IRIDIUM CATALYZED DEHYDROGENATIVE DIBORATION OF ALKYNE, NICKEL AND SILVER COMPLEXES OF AN ALANE/TRIS(PHOSPHINE) LIGAND BUILT AROUND A STRONGLY LEWIS ACIDIC TRIS(N-PYRROLYL)ALUMINUM AND EXPLORATION ON REACTIVITY OF PALP-LIGATED RHODIUM AND IRIDIUM COMPLEXES

A Dissertation

by

QINGHENG LAI

Submitted to the Office of Graduate and Professional Studies of
Texas A&M University
in partial fulfillment of the requirements for the degree of

DOCTOR OF PHILOSOPHY

Chair of Committee,	Oleg V. Ozerov
Committee Members,	Timothy R. Hughbannks
	Michael Nippe
	Hongmin Qin
Head of Department,	Simon W. North

May 2021

Major Subject: Chemistry

ABSTRACT

Phosphination of the *ortho* C-H bond of the pyrrole was developed to form 2-(diisopropylphosphino)pyrrole. The protolysis of $AlMe_3$ with 2-(diisopropylphosphino)pyrrole leads to a new tripodal alane/tris(phosphine) ligand (AlP_3). The synthesis of AlP_3-supported Ni complex was reported. The central tris(pyrrolyl)aluminum moiety acts as a stronger Lewis acid towards Ni than other related group 13 element-centered tripodal ligands, as demonstrated by the binding of H_2 to Ni and ease of reduction.

The Z-type tripodal alane ligand (AlP_3) also reacts with AgOTf by coordination of three phosphines to the Ag center and transfer of triflate to the tris(pyrrolyl) Al site. Reaction with $Ag[HCB_{11}Cl_{11}]$ results in the coordination of two phosphines to Ag and one to Al, indicating, with little to no Ag-Al interaction in either structure.

The synthesis of PAlP and PBP pincer complexes of Rh possessing a central bis(N-pyrrolyl)aluminyl or -boryl unit was developed. Complex $(PAl^{py}P)Rh(CO)_2$ possesses an aluminyl site stabilized by coordination of pyridine, resulting in a four-coordinate Al. Attempts to the three-coordinate aluminyl by abstraction of pyridine with $BF_3{\cdot}Et_2O$ unexpectedly led to the B/Al metathesis with the preservation of the pincer structure in the product $(PBP)Rh(CO)_2$. Abstraction of pyridine was carried out using $B(C_6F_5)_3$, but the desired $(PAlP)Rh(CO)_2$ underwent dimerization via isocarbonyl bridging, reflecting the elevated Lewis acidity of the N-pyrrolyl-substituted aluminyl.

The direct cyclometalation of PCP ligand with $Fe_2(CO)_9$ under UV irradiation leads to a C-H activation product (PCP)FeH$(CO)_2$. 1 e- oxidation of (PCP)FeH$(CO)_2$ in C_6H_5F affords C-H reductive elimination product with [(PCHP)Fe $(CO)_2$] cation with agostic C_{aryl}-H-Fe interaction. While 1 e^- oxidation of (PCP)FeH$(CO)_2$ in CH_3CN gives rise to H_2 and [(PCP)Fe$(CO)_2NCCH_3$] cation.

Catalytic dehydrogenative diboration (DHDB) of alkyne with HBpin was achieved using $[Ir(COD)Cl]_2$ and other related Ir precursors under CO atmosphere. The selectivity for DHDB over hydroboration is higher in less polar solvent and under increasing CO pressure. It was further improved when catalytic amount of ^{t}BuNC was added to the reaction. It was possible to achieve DHDB of both terminal and internal alkynes with selectivity for DHDB of up to 9:1 under the best conditions. Some DHDB products were isolated on the preparative scale.

DEDICATION

To Dad and Mom

ACKNOWLEDGEMENTS

I would like to thank my research advisor Dr. Oleg Ozerov for his guidance over the past six years. I appreciate his helpful suggestions and great effort on my research. I would also like to thank my committee members Dr. Timothy R. Hughbannks, Dr. Michael Nippe and Dr. Hongmin Qin.

I would also like to thank the Ozerov research group, especially my elders who helped me get through the first few tough years: Dr. Loren Press, Dr. Jessica DeMott, Dr. Chandra Mouli Palit, Dr. Christopher Pell and Dr. Wei-Chun Shih. I really appreciated having Dr. Alex Kosanovich as a classmate who is a very kind person full of passion in chemistry. I would also like to thank the Ozerov group members that I have been great to work with: Dr. Bryan Foley, Soomin Park, Dr. Andy Yu, Ming-Uei Hung, Olivia Gunther, Yanwu Shao, Yihan Cao, Mario Cosio, Vinh Nguyen, Brandy Adolph, Derek Leong and Sam Lee.

Finally, I would like to thank my family who made all of my accomplishments possible. Thanks to my mom, dad, and sisters for their encouragement and consistent love.

I am proud to be a graduate student of Texas A&M University. The spirit and traditions of A&M are contagious, and I am glad that I have become a part of this community.

CONTRIBUTORS AND FUNDING SOURCES

This work was supervised by a dissertation committee consisting of Professor Oleg V. Ozerov, Professor Michael Nippe, and Professor Timothy R. Hughbannks of the Department of Chemistry, and Professor Hongmin Qin of the Department of Biology.

IR data in Chapter 5 was collected with assistance from Haomiao Xie during his time as a graduate student in the Dunbar group at Texas A&M University. The XRD structure of **519** in Chapter 5 was solved by Wei-Chun Shih during his time as a graduate student in the Department of Chemistry at Texas A&M University. The XRD structures of **303** (Chapter 3), **405** (Chapter 4)**,** and **706** (Appendix A) were solved by Dr. Nattamai Bhuvanesh. **174** catalyst (Chapter 6) was made by Chun-I Lee during his time as a graduate student in the Department of Chemistry at Texas A&M University.

All other work conducted for the dissertation was completed by the student independently.

This work was made possible in part by the US National Science Foundation (grants CHE-1300299 and CHE-1565923), Welch Foundation (grant A-1717), and support from Dow Chemical Co. Its contents are solely the responsibility of the authors and do not necessarily represent the official view of the U.S. National Science Foundation, the Welch Foundation, or Dow Chemical Co.

NOMENCLATURE

Ar	Aryl
$BArF_{20}$	Tetrakis(pentafluorophenyl)borate
B_2pin_2	Bis(pinacolato)diboron
B_2cat_2	Bis(catcolato)diboron
TMP	2,2,6,6-tetramethylpiperidide
Boc	*tert*-Butoxycarbonyl
TBE	*tert*-butylethylene
COD	Cyclooctadiene
COE	Cyclooctene
Cp	Cyclopentadienyl
Ph	phenyl
CAAC	cyclic alkylaminocarbenes
DFT	Density Functional Theory
DHBTA	Dehydrogenative Borylation of Terminal Alkynes
Dipp	2,6-diisopropylphenyl
Et	Ethyl
FLP	Frustrated Lewis Pair
HBpin	Pinacolborane, 4,4,5,5-tetramethyl-1,3,2-dioxaborolane
HBdan	1,8-naphthalenediaminatoborane
^{i}Pr	*iso*-propyl

NBS	*N*-bromosuccinimide
^{n}Bu	*n*-butyl
DHDB	Dehydrogenative diboration
nbd	norbornadiene
NMR	Nuclear Magnetic Resonance
OA	Oxidative Addition
OAc	Acetate
OTf	Triflate
py	pyridine
RE	Reductive Elimination
TBE	*tert*-butyl ethylene, 2,2-dimethyl-3-butene
^{t}Bu	*tert*-butyl
THF	Tetrahydrofuran
PhF	fluorobenzene
XRD	X-Ray Diffraction

TABLE OF CONTENTS

Page

LIST OF FIGURES

Page

LIST OF SCHEMES

Page

LIST OF TABLES

Page

CHAPTER I

INTRODUCTION

1.1 Pincer ligands

Pincer ligands are tridentate chelating ligands coordinate to a metal with meridional configuration, which provide high thermal stability to the resulted complexes. While tridentate ligands bind to a metal in *fac* manner was referred as scorpionate ligands, which will be discussed in the later sections. The seminal project on pincer complex was first reported by Shaw and co-workers back to 1976.[1] The last few decades have witnessed the continuous booming in the development of pincer chemistry with a wide variety of applications.[2]

The terminology of pincer ligand is very closely related to their donor atoms and the link between the central donor and the other two side donors. Due to the presence of diverse donor atoms as well as various linkers, Pincer ligands are synthetically variable for chemist to achieve more control on both electronic and steric properties of the metal center, more importantly either electronic or steric properties of the metal can be tuned independently without significant influence on each other.

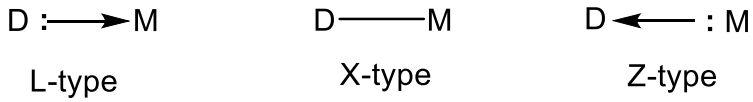

Scheme I-1. A generic L, X, and Z-type ligand interactions with a generic metal center

There are 3 basic types of ligand-metal coordination differentiated by the electronic binding nature between ligand and the metal (**Scheme I-1**): L-type interaction

is referred to binding via lone pair, or two-electron donation from ligands to the metal center; X-type interaction is categorized by binding via sharing one electron from the ligand and the other from the metal; Z-type interaction is characterized with two-electron donation for metal to ligand. In general, L-, X- and Z-type lignads donate 2, 1, 0 electron to a metal center when using the neutral ligand method of electron counting.[3]

Theoretically three donors of pincer ligands could be any type of ligands with any combination, and are used for abbreviation of pincer ligands in most cases. The classic representative examples of pincer ligands are generally separated into four main categories as shown in **Figure I-1**. The first category, one of the most common pincer ligands, are neutral (LLL-type) ligands with terminal *tert*-phosphine groups and central heteroatom-(**101A**)[4] or carbene-based (**101B**, **101C**)[5] donor groups. The second pincer platform are anionic (LXL-type) ligands. The most common combination is anionic X-type central donor with 2 L-type neutral side arms ligands including widely used PCP (**101D**) ligands[1], POCOP ligands (**101E**),[6,7] diarylamino PNP ligands (**101F**) developed by Liang[8] and Ozerov[9], Fryzuk's PNP ligands (**101G**),[10] Peters' NNN ligand (**101H**),[11] and PSiP ligands (**101I**)[12]. The dianionic (LXX-type) and trianionic (XXX-type) ligands are relatively rare but did find their ways into the literatures.[13-20]

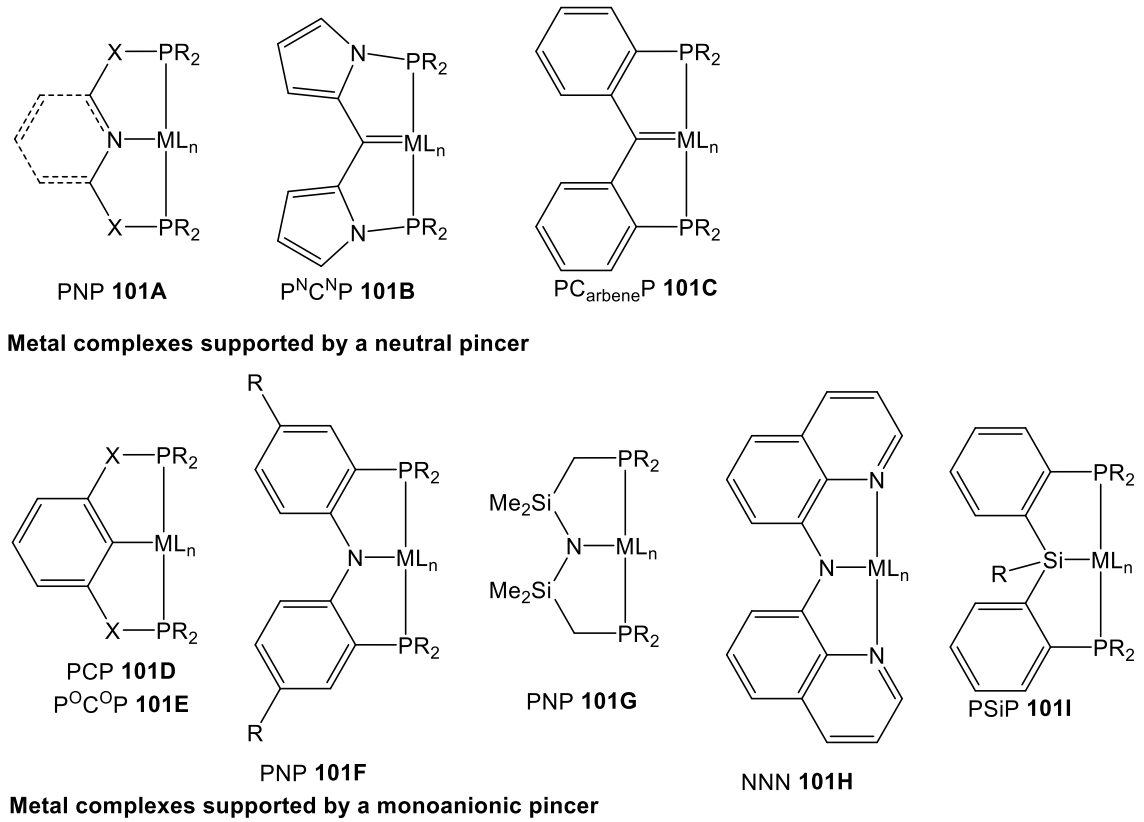

Figure I-1. Representative LLL-type and LXL-type pincer ligands

1.2 Pincer ligands with a group III atoms as central donor

Among those pincer ligands, pincer ligands bear a group III atoms (B, Al) have drawn increased attention over the past 20 years due to the unique feature of empty orbital on the central donors which lead to unusual modes of metal-ligand-cooperativity.[21-32] The central donors of the pincer ligand can bind to a metal center in various manners. There are three common fashions for a tri-substituted boron ligation with a metal (**Scheme I-3**)[33]: a Z-type interaction would be expected when a neutral borane moiety accepts 2 e^- from a metal, while a ligand stabilized borylene moiety binds to a metal in L-type fashion

similar to cyclic alkylaminocarbenes (CAACs) or carbon monoxide;[34-36] the third category is the X-type bonding between a boryl $[R_2B]^-$ and a metal.[27-32,37,38]

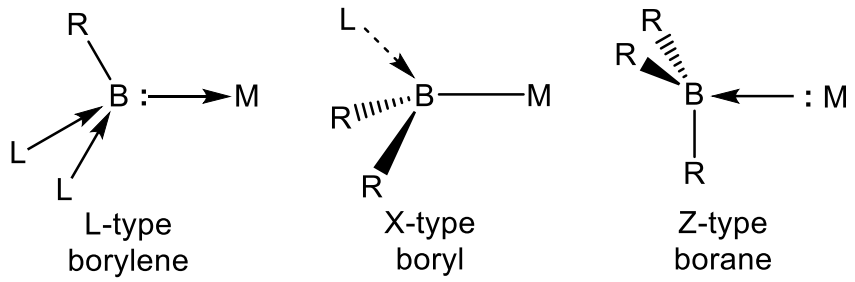

Figure I-2. Classification of ligand-metal interaction between a tri-coordinate boron and a metal

The coordination pattern of the boron centers to a metal (**Figure I-2**) can be more flexible depends on the nature of the metal and substituents on the boron, which is well demonstrated by Ozerov's study on triaryl-PBP-ligated rhodium complexes.[37]

1.2.1 Boryl-centered pincer

The boron-containing pincer complexes were an exciting class of pincers present a strong donor and *trans* influence ligand. The boron centered pincers were mainly subdivided into three categories according to their back bones (**Figure I-3**): diaminoboryl pincer complexes (**101J**) diarylboryl pincer complexes and carborane-derived pincer complexes (**101K**).

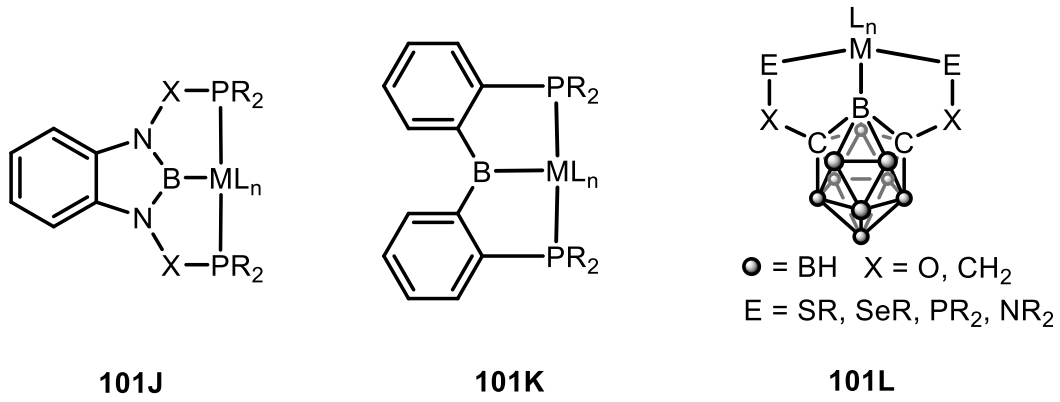

101J **101K** **101L**

Figure I-3. Boryl-centered pincer ligands

1.2.1.1 Diamino-based PBP pincers

Incorporating boron into a pincers is not synthetically challenging, meanwhile transition metal complexes with a X-type boryl group have been reported a lot especially in the field of C-H borylation catalysis, however, The draught for the boryl-centered pincer continued until Nozaki and Yamashita disclosed the first boryl-centered PBP-type pincer complex (**104**) in 2009.[30] The borylation of ligand back bone was inspired by the synthesis of well-know borylation reagents chelated with diols (**HBpin** and **HBcat**): 1,2-bis(phosphinomethylamino)benzene (**102**) was obtained via condensation of *ortho*-phenylenediamine with phosphinomethanol generated by the reaction of formaldehyde with secondary phosphine *in situ*. Then 3 equiv BH_3•SMe_2 was treated to **102** to form amino-chelated hydroborane back bone. The excess borane bind to phosphine was removed with alkylamine to afford the desired PBP ligands **103.**

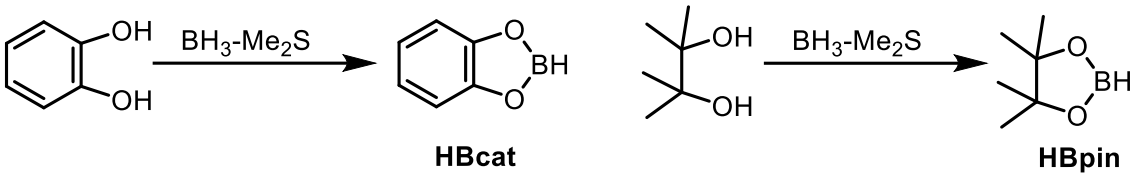

Scheme I-2. Synthesis of HBcat and HBpin

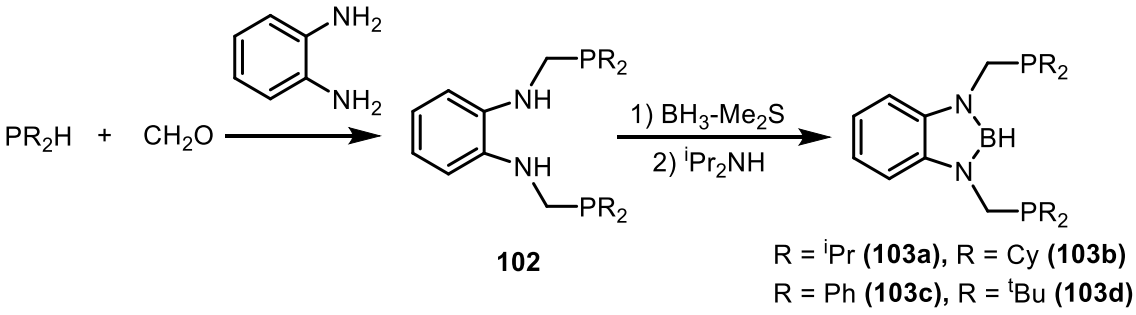

Scheme I-3. Synthesis of diaminoboryl pincer ligands

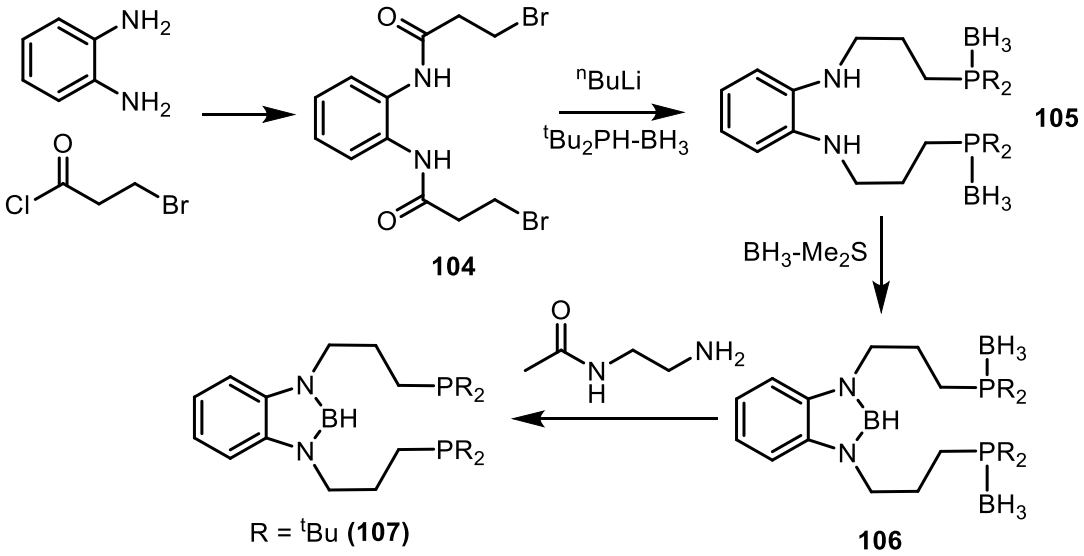

Scheme I-4. Synthesis of diamino-boryl pincer ligand with extended side arms

The synthesis of boryl-centered pincer with longer phosphine side arms was developed by Yamashita and co-workers in 2016.[39] The condensation of 3-

bromopropionyl chloride with *ortho*-phenylenediamine gave rise to **104**. The di-*tert*-butylphosphinoborane and ^{n}BuLi was added to form **105** with phosphinoborane side arms. The BH_3•SMe_2 was introduced to formed broyl-centered pincer **106** with phosphine side donors protected with BH_3, which was removed with *N*-acetylethylenediamine to generate desired ligand **107**. The similar pincer **108** with tetramethylethyl back bone can be obtained using the same procedure with 2,3-dimethylbutane-2,3-diamine.[40]

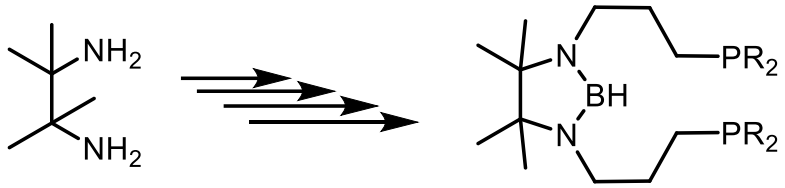

R = ^{t}Bu **(108)**

Scheme I-5. Synthesis of boryl pincer ligand with aliphatic back bone

B-H oxidative addition to the group VII transition metal such as Ir or Rh took place at room temperature to generate corresponding (PBP)IrHCl(**110-112**)[30,39-41] and (PBP)RhHCl complexes (**109**)[30,31] with a 3-coordinate boryl center, which is a strongly σ-donating group. These amino-based (PBP) metal complexes were found to facilitates a number of bond activation reaction and catalytic applications, such as the transfer dehydrogenation of alkanes,[32,39] the dehydrogenation of dimethylamine-borane[40,42] or the hydrogenation and hydrosilylation of olefins[32,42,43]

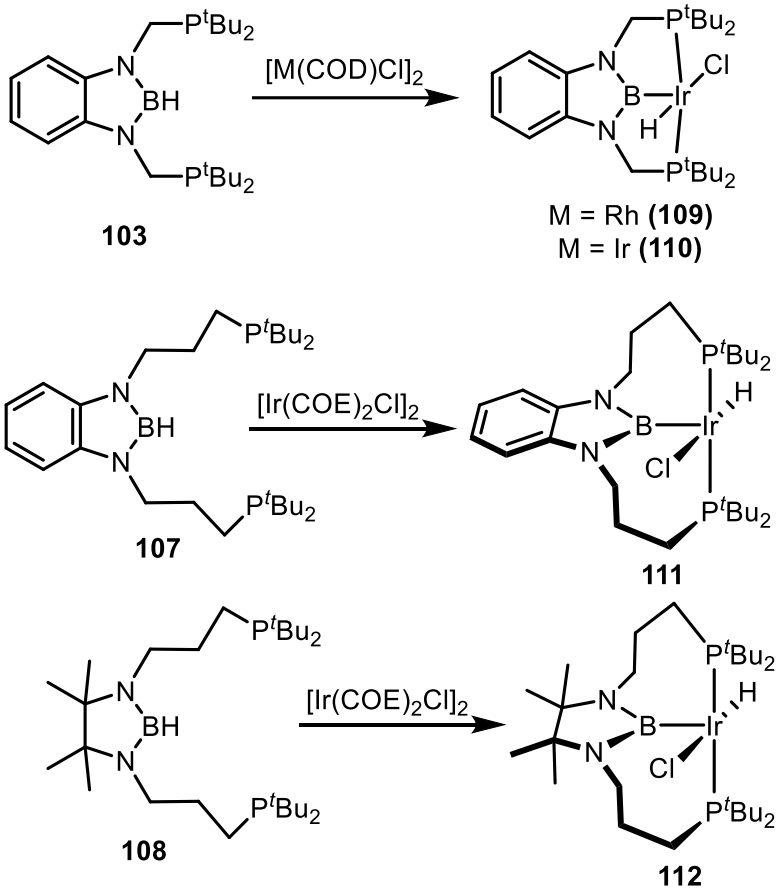

Scheme I-6. Cyclometalation of amino-based boryl pincers

The amino-based PBP ligands can also react with other transition metal precursors via B-H oxidative addition to give boryl-based pincer-type complexes.[32,43]

1.2.1.2 Diaryl-based PBP pincers

The synthesis of boron-centered pincers (**113**) with similar back bone to Ozerov PNP was developed earlier by Bourissou and co-workers than amino-based PBP ligands: The reaction of ortho-lithiated phosphinobenzene generated in situ with PhBCl2 in 2:1 ratio give rise to aryl-based PBP with a B-Ph moiety.[44,45]

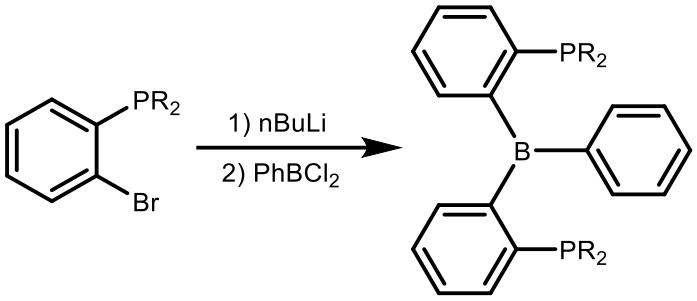

R = iPr, **113A**
R = Ph, **113B**

Scheme I-7. Synthesis of aryl-based PBP

Unlike those amino-based PBP with B-H bond, the stronger B-C bond make it challenging to form X-type boryl pincer ligation via oxidative addition of B-C bond to a metal. The central boron of aryl-based PBP bind to a metal with Z-type interaction dominantly until 2016. Direct oxidative addition B-C to Ir center was achieved and generates X-type boryl (PBP)IrPhCl by Ozerov and co-workers.[27]

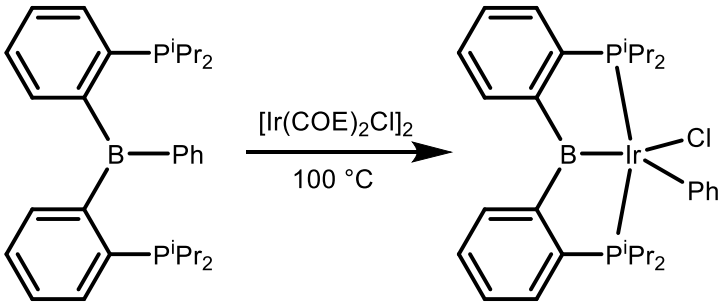

113A **114**

Scheme I-8. Synthesis of X-type boryl-centered (PBP)IrPhCl

In the same year, Tauchert and co-workers developed a method to enforce the X-type boryl bonding from Z-type bonding: oxidative addition of aryliodide to **115** would generate **116**, which release the C-C reductive coupling biaryl to formed **117**.[26] The mechanism for the conversion from **116** to **117** was proposed: ligand exchange between

B and Pd gives rise to **118** with two aryl groups *cis* to each other, then C-C reductive elimination forms a palladium(0) **119**, which can oxidatively activate the B-I bond to afford **117**.

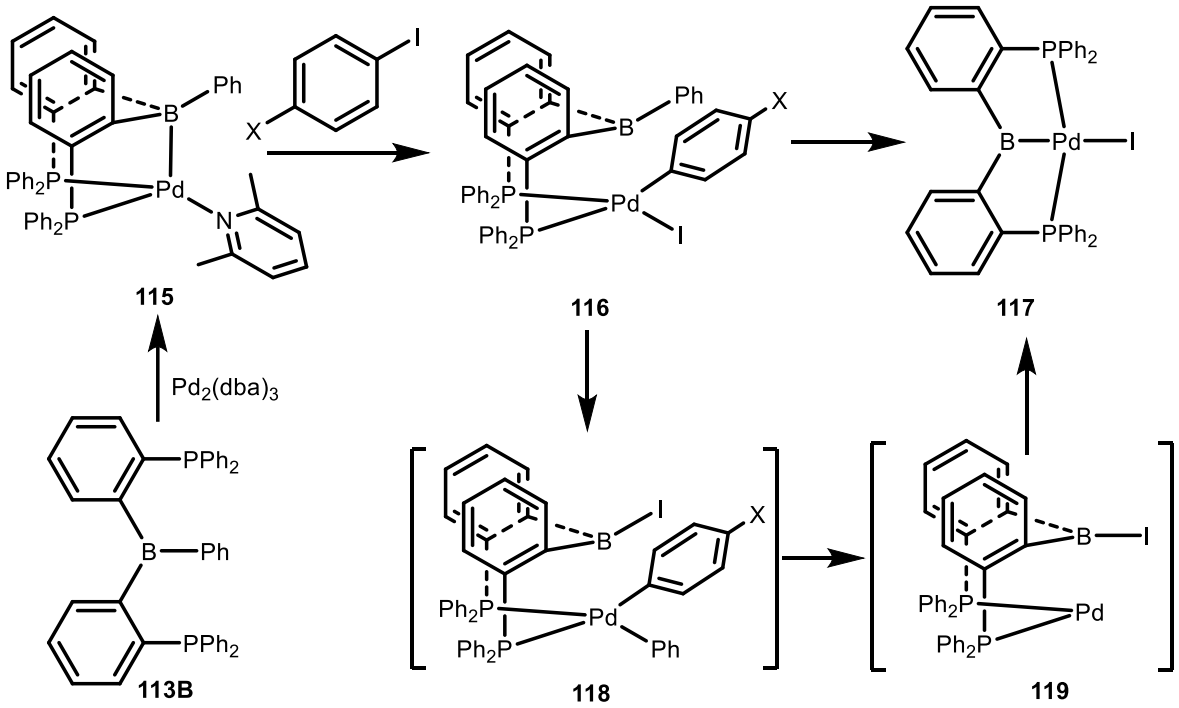

Scheme I-9. Synthesis of X-type boryl-centered (PBP)PdI and proposed mechanism.

The diarylboron center in this PBP ligand is likely to be more Lewis acidic than those of diamino-based PBP which possess π-donating amino substituents on the boron. Extensive studies of the aryl-based PBP supported iridium complexes revealed the aryl-based PBP platforms facilitates bond activations in a unique way. Directed CH activation generally relies on the formation of five- and sometimes six-membered cyclometallo-rings, therefore C-H activation of quinoline usually occurred to the C-H bond of phenyl. While Thermolysis of compound **120** with quinoline at 100 ℃ resulted in 97% **121**, an

ortho-CH activated product with a four-member rings containing boron and iridium, and 3% of C-H activation product of phenyl position to form classic 5-member rings. In addition, **123** with mono CO attached to iridium center, obtained via comproportionation of **120** with **122** at room temperature, was demonstrated to be more effective for *ortho*-CH activation of pyridine derivatives.[38]

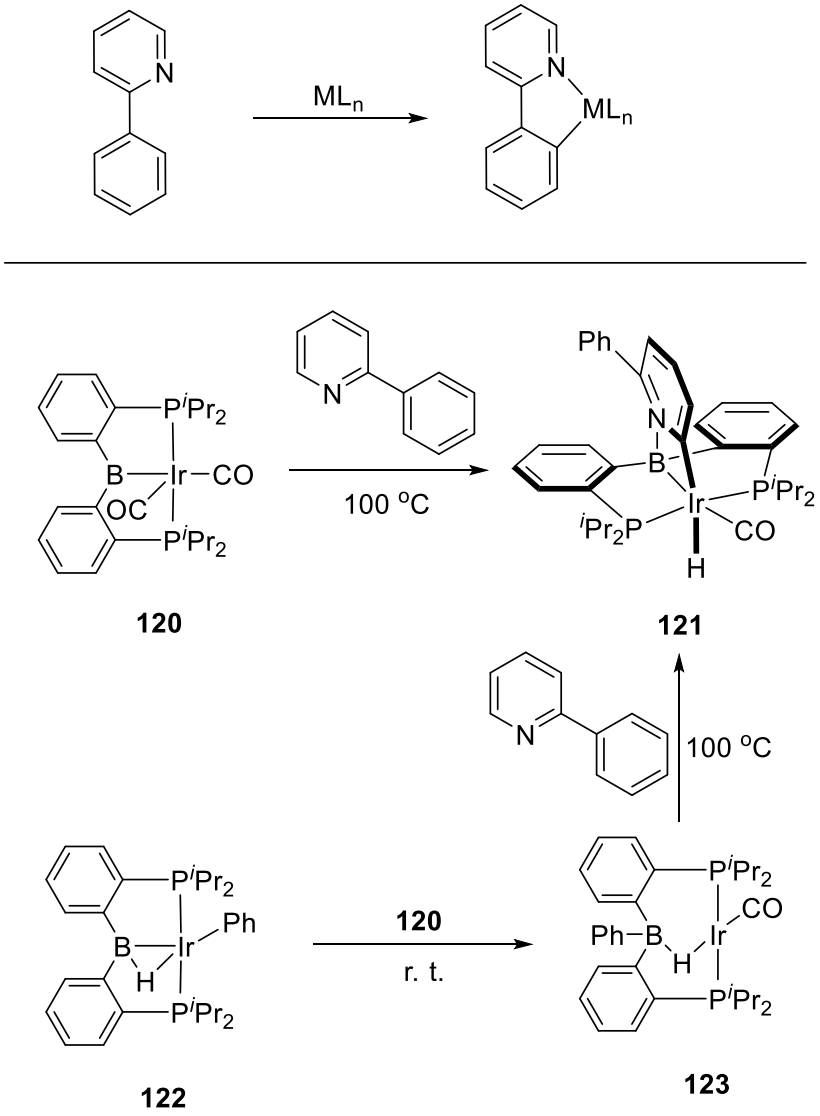

Scheme I-10. Ortho C-H bond activation of quinoline

In the proposed mechanism, pyridine binding occurs before or after CO dissociation from **120**. The Lewis acid-base adduct can be isolated prior C-H activation when stronger pyridine derivative such as DMAP was used. It is very unlikely that pyridine will bind to the 4-coordinate borane in **122**, instead pyridine most likely bind to **126**, a Ph-H reductive elimination product. The iridium insertion of **125** into a directed *ortho*-C–H bond of pyridine should give isomer **127** with a *cis*-disposition of the H and $C_{pyridyl}$ ligands around Ir. Then rearrangement of 127 gives rise to observed product **128** with a CO trans to boryl moiety.[38]

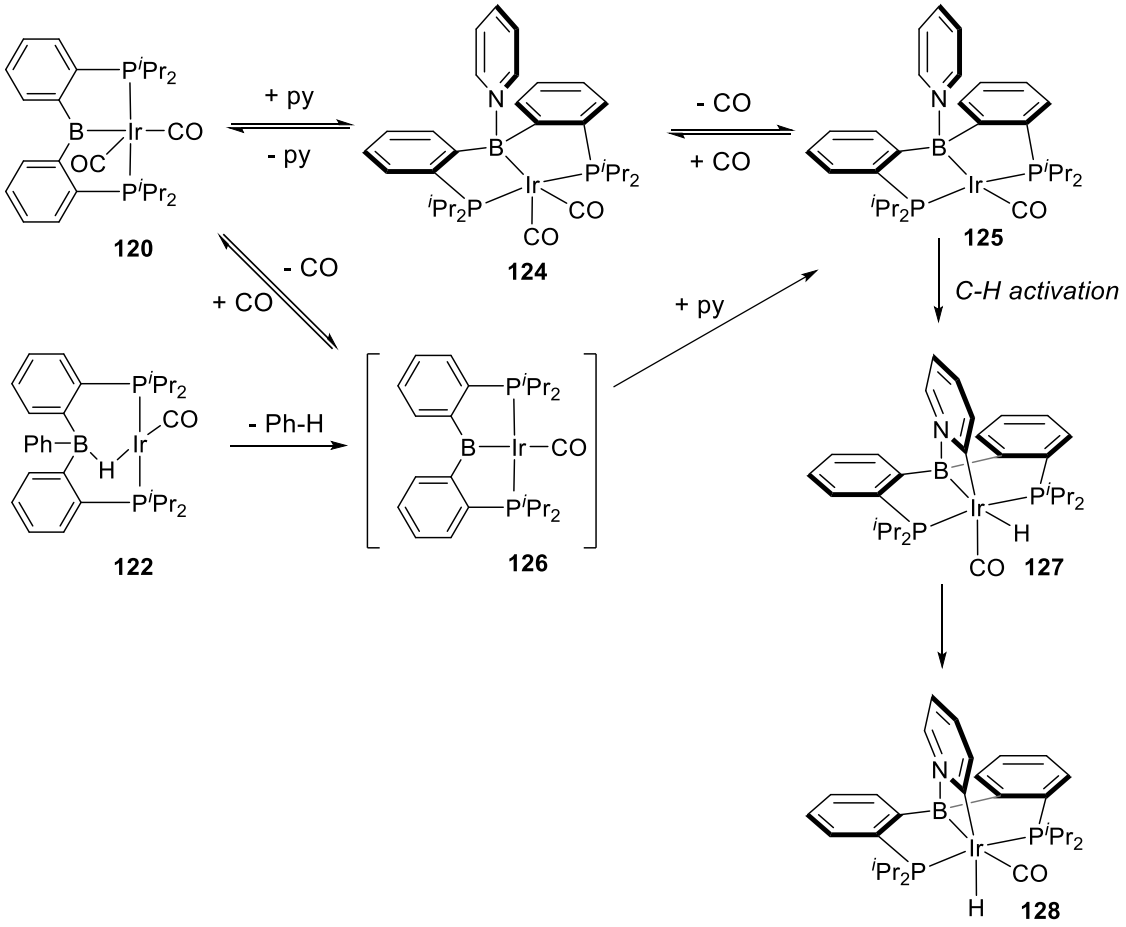

Scheme I-11. Proposed mechanism for Py ortho-C-H activation

Heterolytic cleavage of O–H, N–H, and F–H bonds by **120** was demonstrated in 2019 by Ozerov and co-workers.[46] This diaryl-based PBP supported complexes are proved to catalyze the transfer dehydrogenation of olefin in 2017. [47]

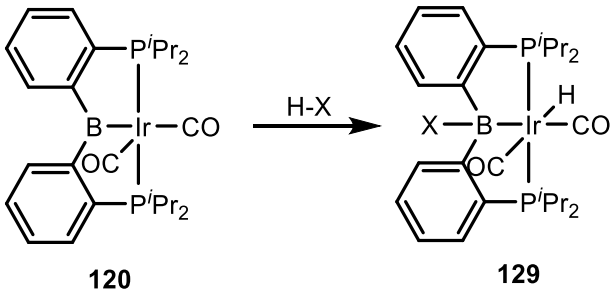

120 **129**

Scheme I-12. H-X cleavage across Ir-B

The complexation of **113** with other group metals such as Fe,[48,49] Ni[50], Ru,[51,52] Cu,[53] Ag[54] and Au[45] was achieved, however none of the above complexes bear X-type boryl-metal interaction.

1.2.1.3 Carborane-based PBP pincer ligands

Icosahedral *meta*-dicarbaboranes present a good platform for the design of pincer ligands, due to a wide range of accessible methods for C-H functionalization of the *m*-carborane. In addition, carborane unit exhibits extraordinary stability which work well with the main purpose of a supporting pincer ligand. The first carborane-based pincer ligand family was developed by Mirkin in 2009.[28] The SBS (**131**) was synthesized in 1 step: the deprotonation C-H of **130** with MeLi followed by a SN2 reaction of the carba anions generated in *situ* with $PhSCH_2Cl$ give rise to **131**. The synthesis of SeBSe (**134**) required 3 steps: Firstly paraform was reacted with deprotonated 130 to install hydroxylmethyl side arms. Secondly bromination was achieved using Br_2 in the presence of PPh_3. Thirdly SePh group was attached via reaction of PhSeSePh with Lithiated **133**.

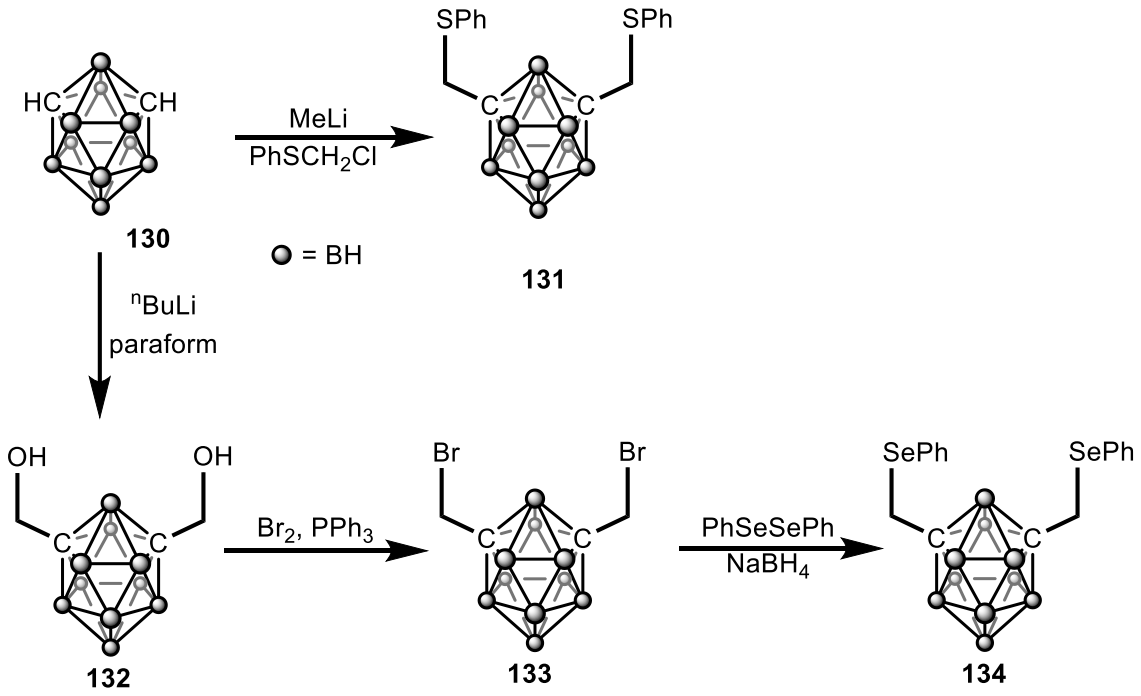

Scheme I-13. Synthesis of carborane-based SBS and SeBSe

The cyclometalation conditions of **131** and **134** with Pd are the same, which is reacting ligand with $Pd(CH_3CN)_4[BF_4]_2$ in acetonitrile followed by addition of 2 equiv of $(nBu)_4NCl$. According to the calculation, there is a net negative charge localized on the Pd atom and a relative positive charge on the boryl center connected to Pd, compared to other borons in the cage, suggesting an X-type boryl center in **135** and **136**. The Pd-B bonds in complexes **135** and **136** exhibit strong σ-electron donation with little π-back bonding.

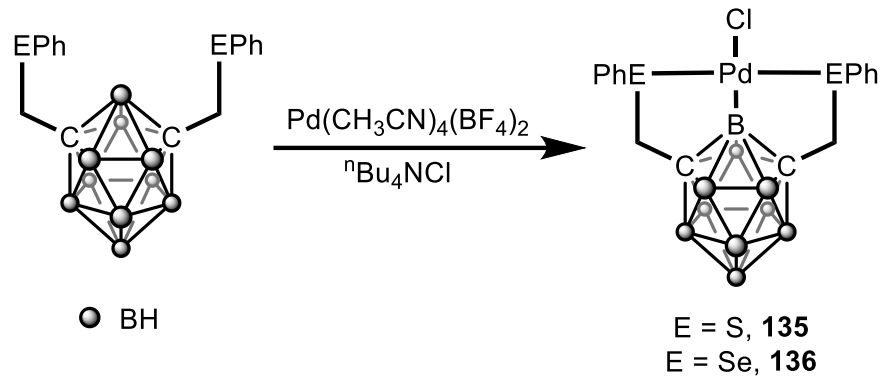

Scheme I-14. Synthesis of carborane-base[55] (EBE)PdCl

More m-carborane-based LBL pincer ligands were developed. The synthesis of a series chiral NBN pincer ligands were reported by Nakamura and co-workers in 2011.[56] The *m*-carborane-based pincer complexes of rhodium(III), nickel(II), and palladium(II) were synthesized by the oxidative addition of the ligands to $RhCl_3 3H_2O$, $Ni(COD)_2$, and $Pd(CH_3CN)_4[BF_4]_2$ respectively. The air stable rhodium complexes can catalyzed asymmetric conjugate reduction of α,β-unsaturated esters with good enantioselectivity.

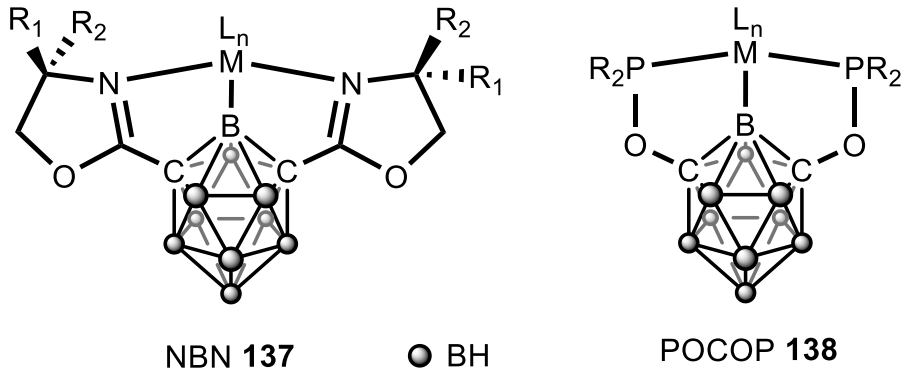

Figure I-4. *m*-carborane-based pincer ligands

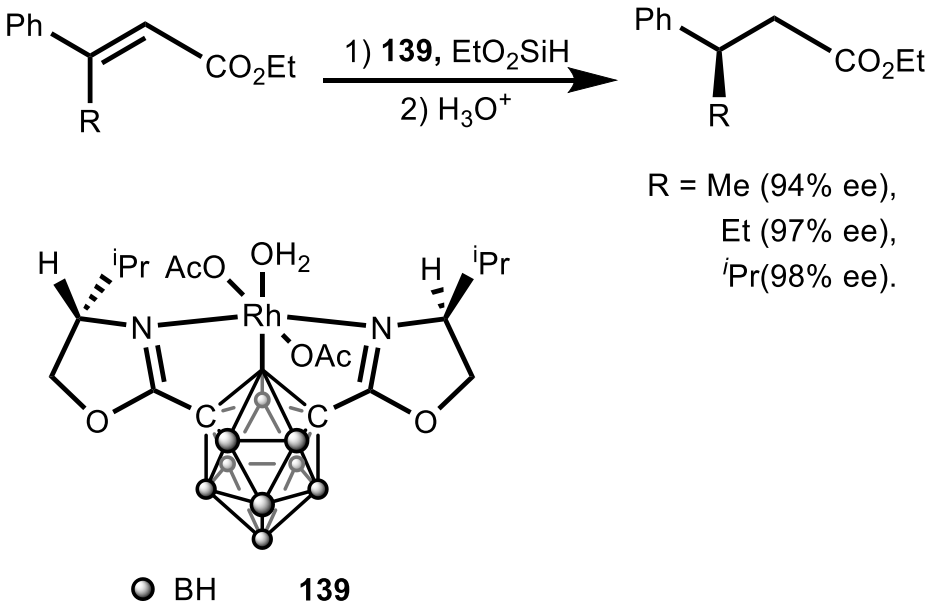

Scheme I-15. Catalytic asymmetric conjugate reduction of α,β-unsaturated esters with **139**

In 2016, Peryshkov and co-workers succeeded to install a phosphinite side arms in to the *m*-carborane unit.[29] The complexation of carborane-based POCOP (**138**) ligands with $Rh(PPh_3)_3Cl$ proceed at room temperature to afford **140** with octahedral geometry. In the presence of Et_3N, **140** would reductive eliminate HCl quickly even at room temperature to form 4-coordinate rhodium complex **141**. The complexation of **138** with $[Ru(CO)_3Cl]_2$ required Et_3N to achieve clean metalation product **142**, a double B-H activation product with rhodium boryne moiety.[57] The rhodium-BB moiety showed novel reactivity towards some chemical bonds such as CC triple bonds, C_{sp}-H bond and I-I bond.

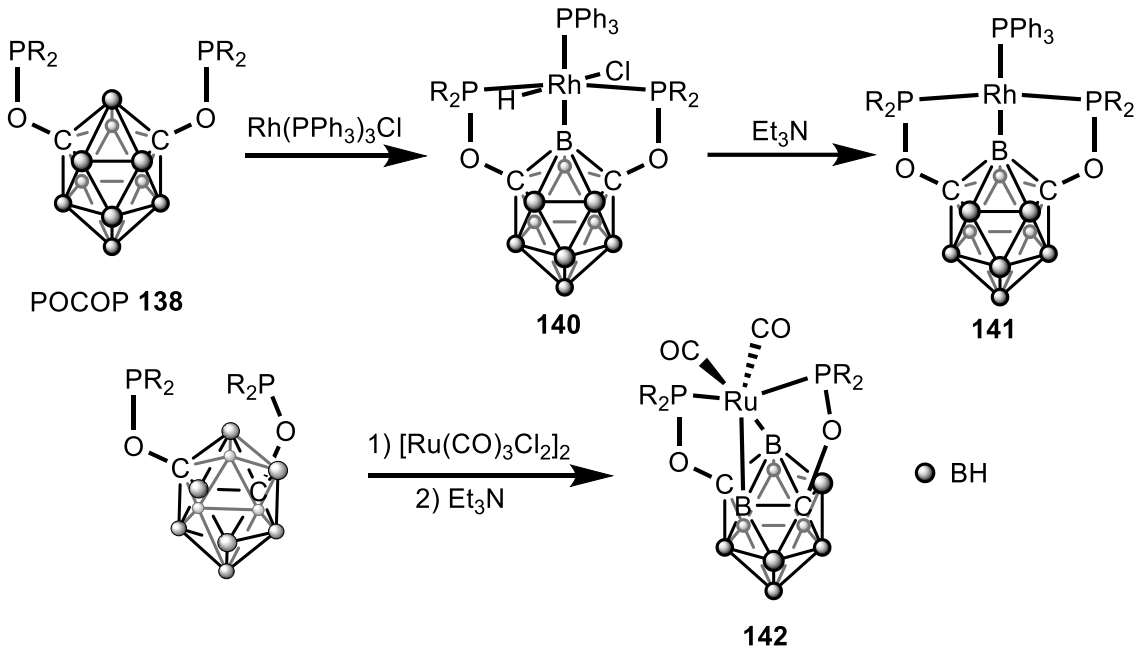

Scheme I-16. Cyclometalation of carborane-based POCOP

1.2.2 Aluminum-centered pincer ligands

In comparison the aluminum-centered pincer ligands ligated metal complexes have been scarcely explored, among which electro-static or Z-type boding between Al and a metal are most commonly seen. The X-type aluminyl is arguably equal if not more strongly σ-donating as X-type boryl, while 3-coordinate aluminyl center should be much more Lewis acidic than boryl center due to the higher electro-positivity of Al. In addition, the structure of Al could be more diversified due to the higher coordination number of Al. All of the above factors make Al-centered pincer ligands very appealing ambiphilic ligands. However, the relatively high sensitivity of Al-C or Al-N bond (due to protolysis or redistribution of Al–C bonds) represents a synthetic limitation.[21,58]

1.2.2.1 Diaryl-based PAlP

The first Al-centered pincer ligands was synthesized by Bourissou and co-workers in 2008.[21] The same building block for diaryl-based PBP synthesis was used to construct PAlP (**143**) via similar steps. Treatment of the **143** with [AuCl(SMe_2)] resulted in chloride transfer from Au to Al and readily afforded the **144** without significant Al-Cl-Au bridging interaction. When the **143** was treated with CuCl, zwitterionic polymer **145** was formed through Cu-Cl-Al bridges.[59] In both complexes, the direct M-Al interaction was missing.

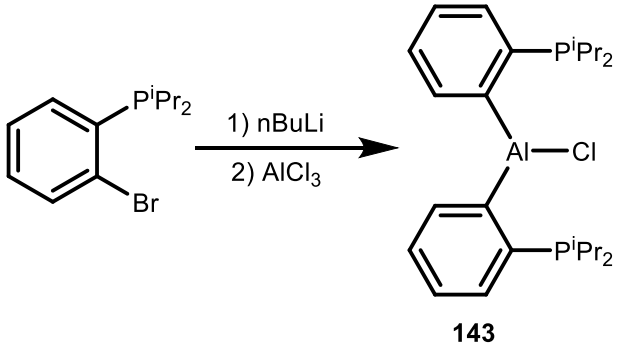

143

Scheme I-17. Synthesis of PAlP pincer

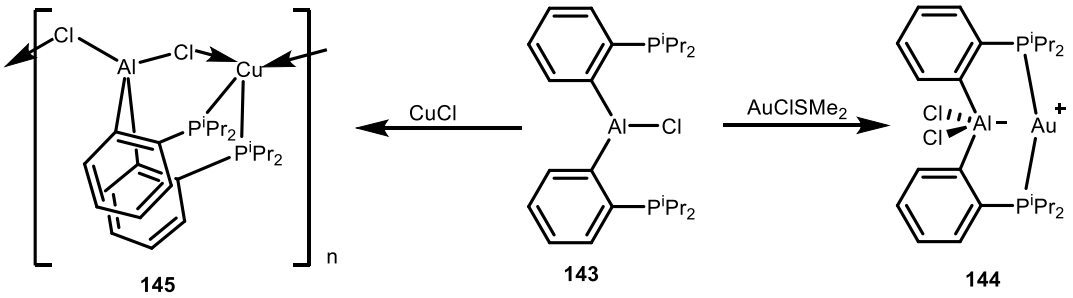

145 **143** **144**

Scheme I-18. Activation of M−Cl Bonds with PAlP

1.2.2.2 NNN-based PAlP and heavier PEP pincer ligands

In 2017, Iwasawa and Takaya utilized a NNN pincer frame work to enforce a X-type Al-Pd interaction.[22] The cyclometalation of **146** with excess $AlCl_3$ occurred at room temperature to give **147a** with two type of Al center: 5-coordinate Al cation and 4-coordinate Al anion. The Pd_2dba_3 was then used to further cyclometalate **147a** to form **148a**, the first pincer complexes bear a X-type Al moiety. Pd−Cl bond (2.5475(9) Å) is the longest among reported pincer palladium complexes, consistent with expected strongly *trans* influence of an X-type aluminyl donor. The Pd-Al (2.461(1) Å) bond is slightly longer than a Z-type Pd→Al interaction. Both the incorporation of heavier group III elements to **146** and the subsequent cyclometalation with palladium were successful. **148a**, **148b** and **148c** were proved to be effective catalyst for CO2 hydrosilylation, and the aluminyl-centered **148a** showed significant higher reactivity.

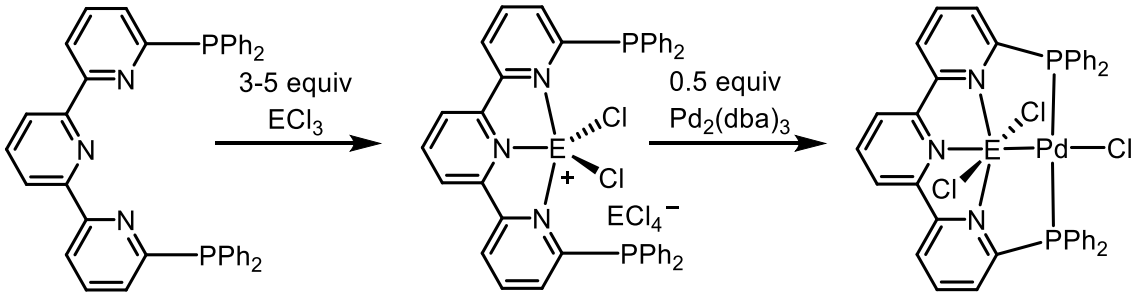

146

E = Al, **147a**
E = Ga, **147b**
E = In, **147c**

E = Al, **148a**
E = Ga, **148b**
E = In, **148c**

Scheme I-19. Cyclometalation of PEP with Pd

The same method worked well for the incorporation of Ga into 2,6-dimethyl substituted **149** ligand.[60] Then cyclometalation of 149 with $[Ir(COD)Cl]_2$ led to a

gallylene-centered pincer iridium complex **151**. Replacing the neutral py moiety with pyrroly would require deprotonation in order to introduce group III element. The pincer ligand with pyrrolyl back bone was neutral. Complexation of **153b** and **153c** with $[Ir(coe)_2Cl]_2$ give rise to **154b** and **154c** respectively.[61]

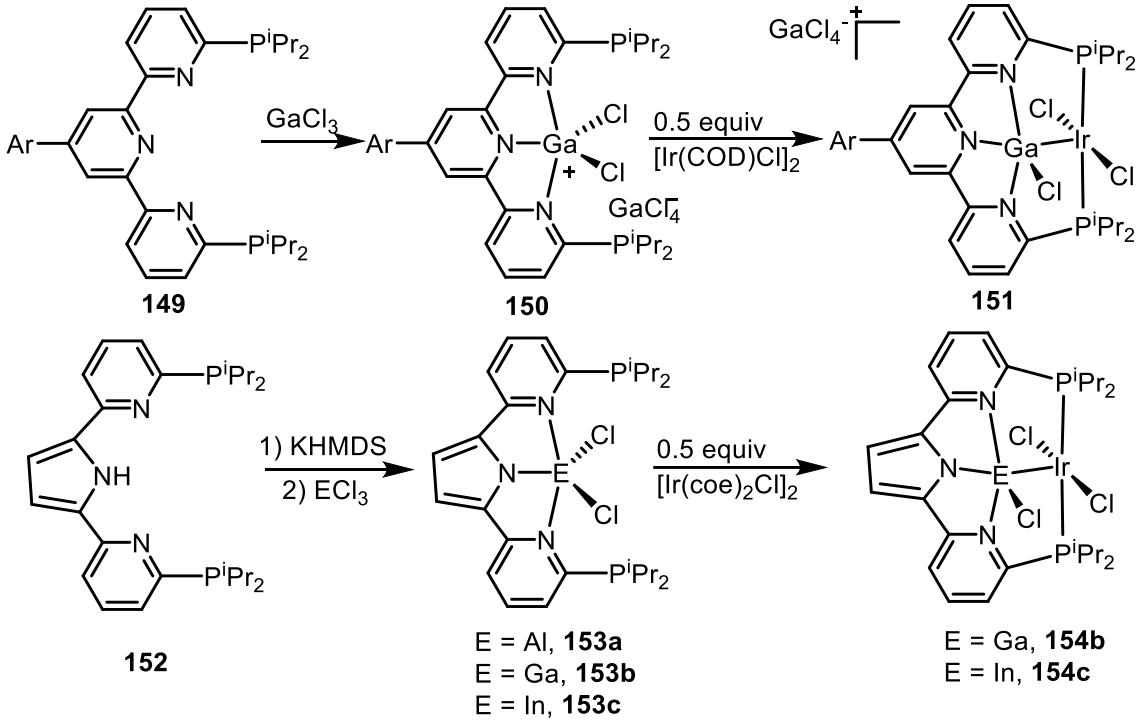

Scheme I-20. NNN-supported group 13 elements centered pincer ligands

In 2018, Nakao and co-workers developed the synthesis of similar NNN-chelated-Al pincer, but instead of 2 or 3 L-type N donors, there is only one L-type N donor in the back bond. [23] The reaction of lithiated **155** with $AlCl_3$ in 1:1 ratio give rise to PAlP pincer **156** with 4-coordinate Al center. Thermolysis of 156 with $[RhCl(nbd)]_2$ led to rhodium dimer **157** with Z-type Al-Rh interaction. X-type aluminyl pincer complex **158** was obtained via reduction of **157** in the presence of nbd. The X-type Al−Rh bond [2.5487(8) Å] is longer than a reported Z-type Al-Rh (2.425 Å). **158** activates ortho C-H of pyridine

when nbd was removed via hydrosilylation, and was found to effect pyridine alkylation with olefin. The catalytic system did suffer from poor reactivity even though high ortho selectivity was observed.

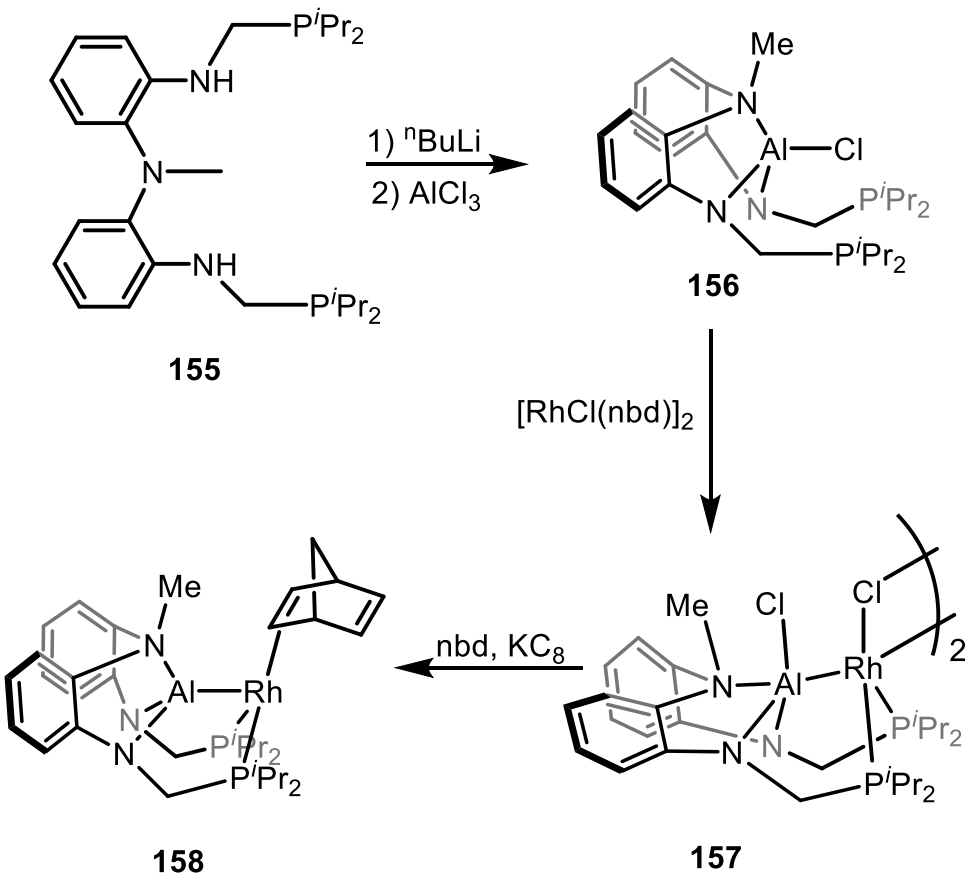

Scheme I-21. Synthesis of aluminyl-PAlP rhodium complex

159 generated in situ also activates C_{ary}-F bond across Rh-Al moiety. The oxidative product **161** can be reduced by Mg to regenerate **159**. The catalytic C_{aryl}-F bond reduction products generated this way are well-known Greenard reagents, which readily react with all kinds of electrophile to form new C-X bond.[25]

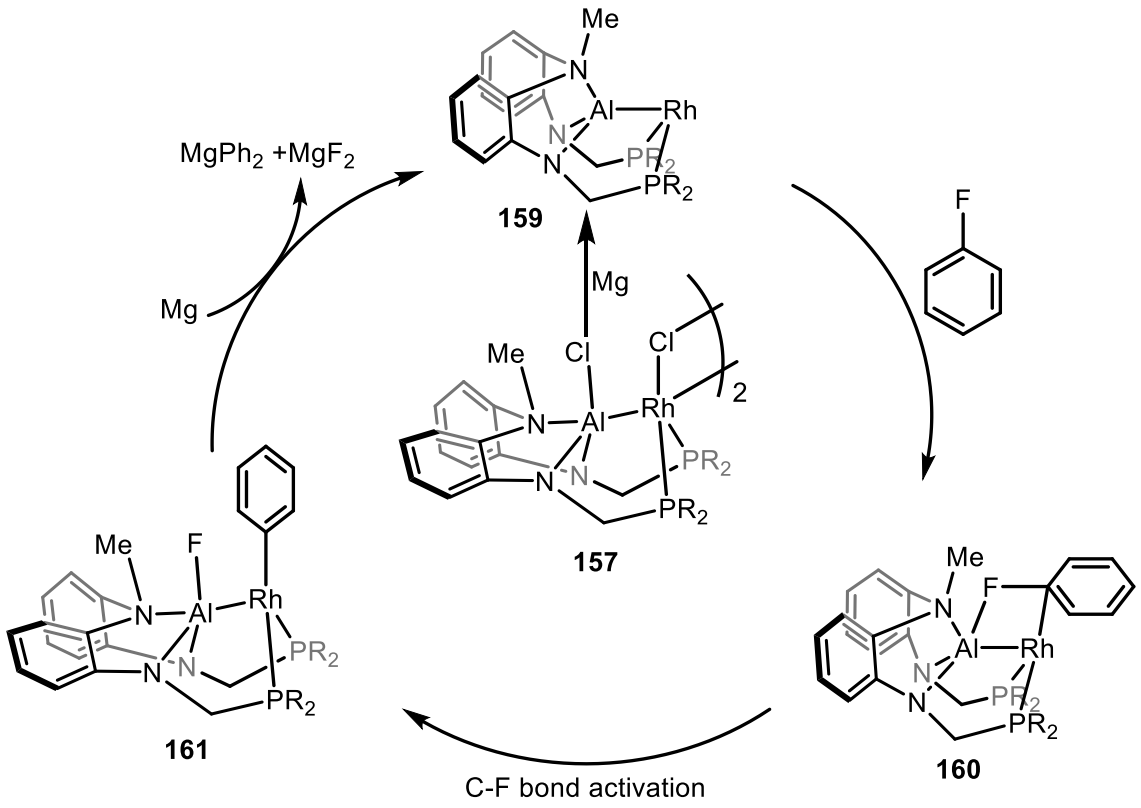

Scheme I-22. Mechanism for aryl C-F magnesiation

1.2.2.3 diamino-based PAlP

Yamashita reported the first aluminyl-center pincer iridium complexes with a 3-coordinate Al center in 2019.[24] The similarity of Al and B in reactivity provides benefit for the PAlP synthesis from PBP synthesis. The synthesis of **163** is very similar to the boryl version via protolysis of E-H with N-H bond. Then cyclometalation of **163** was achieved with $[Ir(COD)Cl]_2$. X-type Al-Ir bond [2.3819(14) Å] of **164** is significantly shorter than the sum of the covalent radii of the Al and Ir atoms.

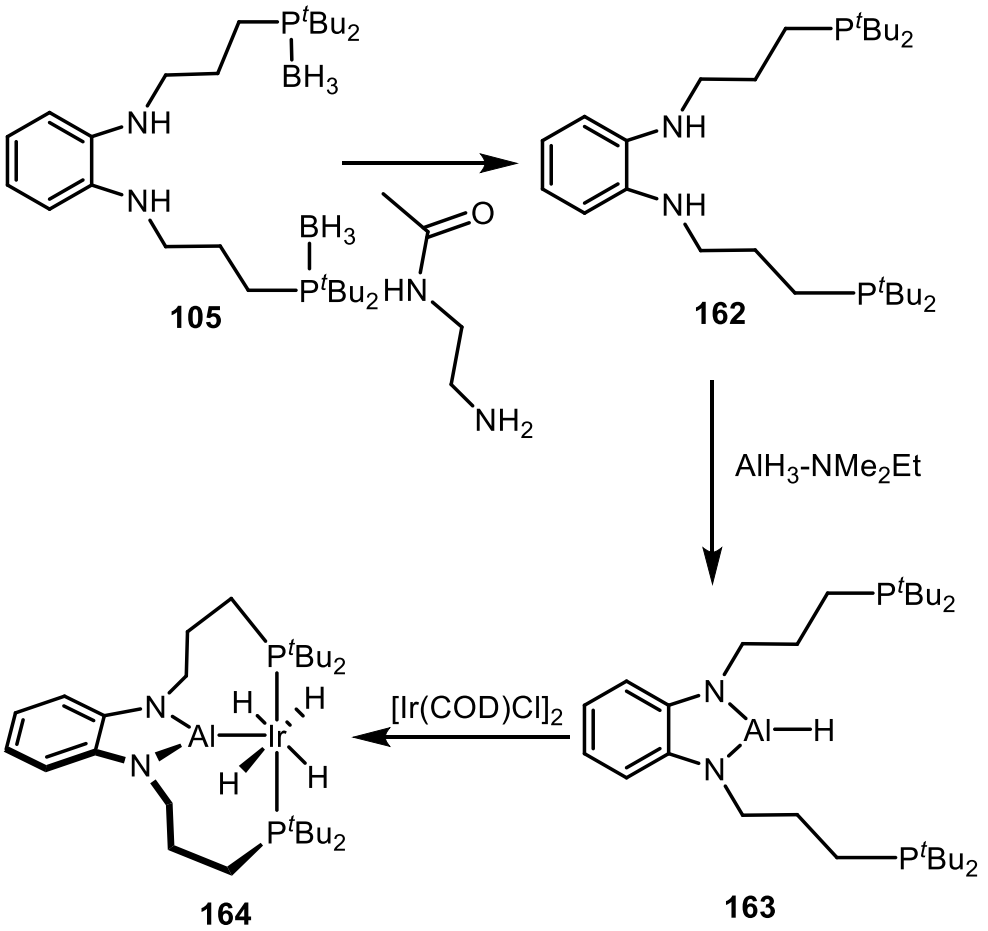

Scheme I-23. Synthesis of diamino-based PAlP

1.3 Tripodal ligands

Tripodal ligands are C_3 symmetric tri- and tetradentate ligands with 3 side arms containing donor atoms that are connected to the central atom. In contrast to pincer ligands, the tridentate tripod ligands typically bind to the transition metal with facial configuration, which is also common configuration for tetradentate tripod ligands when the fourth coordination site is not available.

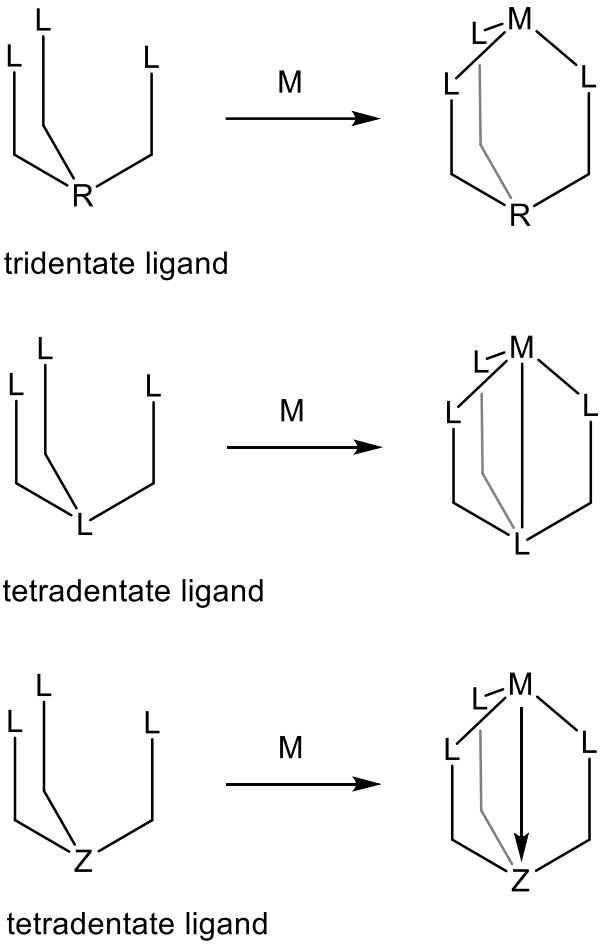

Scheme I-24. Complexation of tripodal ligands

Since their first discovery in 1966 by Trofimenko,[62] hydrotris(pyrazolyl)borates (**Tp**) have played a great role of designing novel compounds in the field of coordination chemistry.[63,64] In 1986, Trofimenko developed a second generation of **Tp*** ligands with substituents on pyrazole-3 position to prevent the formation of the homoleptic $M(Tp)_2$ complexes, which are proven to be more valuable ligands in the preparation of catalysts and models for enzyme active sites.

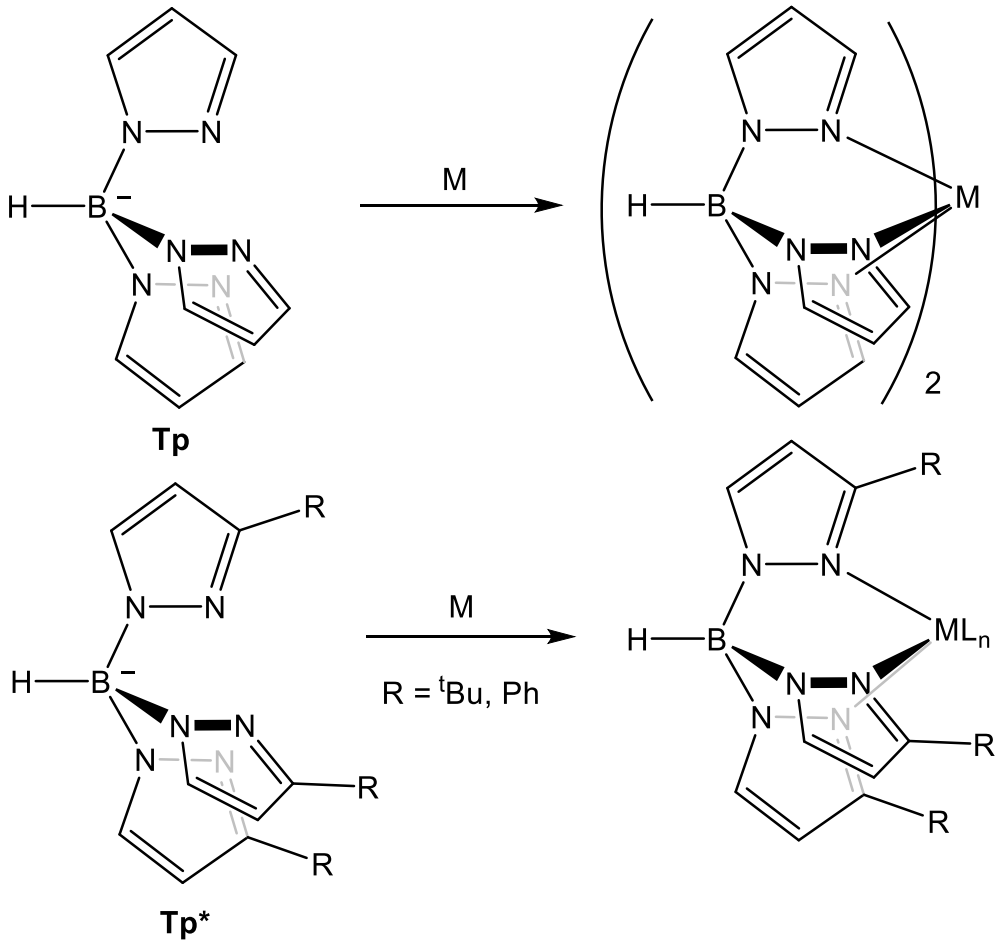

Scheme I-25. First and second generation of Tp ligands

The steric environment of **Tp*** can be tuned via substitutions on the pyrazolyl ring, however it is more difficult to tune the donor/acceptor properties of **Tp***. Hydrotris(methimazolyl)borate with three sulfur donors, a soft analogue of **Tp**, was developed by Reglinski and co-workers in 1996.[65]

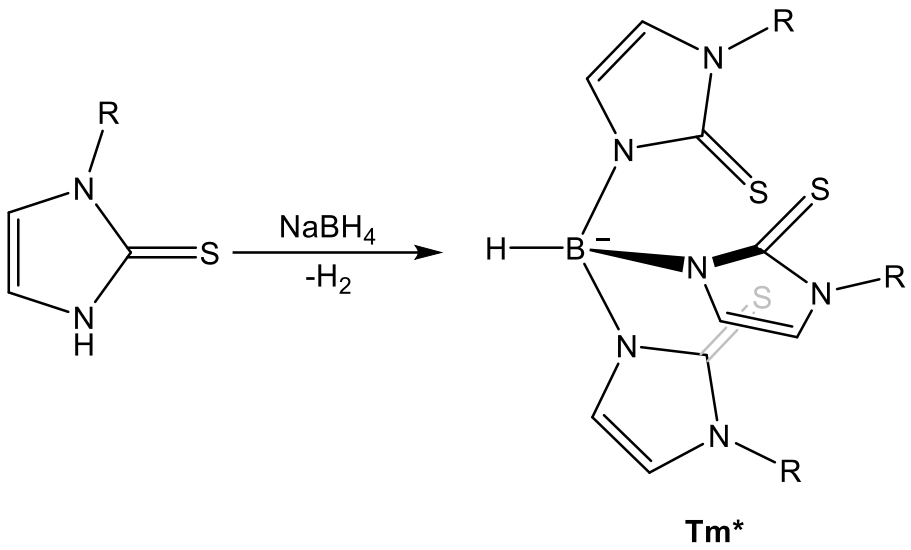

Scheme I-26. Synthesis of Tm* ligands

Varieties of other donor atoms can be incorporated into the tripod ligands, such as Oxygen and Phosphorus. The tripodal ligand with other central atoms including group III, IV, or V elements have been vastly designed and studied.[66-69] The tripodal ligands can be further diversified by the design of linkage between central atoms and 3 donor sites to achieve different goals in organometallic chemistry. One tripodal ligand of commercial significance is nitrilotriacetate, $N(CH_2CO_2^-)_3$, where worldwide capacity is estimated at 100 thousand tons per year, due to the cheap synthesis and wide applications based on its ability to form water soluble chelates with multivalent metal ions. [70]

1.4 Various Z-type tripodal ligands

In 1999, Hill and co-workers demonstrated the greater flexibility of **Tm*** ligand (**165**) derived from an additional atom between boron and donor atoms: where B-H activation results in the formation of a metal-to-boron dative bond in the first metallaboratrane complex.[71] Compared to the well-known tripodal ligands with 3 or 4

donor sites (L_4 or L_3X), the ligand design (ZL_3)with an σ-acceptor (Z-type ligand) was far less developed, however due to the unique properties arose from the combination of donor and acceptor coordination sites, significant advance on the chemistry based on the ambiphilic tripod ligands has been achieved over the last decades.[66,72-77]

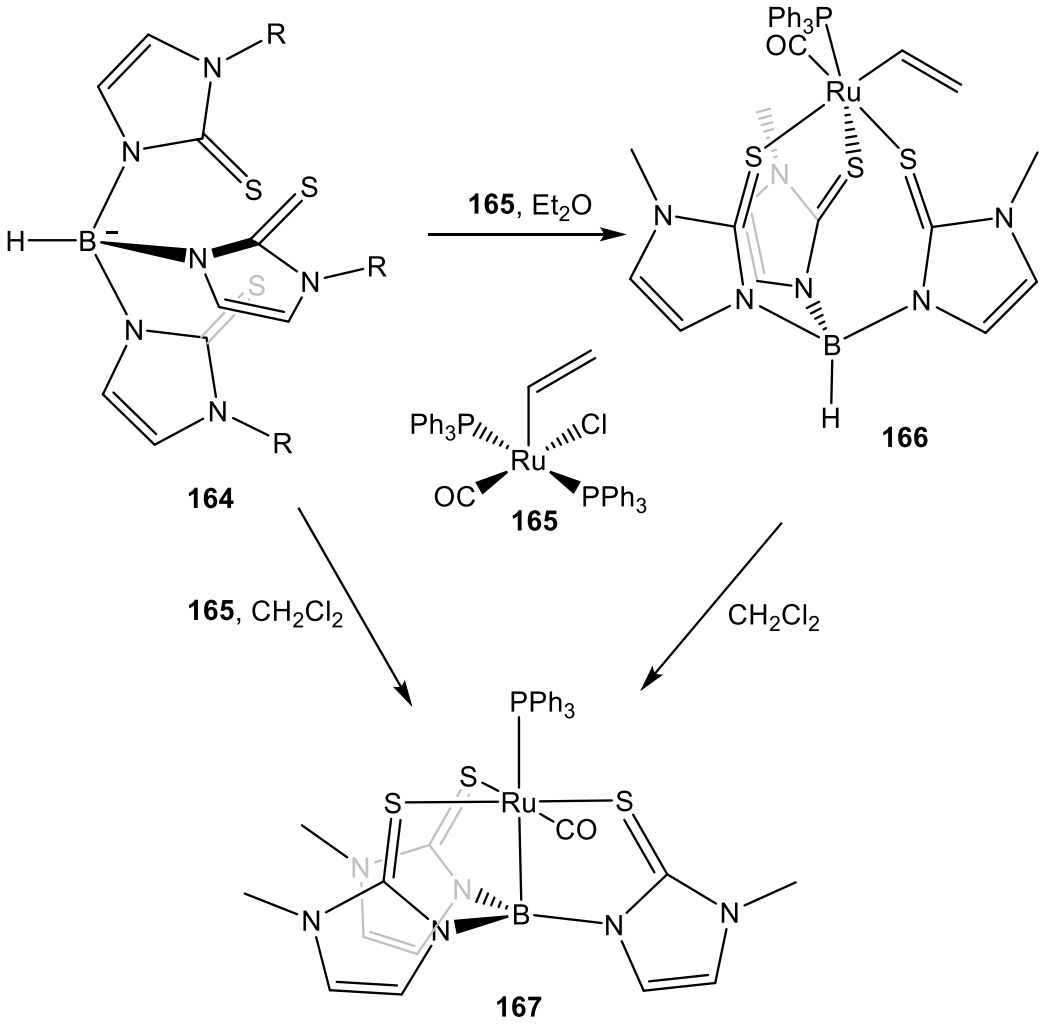

Scheme I-27. Synthesis of ruthenium borotrane

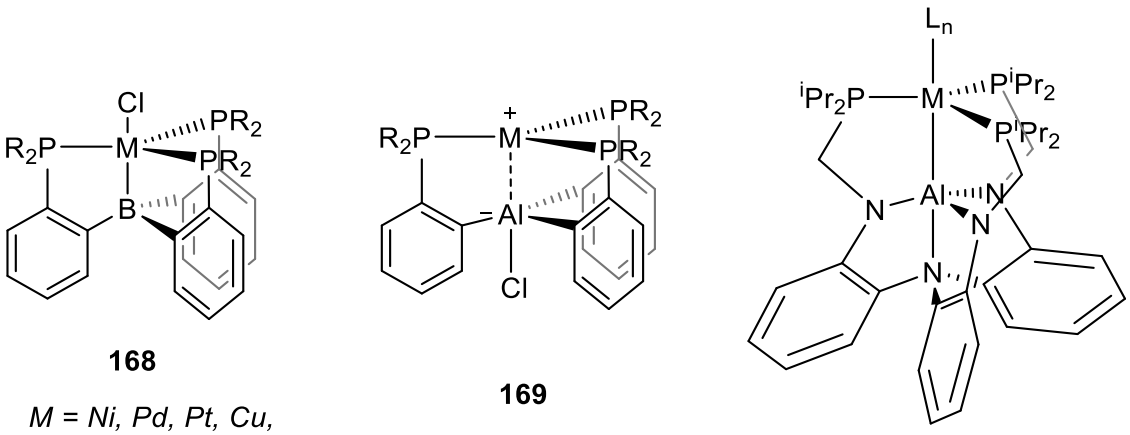

Figure I-5. Representative examples of other Z-type tripod ligand-ligated complexes

Inspired by the pioneering work on boron based Z-type tripodal ligands to enforce the strong M→B interaction,[72] stronger Lewis acidic Al center was incorporated into tripodal ligand to study the unusual M→Al bonding.[59,78] However, due to the high chloro affinity of Al center, the corresponding M-Cl bond was activated, which resulted in a very weak M→Al interaction (**Figure I-5**). Lu and co-workers were not only able to extend the Z-type tripodal ligands further down the group III elements with their own ligand design, but also blocking the potential halide abstraction with extra Lewis N donor on the back bone.[73,74,79] Well defined Co and Ni catalytic systems for hydrogenation of CO_2 or olefin were developed by tuning the electronic properties of the transition metals with various central Z-type acceptors. [80]

The aryl, imidazole, pyrazole and alkyl are very common linkage for the tripod ligands to connect the side arm donors and the central atoms. While the tripod ligands incorporate the commercial available and cheap pyrrole into the backbone was far rare studied,[81,82] especially for Z-type tripodal ligands.[83] Considering the ease of N-H

functionalization, Z-type tripod ligands linked via pyrrole back bone would be feasible. In addition, with N directly attach to central acceptor, the Lewis acidity of which can be increased while maintain the similar donating ability of the three donors compared to the aryl-based Z-type tripod ligands.

1.5 Alkyne diboration.

1.5.1 Introduction to bisborylalkene

Borylated organic compounds have become staple reagents for synthetic chemistry as they are generally considered relatively stable for storage and nontoxic to plants, mammals, and other complex life forms and are therefore environmentally benign,[84] In addition, the boron functionality are found to be an ideal temporary functional group due to the development of diverse facile transformations,[85,86] among which both hydroboration-oxidation and C-C cross coupling reactions were awarded with Nobel prizes in chemistry in 1979[87] and 2010[88] respectively. Additionally, boryl groups is widely dispersed in natural products and synthetic drugs, such as antibiotics aplasmomycin, boromycin, tartolon B, Tavaborole, Bortezomib, et al.[89-95]

1.5.2 Synthesis of bisborylalkene

Due to the diverse utilities of organoboron compounds, massive efforts have been made to develop the effective methods for the installation of boron functionalities over the past few decades, among which 1,2-diborylalkenes typically conceived as addition of B-B diboron moieties across the CC triple bonds have been widely used in organic synthesis, especially for the synthesis of asymmetric alkene derivatives.[96-99]

1.5.2.1 alkyne diboration with Cl_2BBCl_2

The first 1,2-bisborylalkene synthesis was reported in 1954, where Cl_2BBCl_2 was directly added across CC triple bonds of acetylene to form $Cl_2BCHCHBCl_2$ in the absence of catalyst.[100,101]

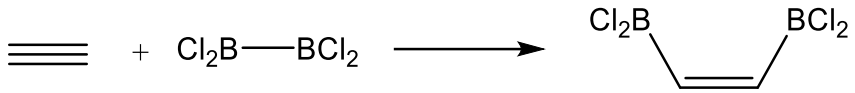

Scheme I-28. Reaction of tetrachlorodiborane with acetylene

The alkyne substrate was not limited to acetylene. Substituent as bulky as tBu can afford 83% yield, in addition further functionalization of B-Cl was achieved due to the reactive B-Cl bond, which however is not ideal for storage as a useful synthetic material. Neither the BCl_2 group was a good for cross coupling reactions, which is one of main reasons why organoborons are widely used in organic synthesis.

Much more stable and easy to handle tetrakisalkoxyldiboron reagents were then developed by Brotherton and co-workers, where hydrolysis of $B_2(NMe_2)_4$ with corresponding alcohols,[102] especially the 1,2-diols supported diborons really shined in catalytic borylation of hydrocarbons.

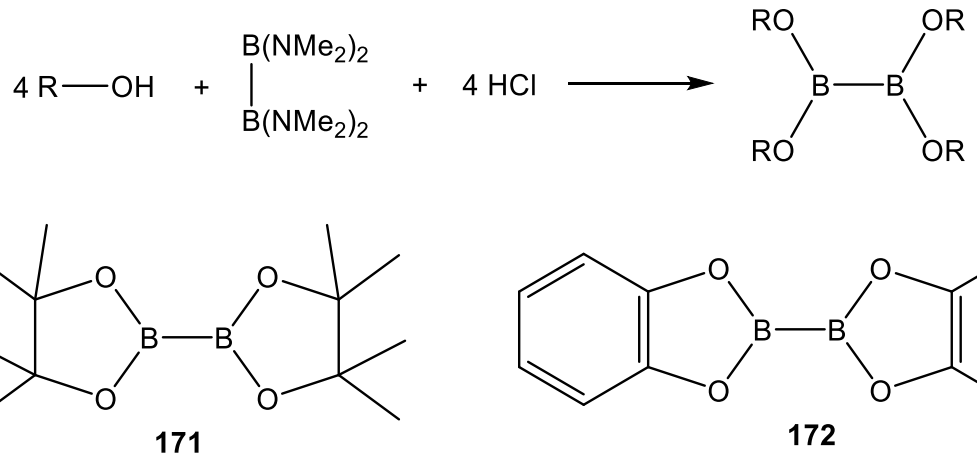

Scheme I-29. Synthesis of tetrakisalkoxyldiboron and representative examples

Unlike the Cl_2BBCl_2, the tetrakisalkoxyldiborons bear a high energy B-B bond do not readily add to the alkyne in the absence of catalysts.

1.5.2.2 Transition metal catalyzed alkyne diboration with diboron reagents

In the seminal catalytic alkyne diboration reported by Suzuki, Miyaura, and co-workers in 1993, the addition of B2pin2 to alkyne was catalyzed by a platinum phosphine complexes.[103]

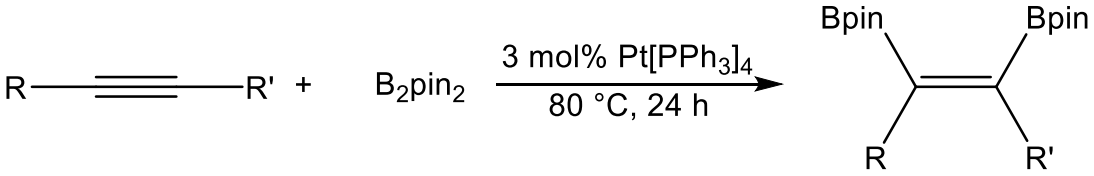

Scheme I-30. Platinum catalyzed alkyne diboration

A mechanism involving oxidative addition of B-B to Pt(0) was proposed. Then the insertion of CC triple bond into Pt-B followed by C-B reductive elimination regenerates Pt(0) species to turn over the catalytic cycle.

In 2001, further investigation of the Pt-based alkyne diboration was made by Marder and co-workers.[104] They disclosed the optimal 1:1 ratio of Pt to phosphine for the alkyne diboration, in addition, more electron rich PCy_3 enhance the reactivity dramatically, where reaction was completed within hours even at ambient temperature.

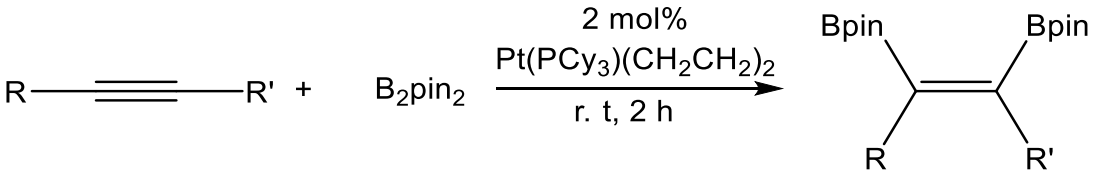

Scheme I-31. Monophosphine-platinum catalyzed alkyne diboration

Apart from platinum, copper was proved to be effective for alkyne diboration in the presence of phosphine as well in 2012.[105] The Cu-PCy_3 system was found to borylated C-O bond of the propargyl ether while in the platinum-based system C-O of the propargyl ether remains untouched.

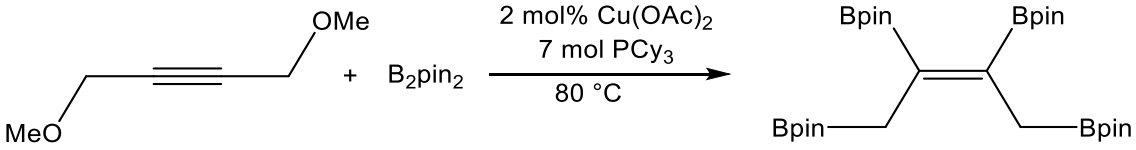

Scheme I-32. Copper catalyzed alkyne diboration

More interestingly, the selective asymmetric diboration of alkyne was achieved with Bpin-Bdan reagent catalyzed by Iwadate, Suginome and co-workers in 2010.[99] The regioselectivity was controlled by the steric effect, where bulkier Bdan group located cis to smaller R group.

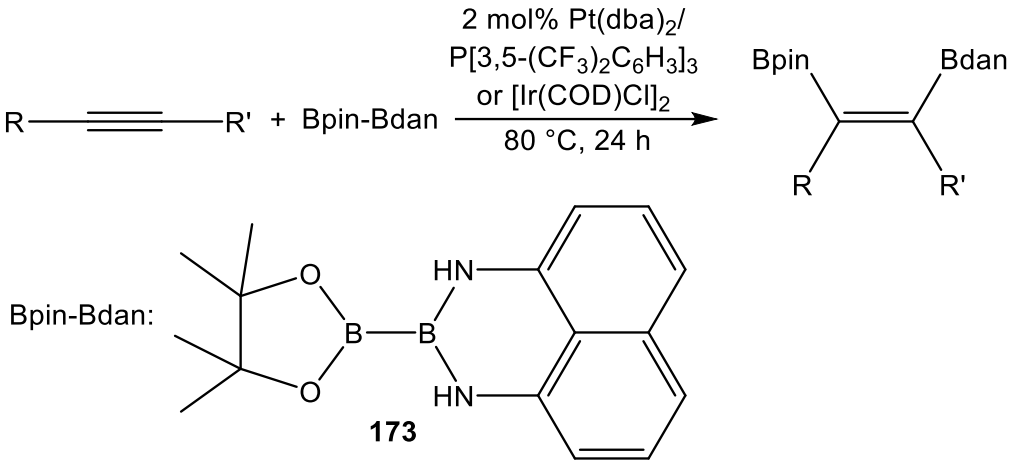

Scheme I-33. Catalytic asymmetric alkyne diboration with Bpin-Bdan

The addition product has two different boryl group attached to CC double bond, where Bpin group is more reactive towards Suzuki coupling even though it is more steric hindered, which show different regioselectivity from the addition product with B_2Pin_2.

The palladium complex for alkyne diboration was also disclosed to undergo very similar catalytic cycle as platinum-based system but with much slower reactivity.[106]

More recently simple $FeBr_2$ was found to catalyze the alkyne diboration under certain conditions.[107] Atomic efficiency was quiet poor for this system as 4.5 equiv of Bpin in total was used for one CC triple bond. However, the asymmetric diboration can be achieved since the boryl group in the addition products coming from different boron reagents.

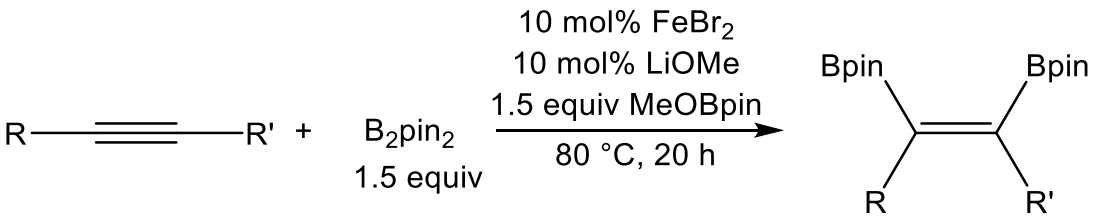

Scheme I-34. Iron-catalyzed alkyne diboration

In 2017, the first alkyne diboration catalyzed by Au nanoparticles was reported by Stratakis' group. The Au nanoparticle system was also effective for disilylation of alkyne, in addition, regioselective silylborylation of alkyne can be obtained when dibroron and disilane was used in 1:1 ratio.

1.5.2.3 Catalytic alkyne diboration with diboron reagents in the absence of transition metal

The transition metal catalyzed diboration of alkyne with diboron reagents only afford *syn*-1,2-bisborylalkene, because the reaction is generally triggered by the insertion of alkyne to M-B followed by reductive elimination of C-B bond regardless the nature of transition metals. In order to break the dominant cis-addition in alkyne diboration, Hirano, Uchiyama and co-workers proposed accomplished a *trans*-addition by adding a boryl anion equivalent to acetylene, however, based on the model calculation this intermolecular path way need to overcome an insurmountable activation barrier as high as 51.9 kcal/mol despite the process was thermodynamic favored by 11.1 kcal/mol.[108]

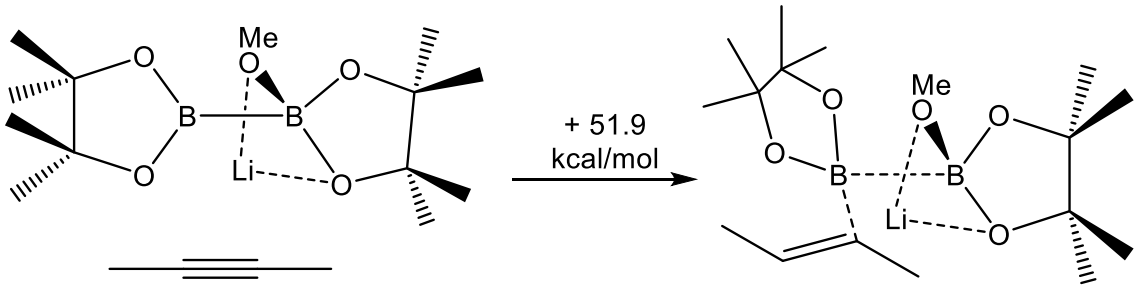

Scheme I-35. DFT calculation for intermolecular B-B addition to CC triple bonds

So they moved on to calculate the *pseudo*-intramolecular reaction strategy, where a heteroatom(s) was installed on the acetylene skeleton to coordinate/activate diboron to stabilize the transition state. Extensive studies on the substrates revealed propargyl

alkoxide would direct the B-B addition to CC triple bond without any catalyst. The more reactive pinBBMes$_2$ was used in the base catalyzed system by Yamashita and co-workers in 2016 to expand the alkyne substrate scope, however *trans* addition of B-B across CC triple bond was dominant but no longer 100%.[109]

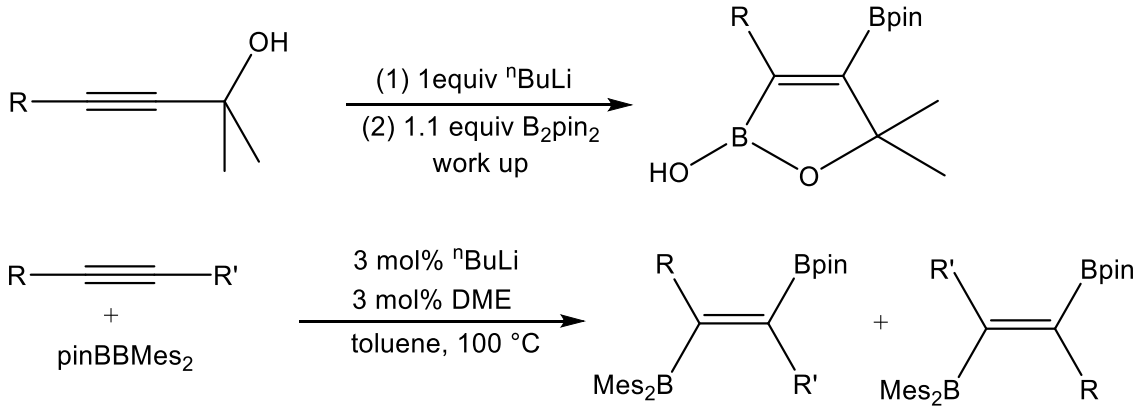

Scheme I-36. Alkali base catalyzed alkyne diboration

In 2015, The complete metal-free alkyne diboration system was also developed with PBu$_3$ catalyst by Sawamura and co-workers.[110] It was proposed that the ester group plays similar role as propargyl ether to stabilize the intramolecular transition state.

The same year organosulfur was discovered to effect alkyne diboration under light by Ogawa and co-workers respectively.[111] This photo catalyst worked for wider alkyne substrate scope, however the mixture of *syn* and *anti*-diborylalkenes were obtained due to the radical mechanism.

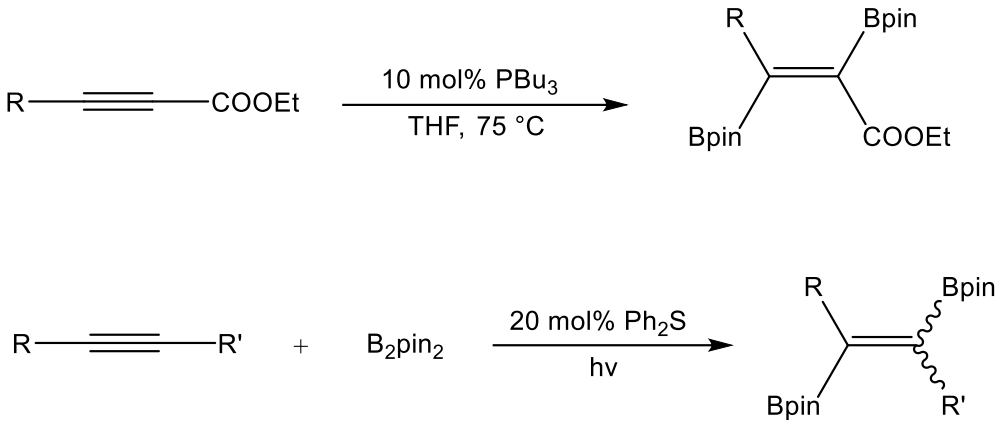

Scheme I-37. Metal-free catalytic alkyne diboration

1.5.2.4 Dehydrogenative diboration (DHDB) of alkyne

The synthesis of 1,2-diborylalkene via dehydrogenative diboration (DHDB) of alkyne with hydroborane remains elusive due to the ease of hydroboration of unsaturated CC bonds to generate borylalkenes or bisborylalkanes. The B-H bonds of dialkylboranes, such as 9-borabicyclo [3.3.1] nonane (9-BBN) can even easily add across unsaturated C-C bonds without the aid of catalysts.[112] In addition, the unsaturated CC bond in both products and alkynes could be hydrogenated in the presence of H_2, which is the byproduct of DHDB reaction.

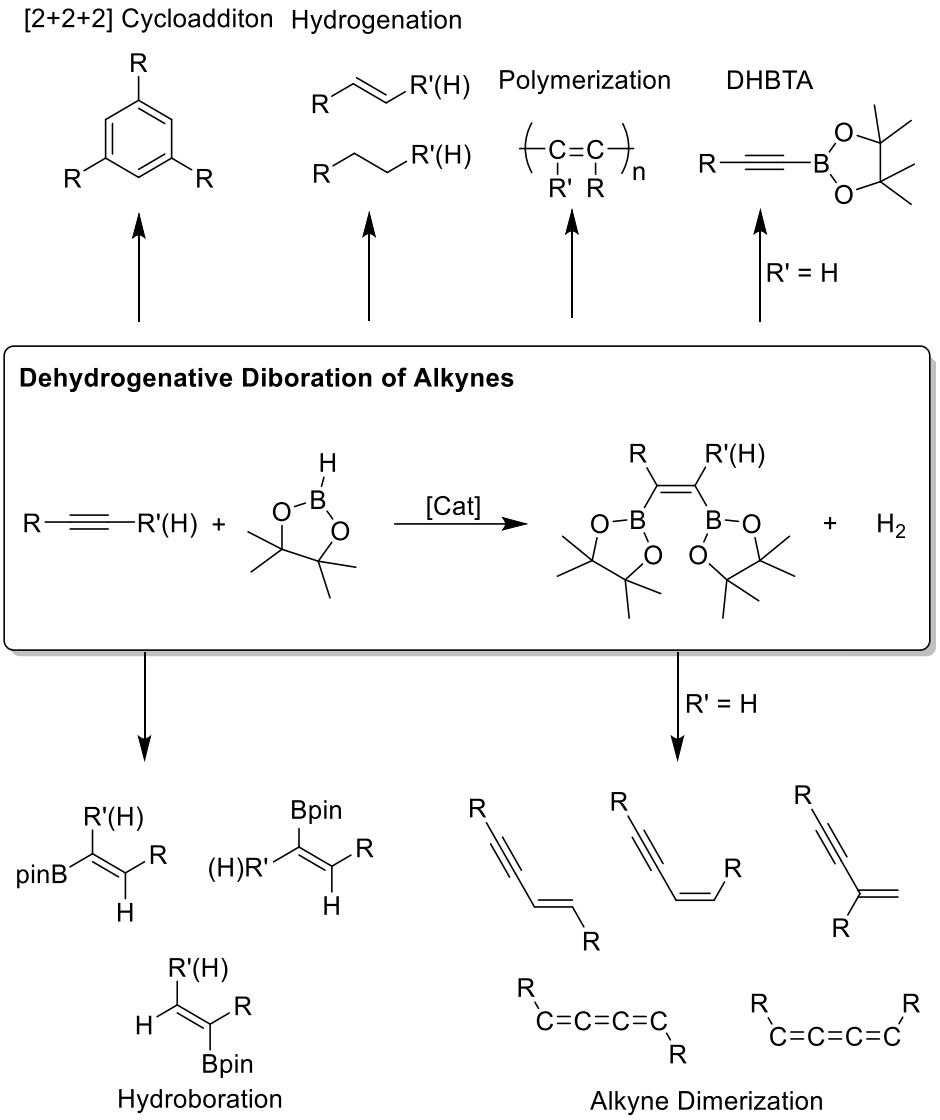

Scheme I-38. Reactions of HBpin with alkyne

The DHDB reaction could be further complicated due to the fact that the products of one side reactions could be the substrates of the others. Taking all the possibilities into consideration, clean DHDB of alkynes is almost impossible and has not been reported until Ozerov's work in 2013, where under 1 atm CO the DHBTA products,

alkynylboronates, would undergo DHDB to afford trisborylalkene with moderate to high selectivities.[113]

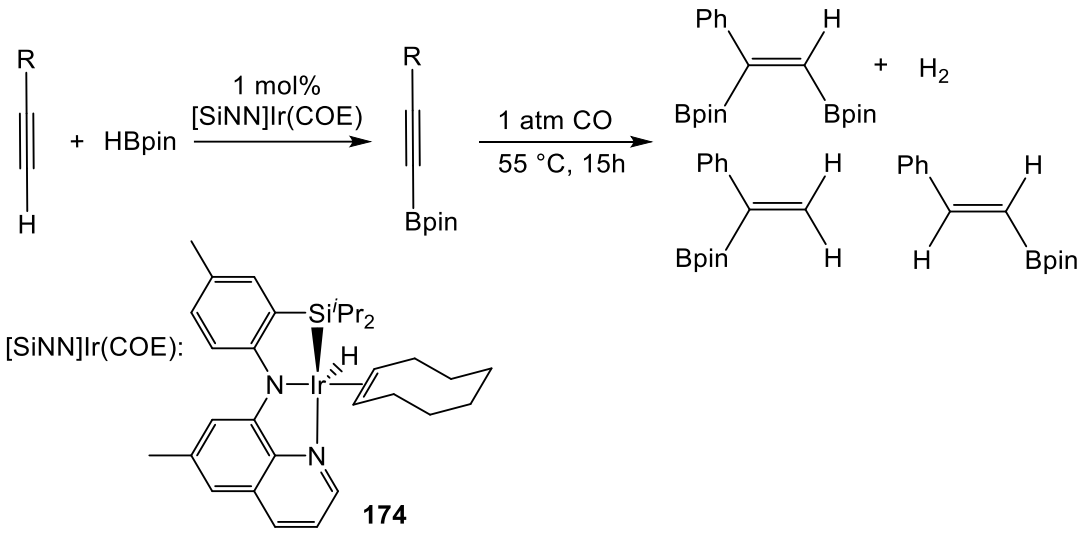

Scheme I-39. [SiNN]Ir(COE) **174** catalyzed DHBTA and DHDB of DHBTA product

CHAPTER II

NI COMPLEXES OF AN ALANE/TRIS(PHOSPHINE) LIGAND BUILT AROUND A STRONGLY LEWIS ACIDIC TRIS(N-PYRROLYL)ALUMINUM*

2.1 Introduction

Z-type ligand is a term that arose to describe the binding of typical σ-Lewis acids to transition metal centers functioning as Lewis bases.[114] Such M→Z complexes have attracted considerable attention because of the potential for the modulation of the properties of the transition metal center via changes in the nature of the Z-Lewis acid, including for applications in catalysis.[66,74,75,115-117] Z-ligands are often incorporated into polydentate chelates.[75,114] The ZL_3 type, combining a central Z site with three outer neutral donors has been commonly explored (**167**, **168**, **170**, **Figure II-1**).[73,76,77,79,118-121] The known ZL_3 ligands typically position the Z and the L sites in a 1,2-relationship to each other. 1,2-Disposition on an aromatic ring such as in **168** provides significant rigidity and preorganization to the structure that is geometrically well set up for binding a transition metal.

We surmised that using a 1,2-pyrrolediyl connection presents an attractive alternative to 1,2-benzenediyl in **168**. Both are flat aromatic connectors, but N-pyrrolyl is a very electron-withdrawing substituent compared to a C-aryl,[122] introducing intrinsic electronic asymmetry. We note that the pyrrole backbone has not been widely used in

---

* [Lai, Q; Cosio, M.; Ozerov, O.V. Ni Complexes of an Alane/Tris(phosphine) Ligand Built Around a Strongly Lewis Acidic Tris(N-pyrrolyl)aluminium. *Chem. Comm*. **2020**, *56*, 14845-14848.] Reproduced by permission of The Royal Society of Chemistry.

ligand construction,[5,82,83,123,124] in contrast to the benzene ring connectors which are ubiquitous in many ligand types far beyond ZL_3. A reliable synthesis of a 2-phosphinopyrrole precursor should permit a more active exploration of these options. The only known derivative is 2-diphenylphosphinopyrole,[81,125-127] which was most recently used by Tonks et al.[128,129] Its synthesis is not high-yielding and we have not had success in adapting it for other phosphino variations.[130,131] In this work, we wish to report two synthetic pathways leading to 2-(diisopropylphosphino)pyrrole (**204**, Scheme II-2), as well as the straightforward use of **204** in the construction of a new AlP_3 ligand (Figure II-1) and AlP_3 complexes. The AlP_3 ligand combines a central Z-type alane site with three outer phosphine donors. We were attracted to exploring AlP_3 because the pyrrolyl substituents on Al should render it more electron-poor than the C-aryl substituents on boron in **168** or the dialkylamido substituents on Al in **170**. Coupled with the absence of the extra amine donor such as in **170**, we expected that the alane site in AlP_3 should be considerably more Lewis acidic than other common ZL_3 systems with a central group 13 Lewis acid.

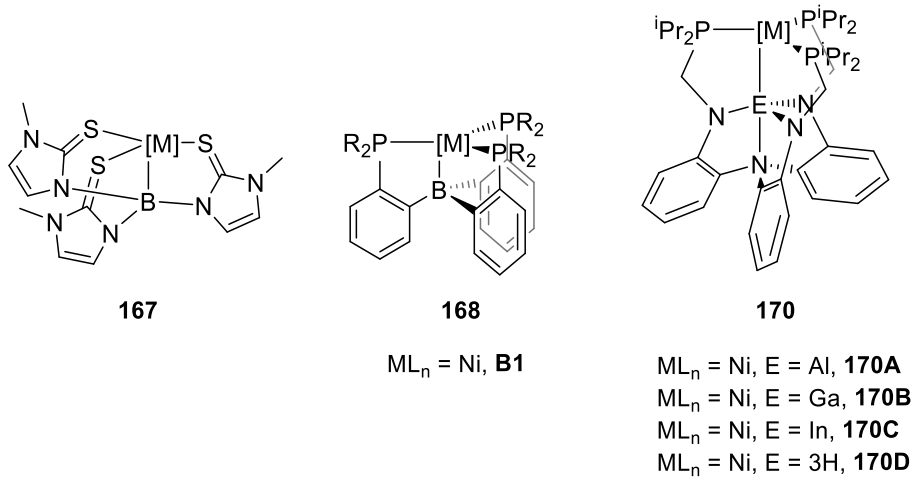

Figure II-1. Key examples of transition metal complexes of ZL_3 ligands from the literature.

2.2 Results and discussion

2.2.1 Synthesis of 1H-2-diisopropylphosphinopyrrole

N-Boc protected 2-bromopyrrole (**201**) was prepared according to a published procedure.[132] Lithium/bromine exchange presumably generated the unobserved **202** in situ, which was allowed to react with ClP^iPr_2, resulting in the formation of crude **203** (Method A, **Figure II-2**). Deprotection of the Boc group produced **204** in good yield, but in sub-optimal purity, which can be traced to the 87% purity of **201**. Purification of **204** can be accomplished via the synthesis of the lithio derivative **205**, which was isolated in a 60% yield. Air-free hydrolysis of **205** then gave **204** of >98% purity (47% yield based on $^iPr_2PCl$). An alternative synthesis (Method B) generates the presumed intermediate **202** via deprotonation of **206**[133] with LiTMP,[126] followed by phosphination and Boc-deprotection. Distillation of the crude product, followed by recrystallization from isooctane yielded **204** in high purity and 75% yield.

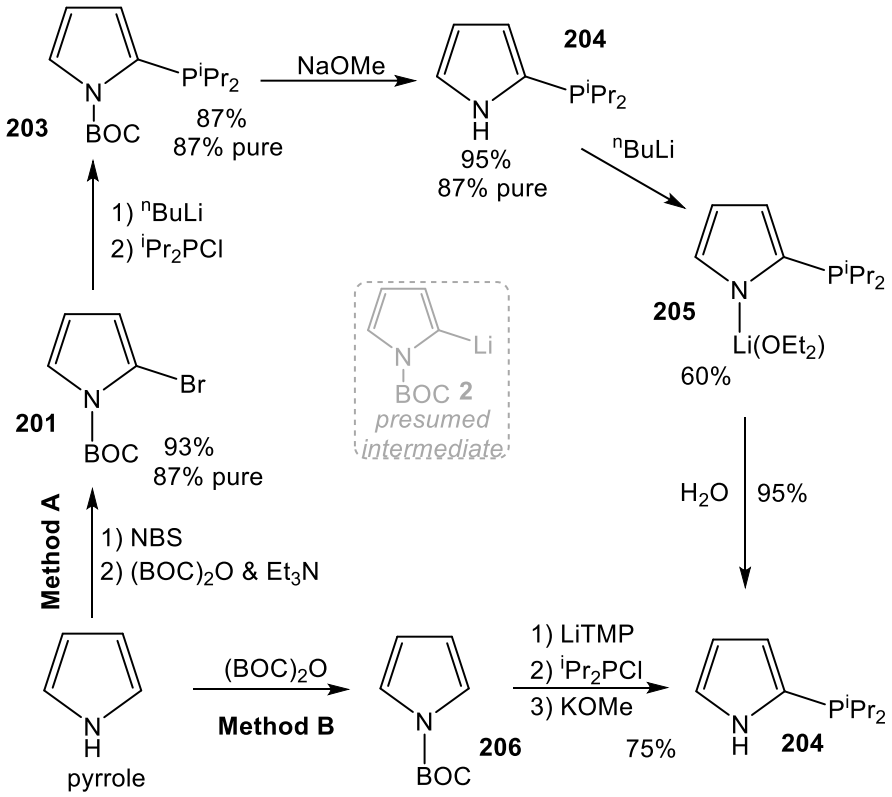

Figure II-2. Synthesis of **204**

2.2.2 Synthesis of tris-(2-diisopropylphosphinopyrrolyl) alane (ALP_3) ligand and its complex with Ni

The tripodal ligand AlP_3 (**207**) was synthesized via protolysis of $AlMe_3$ with 3 equiv of pyrrolylphosphine (**204**) at 100 ℃ for 1 h in toluene. After all the volatiles were removed under vacuum, AlP_3 was obtained as an orange oil of >95% purity (NMR evidence). Attempts to purify AlP_3 (**207**) further were hampered by its high lipophilicity and sensitivity towards water and other protic sources, but the crude material could be used effectively in the next step. Thermolysis of **207** with $Ni(COD)_2$ at 100 ℃ for 4 h in toluene led to the formation of (AlP_3)Ni (**208**, Scheme II-2), which was isolated in the form of analytically pure dark-green crystals in 75% yield after filtration and

recrystallization. Both **207** and **208** displayed apparent C_{3v} symmetry in their NMR spectra at ambient temperature, although the signals of **208** appeared broadened.

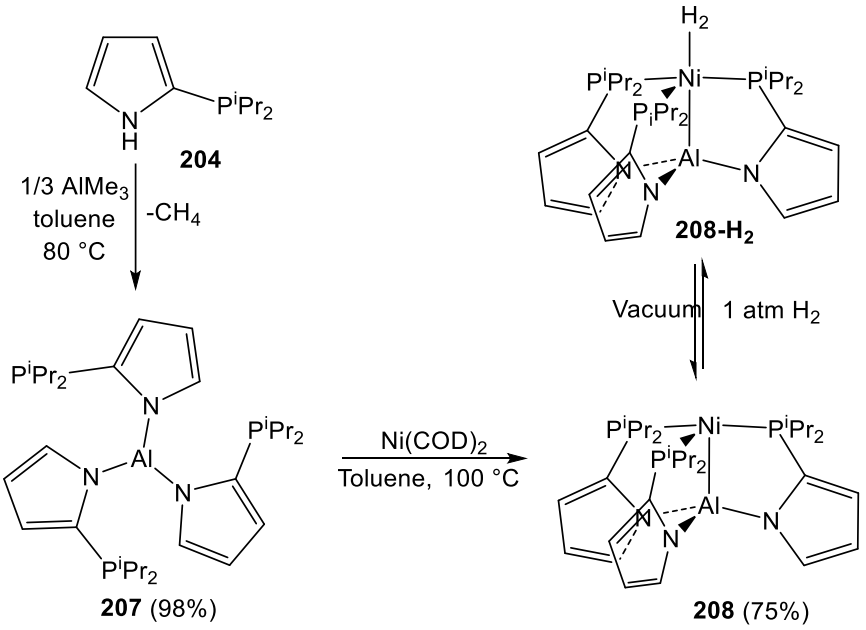

Scheme II-1. Synthesis of **207** and its complexation with Ni

2.2.3 XRD and electrochemical studies of Ni(AlP$_3$)

Single crystals suitable for an X-ray study were obtained via vapor diffusion of pentane into a toluene solution of (AlP$_3$)Ni. An XRD study revealed an approximately C_3-symmetric structure for **208** in the solid state (**Figure II-3**). The Ni centre is only slightly displaced from the plane defined by the three phosphorus atoms (ΣP-Ni-P = 357.4°), while the geometry of the Al center is decidedly tetrahedral with an average Ni-Al-N angle of 112.6°. The Ni-Al distance in **208** (2.2695(16) Å) can be contrasted with the much longer Ni-Al distance in Lu's **170A** (ca. 2.45 Å)[73] and the sum of the corresponding covalent radii per Alvarez et al (also 2.45 Å).[134] Furthermore, the Ni-Al distance in **208** is only ca. 0.1 Å longer than the N-B distance in **168**,[76] in spite of a 0.37

Å larger covalent radius for Al vs B.[135] These data suggest a strong Ni-Al interaction. It is best viewed as σ-donation from a zerovalent Ni to the Al Lewis acid. The presence of this interaction renders the Ni center divalent because two electrons of the original d^{10} configuration at Ni are being used for Ni→Al bonding.[135] The semantics and the nuanced theoretical underpinnings of the nomenclature pertaining to the oxidation state and d^n configuration assignments in M→Z complexes have been debated and analyzed elsewhere.[66,73,76,136-138]

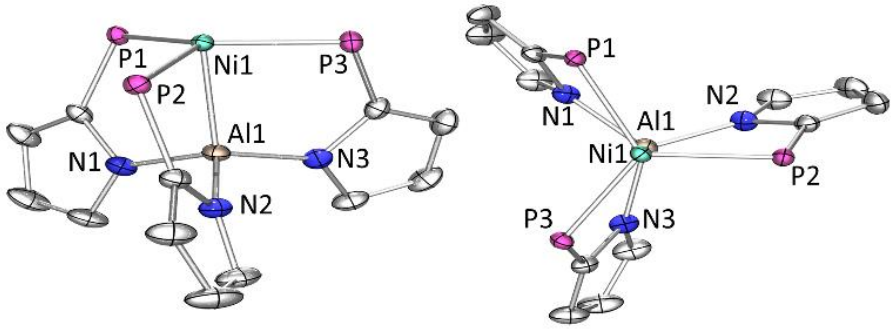

Figure II-3. ORTEP drawing (50% thermal ellipsoids) of **208** showing selected atom labeling. Hydrogen atoms and isopropyl groups were omitted for clarity. Selected bond distances (Å) and angles (°): Ni1-P1, 2.2217(13); Ni1-P2 2.2227(13); Ni1-P3 2.2197(17); Ni1-Al1, 2.2695(16); Al-N1, 1.8591(19); Al1-N2, 1.8545(16); Al-N3 1.8483(19); P1-Ni1-P2, 117.61(5); P1-Ni1-Al1, 86.18(4); P2-Ni1-Al1, 84.18(3); P3-Ni1-P1, 118.91(2); P3-Ni1-P2 120.89(4); P3-Ni1-Al1 83.60(2); N1-Al1-Ni1, 106.55(5); N2-Al1-Ni1, 104.57(6); N2-Al1-N1, 112.91(7); N3-Al1-Ni1, 107.39(4); N3-Al1-N1, 113.03(6), N3-Al1-N2, 111.73(7).

Further evidence of the strong Ni→Al donation can be deduced from the electrochemical study of (AlP_3)Ni (**208**). Cyclic voltammogram of **208** (Figure II-4) displayed two quasi-reversible waves with $E_{1/2}$ values of -0.49 V and -1.65 V vs the Fc/Fc^+ couple. We assign these two redox events as oxidation and reduction of **208**, respectively. The contrast with the complexes by Lu et al. is instructive. Reversible oxidation was

reported for **170A** (-0.74 V), **170B** (-0.57 V), and the Lewis-acid free complex **170D** (-1.02 V), indicating that **208** is more difficult to oxidize than any of these. A reversible reduction for **170A** was not reported, but the Ga analog **170B** displayed a reversible reduction at -2.48 V.[73,79] The overall analysis by Lu et al. suggested that Ga is more electron-withdrawing than Al with respect to Ni in their compound series.[79] Thus the much greater ease of reduction of **208** is striking. The larger difference in the potentials for the reduction events between **208** and **170B** ($\Delta E_{1/2}$ = 0.83 V), compared to a modest difference in potentials for the oxidation event ($\Delta E_{1/2}$ = 0.08 V) is likely a reflection of that the Ni→Al interaction is much more influential on the LUMO than on the HOMO of an (L_3Z)Ni molecule.[73]

Lu et al. investigated the binding of H_2 to Ni in their series of compounds **170A-170C**, including demonstrating that catalysis of olefin and CO_2 hydrogenation was possible.[74,79] Notably, they observed no binding of H_2 to **170A** at RT, and only to the Ga and In analogs **170B** and **170C**. In contrast, the dark-green solution of **208** in C_6D_6 turned pale green immediately when it was exposed to 1 atm H_2. NMR spectroscopy indicated the formation of a new complex **208-H_2**, with a broad resonance at -2.1 ppm in the ^{1}H NMR spectrum, and new, considerably shifted resonances in the $^{31}P\{^1H\}$ (24.3 ppm vs 13.0 ppm for **208** and ^{27}Al NMR spectra (138.0 ppm vs 104.4 ppm for **208**). Variable temperature NMR experiments showed that below -20 ℃, the resonance for the Ni-bound H_2 shifted to ca. -2.5 ppm, the signal for free H_2 appeared, and no trace of **208** was evident. This suggests that **208-H_2** constitutes ca. 90% of the mixture at RT and is in rapid equilibrium with **208** and free H_2. At temperatures below -20 ℃, however, the formation

of **208-H2** is complete under 1 atm of H_2. Collecting NMR spectra at temperatures down to -75 ℃ did not allow for an unambiguous T_{1min} value, but the lowest obtained values of <25 ms were consistent with a classical dihydrogen complex.[139] This was corroborated by the $J_{H\text{-}D}$ = 35 Hz determined for **208-HD** isotopomer prepared from **208** and HD gas.[140] This value can be compared against those for the HD adducts of **170C** (34 Hz) and **170D** (32 Hz) analyzed by Lu et al (**Figure II-1**).[74,141] The slightly higher value in **208-HD** suggests less back-donation to HD from Ni and is consistent with the notion of a more electron-poor Ni center in **208-HD**. However, all these values are near the upper limit for HD complexes, and are similar to that observed by Peters et al. in the closely related **209-HD** (**Figure II-1**).[142]

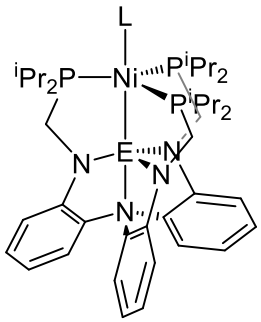

L = none, E = Al, **170A**
L = none, E = Ga, **170B**
L = HD, E = Ga, **170B-HD**
L = HD, E = In, **170C-HD**
L = CO, E = Al, **170A-CO**

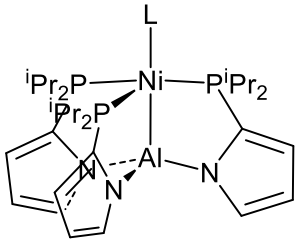

L = none, **208**
L = HD, **208-HD**
L = CO, **208-CO**

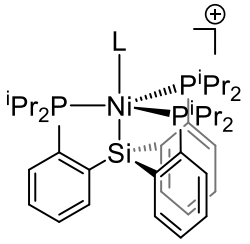

L = none, **209**
L = HD, **209-HD**
L = CO, **209-CO**

$E_{1/2}$ (ox):	-0.74 V (**170B**) -0.57 V (**170C**)	-0.49 V (**208**)	N/A
$E_{1/2}$ (red):	N/A (**170A**) -2.48 V (**170B**)	-1.65 V (**208**)	N/A
J_{H-D}:	34 Hz (**170B-HD**) 32 Hz (**170C-HD**)	35 Hz (**208-HD**)	35 Hz (**209-HD**)
ν(CO):	1953 cm^{-1} (**170A-CO**)	1972 cm^{-1} (**208-CO**)	2036 cm^{-1} (**209-CO**)

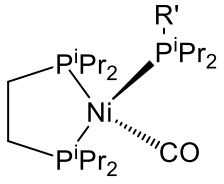

210-CO

ν(CO) = 1902 cm^{-1}

R′ = $CH_2CH_2P(O)^iPr_2$

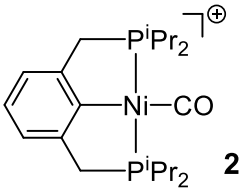

211-CO

ν(CO) = 2096 cm^{-1}

Figure II-4. Comparison of selected properties of 8 and its HD and CO adducts with literature examples.

Exposure of a C_6D_6 solution of **208** to 1 atm of CO resulted in complete conversion to the new complex **208-CO** (**Figure II-4**). Its ν(CO) value can be used to compare the capacity of the Ni center for π-back-donation in the three locally isoelectronic systems **170A-CO**,[143] **208-CO**, and **209-CO**[142] (**Figure II-4**). The ν(CO) values for these three

complexes lie in between the values for complexes **210-CO** and **211-CO** (Figure II-4), which possess the more traditional, four-coordinate geometries about zerovalent Ni (**210-CO**, tetrahedral)[144] and low-spin divalent Ni (**211-CO**, square-planar).[145] The values for **170A-CO** and **208-CO** are closer to the value of the zerovalent **210-CO**, whereas the value for **209-CO** is closer to **211-CO**. However, it must be noted that the difference between **208-CO** and **211-CO** (74 cm^{-1}) is similar to the differences between **8-CO** and **210-CO** (70 cm^{-1}), or **209-CO** and **211-CO** (60 cm^{-1}). Thus, the triad of **170A**/**208**/**209** can be viewed as part of a continuum of possible structures in which Ni is rendered to be more electron-poor by the donation to a progressively stronger Lewis acid: base-stabilized tris(amido)alane in **170A**, tris(pyrrolyl)alane in **208**, and formally triarylsilylium cation in **209**.

2.3 Conclusion

All in all, our observations indicate with that the central Lewis acid in AlP_3 (**207**) is considerably stronger than the Z fragments in other common group 13-centered ZL_3 ligands. The greater degree to which the alane site in **208** withdraws electron density from Ni is consistent with the short Al-Ni distance, ease of reduction of (AlP_3)Ni (**208**), and the ability of Ni in **208** to bind H_2. We thank the US National Science Foundation (grant CHE-1565923 to O.V.O.) for the support of this research. We thank Dr. Weixing Gu for conducting early experiments on the lithiation of pyrrole, and Profs. Ian Tonks and Miles Johnson for helpful discussions with regard to the synthesis of phosphinopyrroles.

2.4 Experimental section

2.4.1 General consideration

Unless otherwise specified, all reactions and manipulations were carried out inside an argon-filled glove box or using Schlenk line techniques. THF, diethylether, toluene, and pentane were dried and deoxygenated via the solvent purification system and stored over molecular sieves in the glove box filled with argon. C_6D_6 were dried over NaK /Ph_2CO/18-crown-6, distilled and stored over molecular sieves in an Ar-filled glove box. Fluorobenzene was dried over CaH_2, distilled and stored over molecular sieves in an Ar-filled glove box. 1H-pyrrole was purchased from Oakwood chemicals, then was dried with CaH_2 and distilled before use. Other chemicals were purchased from commercial vendors and used without further purification. N-tert-butoxycarbonyl-2-bromopyrrole (**201**)[132] and N-tert-butoxycarbonylpyrrole (**206**)[133] were synthesized according to the literature.

2.4.2 Physical method

NMR spectra were recorded on a Varian Inova 500 spectrometer (^{1}H NMR, 499.703 MHz, ^{13}C NMR 125.580 MHz), Varian Inova 400 (^{11}B NMR, 128.191 MHz, ^{27}Al NMR, 104.223 MHz) spectrometer. Chemical shifts are reported in δ (ppm). For ^{1}H and ^{13}C NMR spectra, the residual solvent peak was used as an internal reference (^{1}H NMR: δ 7.16 for C_6D_6, 5.32 for CD_2Cl_2, 2.08 for d_8-toluene; ^{13}C NMR: δ 128.06 for C_6D_6, 53.84 for CD_2Cl_2, 20.43 for CD_3CN). UV-Vis spectra were collected on a Hitachi U-4100 UV-Vis spectrophotometer. Elemental analyses were performed by CALI Labs, Inc. (Highland Park, NJ).

2.4.3 Synthesis of 1H-2-diisopropylphosphinopyrrole

Method A:

Synthesis of N-tert-butoxycarbonyl-2-diisopropylphosphinopyrrole (203). To a 250 mL Schlenk flask, 19.4 g (78.8 mmol) **201** (prepared according to the previous procedure with 87% purity) was loaded with 100 mL THF. The resulting solution was cooled in an acetone/dry ice bath for 10 min, before 31.5 mL 2.5 M ^{n}BuLi (78.8 mmol, 1.0 equiv) was added drop wise via syringe over a course of 30 min. The colorless solution turned orange upon the addition of ^{n}BuLi solution. Then 13.8 mL $^{i}Pr_2PCl$ (86.6 mmol, 1.1 equiv) was added to the orange solution via a syringe over a course of 30 min. The resulting mixture was allowed to warm up to r.t., and then THF was removed under vacuum. 6.0 g silica gel and 40 mL pentane were added to the residue and stirred at r.t. for 10 min, then was filtered through a short pad of Celite. The colorless pentane filtrate was concentrated under vacuum to afford 21.2 g (85% yield with 87% purity) of **203** as colorless oil.^{1}H NMR (500 MHz, C_6D_6) δ 7.54 (dt, *J* = 3.2, 1.6 Hz, pyrrole-*H*, 1H), 6.38 (brs, pyrrole-*H*, 1H), 6.19 (t, *J* = 3.3 Hz, pyrrole-*H*, 1H), 2.13 – 2.06 (m, $(CH_3)_2CH$, 2H), 1.33 (s, $(CH_3)_3C$, 9H), 1.13 (dd, *J* = 14.5, 7.0 Hz, $(CH_3)_2CH$, 6H), 1.10 (dd, $J_{C\text{-}P}$ = 14.0, 7.0 Hz, $(CH_3)_2CH$, 6H). $^{13}C\{^{1}H\}$ NMR (125.7 MHz, C_6D_6): δ 149.6 (s, C=O), 131.3 (d, $J_{C\text{-}P}$ = 29.3 Hz, pyrrole-*C*), 125.1 (s, pyrrole-*C*), 121.2(brs, pyrrole-*C*), 111.4 (s, pyrrole-*C*), 83.5 (s, $(CH_3)_3C$), 27.9 (s, $(CH_3)_3C$), 24.6 (d, $J_{C\text{-}P}$ = 14.6 Hz, $(CH_3)_2CH$), 20.4 (d, $J_{C\text{-}P}$ = 14.1 Hz, $(CH_3)_2CH$), 19.93 (d, $J_{C\text{-}P}$ = 17.0 Hz, $(CH_3)_2CH$). $^{31}P\{^{1}H\}$ NMR (202 MHz, C_6D_6): δ -5.4 (brs).

Deprotection of N-tert-butoxycarbonyl-2-diisopropylphosphinopyrrole (203) to give crude 204. 21.2 g (74.8 mmol) of **203** with 87% purity was dissolved with 50 mL THF in 250 mL Schlenk flask, which was cooled in an ice/water bath. 40 mL methanol solution containing 20.0 g NaO^tBu (205 mmol, 3 equiv) was degassed by bubbling Ar through for 30 min, then was cannula transferred to the precooled THF solution. The resulting mixture was stirred for 45 min before 40 mL degassed distilled water was added via cannula transferred. The suspension formed after water addition was further stirred at r.t. for 30 min. The desired product was extracted with degassed hexane (3×20 mL). The hexane solution was concentrated to afford 13.7 g (83% yield, 87% pure) of **204** as light yellow oil.

Purification of 204 via deprotonation followed by reprotonation. 6.77 g (37.0 mmol) of the crude product **204** (87% pure) was loaded in a 100 mL Schlenk flask and dissolved with 30 mL diethyl ether. The solution was cooled in -35 ℃ for 30 min before the addition of 14.8 mL 2.5 M ^{n}BuLi (37.0 mmol, 1.0 equiv) via syringe. The resulting orange solution was stirred at r.t. for 30 min and then was concentrated under vacuum. The saturated diethyl ether solution was cooled in a -35 ℃ freezer overnight to yield 7.00 g (60%) of **205** as white crystals. The white crystals **205** was dissolved in 30 mL THF, and then 20 mL degassed water was added via cannula transfer. The resulting suspension was stirred at room temperature for 30 min and then extracted with degassed hexanes. The hexanes extraction was concentrated after passing through a short pad of silica gel to yield 4.6 g (47% based on phosphine) of desired product **204** as white solid. NMR data for **205** follow. ^{1}H NMR (500 MHz, C_6D_6) δ 7.53 (s, pyrrole-*H*, 1H), 6.82 (s, pyrrole-*H*, 1H), 6.77

(s, pyrrole-*H*, 1H), 2.11 (septd, *J* = 7.0, 3.4 Hz, $(CH_3)_2CH$, 2H), 1.19 (dd, *J* = 14.4, 7.1 Hz, $(CH_3)_2CH$, 6H), 1.15 (dd, *J* = 11.9, 6.9 Hz, $(CH_3)_2CH$, 6H). $^{13}C\{^1H\}$ (125.7 MHz, C_6D_6): δ. 132.15 (d, $J_{C\text{-}P}$ = 12.9 Hz, pyrrole-*C*), 131.64 (d, $J_{C\text{-}P}$ = 17.2 Hz, pyrrole-*C*), 115.72 (s, pyrrole-*C*), 111.63 (s, pyrrole-*C*), 65.72 (s, CH_2CH_3), 24.49 (d, $J_{C\text{-}P}$ = 5.9 Hz, $(CH_3)_2CH$), 20.62 (d, $J_{C\text{-}P}$ = 15.4 Hz, $(CH_3)_2CH$), 20.08 (d, $J_{C\text{-}P}$ = 8.8 Hz, $(CH_3)_2CH$), 14.35 (s, CH_2CH_3). $^{31}P\{^1H\}$ NMR (202 MHz, C_6D_6): δ -6.6 (brs).

Method B:

A 300-mL round bottom flask was charged with TMP (7.6 g, 54 mmol) and THF (50 mL). The solution was cooled to -78 ℃ in a dry ice/acetone bath. To the TMP solution, n-BuLi (2.5 M, 21 mL, 52.5 mmol) was added slowly via syringe. The solution was stirred for 10 min in the dry ice/acetone bath before being placed in an ice water bath for 20 min. After the 20 min, the solution was placed back in the dry ice/acetone bath and allowed to cool for 5 min. N-Boc pyrrole **206** (8.4 g, 50 mmol) in THF (12 mL) was added drop wise via an addition funnel. The solution began to turn orange before becoming opaque and brown. The resultant solution was stirred for 20 min then transferred via cannula to a flask containing diisopropylchlorophosphine (8.6 g, 56 mmol) cooled in a dry ice/acetone bath. The reaction was stirred for 1 h. After 1 h, a degassed solution of sodium methoxide (formed by stirring sodium *tert*-butoxide (28 g, 250 mmol) in degassed methanol (80 mL)) was cannula transferred into the phosphine solution and then stirred for 3 hours. Volatiles were removed under reduced pressure and the crude extracted with water (100 mL) and ethyl acetate (3 × 50 mL) and concentrated under vacuum to afford a black/brown oil. The final product **204** was isolated via vacuum distillation as an oil and then recrystallized

from isooctane to afford a white solid (6.6 g, 75% yield) in above 95% purity. ^{1}H NMR (500 MHz, C_6D_6) δ 7.45 (brs, pyrrole-N*H*, 1H), 6.52 – 6.49 (m, pyrrole-*H*, 2H), 6.37 (dd, *J* = 5.3, 2.6 Hz, pyrrole-*H*, 1H), 1.91 – 1.78 (dsept, *J* = 7.0, 1.0 Hz, $(CH_3)_2CH$, 2H), 1.01 (dd, *J* = 15.8, 7.0 Hz, $(CH_3)_2CH$, 6H), 0.95 (dd, *J* = 11.1, 6.9 Hz, $(CH_3)_2CH$, 6H). ^{13}C{^{1}H} (125.7 MHz, C_6D_6): δ 19.7 (d, $J_{C\text{-}P}$ = 7.5 Hz, $(CH_3)_2CH$), 20.8 (d, $J_{C\text{-}P}$ = 19.0 Hz, $(CH_3)_2CH$), 24.4 (d, $J_{C\text{-}P}$ = 7.9 Hz, $(CH_3)_2CH$), 110.3 (d, $J_{C\text{-}P}$ = 3.5 Hz, pyrrole-*C*), 117.6 (d, $J_{C\text{-}P}$ = 7.7 Hz, pyrrole-*C*), 121.5 (d, $J_{C\text{-}P}$ = 4.6 Hz, pyrrole-*C*), 124.3 (d, $J_{C\text{-}P}$ = 12.7 Hz, pyrrole-*C*). ^{31}P{^{1}H} NMR (202 MHz, C_6D_6): δ -10.1 (s).

2.4.4 Synthesis and characterization of AlP_3 ligand and nickel complex

Synthesis of AlP_3 (207). To a 10 mL toluene solution dissolving 272 mg of **204** (1.5 mmol) in a culture tube, 250 μL $AlMe_3$ solution (0.50 mmol, 2.0 M in heptane) was added. The culture tube was then heated in a 80 ℃ oil bath for 2 h. All the volatile was removed under vacuum to afford 312 mg (98% yield) a light orange oil. The ligand was used without further purification (purity is greater than 95% according to ^{31}P{^{1}H} NMR). ^{1}H NMR (500 MHz, C_6D_6) δ 7.54 (d, *J* = 0.9 Hz, 3H, pyrrole-*H*), 6.79 – 6.74 (m, 3H, pyrrole-*H*), 6.60 (d, *J* = 3.0 Hz, 3H, pyrrole-*H*), 1.93 – 1.87 (m, 6H, $(CH_3)_2CH$), 0.96 – 0.92 (m, 36H, $(CH_3)_2CH$). ^{13}C{^{1}H} (125.7 MHz, C_6D_6): δ ^{31}P{^{1}H} NMR (121 MHz, C_6D_6): δ -4.0 (s).

Synthesis of Ni(AlP_3) (208). To a top-screw cap culture tube, 340 mg (0.59 mmol) of **207** was loaded with 163 mg $Ni(COD)_2$ (0.59 mmol, 1.0 equiv) in 10 mL toluene. The resulting light green solution was heated in 100 ℃ oil bath for 4 h and turned deep green. The deep green solution was filtered through a short pad of Celite, then removed toluene

under vacuum to afford green solid. The crude **208** was recrystallized by slow diffusion pentane into concentrated toluene solution in the freezer, and 280 mg (75%) dark green crystal was obtained. Single crystal was obtained via slow diffusion of vapor pentane into a concentrated toluene solution. ^{1}H NMR (500 MHz, C_6D_6): δ 7.05 (brs, 3H, pyrrole-*H*), 6.69 (d, J = 2.9 Hz, 3H pyrrole-*H*), 6.63 – 6.62 (m, 3H, pyrrole-*H*), 2.51 (m, 6H, $(CH_3)_2CH$), 1.10 (br, 18H, $(CH_3)_2CH$), 0.85 (bm, 18H, $(CH_3)_2CH$). ^{31}P{^{1}H} NMR (202 MHz, C_6D_6): δ 13.0 (s). ^{27}Al{^{1}H} NMR (104 MHz, C_6D_6): δ 104.4 (brs). UV-Vis (in toluene): nm (ε [$L \cdot mol^{-1} \cdot cm^{-1}$]) 342 (1900), 460 (2220), 616 (520). calcd for $C_{30}H_{51}NiAlP_3N_3$: C 56.98; H 8.13, N 6.65; found: C 56.81; H 8.07; N 6.46.

Synthesis of 208-H$_2$. To a J. Young tube, 12.6 mg of **203** (0.02 mmol) was loaded with 0.5 mL C_6D_6. The solution was degassed via freeze-pump-thaw 3 cycles and then back filled with 1 atm H_2. The dark green solution turned pale green (almost colorless) within 5 min. ^{1}H NMR (500 MHz, C_6D_6, 298K): δ 7.27 (s, 3H, pyrrole-*H*), 6.67 (d, *J* = 3.0, 2.4 Hz, 3H, pyrrole-*H*)), 6.57 (dd, *J* = 3.1, 0.6 Hz, 3H, pyrrole-*H*), 2.08 (m, 6H, $(CH_3)_2CH$), 0.96 (dd, *J* = 13.6, 6.8 Hz, 18H, $(CH_3)_2CH$), 0.52 (dd, *J* = 5.2 Hz, 18H, $(CH_3)_2CH$), -2.09 (brs, 2H). ^{1}H NMR (500 MHz, d_6-toluene, 193K) δ 7.30 (s, 3H, pyrrole-*H*), 6.78 (s, 3H, pyrrole-*H*)), 6.57 (s, 3H, pyrrole-*H*), 2.16 (m, 3H, $(CH_3)_2CH$), 1.73 (m, 3H, $(CH_3)_2CH$), 0.97 (brs, 9H, $(CH_3)_2CH$), 0.79 (brs, 18H, $(CH_3)_2CH$), 0.02 (brs, 9H, $(CH_3)_2CH$), -2.49 (brs, 2H). ^{31}P{^{1}H} NMR (202 MHz, d_6-toluene): δ 24.3 (s). ^{27}Al{^{1}H} NMR (104 MHz, C_6D_6): δ 138.0 (brs).

*2.4.5 Characterization of **208-H_2***

Variable-Temperature Spectroscopic Analysis of 208-H_2. To a J. Young tube, 12.6 mg of **208** (0.02 mmol) was loaded with 0.5 mL d_8-toluene. 3 cycles of freeze-pump-thaw were performed to evacuate the headspace of the J. Young tube before 1 atm H_2 was back filled. The resulting **208-H_2** pale green solution was cooled from 25 ℃ to -80 ℃ and monitored by ^{1}H NMR. Upon cooling, the bound H_2 resonance sharpens and free H_2 resonance appears as a broad signal at 253 K, which is not visible at r.t. T1 values for **208-H_2** above 253 K could not be reliably obtained due to the quick exchange of free and bounded H_2 at those temperatures. T_1 = 22 ms was observed at 228 K for **208-H_2** (**Table II-1**)

Table II-1. Variable temperature T1 inversion recovery data collected on hydride resonance at -2.1 ppm in toluene-d8 for **208-H_2** using a Varian iNova 500 MHz spectrometer.

T(temperature/K)	T1/ms
228	22.2(2)
223	24.2(1)
218	26.1(2)
213	28.6(2)
208	36.0(4)
203	43.9(8)
198	56.6(2)
193	98(3)

Variable-Temperature Spectroscopic Analysis of 208-HD. To a J. Young tube, 12.6 mg of **208** (0.02 mmol) was loaded with 0.5 mL d_8-toluene. 3 cycles of freeze-pump-thaw were performed to evacuate the headspace of the J. Young tube before 1 atm HD was back filled. HD gas was generated by treating D_2O with excess CaH_2 in a top-screw-cap Schlenk flask, where the head space was evacuated via freeze-pump-thaw cycle before mixing. The pale green solution containing mixture of **208-H$_2$** and **208-HD** was cooled from 25 to -80 ℃ and monitored by ^{1}H NMR. ^{1}H NMR (500 MHz, d_6-toluene, 203K): δ 7.31 (s, 3H, pyrrole-*H*), 6.80 (s, 3H, pyrrole-*H*)), 6.58 (s, 3H, pyrrole-*H*), 2.17 (m, 3H, $(CH_3)_2CH$), 1.73 (m, 3H, $(CH_3)_2CH$), 0.96 (brs, 9H, $(CH_3)_2CH$), 0.79 (brs, 18H, $(CH_3)_2CH$), 0.01 (brs, 9H, $(CH_3)_2CH$), -2.50 (t, J_{HD} = 35 Hz, *H*D).

2.4.6 Electrochemical study of Ni(AlP$_3$)

Electrochemical studies were carried out using a CH Instruments Model 700 D Series. Electrochemical Analyzer and Workstation in conjunction with a three electrode cell. The working electrode was a CHI 104 glassy carbon disk with a 3.0 mm diameter and the auxiliary electrode was composed of platinum wire. The third electrode, the reference electrode, was a $Ag/AgNO_3$ electrode. This was prepared as a bulk solution composed of 0.01 M $AgNO_3$ and 0.2 M $[^nBu_4N][PF_6]$ in fluorobenzene. This was separated from solution by a fine porosity frit. CVs were conducted in fluorobenzene with 0.2 M $[^nBu_4N][PF_6]$ as supporting electrolyte and were reported with a scan rate of 100 mV/s. The concentration of the analyte solutions were approximately 1.00×10^{-3} M. CVs were referenced to $Fe(\eta\text{-}Cp)_2^+/ Fe(\eta\text{-}Cp)_2$ redox couple. The Cyclic voltammograms of **208** was shown in **Figure II-5** with 2 reversible redox events**.**

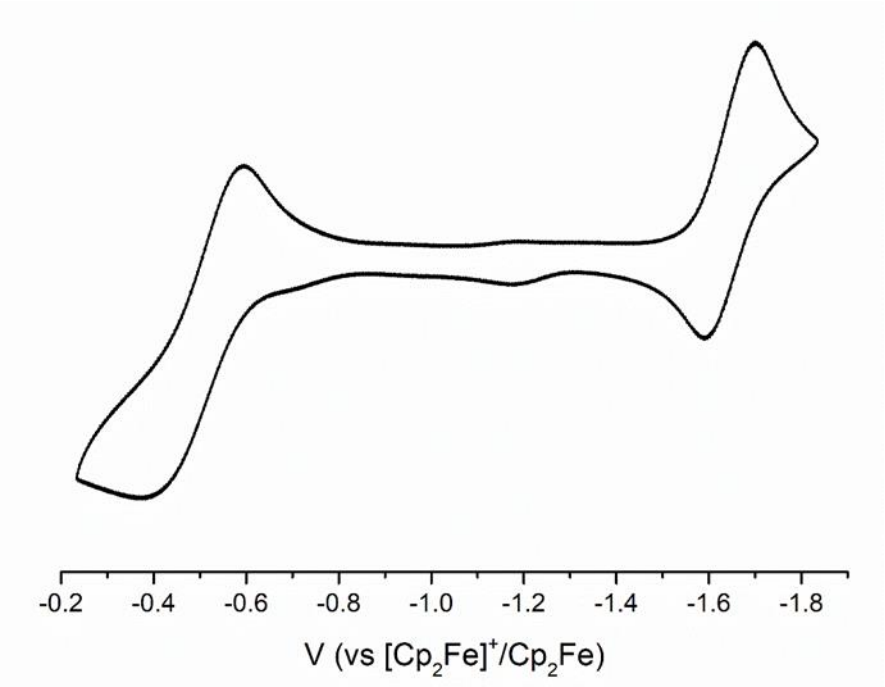

Figure II-5. Cyclic voltammograms of **208** scanned in 0.2 M [^{n}Bu$_4$N][PF$_6$] in PhF at 100 mV/s.

2.4.7 X-Ray structural determination details

A dark green block of **208 (CCDC 1915840)** was mounted onto a nylon loop and placed in a cold stream of nitrogen. Low temperature (110 K) X-ray data were obtained on a Bruker APEXII CCD based diffractometer (Mo sealed X-ray tube, Kα = 0.71073 Å). All diffractometer manipulations, including data collection, integration and scaling were carried out using the Bruker APEXII software. An absorption correction was applied using SADABS. The space group was determined on the basis of systematic absences and intensity statistics and the structure was solved by direct methods and refined by full-matrix least squares on F^2. The structure was solved in the monoclinic P21/n space group using XS (incorporated in SHELXLE).[146,147] All non-hydrogen atoms were refined with anisotropic thermal parameters. All hydrogen atoms were placed in idealized positions

and refined using riding model with the exception of the hydrogen bridged to iron and carbon which was located from the difference map. The structure was refined (weighted least squares refinement on F^2) and the final least-squares refinement converged.[146-148] No additional symmetry was found using ADDSYM incorporated in PLATON program.[149]

CHAPTER III

FORMATION OF AN AG→AL DATIVE BOND IS AVOIDED IN REACTIONS OF AN ALANE/TRIS(PHOSPHINE) LIGAND WITH MONOVALENT SILVER*

3.1 Introduction

Tripodal ligands combining a central main group Lewis acid with three neutral outer donors (ZL_3) have played a pivotal role in the development of the understanding of the nature of the interaction of Z-type ligands with transition metals,[114] and in the development of catalytic applications.[66,74,75,115-117] The ligands comprised of a central group 13 element and three phosphine donors (such as **167**, **168**, **169**, and **170** in Figure III-1) have been particularly prominent.[73,76,77,79,118-121]

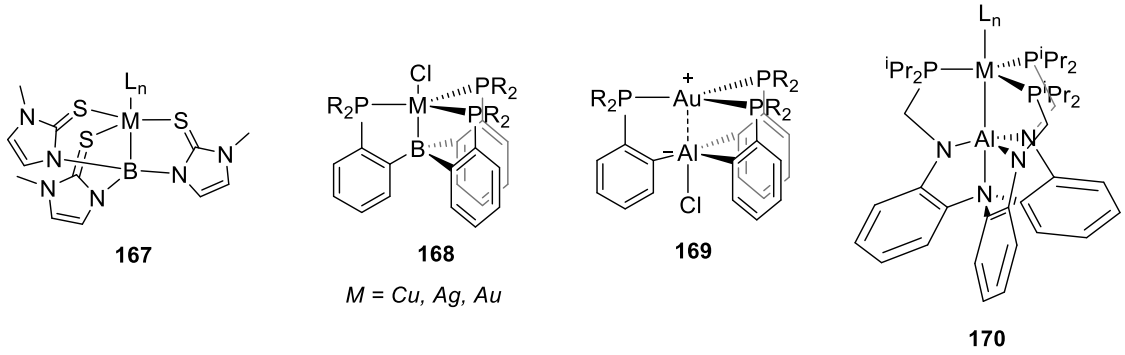

Figure III-1. Selected literature examples of complexes of boron- and aluminum-centered ZL_3 ligands.

We have recently reported a new AlP_3 ligand (chapter II) of this class which features one of the arguably strongest group 13 Lewis acids in the ZL_3 designs, courtesy

* [Lai, Q.; Bhuvanesh, N.; Zhou, J.; Ozerov, O. V. Formation of an Ag→Al Dative Bond Is Avoided in Reactions of an Alane/tris(phosphine) Ligand with Monovalent Silver. *Dalton Transactions*, **2021**, Accepted.] Reproduced by permission of The Royal Society of Chemistry

of a tris(N-pyrrolyl) substitution about the Al center. Interactions of ZL_3 ligands with coinage metal-based MX or M^+ fragments with the system **168** (Figure III-1) have been studied and generally showed that the ability to donate to the Lewis acid decreases in the order Au > Cu > Ag.[76] We became interested in whether the AlP_3 ligand and its higher central Lewis acidity can enforce a stronger interaction with an Ag center. However, we discovered that the combination of AlP_3 with the AgOTf or Ag^+ fragments did not result in the expected tripodal complexes with simple Ag→Al interaction. In this report, we present the structural changes that were observed instead.

3.2 Results and discussion

3.2.1 Synthesis of AlP_3 complexes with silver

The reaction of AlP_3 with AgOTf proceeded smoothly to result in a single product, which was isolated in 77% yield. The ^1H, ^{31}P, and ^{13}C NMR spectra were consistent with C_3 symmetry. In particular, we noted a single set of ^{31}P NMR resonances displaying characteristic coupling to the two S = ½ isotopes of Ag. However, the XRD study on a suitable single crystal revealed that while the three phosphines are indeed bound to the Ag center, the triflate has migrated to Al. This has the apparent effect of quenching the Lewis acidity of Al towards the Ag center. The Al-Ag distance is quite long at 3.1834(7) Å vs 2.56 Å as the sum of covalent radii per Alvarez et al.[134] The Al center is displaced from the N_3 plane towards the oxygen of the triflate, but the geometry falls short of taking on a strictly tetrahedral ($\Sigma_{N\text{-}Al\text{-}N}$ = ca. 352.5°). The Ag center is slightly displaced from the P_3 plane, away from Al ($\Sigma_{P\text{-}Ag\text{-}P}$ = ca. 354.9°). Based on these metrics, although some Al…Ag

interaction cannot be excluded, it would clearly be quite weak at best. The incomplete pyramidalization of Al may be related to the chelate constraint.

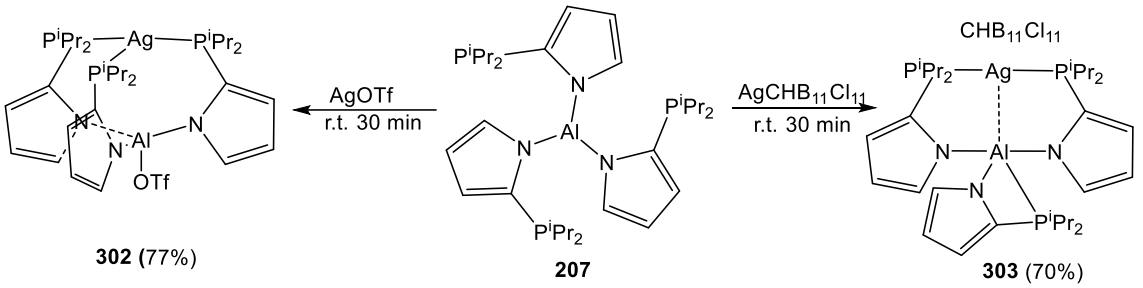

Scheme III-1. Synthesis AlP_3 complexes with silver

The transfer of triflate to Al is reminiscent of the observation of Bourissou et al. who recorded the transfer of chloride from Au to Al resulting in structure **169** (Figure III-1).[59] It is also related to the abstraction of the halide from group 11 metal halides by certain ZL_2 ligands.[54,59] We surmised that removing the triflate from the equation and instead utilizing a more weakly coordinating anion might result in the retainment of Lewis acidity at Al in the adduct with Ag^+. To this end, AlP_3 was subjected to a reaction with $Ag[HCB_{11}Cl_{11}]$.[150-155] It resulted in the clean formation of a single product, but it was apparent from the NMR spectra that it did not possess the expected tripodal symmetry. Two resonances in a 2:1 ratio were observed in the ^{31}P NMR spectrum, with only the larger resonance displaying the telltale coupling to $^{107/109}Ag$.

3.2.2 XRD studies of Ag(AlP_3) complexes

A single-crystal XRD study (Figure III-2) revealed that one of the phosphine arms has rotated away from Ag and brought the phosphine donor around to make a bond to Al. The 1,2-disposition of the Lewis acid and Lewis base (P) mimics some of the common designs for intramolecular frustrated Lewis pairs.[154,155]

Although the P-Al interaction should be challenged by the strain of the four-membered ring it creates, the P-Al distance in **303** (2.4395(8) Å) is not especially long. Barron et al. analysed Al-P distances in alane-phosphine adducts as a function of the number of carbon (R) vs heteroatom (X) substituents on Al and noted that $X_3Al\text{-}PR_3$ adducts possess the shortest Al-P distance on the order of 2.40 Å, and the corresponding $RX_2Al\text{-}PR_3$ giving rise to distances (2.44 Å) similar to that in **303**.[156] An adduct of an alkyldiisopropylphosphine with $AlCl_3$ has been structurally characterized by the Fryzuk group, revealing a ca. 2.41 Å Al-P distance.[157]

The value of $\Sigma_{N\text{-}Al\text{-}N}$ = ca. 355.6 ° in **303** is similar to that in **302**, indicating that Al largely remains in the N_3 plane. Thus it is also possible to contemplate that the structure can be viewed as trigonal bipyramidal about Al, with bonding interactions with both P and Ag. The Ag-Al distance in **303** (2.9629(7) Å) is shorter than in **302** but is still about 0.4 Å longer than the sum of the covalent radii. Furthermore, the P-Ag-P angle is ca. 159 °, but the deviation from linearity positions Ag away from Al. Thus here, too, we are forced to conclude that any Ag-Al interaction is minimal.

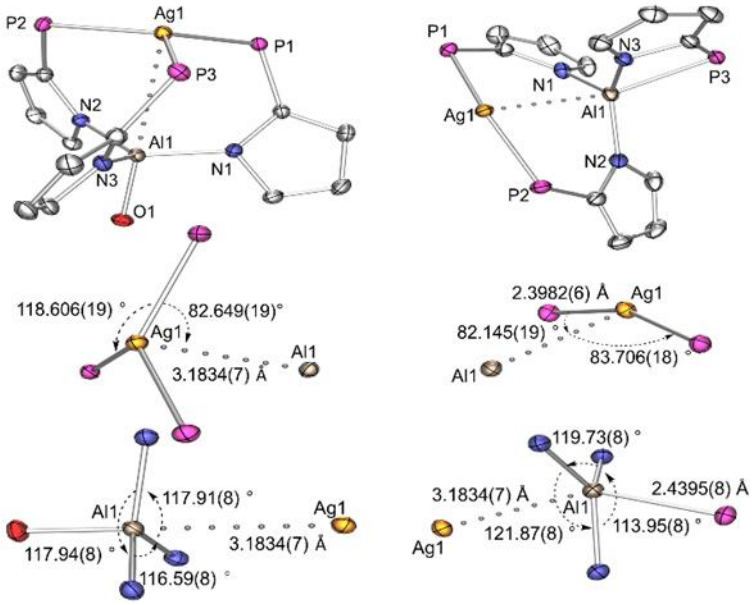

Figure III-2. POV-Ray rendition of the ORTEP drawing[158] (50% thermal ellipsoids) of **302** (left) and **303** (right). Top: A view showing selected atom labelling. Hydrogen atoms, solvent molecules, and isopropyl groups are omitted for clarity. Middle: Truncated molecules showing the Ag center and atoms around Ag. Bottom: Truncated molecules showing the Al center and atoms around Al.

3.3 Conclusion

In summary, reactions of the AlP_3 ligand with AgOTf and Ag^+ do not lead to a well-defined Ag→Al bond. Instead, Al manages to abstract either the triflate anion or one of the phosphine donors away from silver. This reinforces the notion that monovalent silver is not a good partner for Z-type ligands. Employing a stronger Lewis acid such as in AlP_3 causes the Al center to seek alternatives to Ag as a Lewis basic partner, even in spite of the significant structural preorganization favouring a direct silver-aluminum contact.

3.4 Experimental section

3.4.1 General consideration

Unless otherwise specified, all reactions and manipulations were carried out inside an argon-filled glove box or using Schlenk line techniques. Toluene and pentane were dried and deoxygenated via the solvent purification system and stored over molecular sieves in the glove box filled with argon. C_6D_6 were dried over NaK /Ph_2CO/18-crown-6, distilled and stored over molecular sieves in an Ar-filled glove box. Fluorobenzene and C_6D_5Br were dried over CaH_2, distilled and stored over molecular sieves in an Ar-filled glove box. 1H-pyrrole was purchased from Oakwood chemicals, then was dried with CaH_2 and distilled before use. Other chemicals were purchased from commercial vendors and used without further purification. $AgCHB_{11}Cl_{11}$[159] and N-tris(2-diisopropylphophinopyrrolyl)alane (**201** AlP_3) ligand was synthesized according to the literature.

3.4.2 Physical method

NMR spectra were recorded on a Varian Inova 500 spectrometer (^{1}H NMR, 499.703 MHz, ^{13}C NMR 125.580 MHz, ^{19}F NMR, 469.854 MHz), Varian Inova 400 (^{11}B NMR, 128.191 MHz) spectrometer. Chemical shifts are reported in δ (ppm). For ^{1}H spectra, the residual solvent peak was used as an internal reference (δ 7.16 for C_6D_6, 7.30 for C_6D_5Br).

3.4.3 Synthesis and characterization of Ag(AlP_3) complexes

Synthesis of Ag(AlP_3OTf) (302). To a toluene solution containing 540 mg (0.94 mmol) Al_3P, 240 mg AgOTf (0.94 mmol, 1.0 equiv) was added. The resulting mixture

was stirred at r.t. for 2 h. The light orange solution was then filtered through a short pad of Celite. The filtrate was concentrated under vacuum, and then layered with pentane to allow slow diffusion in the freezer. 600 mg of **302** (77%) was obtained as colorless crystal. ^{1}H NMR (500 MHz, C_6D_6): δ 8.10 (brs, 3H, pyrrole-CH), 6.52 (t, J = 3.0 Hz, 3H, pyrrole-CH), 6.39 (d, J = 3.2 Hz, 3H, pyrrole-CH), 2.20 - 2.12 (m, 3H, $(CH_3)_2CH$), 1.61 – 1.52 (m, 3H, $(CH_3)_2CH$), 1.07 – 1.02 (m, 9H, $(CH_3)_2CH$), 0.85 – 0.81 (m, 9H, $(CH_3)_2CH$), 0.78 – 0.75 (m, 9H, $(CH_3)_2CH$), 0.04 – 0.01 (m, 9H, $(CH_3)_2CH$). ^{31}P{^{1}H} NMR (202 MHz, C_6D_6): δ 7.43 (d, J_{Ag-P} = 286.6 Hz, J_{Ag-P} = 330.9 Hz). ^{19}F (470 MHz, C_6D_6): δ -75.7. calcd for $C_{35}H_{59}AgAlN_3P_3O_4SF_3$: C 46.57; H 6.59, N 4.65; found: C 46.16; H 6.54; N 4.53.

Synthesis of $Ag(AlP_3)CHB_{11}Cl_{11}$ (303). 287 mg (0.50 mmol) of Al_3P was loaded in a culture tube with 10 mL fluorobenzene. 315 mg (0.50 mmol, 1 equiv) $AgCHB_{11}Cl_{11}$ was added to the above toluene solution. The mixture was stirred at r.t. for 2 h. The light orange solution was then filtered through a short pad of Celite. The filtrate was concentrated under vacuum, and slow diffusion of pentane would result in 420 mg (70%) colorless crystal of **303**. ^{1}H NMR (500 MHz, C_6D_5Br): δ 7.61 (brs, 1H, pyrrole-CH), 7.21 (brs, 2H, pyrrole-CH), 6.67 (t, J = 2.4 Hz, 1H, pyrrole-CH), 6.56 (t, J = 2.5 Hz, 2H, pyrrole-CH), 6.52 (d, J = 3.2 Hz, 1H, pyrrole-CH), 6.45 (d, J = 3.2 Hz, 2H, pyrrole-CH), 2.92 (m, 1H, $(CH_3)_2CH$), 2.25 - 2.16 (m, 1H, $(CH_3)_2CH$), 2.11 – 2.04 (m, 2H, $(CH_3)_2CH$), 1.81 – 1.73 (m, 2H, $(CH_3)_2CH$), 1.08 (dd, J = 18.9, 7.0 Hz, 6H, $(CH_3)_2CH$), 0.81 – 0.60 (m, 30H, $(CH_3)_2CH$). ^{31}P{^{1}H} NMR (202 MHz, C_6D_5Br): δ 19.5 (d, J_{Ag-P} = 424.2 Hz, J_{Ag-P} = 489.3 Hz, 2P), -1.8 (brs, 1P). EA (%) calcd for $C_{31}H_{52}AgAlN_3P_3B_{11}Cl_{11}$: C 30.94; H 4.36, N 3.49; found: C; H; N.

3.4.4 X-ray structural determination details

Y Colorless block crystals of **302 (CCDC 1915843)** was mounted onto a nylon loop and placed in a cold stream of nitrogen respectively. Low temperature (110 K) X-ray data were obtained on a Bruker APEXII CCD based diffractometer (Mo sealed X-ray tube, Kα = 0.71073 Å). All diffractometer manipulations, including data collection, integration and scaling were carried out using the Bruker APEXII software. An absorption correction was applied using SADABS. The space group was determined on the basis of systematic absences and intensity statistics and the structure was solved by direct methods and refined by full-matrix least squares on F^2. The structure was solved in the monoclinic P21/n space group using XS/XT (incorporated in SHELXLE).[146,147] All non-hydrogen atoms were refined with anisotropic thermal parameters. All hydrogen atoms were placed in idealized positions and refined using riding model with the exception of the hydrogen bridged to iron and carbon which was located from the difference map. The structure was refined (weighted least squares refinement on F^2) and the final least-squares refinement converged.[146-148] No additional symmetry was found using ADDSYM incorporated in PLATON program.[149]

Colorless block crystals of **303 (CCDC 1915844)** were mounted onto a nylon loop and placed in a cold stream of nitrogen respectively. Low temperature (110 K) X-ray data were obtained on a Bruker APEXII CCD based diffractometer (Mo sealed X-ray tube, Kα = 0.71073 Å). All diffractometer manipulations, including data collection, integration and scaling were carried out using the Bruker APEXII software. An absorption correction was applied using SADABS. The space group was determined on the basis of systematic

absences and intensity statistics and the structure was solved by direct methods and refined by full-matrix least squares on F^2. Integrated intensity information for each reflection was obtained by reduction of the data frames with the program APEX2. The integration method employed a three-dimensional profiling algorithm and all data were corrected for Lorentz and polarization factors, as well as for crystal decay effects. Finally the data was merged and scaled to produce a suitable data set. The absorption correction program SADABS was employed to correct the data for absorption effects.

Systematic reflection conditions and statistical tests of the data suggested the space group *P*-1. A solution was obtained readily using XT/XS in APEX2.[146,147] Two molecules of toluene were found solvated. One of them located on a symmetry element and hence disordered, which was modeled successfully. Hydrogen atoms were placed in idealized positions and were set riding on the respective parent atoms. All non-hydrogen atoms were refined with anisotropic thermal parameters. Also, residual electron density (Q) peaks suggested the isopropyl group (C26, C27, C28) was disordered and was modeled between two positions with an occupancy ratio of 0.88 : 0.12. Appropriate restraints and/or constraints were added to keep the bond distances, angles, and thermal ellipsoids meaningful. Absence of additional symmetry and voids were confirmed using PLATON (ADDSYM).[149] The structure was refined (weighted least squares refinement on F^2) to convergence.[146,147] Olex2 was employed for the final data presentation and structure plots.[148]

CHAPTER IV

UNEXPECTED B/AL TRANSELEMENTATION WITHIN A RH PINCER COMPLEX*

4.1 Introduction

Pincer ligands, binding to a metal in a meridional tridentate fashion, have become a widely used class of auxiliary ligands with many applications in catalysis and fundamental studies of bond-breaking and making.[160-164] Pincer ligands, and polydentate ligands in general, enable precise positioning of donor sites in the desired molecule and utilization of different pincer ligands permits systematic variation of these donor sites with the preservation of the overall geometry and control of the overall charge.[165] Among pincer ligands with a central X-type[166] donor, boryl- and aluminyl-centered pincer ligands are arguably the most donating towards the metal and the most *trans*-influencing.[167] The first boryl-centered PBP-type pincer was reported by Nozaki and Yamashita in 2009 (**101J**, Figure IV-1).[30] This and the closely related diaminoboryl-centered ligands have been used further by Yamashita[39,41] and other groups.[32,168] The boryl pincer family also includes examples of ligands based on the *meta*-carborane cage pioneered by Mirkin and Spokoyny (**135,136**, Figure IV-1).[28,29,56,57] Our group has reported on the reactivity of Rh and Ir complexes based on the ligand shown in **120**.[27,37,46,47] The boryl center in **101J**

* Reprinted with permission from "Unexpected B/Al Transelementation within a Rh Pincer Complex." Lai, Q; Bhuvanesh, N.; Ozerov, O.V. *J. Am. Chem. Soc*. **2020**, *142*, 20920–20923. Copyright [2020] by The American Chemical Society

carries two strongly π-donating amino substituents which may diminish its Lewis acidity, while carborane-derived ligands such as **135** and **136** do not possess an accessible empty orbital at boron at all. In contrast, the diarylboryl center in **120** lacks such stabilization. The aluminyl-centered pincer ligands are an even more recent development. In the last few years, aluminyl pincer ligands with six-,[22] four-,[23,169] and three-coordinate[24] Al have been reported by the Iwasawa, Nakao, and Yamashita groups, respectively (**148**, **158**, and **164**, Figure IV-1).

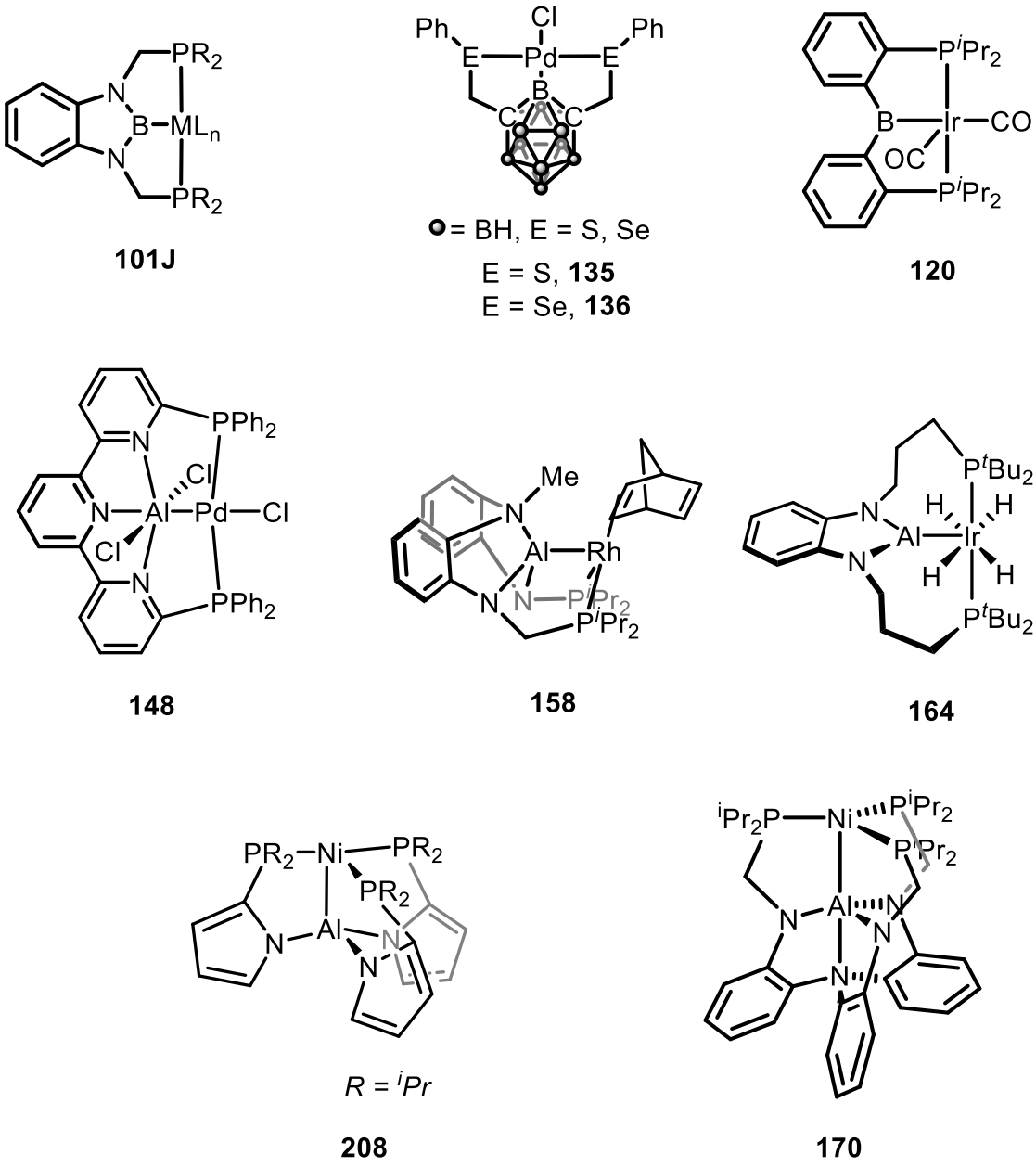

Figure IV-1. Structures of selected previously reported pincer complexes with central boryl and aluminyl donors, and examples of complexes of alane/tris(phosphine) ligands.

Pincer ligands with a central three-coordinate boryl unit retain Lewis acidity at the boron atom but it is completely quenched by addition of a single Lewis base.[27,37,46,47,114] On the other hand, the Lewis acidity of Al in an aluminyl is not completely quenched by

binding one Lewis base. The triply base-stabilized aluminyl in **148** is no longer Lewis acidic,[22] but the singly base-stabilized Al in **158** retains enough Lewis acidity to interact with Lewis bases while maintaining an Al-Rh bond.[23]

We recently reported a new tripodal alane/tris(phosphine) ligand based on the phosphinopyrrolyl construction (Chapter 2). Its Ni complex **208** was shown to be more electron deficient than Lu's compound **170**.[73,79] We surmised that a bipodal analog of **208**, an aluminyl pincer ligand with pyrrolyl substituents on Al and no additional built-in neutral donor for Al would furnish a metal-bound Al site that should be more Lewis acidic than that in **158** or **164**.[23,24]

The role and of the Z-type[114] borane or alane ligands such as in **208** and **170** is different from the potential role of boryl or aluminyl donors in chelating ligands. Group 13-based Z-type ligands primarily affect the reactivity by electronically modulating what may take place solely at the transition metal site. In contrast, the boryl and aluminyl sites possess Lewis acidity that is directed not at the transition metal, but potentially at a substrate. This offers promise of new reactivity routes that exploit the main group Lewis acidity either for dramatically enhanced reactivity or unusual selectivity. Such approaches have only recently begun to be explored. Examples include our group's demonstration of selective C-H activation of azines by derivatives of **120**,[38] and Nakao's work showing that Rh complexes related to **158** can catalyze C-H functionalization in pyridines and aromatic C-F bond activation.[23,25,167] In this context, accessing new systems with enhanced Lewis acidity appears to be a promising expansion.

4.2 Results and discussion

*4.2.1 Synthesis of bis-(2-diisopropylphosphinopyrrolyl)dihydroaluminate ligand **(402)***

Treatment of 1H-2-diisopropylphosphinopyrrole (**204**) with $LiAlH_4$ in 2:1 ratio in THF at room temperature for 2 h led to the new dihydroaluminate compound **402** accompanied by gas evolution. After removing all the volatiles, the residual colorless oil was triturated with pentane to yield crude **402** as a white powder which contained ca. 1 equiv THF. THF-free compound **402** was obtained via trituration with toluene and recrystallized as colorless block crystals (84%) from toluene/pentane solution. The difference between the ^{31}P NMR chemical shifts of **402** in the presence or absence of THF was insignificant, but the latter gave rise to a broader ^{31}P NMR resonance, possibly due to the coordination of phosphines to Li.

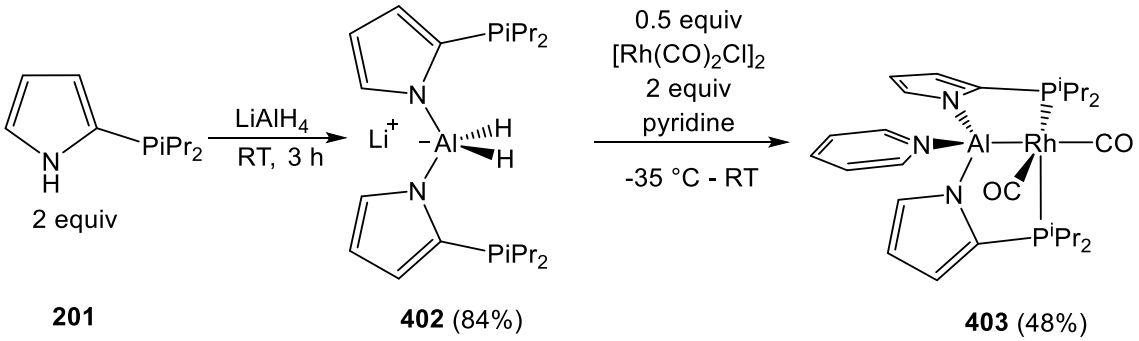

201 **402** (84%) **403** (48%)

Scheme IV-1. Synthesis of $(PAl^{py}P)Rh(CO)_2$ **(403).**

*4.2.2 Synthesis of $(PAl^{Py}P)Rh(CO)_2$ **(403)** complex and its reactivities*

In the presence of 2.0 equiv pyridine, the reaction of 1.0 equiv ligand **402** with 0.5 equiv $[Rh(CO)_2Cl]_2$ at -35 ℃ led to a major product **403**. Filtration followed by cooling a saturated THF solution allowed the isolation of **403** as light-yellow block crystals in 48% yield. The ^1H NMR spectrum of **403** afforded 2 methine C-H resonances and 4 methyl C-

H resonances, suggesting that **403** has C_s symmetry. In addition, the aromatic region of the ^{1}H NMR spectrum contained only the pairwise resonances of pyrrolyl C-H sites and a set of pyridine resonances in a 2:2:1 ratio. The presence of two carbonyl ligands in **403** was inferred from the two resonances in the $^{13}C\{^1H\}$ NMR spectrum (δ 207.6 ppm, br d, J_{Rh-C} = 60.9 Hz; and 203.1 ppm, dt, J_{Rh-C} = 73.2 Hz, J_{C-P} = 21.5 Hz) and two IR bands (ν_{CO} = 1966 and 1915 cm^{-1}). These data are similar to those in Nakao's **158** (e.g., ν_{CO} = 1973/1907 cm^{-1}).[23] The structural assignment was confirmed by an X-ray diffraction study on a single crystal of **403** (vide infra).

We envisioned that a suitable Lewis acid might abstract pyridine from **403** and lead to a PAlP pincer rhodium complex with a three-coordinate aluminyl moiety. It was anticipated that the putative **404** would possess C_{2v} symmetry on the NMR timescale, similarly to **120** and **164**.[24,47] Towards this end, thermolysis of **403** with 2.1 equiv $BF_3{\cdot}Et_2O$ at 60 ℃ for 1 h was carried out. This resulted in the expected formation of the $BF_3{\cdot}Py$ byproduct (^{19}F and ^{11}B NMR evidence)[170] and a new complex displaying C_{2v} symmetry by NMR spectroscopy and two IR carbonyl stretching bands at 1981 and 1930 cm^{-1}. However, initial excitement was subdued when additional data pointed to that this product was not **404**. Utilization of 1 equiv of $BF_3{\cdot}Et_2O$ in the thermolysis with **403** resulted in only 50% conversion of **403**, with 50% formation of $BF_3{\cdot}Py$ and the same C_{2v}-symmetric product. A downfield ^{11}B NMR resonance was detected (62.7 ppm), which is typical for a three-coordinate, heteroatom-substituted boron species.[171,172] Finally, an X-ray study on a suitable single crystal (Figure IV-3) revealed that the C_{2v}-symmetric product formed in thermolysis of **403** with $BF_3{\cdot}Et_2O$ is the new boryl pincer complex **405**.

We have not established the fate of Al, but we tentatively assume that insoluble AlF_3 is formed (a precipitate is evident in the reaction mixture). The overall transformation is probably driven by the thermodynamics of making stronger Al-F bonds and perhaps also stronger Rh-B bonds, as well as the formation of a more favorable adduct with pyridine. Ostensibly, two equiv of $BF_3{\cdot}Et_2O$ are necessary for the reaction to proceed to completion because one equivalent is used to form $BF_3{\cdot}Py$ and the other undergoes a metathesis with Al in the PAlP pincer. However, it is not clear whether the abstraction of pyridine plays only a thermodynamic role or is also kinetically necessary prior to the "transelementation" step(s).

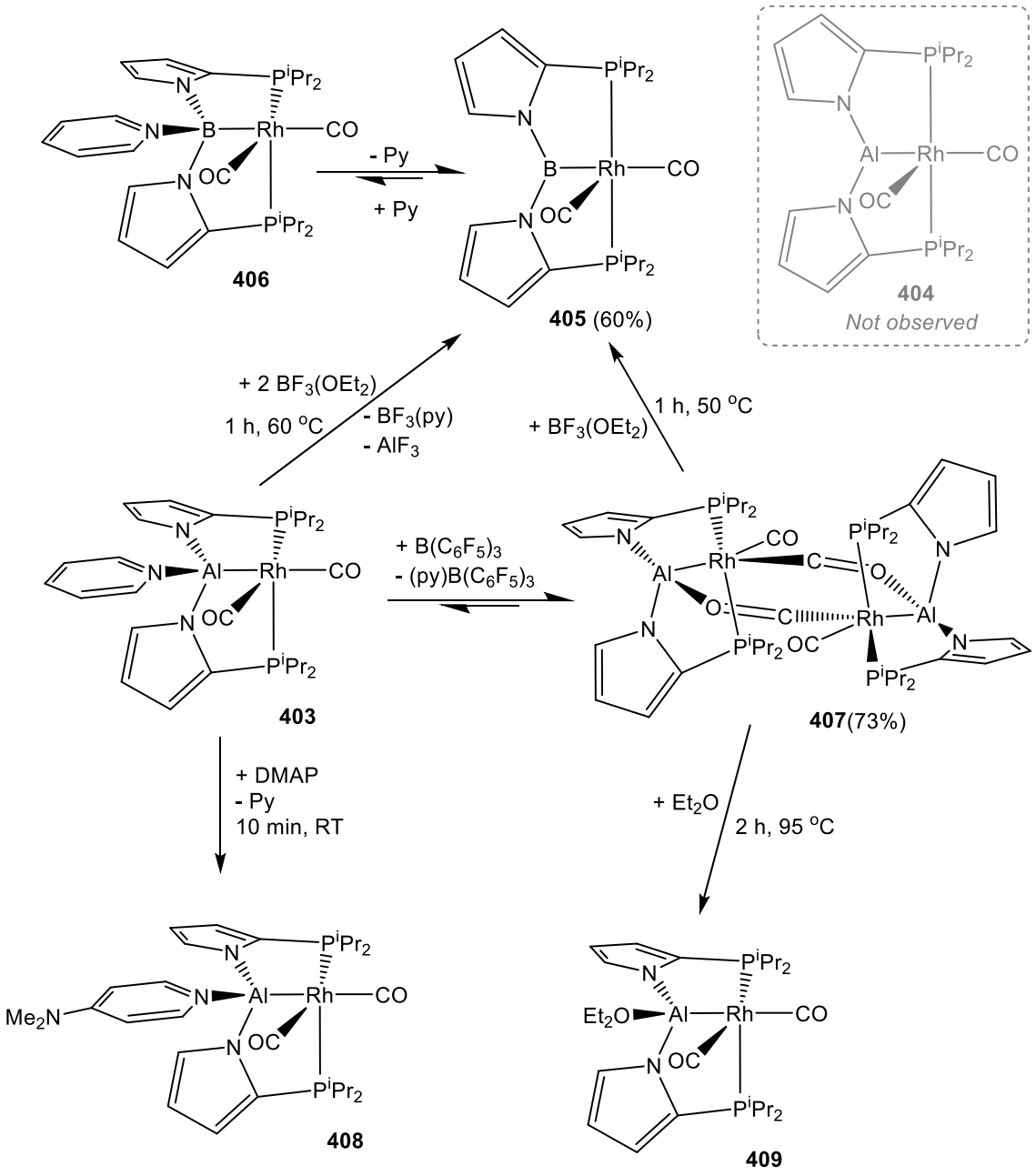

Scheme IV-2. Reactions of (PAlpyP)Rh(CO)$_2$ (**403**) with boranes

Although **405** was not the target of our study as it was conceived, it nonetheless represents a complex of a previously unknown PBP pincer ligand. In order to evaluate the Lewis acidity of the boron center, the reaction of **405** with pyridine was examined.

Addition of 2.1 equiv of pyridine to a solution of **403** induced minor changes in the positions and shapes of the ^{1}H NMR resonances. The overall C_{2v} symmetry was maintained and only one set of pyridine resonances was evident. From this it was concluded that the binding of pyridine to **405** is rapidly reversible on the NMR timescale. A Van't Hoff study permitted determination of the thermodynamic parameters (ΔH = -14(1) kcal/mol; ΔS = -43(3) cal/(mol·K)), **Figure IV-5**). Since **405** does not bind 1 equiv of pyridine fully, the Lewis acidity of B in **405** is less than that of Al in **403**.

We surmised that a boron Lewis acid without B-F bonds or any other labile B-X bonds might be suitable to perform pyridine abstraction from **403** while avoiding transelementation, and settled on $B(C_6F_5)_3$. Indeed, in situ ^{1}H NMR and ^{31}P NMR analysis revealed that heating the mixture of **403** and 1.1 equiv of $B(C_6F_5)_3$ at 80 ℃ resulted in 88% conversion of **403** to a new product. The expected byproduct $B(C_6F_5)_3 \cdot Py$ was observed in the ^{19}F and ^{11}B NMR spectra.[173] Utilization of 1.5 equiv $B(C_6F_5)_3$ led to 90% conversion of **403**. The abstraction is apparently not sufficiently favorable to completely remove pyridine, but it proceeds far enough to allow isolation of the new Rh product **407**. Treatment of an isolated sample of **407** with 1 equiv. pyridine regenerated **403** quantitatively within 5 min at ambient temperature, while heating **407** with 2 equiv. of Et_2O in benzene at 95 °for 2 h resulted in the clean formation of **409.**

The reaction of **403** with $B(C_6F_5)_3$ is independent of $[B(C_6F_5)_3]$ and is slower than the reaction of **403** with $BF_3 \cdot Et_2O$, which displays a positive dependence of the rate on $[BF_3 \cdot Et_2O]$. Both are much slower than the reaction of **403** with DMAP, complete in 10 min at RT to give the DMAP adduct **408**. We propose that the abstraction of pyridine

from **403** using $B(C_6F_5)_3$ occurs by a dissociative mechanism via the intermediate formation of **404**, while the displacement of pyridine by DMAP takes place by an associative mechanism, via a five-coordinate Al transition state or an intermediate. The reaction with $BF_3{\cdot}Et_2O$ evidently does not proceed by a purely dissociative mechanism and may involve an attack of $BF_3{\cdot}Et_2O$ on **403**. Further, we cannot exclude that the reaction with $BF_3{\cdot}Et_2O$ is catalysed by protic impurities in $BF_3{\cdot}Et_2O$. Judging by that a) **407** reacted with 1.1 equiv of $BF_3{\cdot}Et_2O$ to give **405** and b) **409** was observed at the intermediate stages of the reaction of **403** with $BF_3{\cdot}Et_2O$, pyridine is not critical for the B/Al exchange.

The rhodium complex **407** displayed a lower symmetry in its NMR spectra than expected for **404**, with four different methyl resonances. In addition, its solubility in organic solvents was surprisingly poor vs what might be expected for a monometallic pincer complex. The poor solubility was beneficial for the purification and isolation: cooling the reaction mixture to room temperature afforded light-yellow crystals in 73% yield, from which suitable ones for X-ray diffractometry could be retrieved.

4.2.3 XRD studies of pincer rhodium complexes

The X-ray study (Figure IV-2) demonstrated that compound **407** is formally a dimer of **404** connected via a pair CO ligands bridging between Rh and Al. The formation of isocarbonyl complexes by means of attachment of an oxophilic Lewis acid (including Al) to the oxygen terminus of a transition metal carbonyl is well precedent.[174-176]

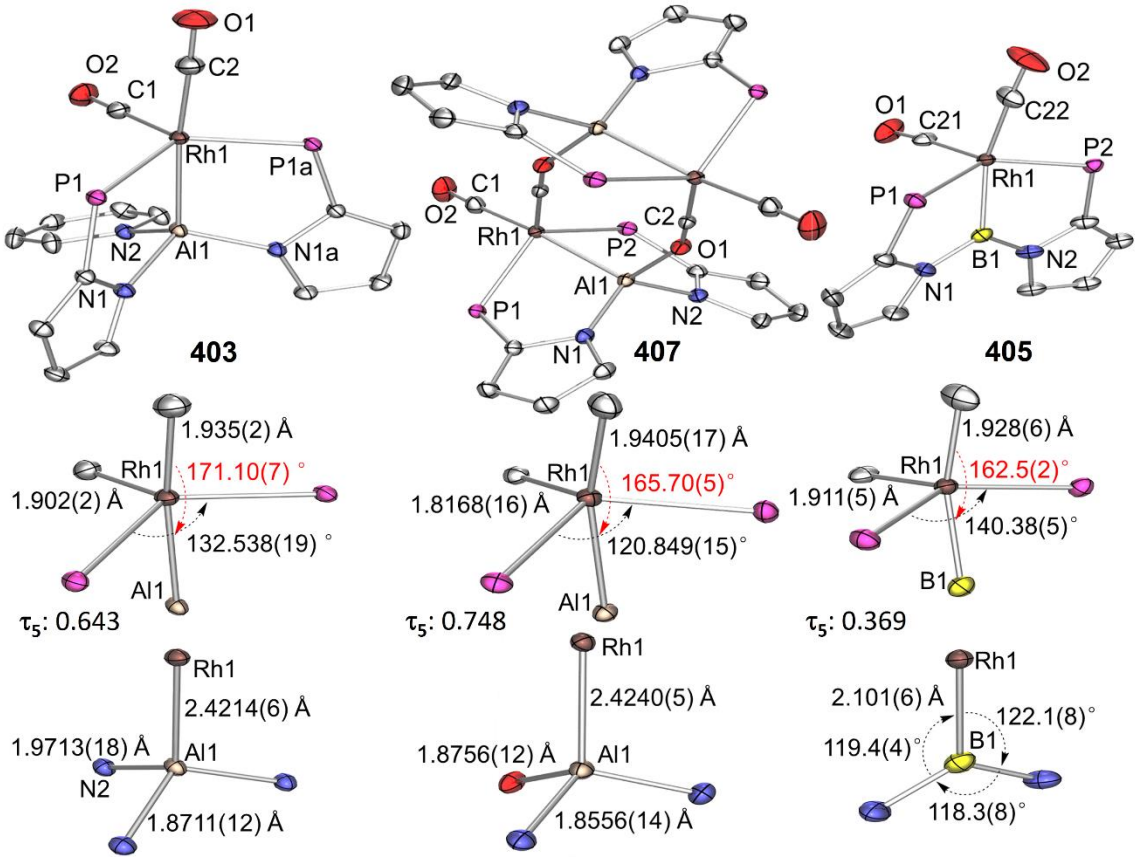

Figure IV-2. Top: ORTEP drawings (50% probability ellipsoids) of **403**, **407** and **405**, showing selected labeling. Hydrogen atoms, isopropyl arms, toluene molecules in 403 and **407**, and disorder in the pyrrole rings in **405** are omitted for clarity. Middle: Truncated molecules showing only the immediate Rh coordination environment. Bottom: Truncated molecules showing only the immediate Al or B coordination environment.

The coordination geometries about Rh and Al in **403** and **407** are quite similar. Both rhodium centers in **403** and **407** adopt a similar distorted trigonal bipyramidal geometry. The Al donor and one of the CO ligands can be viewed as axial, while the two phosphorus atoms and the other CO define the equatorial plane. The Rh-Al distances in **403** and **407** are almost identical and comparable to **158** (ca. 2.44 Å).[23] The geometries of Al centers in both **403** and **407** are distorted tetrahedral, and the Al-$N_{pyrrolyl}$ distances of **407** are slightly shorter than that of **403**. The Al1-O1 distance (ca. 1.88 Å) of **407** is almost

identical to the sum of Al and O covalent radii (1.87 Å),[134] and the O1-C2 distance (ca. 1.20 Å) is elongated by 0.07 Å compared to the terminal CO ligand. The IR stretching frequency of isocarbonyl is 1707 cm^{-1}, typical for the isocarbonyl complexes,[174-176] and similar to the stretches arising from double C=O bonds in organic compounds.

The geometry about Rh in **405** can be classified as closer to square pyramidal, but as can be seen in Figure IV-3, the differences in the requisite angles from **403** and **407** are modest. The structure of **405** is quite similar to that of **120**.[47] The boron center in **405** is also strictly planar ($\Sigma_{N\text{-}B\text{-}N(Rh)}$ = ca. 359.8 °). The Rh1-B1 bond distance in **405** (ca. 2.10 Å) is longer than most Rh-B_{boryl} bonds[177] but is close to the Ir-B distance in **120** (ca. 2.15 Å; Ir and Rh are nearly identical in size). The geometry about Rh in **405** is very close to that about Ir in **120** (cf. τ = 0.33). The B-N distances in **5** are similar to those in Ar_2B(N-pyrrolyl) compounds,[i] at ca, 1.46-1.47 Å.[178]

4.3 Conclusion

In conclusion, Rh complexes supported by new aluminyl-centered pincer ligands have been described. The two N-pyrrolyl substituents on Al were expected to augment the Lewis acidity at Al. This is reflected in the dimerization via isocarbonyl formation upon attempts to isolate a complex with a three-coordinate aluminyl site. The unexpected B/Al transelementation that preserves the pincer structure is potentially intriguing as a more general synthetic tool for the construction of templated pincer complexes with various main group elements in the central site.

4.4 Experimental section

4.4.1 General consideration

Unless otherwise specified, all reactions and manipulations were carried out inside an argon-filled glove box or using Schlenk line techniques. Solvents were dried and deoxygenated via the solvent purification system and stored over molecular sieves in the glove box filled with argon. C_6D_6 were dried over NaK /Ph_2CO/18-crown-6, distilled and stored over molecular sieves in an Ar-filled glove box. Fluorobenzene and C_6D_5Br were dried over CaH_2, distilled and stored over molecular sieves in an Ar-filled glove box. 1H-pyrrole was purchased from Oakwood chemicals, then was dried with CaH_2 and distilled before use. Other chemicals were purchased from commercial vendors and used without further purification. 1H-2-diisopropylphosphinopyrrole was synthesized according to the published procedure.

4.4.2 Physical method

NMR spectra were recorded on a Varian Inova 500 spectrometer (^{1}H NMR, 499.703 MHz, ^{13}C NMR 125.580 MHz), Varian Inova 400 (^{11}B NMR, 128.191 MHz, ^{27}Al NMR, 104.223 MHz) spectrometer. Chemical shifts are reported in δ (ppm). For ^{1}H and ^{13}C NMR spectra, the residual solvent peak was used as an internal reference (^{1}H NMR: δ 7.16 for C_6D_6, 5.32 for CD_2Cl_2, 2.08 for d_8-toluene; ^{13}C NMR: δ 128.06 for C_6D_6, 53.84 for CD_2Cl_2, 20.43 for CD_3CN). Infrared spectra were obtained on an Agilent CARY 630 ATR-FTIR, Mattson 4020 Galaxy Series. Elemental analyses were performed by CALI Laboratories, Inc. (Highland Park, NJ).

*4.4.3 Synthesis of the proto-pincer PAlP ligand **(402)** and its complexes*

Synthesis of $LiAlH_2P_2$ (402). To a 50 mL culture tube, 1.0 mL $LiAlH_4$ 2.0 M in THF solution (2.0 mmol) was loaded. 0.73 g of 1H-2-diisopropylphosphinopyrrole (4.0 mmol) was dissolved in 10 mL THF and was added to $LiAlH_4$ solution drop wise via pipette. The resulting mixture was stirred at r.t. for 5 h until visible gas evolution stopped. All the volatile was then removed under vacuum to yield colorless oil which was triturated with toluene 3 times to remove residual THF. 0.82 g (84%) of **402** as white crystalline solid was obtained after recrystallization by layer pentane over toluene solution. ^{1}H NMR (500 MHz, C_6D_6): δ 7.60 (br s, Pyrrole*H*, 2H), 6.71 – 6.66 (m, Pyrrole*H*, 4H), 4.60 (br s, AlH_2, 2H), 1.92 (dsep, $J_{H\text{-}H}$ = 6.9 Hz, $J_{P\text{-}H}$ = 3.5 Hz, C*H*$(CH_3)_2$, 4H), 0.98 (dd, $J_{H\text{-}H}$ = 6.9 Hz, $J_{P\text{-}H}$ = 12.5 Hz, CH(C$H_3)_2$, 12H), 0.92 (dd, $J_{H\text{-}H}$ = 6.9 Hz, $J_{P\text{-}H}$ = 15.8 Hz, CH(C$H_3)_2$, 12H). ^{1}H NMR (500 MHz, C_6D_6) (THF free): δ 7.37 (br s, Pyrrole*H*, 2H), 6.69 (m, Pyrrole*H*, 4H), 4.38 (br s, AlH_2, 2H), 1.93 (hepd, $J_{H\text{-}H}$ = 7.0 Hz, $J_{P\text{-}H}$ = 4.0 Hz, C*H*$(CH_3)_2$, 4H), 0.98 (m, CH(C$H_3)_2$, 24H). ^{13}C{^{1}H} NMR (125 MHz, C_6D_6): δ 132.7 – 131.9 (m, Pyrrole*C*), 124.0 (d, $J_{C\text{-}P}$ = 28.9 Hz, Pyrrole*C*), 118.1 (s, Pyrrole*C*), 111.4 (s, Pyrrole*C*), 23.9 (d, $J_{C\text{-}P}$ = 6.2 Hz, *C*H$(CH_3)_2$), 20.2 – 19.8 (m, CH(*C*$H_3)_2$), 18.8 (t, $J_{C\text{-}P}$ = 2.3 Hz, CH(*C*$H_3)_2$). ^{31}P{^{1}H} NMR (202 MHz, C_6D_6): δ -9.8 ppm. ^{27}Al NMR (104 MHz, C_6D_6): δ 113.7 ppm.

Synthesis of $(P^{Py}AlP)Rh(CO)_2$ (403). 388 mg (1.0 mmol) $[Rh(CO)_2Cl]_2$ and 320 μL (4.0 mmol) pyridine was dissolved in 10 mL toluene and cooled in the freezer (-35 °C)**.** 880 mg (2.2 mmol) ligand **402** was dissolved in 10 mL toluene and precooled in the freezer before the addition to the rhodium pyridine mixture dropwise. The resulting orange

solution was further stirred at r.t. for 1 h before filtration. The filtrate was concentrated and then recrystallized by slow pentane vapor diffusion to yield 500 mg **403** as yellow crystals (48%). ^{1}H NMR (500 MHz, C_6D_6): δ 7.66 (d, $J_{H\text{-}H}$ = 5.1 Hz, Pyridine*H*, 2H), 6.91 (m, Pyrrole*H*, 2H), 6.89 (t, $J_{H\text{-}H}$ = 2.5 Hz, Pyrrole*H*, 2H), 6.78 (d, $J_{H\text{-}H}$ = 3.0 Hz, Pyrrole*H*, 2H), 6.52 (t, $J_{H\text{-}H}$ = 7.7 Hz, Pyridine*H*, 1H), 6.21 – 6.10 (m, Pyridine*H*, 2H), 2.41 (dhep, $J_{P\text{-}H}$ = 14.1, $J_{H\text{-}H}$ = 7.1 Hz, C*H*$(CH_3)_2$, 2H), 2.24 – 2.14 (m, C*H*$(CH_3)_2$, 2H), 1.26 (dd, $J_{H\text{-}H}$ = 6.9 Hz, $J_{P\text{-}H}$ = 10.2 Hz, CH(C*H*$_3)_2$, 6H), 1.16 – 1.03 (m, CH(C*H*$_3)_2$, 18H). ^{13}C{^{1}H} NMR (125 MHz, C_6D_6): δ 207.6 (br d, $J_{Rh\text{-}C}$ = 60.9 Hz, CO), 203.1 (dt, $J_{Rh\text{-}C}$ = 73.2, $J_{C\text{-}P}$ = 21.5 Hz, CO), 147.4 (s, Pyridine*C*), 141.1 (s, Pyridine*C*), 137.8 – 137.2 (m, Pyrrole*C*), 125.4 (t, $J_{C\text{-}P}$ = 8.1 Hz, Pyrrole*C*), 125.2 (s, Pyridine*C*), 115.7 (t, $J_{C\text{-}P}$ = 1.6 Hz, Pyrrole*C*), 113.5 (s, Pyrrole*C*), 31.9 (t, $J_{C\text{-}P}$ = 9.6 Hz, *C*H$(CH_3)_2$), 30.0 (t, $J_{C\text{-}P}$ = 16.7 Hz, *C*H$(CH_3)_2$), 19.6 (t, $J_{C\text{-}P}$ = 2.7 Hz, CH(*C*H$_3)_2$), 19.3 (s, , CH(*C*H$_3)_2$), 19.2 (t, $J_{C\text{-}P}$ = 2.5 Hz, CH(*C*H$_3)_2$), 19.1 (t, $J_{C\text{-}P}$ = 4.7 Hz, CH(*C*H$_3)_2$). ^{31}P{^{1}H} NMR (202 MHz, C_6D_6): δ 46.9 (d, $J_{Rh\text{-}P}$ = 139.2 Hz) ppm. ^{27}Al NMR (104 MHz, C_6D_6): δ 170.1 ppm. IR (ATR, cm^{-1}): 1966, 1915 cm^{-1}. EA (%) calcd for $C_{27}H_{39}AlN_3O_2P_2Rh$: C, 51.52; H, 6.25; N, 6.68; found: C, 51.52; H, 6.02; N, 6.60.

Synthesis of (PBP)Rh(CO)$_2$ (405). To a 50 mL culture tube, 400 mg (0.64 mmol) of **403** was loaded with 10 mL toluene and 165 μL (1.28 mmol) BF_3-OEt_2. The resulting mixture was then heated in 60 °C oil bath for 1 h. All the volatile was removed under vacuum, and the residue was dissolved in pentane and filtered through a short pad of Celite. The filtrate was concentrated under vacuum to make a saturated solution at r.t. and cooled in the freezer for recrystallization to yield orange crystals **405** 200 mg (60%). ^{1}H

NMR (400 MHz, C_6D_6): δ 7.21 (dt, J_{H-H} = 2.6, 1.3 Hz, Pyrrole*H*, 2H), 6.52 (t, J_{H-H} = 3.0 Hz, Pyrrole*H*, 2H), 6.46 (d, J_{H-H} = 3.2 Hz, Pyrrole*H*, 2H), 2.08 (dhep, J_{P-H} = 7.9 Hz, J_{H-H} = 6.8 Hz, C*H*$(CH_3)_2$, 4H), 1.12 – 1.04 (m, CH(C*H*$_3)_2$, 12H), 1.00 (dvt, J_{H-H} = 6.9 Hz, J_{P-H} = 7.9 Hz, CH(C*H*$_3)_2$, 12H). $^{13}C\{^1H\}$ NMR (100 MHz, C_6D_6): δ 200.4 (d, J_{Rh-C} = 56.7 Hz, CO), 142.8 (t, J_{P-C} = 29.2 Hz, Pyrrole*C*), 123.2 (t, J_{C-P} = 6.6 Hz, Pyrrole*C*), 117.0 (t, J_{C-P} = 2.7 Hz, Pyrrole*C*), 116.7 (s, Pyrrole*C*), 28.9 (t, J_{C-P} = 13.1 Hz, *C*H$(CH_3)_2$), 19.1 (t, J_{C-P} = 3.7 Hz, CH(*C*H$_3)_2$), 18.7 (s, CH(*C*H$_3)_2$). $^{31}P\{^1H\}$ NMR (162 MHz, C_6D_6): δ 55.8 (d, J_{Rh-P} = 136.1 Hz) ppm. $^{11}B\{^1H\}$ NMR (128 MHz, C_6D_6): δ 62.7 ppm. IR (ATR, cm^{-1}): 1981, 1930 cm^{-1}. EA (%) calcd for $C_{22}H_{34}BN_2O_2P_2Rh$: C, 49.47; H, 6.42; N, 5.24; found: C, 49.53; H, 6.52; N, 5.06.

Synthesis of [(PAlP)Rh(CO)$_2$]$_2$ (407). To a 20 mL culture tube, 63 mg (0.10 mmol) of **403** and 61 mg of $B(C_6F_5)_3$ (0.12 mmol) was loaded with 3 mL toluene. The resulting clear solution was then heated in 100 °C oil bath for 1 h. Upon cooling from 100 °C to room temperature, yellow crystals formed inside the tube. Toluene solution was decanted, and the crystalline residue was washed with 3×1 mL toluene and dried under vacuum to yield 40 mg of **407** (73%). Quality crystals for the X-ray analysis were obtained through this procedure. ^1H NMR (500 MHz, C_6D_6): δ 7.17 (m, Pyrrole*H*, 2H), 6.68 (dd, J_{H-H} = 3.1, 2.3 Hz, Pyrrole*H*, 2H), 6.55 (dd, J_{H-H} = 3.3, 1.0 Hz, Pyrrole*H*, 2H), 2.15 – 2.03 (m, C*H*$(CH_3)_2$, 2H), 1.97 – 1.91 (m, C*H*$(CH_3)_2$, 2H), 1.01 (dd, J_{P-H} = 17.9 Hz, J_{H-H} = 6.8 Hz, CH(C*H*$_3)_2$, 3H), 0.94 (dd, J_{P-H} = 13.5 Hz, J_{H-H} = 6.9 Hz, CH(C*H*$_3)_2$, 4H), 0.70 (dd, J_{P-H} = 17.0 Hz, J_{H-H} = 7.0 Hz, CH(C*H*$_3)_2$, 3H), 0.63 (dd, J_{P-H} = 17.5 Hz, J_{H-H} = 6.8 Hz, CH(C*H*$_3)_2$, 3H). $^{31}P\{^1H\}$ NMR (202 MHz, C_6D_6): δ 43.0 (d, J_{Rh-P} = 122.2 Hz) ppm. (ATR,

cm^{-1}): 1982 (s, CO), 1707 (s, bridging CO) cm^{-1}. EA (%) calcd for $C_{22}H_{34}AlN_2O_2P_2Rh$: C, 48.01; H, 6.23; N, 5.09; found: C, 48.40; H, 5.96; N, 4.89.

Synthesis and observation of 409. 11 mg (0.01 mmol) of **407** was loaded to a J. Young tube along with benzene-d_6 (the solid mostly remained undissolved). 22 μL 1.0 M Et_2O in C_6D_6 stock solution was added to the above suspension. The reaction mixture was then heated at 95 ℃ oil bath for 2 h. **407** was completely converted into **409**. ^{1}H NMR (500 MHz, C_6D_6): δ 6.99 – 6.96 (m, Pyrrole*H*, 2H), 6.82 (t, J_{H-H} = 2.6 Hz, Pyrrole*H*, 2H), 6.69 (d, J_{H-H} = 3.1, 1.0 Hz, Pyrrole*H*, 2H), 3.38 (q, *J* = 7.1 Hz, EtOCH_2CH$_3$, 4H), 2.36 (dsep, J_{P-H} = 14.2, J_{H-H} = 6.8 Hz, C*H*(CH$_3$)$_2$, 2H), 2.14 – 2.03 (m, C*H*(CH$_3$)$_2$, 2H), 1.33 (dd, J_{H-H} = 6.8 Hz, J_{P-H} = 17.1 Hz, CH(CH_3)$_2$, 6H), 1.08 – 0.96 (m, CH(CH_3)$_2$, 18H), 0.59 (t, *J* = 7.1 Hz, EtOCH_2CH$_3$, 6H); ^{13}C{^{1}H} NMR (125 MHz, C_6D_6):δ 203.83 (t, *J* = 21.7 Hz, *C*O), 203.26 (t, *J* = 21.3 Hz, *C*O), 136.29 (s, Pyrrole*C*), 125.24 (t, *J* = 7.6 Hz, Pyrrole*C*), 115.37 (s, Pyrrole*C*), 113.41 (s, Pyrrole*C*), 67.14 (s, EtO*C*H$_2$CH$_3$), 32.08 (t, *J* = 9.8 Hz, *C*H(CH$_3$)$_2$), 29.81 (t, *J* = 16.7 Hz, *C*H(CH$_3$)$_2$), 19.39 (s, EtOCH$_2$*C*H$_3$), 19.34 (t, *J* = 2.7 Hz, CH(*C*H$_3$)$_2$), 19.22 (t, *J* = 2.8 Hz, CH(*C*H$_3$)$_2$), 19.11 (t, *J* = 4.5 Hz, CH(*C*H$_3$)$_2$), 12.90 (dvt, *J* = 5.1 Hz, CH(*C*H$_3$)$_2$) ^{31}P NMR (202 MHz, C_6D_6): δ 46.5 (d, J_{Rh-P} = 138.2 Hz) ppm; ^{27}Al NMR (104 MHz, C_6D_6): δ 165.8 ppm.

4.4.4 Studies of the reactivity of 403 and 407

Thermal stability of 403. After thermolyzing benzene-d_6 solution of **403** in 110 °C oil bath for 14 h, no changes was observed in both ^{1}H and ^{31}P NMR spectra, and after thermolyzing toluene solution of **403** in 150 °C oil bath for 14 h, no changes was observed in both ^{1}H and ^{31}P NMR spectra.

Thermal stability of 407. Compound **407** was loaded into a J. Young NMR tube along with benzene-d_6 (the solid mostly remained undissolved) and subjected to thermolysis at 100 °C for 24 h. This resulted in a suspension. Analysis by solution $^{31}P\{^1H\}$ NMR spectroscopy showed the presence of multiple unidentified products.

Reaction of 403 with 1 equiv of BF_3-OEt_2. To a J. Young tube, a solution of 12.6 mg (0.020 mmol) of **403** in 0.5 mL C_6D_6 was loaded, and then 20 μL 1.0 M BF_3-OEt_2 and 100 μL 0.1 M mesitylene (internal standard) stock solutions were added via syringe. According to the ^1H, $^{31}P\{^1H\}$, $^{11}B\{^1H\}$ and ^{19}F NMR spectra collected in situ, after the resulting mixture was heated in a 60 °C for 1 h, 0.010 mmol of **403** was converted to **405**, and 0.01 mmol of BF_3-Py was formed. The precipitate was observed and presumably contained (AlF_3).

Reaction of 403 with 2.2 equiv of BF_3-OEt_2. To a J. Young tube, a solution of 12.6 mg (0.020 mmol) of **403** in 0.5 mL C_6D_6 was loaded, and then 44 μL 1.0 M BF_3-OEt_2 and 100 μL 0.1 M mesitylene (internal standard) stock solutions were added via syringe. According to the ^1H, $^{31}P\{^1H\}$, $^{11}B\{^1H\}$ and ^{19}F NMR spectra collected in situ, after the resulting mixture was heated in a 60 °C for 1 h, 0.020 mmol of **403** was converted to **405**, meanwhile 0.02 mmol of BF_3-Py was formed. The precipitate was observed and presumably contained (AlF_3).

Reaction of 403 with 1.1 equiv of $B(C_6F_5)_3$. To a J. Young tube, a solution of 12.6 mg (0.020 mmol) of **403** in 0.5 mL C_6D_6 was loaded, and 11.3 mg (0.022 mmol) $B(C_6F_5)_3$ and 100 μL 0.1 M mesitylene (internal standard) stock solutions were added via syringe. After the resulting clear solution was heated at 80 ℃ oil bath for 2 h, 88% of **403**

was converted into **407** according to the ^{1}H, $^{31}P\{^{1}H\}$, $^{11}B\{^{1}H\}$ and ^{19}F NMR spectra. The resulting mixture was heated for 16 h at the same oil bath, no further conversion of **403** was observed.

Reaction of 403 with 1.5 equiv of $B(C_6F_5)_3$. To a J. Young tube, a solution of 12.6 mg (0.020 mmol) of **403** in 0.5 mL C_6D_6 was loaded, and 15.3 mg (0.030 mmol) $B(C_6F_5)_3$ and 100 μL 0.1 M mesitylene (internal standard) stock solutions were added via syringe. After the resulting clear solution was heated at 80 ℃ oil bath for 2 h, 90% of **403** was converted into **407** according to the ^{1}H, $^{31}P\{^{1}H\}$, $^{11}B\{^{1}H\}$ and ^{19}F NMR spectra. The resulting mixture was heated for 16 h at the same oil bath, no further conversion of **403** was observed.

Reaction of 403 with dimethylaminopyridine (DMAP). To a J. Young tube, 12.6 mg (0.020 mmol) of **403,** 17.0 mg (0.14 mmol) of DMAP and 0.5 mL C_6D_6 were loaded, and 40 μL 0.1 M mesitylene (internal standard) stock solutions were added via syringe. The pyridine adduct **403** was converted into **408** within 10 min at room temperature, and 0.02 mmol of free pyridine was observed according to the ^{1}H NMR (500 MHz, C_6D_6): δ 7.42 (d, $J_{H\text{-}H}$ = 7.4 Hz, *Ar*(DMAP)*H*, 2H), 7.11 (m, Pyrrole*H*, 2H), 6.94 (t, $J_{H\text{-}H}$ = 2.6 Hz, Pyrrole*H*, 2H), 6.84 (dd, $J_{H\text{-}H}$ = 3.1, 1.0 Hz, Pyrrole*H*, 2H), 5.32 (d, $J_{H\text{-}H}$ = 7.4 Hz, Ar(DMAP)*H*, 2H), 2.46 (dsep, $J_{P\text{-}H}$ = 13.5, $J_{H\text{-}H}$ = 6.9 Hz, C*H*$(CH_3)_2$, 2H), 2.30 – 2.22 (m, C*H*$(CH_3)_2$, 2H), 1.75 (s, *Me*(DMAP)*H*, 6H), 1.33 (dd, $J_{H\text{-}H}$ = 6.9 Hz, $J_{P\text{-}H}$ = 16.8 Hz, CH(C*H*$_3)_2$, 6H), 1.21 – 1.14 (m, CH(C*H*$_3)_2$, 18H); and ^{31}P NMR (202 MHz, C_6D_6): δ 47.4 (d, $J_{Rh\text{-}P}$ = 141.3 Hz) ppm.

Reaction of 407 with 1.1 equiv BF_3-OEt_2. 11 mg (0.01 mmol) of **407** was loaded to a J. Young tube along with benzene-d_6 (the solid mostly remained undissolved). 22 μL 1.0 M BF_3-OEt_2 in C_6D_6 stock solution was added to the above suspension. **407** fully was converted into **405** after the reaction mixture was heated in 50 ℃ oil bath for 1 h.

Reaction of 407 with 1.1 equiv Py. 11 mg (0.01 mmol) of **7** was loaded to a J. Young tube along with benzene-d_6 (the solid mostly remained undissolved). 22 μL 1.0 M pyridine in C_6D_6 stock solution was added to the above suspension. Upon mixing, the solid **407** dissolved within 5 min to yield **403** at room temperature.

Variable-Temperature Spectroscopic Analysis of 407. To a J. Young tube, 11 mg of 40**7** (0.02 mmol) was loaded with 0.5 mL d_8-toluene. The suspension was then heated from 25 ℃ to 110 ℃, where the sample was allowed to equilibrate at each temperature for 5 minutes prior to data collection.

Reaction of 403 with 2 equiv of BF_3-OEt_2 at 55 ℃. To a J. Young tube, a solution of 12.6 mg (0.020 mmol) of **403** in 440 μL C_6D_6 was loaded, and then 40 μL 1.0 M BF_3-OEt_2 and 20 μL 0.1 M mesitylene (internal standard) stock solutions were added via syringe. The resulting mixture was heated in a 55 °C for 10 min, the reaction progress was monitored by the ^1H and $^{31}P\{^1H\}$ spectra.

Reaction of 403 with 4 equiv of BF_3-OEt_2 at 55 ℃. To a J. Young tube, a solution of 12.6 mg (0.020 mmol) of **403** in 400 μL C_6D_6 was loaded, and then 80 μL 1.0 M BF_3-OEt_2 and 20 μL 0.1 M mesitylene (internal standard) stock solutions were added via syringe. The resulting mixture was heated in a 55 °C for 10 min, the reaction progress was monitored by the ^1H and $^{31}P\{^1H\}$ spectroscopy.

Reaction of 403 with 8 equiv of BF_3-OEt_2 at 55 ℃. To a J. Young tube, a solution of 12.6 mg (0.020 mmol) of **403** in 320 μL C_6D_6 was loaded, and then 160 μL 1.0 M BF_3-OEt_2 and 20 μL 0.1 M mesitylene (internal standard) stock solutions were added via syringe. The resulting mixture was heated in a 55 °C for 10 min, the reaction progress (**Table IV-1**) was monitored by the ^1H and $^{31}P\{^1H\}$ spectroscopy.

Table IV-1. Reaction progress of **403** with BF_3-OEt_2 after heating at 55 ℃ for 10 min

[BF_3-OEt_2](M)	Conversion of 403	Yield of 409	Yield of 405
0.080	54%	12%	42%
0.16	65%	9%	55%
0.32	77%	3%	74%

Reaction of 403 with 1 equiv of $B(C_6F_5)_3$ at 55 ℃. To a J. Young tube, a solution of 12.6 mg (0.020 mmol) of **403** in 480 μL C_6D_6 was loaded, and 10.3 mg (0.020 mmol) $B(C_6F_5)_3$ and 20 μL 0.1 M mesitylene (internal standard) stock solutions were added via syringe. After the resulting clear solution was heated at 55 ℃ oil bath for 1 h, the reaction progress was monitored by the ^1H and $^{31}P\{^1H\}$NMR spectroscopy.

Reaction of 403 with 2 equiv of $B(C_6F_5)_3$ at 55 ℃. To a J. Young tube, a solution of 12.6 mg (0.020 mmol) of **403** in 480 μL C_6D_6 was loaded, and 20.5 mg (0.040 mmol) $B(C_6F_5)_3$ and 20 μL 0.1 M mesitylene (internal standard) stock solutions were added via syringe. After the resulting clear solution was heated at 55 ℃ oil bath for 1 h, the reaction progress was monitored by the ^1H and $^{31}P\{^1H\}$ NMR spectroscopy.

Reaction of 403 with 4 equiv of $B(C_6F_5)_3$ at 55 ℃. To a J. Young tube, a solution of 12.6 mg (0.020 mmol) of **403** in 480 μL C_6D_6 was loaded, and 40.9 mg (0.080 mmol) $B(C_6F_5)_3$ and 20 μL 0.1 M mesitylene (internal standard) stock solutions were added via syringe. After the resulting mixture was heated at 55 ℃ oil bath for 1 h, the reaction progress (**Table IV-2**) was monitored by the ^1H and $^{31}P\{^1H\}$NMR spectroscopy.

Table IV-2. Reaction progress of Py abstraction with $B(C_6F_5)_3$ after heating at 55 ℃ for 1 h

$[B(C_6F_5)_3]$(M)	**Conversion of 403**	**Yield of 407**
0.040	19%	16%
0.080	19%	16%
0.16	24%	17%

*4.4.5 Van't Hoff study of **(PBP)Rh(CO)$_2$** reacting with Py*

The equilibrium between 405 and 406. The coordination of Py to B center would make ^{31}P resonance shift up-field, and the $\Delta\delta$ is dependent on the concentration of Py, indicating the association of Py to B center is a reversible process in nmr time scale. In order to determine the ^{31}P NMR chemical shift of **406**, a series addition of 1.0 M Py solution to a solution containing 5.3 mg (0.01 mmol) **406** was conducted and monitored by ^{31}P NMR. ^{31}P NMR chemical shift of **406** was determined as the minimum value (50.5 ppm) which was obtained in the presence of 140 equiv Py in solution (**Figure IV-3**).

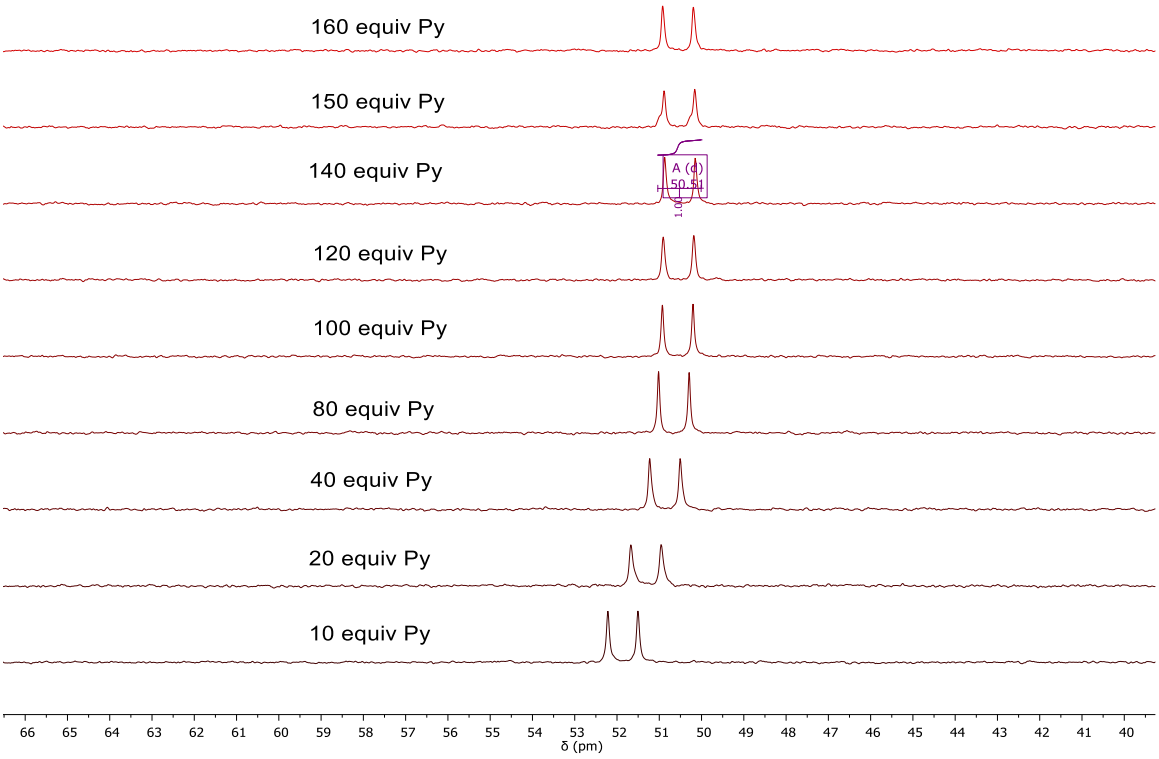

Figure IV-3. $^{31}P\{^{1}H\}$ NMR (202 MHz, C_6D_6) spectra of **405** with different amounts of pyridine added.

Van't Hoff Analysis. In a J. Young tube, 440 µL C_6D_6 was used to dissolve 16.0 mg (0.030 mmol) of **405**, then 60 µL 1.0 M pyridine (0.060 mmol) stock solution was added to the above solution. Equilibrium point at different temperature was monitored by ^{31}P NMR (Figure IV-4), which can be used to calculate the concentration of pyridine adduct **406** with the equation:

$$\delta_{eq} = \frac{([\mathbf{405}]_0 - [\mathbf{406}]) \times \delta_{\mathbf{405}} + [\mathbf{406}] \times \delta_{\mathbf{406}}}{[\mathbf{405}] + [\mathbf{406}]}$$

Where $[\mathbf{405}]_0$ = 0.060 M, $\delta_{\mathbf{405}}$ = 55.8, $\delta_{\mathbf{406}}$ = 50.5.

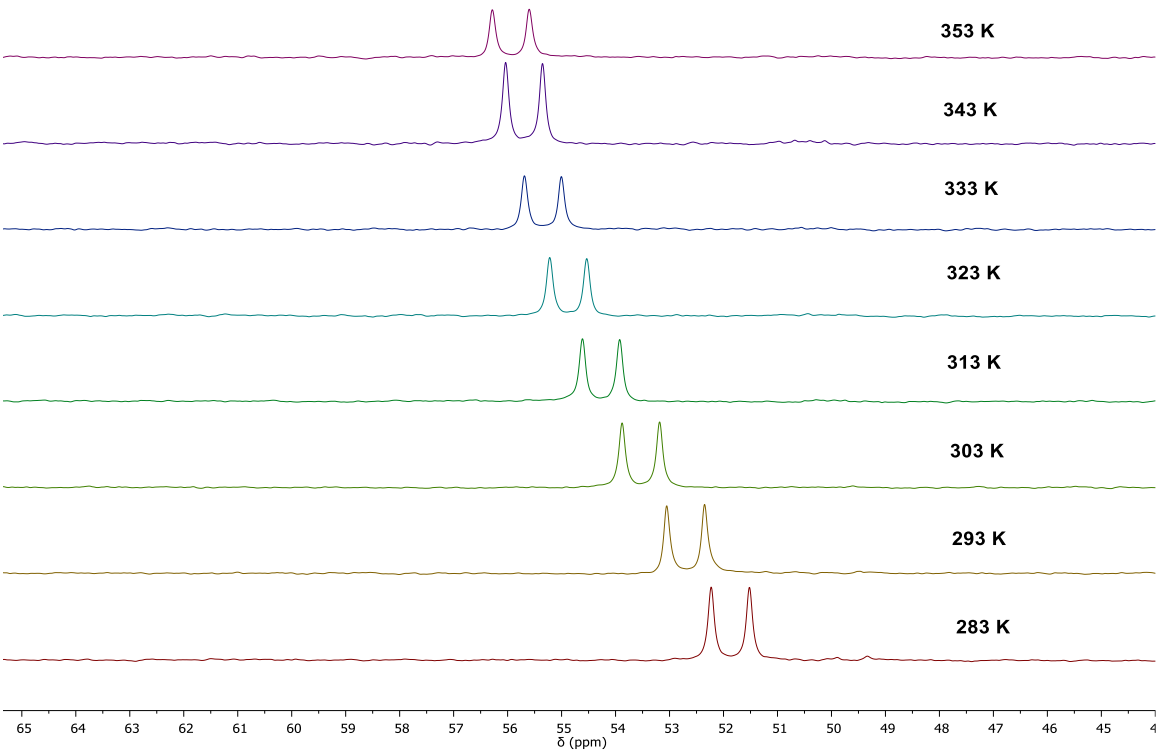

Figure IV-4. $^{31}P\{^{1}H\}$ NMR (202 MHz, C_6D_6) spectra of **405** and 2.0 equiv pyridine at various temperatures.

Then the equilibrium constant at different temperature can be determined with the equation:

$$K_{eq} = \frac{[\mathbf{406}]}{([\mathbf{405}]_0 - [\mathbf{406}])([\boldsymbol{Py}]_0 - [\mathbf{406}])}$$

where $[\mathbf{Py}]_0$ = 0.12 M;

With K_{eq} values at different T, plotting:

$$\mathrm{R}\ln K_{eq} = -\frac{\Delta H}{T} + \Delta S$$

reveals enthalpy change of the reaction equals to the negative slope value and entropy change equals to the y-intercept value (**Figure IV-5**): ΔH = - (14±1) kcal·mol^{-1} and ΔS =

- (43±3) cal·mol^{-1}·K^{-1}, where the errors for the Δ*H* and ΔS values were defined as double the standard errors of the slope and the intercept provided by the linear fit function in OriginPro 9 software.

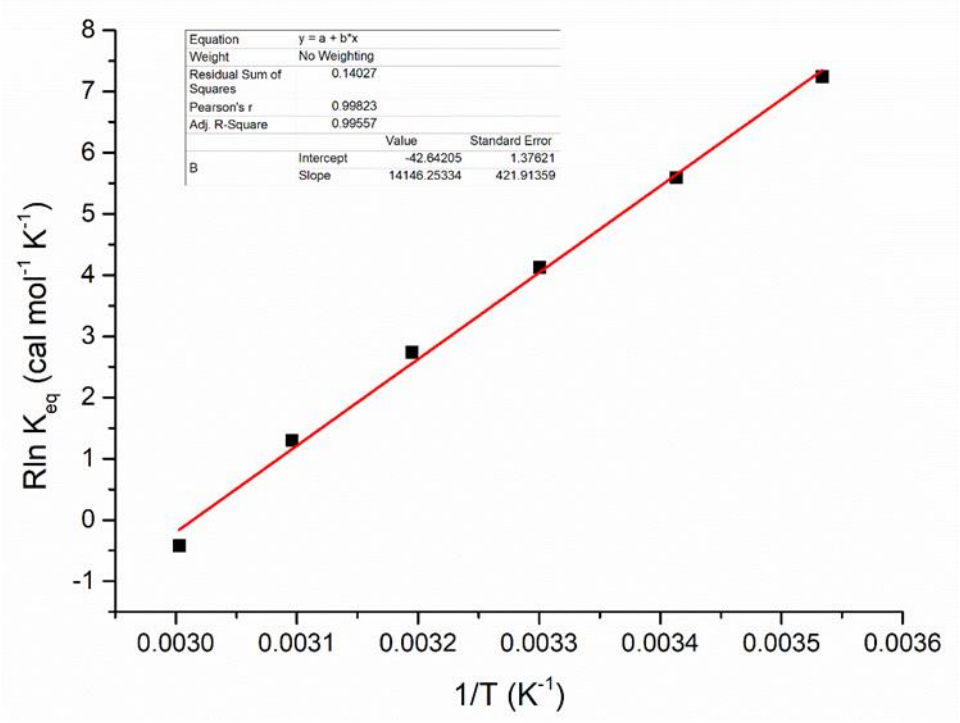

Figure IV-5. Van't Hoff plot for the equilibrium between **405** and **406**

4.4.6 X-Ray structural determination details

X-Ray data collection, solution, and refinement for (PPyAlP)Rh(CO)$_2$ (403) (CCDC 1915845). A Leica MZ 75 microscope was used to identify a light yellow block of **403** with very well defined faces with dimensions (max, intermediate, and min) 0.10 x 0.16 x 0.30 mm^3 from a representative sample of crystals of the same habit. The crystal mounted on a nylon loop was then placed in a cold nitrogen stream (Oxford) maintained at 110 K. X-ray data were obtained on a Bruker APEXII CCD based diffractometer (Mo sealed X-ray tube, Kα = 0.71073 Å). All diffractometer manipulations, including data

collection, integration and scaling were carried out using the Bruker APEX3 software. The absorption correction program SADABS was employed to correct the data for absorption effects. The space group was determined on the basis of systematic absences and intensity statistics and the structure was solved by direct methods and refined by full-matrix least squares on F^2. The structure was solved in the orthorhombic Pnma space group using XS (incorporated in SHELXLE/OLEX2).[146,147] All non-hydrogen atoms were refined with anisotropic thermal parameters. All hydrogen atoms were placed in idealized positions and refined using riding model with the exception of the hydrogen bridged to iron and carbon which was located from the difference map. The structure was refined (weighted least squares refinement on F^2) and the final least-squares refinement converged.[146-148] No additional symmetry was found using ADDSYM incorporated in PLATON program.[149]

X-Ray data collection, solution, and refinement for (PBP)Rh(CO)$_2$ (405) (CCDC 1915846). A yellow, multifaceted block of suitable size (0.50 x 0.30 x 0.10 mm^3) and quality was selected from a representative sample of crystals of the same habit using an optical microscope, mounted onto a nylon loop and placed in a cold stream of nitrogen. Low temperature (110 K) X-ray data were obtained on a Bruker APEXII CCD based diffractometer (Mo sealed X-ray tube, Kα = 0.71073 Å). All diffractometer manipulations, including data collection, integration and scaling were carried out using the Bruker APEX3 software. The absorption correction program SADABS was employed to correct the data for absorption effects. The space group was determined on the basis of systematic absences and intensity statistics and the structure was solved by direct methods and refined by full-matrix least squares on F^2. The structure was solved in the monoclinic $P2_1/c$ space group using XS (incorporated in SHELXLE/OLEX2).[146,147] All non-hydrogen atoms were refined with anisotropic thermal parameters. All hydrogen atoms were placed in idealized positions and refined using riding model with the exception of the hydrogen bridged to iron and carbon which was located from the difference map. The structure was refined (weighted least squares refinement on F^2) and the final least-squares refinement converged.[146-148] No additional symmetry was found using ADDSYM incorporated in PLATON program.[149]

X-Ray data collection, solution, and refinement for [(PAlP)Rh(CO)$_2$] (407) (CCDC 1960229). A Leica MZ 75 microscope was used to identify a light yellow block of **407** with very well defined faces with dimensions (max, intermediate, and min) 0.70 x 0.16 x 0.10 mm^3 from a representative sample of crystals of the same habit. The crystal mounted on a nylon loop was then placed in a cold nitrogen stream (Oxford) maintained at 110 K. X-ray data were obtained on a Bruker APEXII CCD based diffractometer (Mo sealed X-ray tube, Kα = 0.71073 Å). All diffractometer manipulations, including data collection, integration and scaling were carried out using the Bruker APEX3 software. The absorption correction program SADABSwas employed to correct the data for absorption effects. The space group was determined on the basis of systematic absences and intensity statistics and the structure was solved by direct methods and refined by full-matrix least squares on F^2. The structure was solved in the orthorhombic P2$_1$/n space group using XS (incorporated in SHELXLE/OLEX2).[146,147] All non-hydrogen atoms were refined with anisotropic thermal parameters. All hydrogen atoms were placed in idealized positions and refined using riding model with the exception of the hydrogen bridged to iron and carbon which was located from the difference map. The structure was refined (weighted least squares refinement on F^2) and the final least-squares refinement converged.[146-148] No additional symmetry was found using ADDSYM incorporated in PLATON program.[149]

CHAPTER V

EXPLORATION ON REDOX PROPERTY OF PCP IRON DICARBONYL COMPLEXES

5.1 Introduction

Iron as the most abundant transition metal in the earth crust has received tremendous attention in the area of organometallic chemistry over the past few decades due to their involvement in catalysis.[179-183] The iron complexes containing agostic C-H interaction, which are considered the intermediate prior C-H activation, provide fundamental insights to the nature of C-H activation on the iron center, therefore constitute an important class of compounds. However, the isolation and characterization of the iron intermediates with agostic F-H-C interaction was very scarcely reported.[184-186] Previous studies on iron hydrides showed that without a rigid structure enforcing C-H approaching the iron center, the C-H elimination products are either less thermodynamic favorable **(503)** or no evident interaction between C-H and iron center (**505**).[187-189]

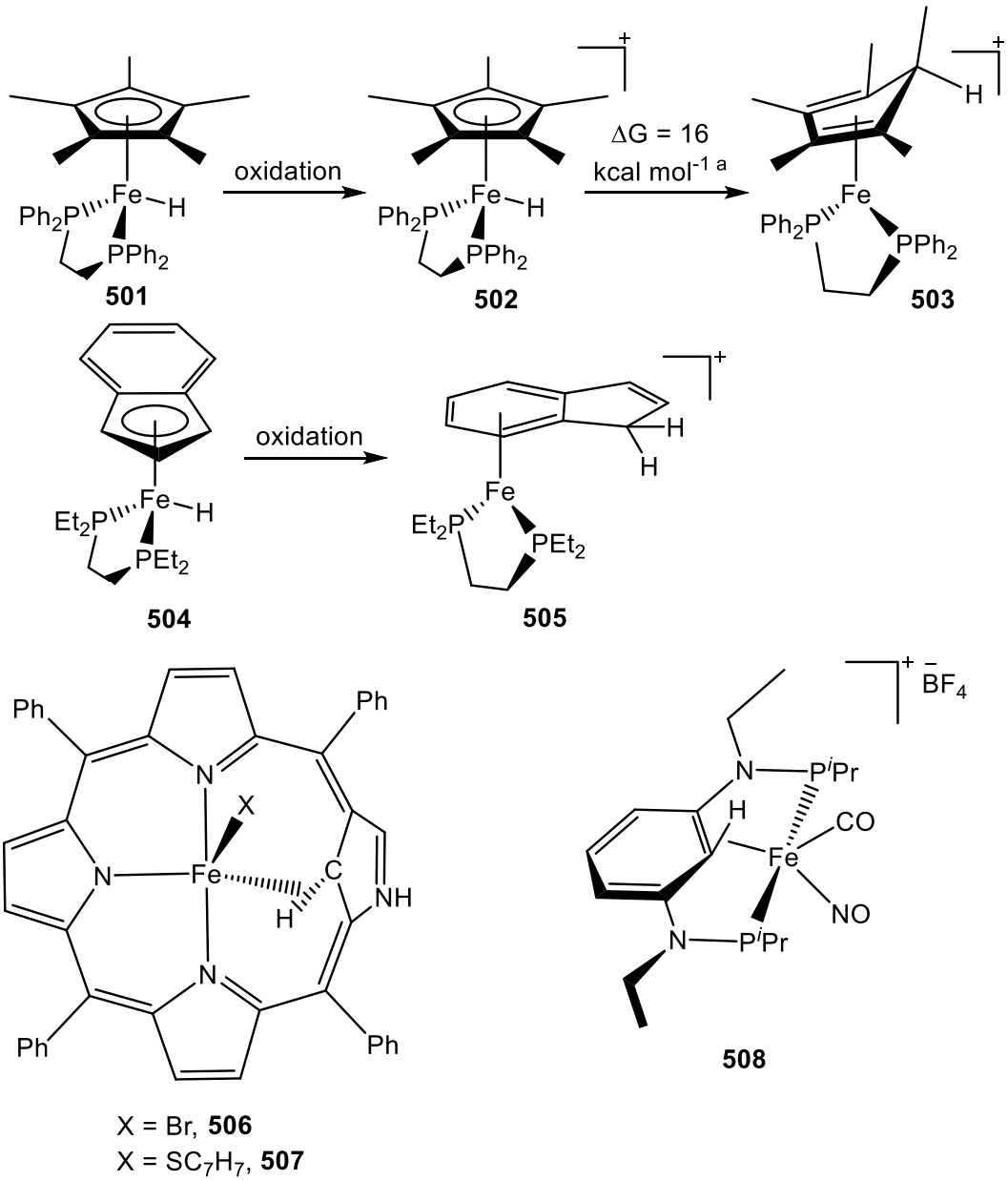

Scheme V-1. 1 e- Oxidation of Fe(II)-H complexes and reported examples containing agostic Fe-H-C. a: DFT calculation using ethyl substituent instead of phenyl

$Fe(PMe_3)_4$[190] or $FeMe_2(PMe_3)_4$[191] are commonly used iron reagents for the cyclometalation of PCP ligands. While processing this work, the activation the C-H bond of POCOP and PCP ligands with liquid $Fe(CO)_5$ under UV irradiation was developed.[192] C-Cl activation of **513** with solid $Fe_2(CO)_9$ was reported by Kirchner in 2018.[184] Carbonyl

iron(0) precursors have also been used to promote the C–H activation on a few Schiff bases ligands.[193,194] Solid $Fe_2(CO)_9$ was chosen for easy handling in this work.

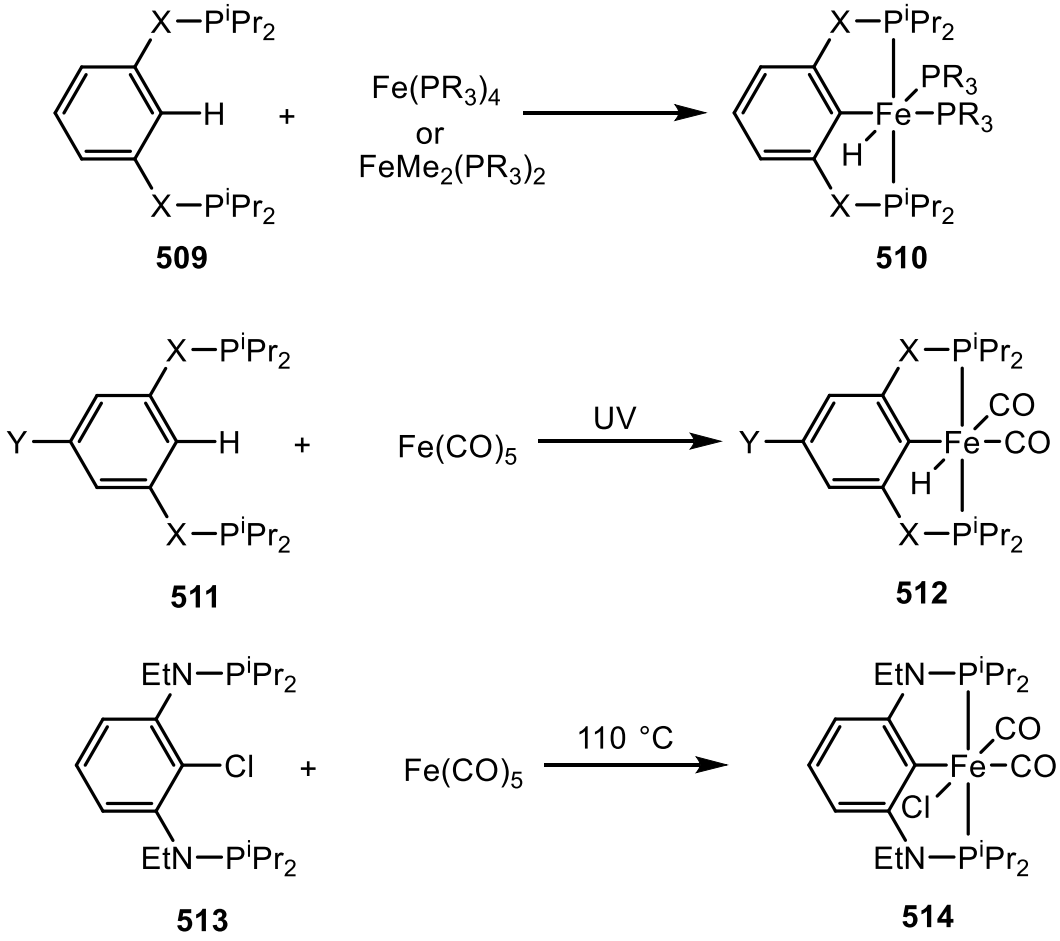

Scheme V-2. Cycloironation of PCP ligands**.**

5.2 Results and discussion

A suspension of $Fe_2(CO)_9$ and 1 equivalent **515** in toluene was loaded into a PPTE-air-tight Schlenk tube and irradiated with UV light for 2 days. The reaction was monitored by $^{31}P\{^1H\}$NMR spectrum where the signal of **515** at 9.8 ppm was converted into new signal at 110.3 ppm. Filtration followed by removing volatile of the filtrate gave 610 as light green powder. Recrystallization by slow diffusion of pentane into a saturated toluene

solution of the green powder yield **516** as green crystals (74%), which were good for X-ray analysis. **516** reacts with 1.1 equiv N-bromosuccinimide at room temperature to yield **517** within 30 min**.**

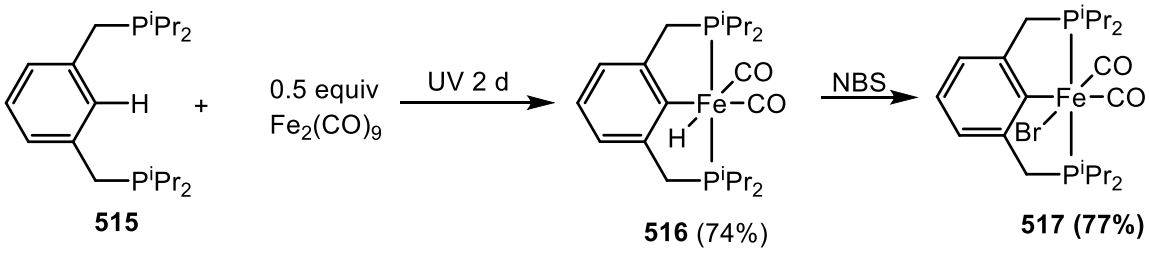

515 **516** (74%) **517 (77%)**

Scheme V-3. Synthesis and reactivity of **516.**

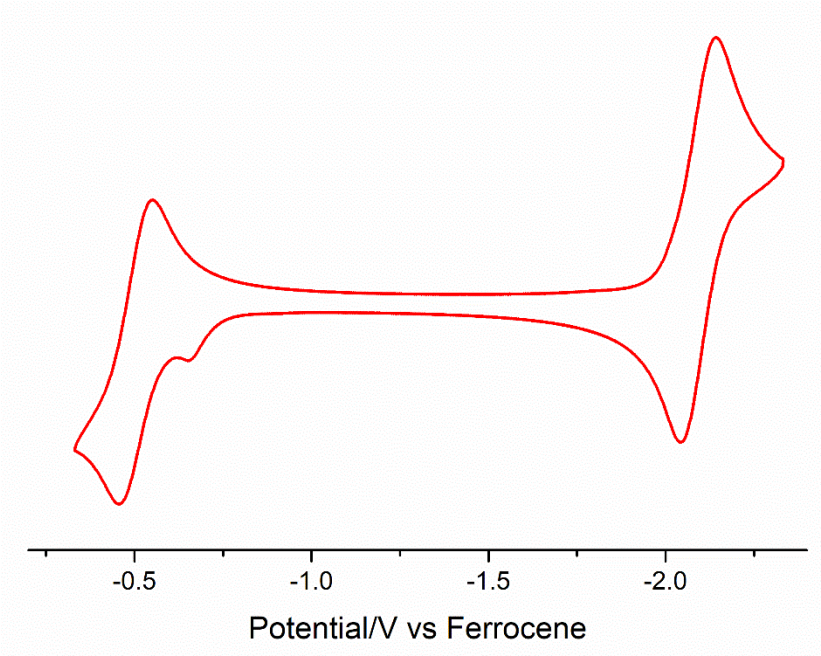

Figure V-1. Cyclic voltammogram of **516** in C_6H_5F at 27 ℃ with a scan rate of 50 mv in the negative direction, and was obtained with 0.1 M $[Bu_4N][BArF^{20}]$ as the supporting electrolyte.

Electrochemical study of **516** (**Figure V-1**) revealed two reversible redox events at -0.50 V (vs E[$Fe(Cp)_2$/$Fe(Cp)_2$]) and -2.09 V (vs E[$Fe(Cp)_2$/$Fe(Cp)_2$]), corresponding to 1 e^- oxidation and reduction of **516** respectively. Therefore $Fe(Cp)_2^+$ should be strong enough to oxidize **516** for the isolation and study of [Fe(III)-H]$^+$. **516** was barely soluble in CH_3CN, but upon addition of $[Fe(Cp)_2][CH_{12}B_{11}]$ (1.1 equiv) solution, the green crystals of **516** slowly dissolved and led to **518** accompanied with gas evolution. After removing the solvent, the oil was triturated with pentane to afford **518** as yellow powder, which was purified via recrystallization from PhF/pentane solution to give 63% isolation yield. The observation of gas evolution indicated isolation of [Fe(III)-H]$^+$ failed, which is not surprising due to the well-studied chemistry that oxidized metal hydride are often acidic and tend to protonate the original hydride and formed adducts with solvent after releasing H_2, especially in the presence of coordinating solvent such as CH_3CN.[195-197]

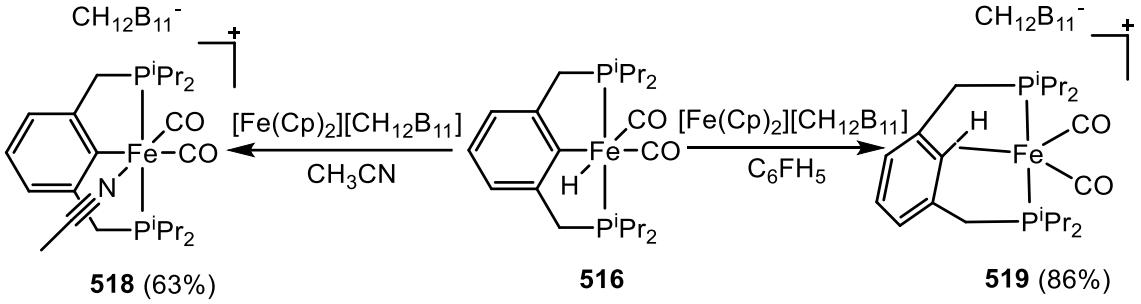

518 (63%) **516** **519** (86%)

Scheme V-4. 1 e^- oxidation of **516** in CH_3CN and C_6FH_5

Since the reversible oxidation wave of **516** was well established in CV study, we proposed the isolation of oxidation product can be accessed with non-coordinating solvent C_6H_5F. The treatment of **516** with 1.1 equiv of $[Fe(Cp)_2][CH_{12}B_{11}]$ in C_6H_5F yield a dark green solution with no gas evolution. We are also pleased that there is no ^{31}P NMR signal

either, which suggesting the protonation of **516** with oxidized **516** was prohibited in C_6H_5F. The dark green solid of **519** (86%) was obtained after removing C_6H_5F and trituration with pentane. Recrystallization of the dark green solid form C_6H_5F/pentane led to dark green crystals suitable for X-ray study.

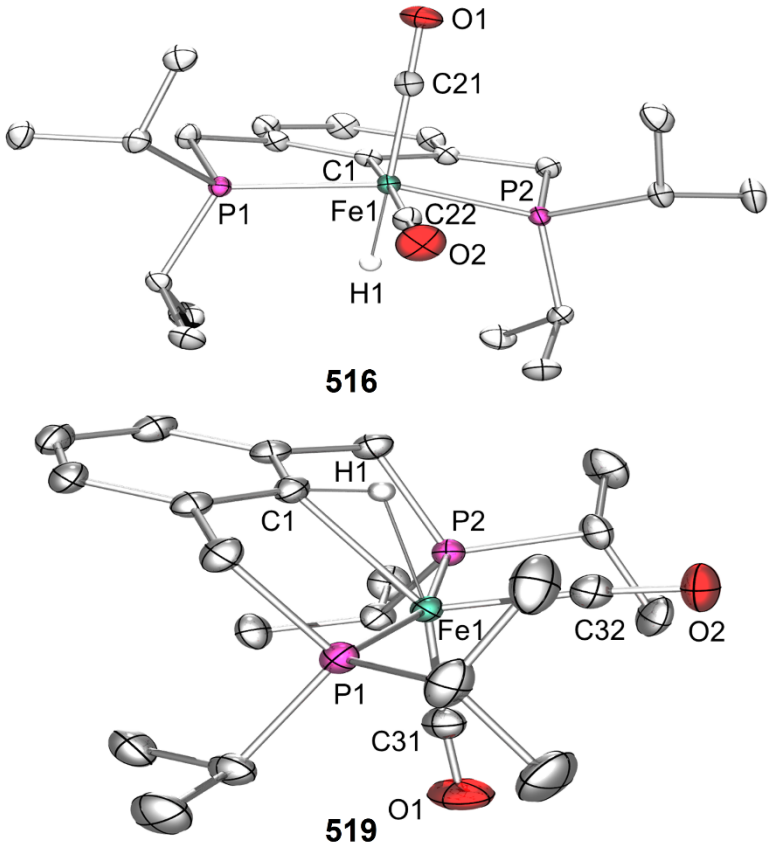

Figure V-2. ORTEP (50% probability ellipsoids) drawing of **516** and **519**. The hydrogen atoms (except the hydride in **516** and C_{aryl}-H in **519**), solvent molecules and anion in 519 are omitted for clarity.

The paramagnetic **519** exhibits a well-defined axial EPR spectrum (**Figure V-3**) where $g_{//} = 2.007$ and $g_{\perp} = 2.054$, of which values are close to free electron g values (g = 2.0023), and is consistent with 1 e^- oxidation process. However, surprisingly the expected $[Fe(III)\text{-}H]^+$ structure was not isolated according X-ray structural study (**Figure V-2**),

instead, C-H reductive elimination occurred to the oxidized Fe(III) center. Due to the coordination of two phosphine to the Fe(I) center, the aryl back bone was significantly displaced from the plane defined by two phosphine side arms in order to avoid strong repulsion between Fe(I) center and C_{aryl}-H bond. The geometry of **519** should be best described as square pyramidal (tau: 0.30), where one carbonyl was located in axial position, and PCHP and the other carbonyl ligands were situated in equatorial plane. The bond distance of the ipso-carbon and the Fe atom [2.2432(15) Å] is rather long when compared to Fe−C_{aryl} σ-bonds in **516** [2.0335(12) Å] but is comparable to the Fe-C_{aryl} in **508** [(2.258(1) Å)].[184] The Fe-CO distance (1.7714(16) Å) for the carbonyl *trans* to aryl C-H bond was slightly shorter than that (1.8139(16) Å) for the carbonyl trans to unpaired d-electron (empty site), indicating that unpaired d-electron is more trans influencing than the C_{aryl}-H in **519**. The Fe-H bond length (1.811(17) Å) as well as *ipso*-C_{aryl}-H-Fe bond angles (102(1) °) were comparable to the values of typical agostic structures (dM-H: 1.8 – 2.3 Å; C-H-M: 90 – 140 °).[198] The paramagnetism of **519** makes quantitative measurement of the agostic interaction by NMR problematic.

The molecular structure of **519** displayed a distorted octahedral coordination geometry as expected for a d_6-Fe(II) center, where two carbonyl ligands were situated *cis* to each other, and the Fe1-C21 distance [1.7773(13) Å] was almost identical to the Fe1-C22 distance [1.7734(14) Å] indicating very similar *trans* influence of hydride to aryl. The bond distances and angles around Fe(II) center in **516** are comparable to those in (POCOP)Fe$(CO)_2$H despite the difference in phosphine linker. So are the carbonyl

stretching frequencies (**516** appeared at 1968 and 1935 cm^{-1}, while (POCOP)Fe$(CO)_2$H appeared at 1980 and 1930 cm^{-1}).[191]

5.3 Conclusion

In this project, we described the synthesis of **516** with iron nonacarbonyl, which showed interesting redox properties. The novel **519** compound with agostic aryl C-H moieties was isolated via oxidation of **516**. Through the reactivity study of these (PCP)Fe complexes, it provided the fundamental understanding of aryl C-H activation on a PCP ligated Fe: where **519** with two carbonyl coordinated to a Fe(I) center was too electron deficient to oxidatively activate C-H bond, while electron rich Fe(0) upon coordination of two phosphine of **515** activated C-H bond to afford **516**.

5.4 Experimental section

5.4.1 General consideration

Unless otherwise specified, all reactions and manipulations were carried out under an argon atmosphere using glovebox or Schlenk line techniques. Solvents were dried and deoxygenated via the solvent purification system and stored over molecular sieves in the glove box filled with argon. C_6D_6 were dried over NaK /Ph_2CO/18-crown-6, distilled and stored over molecular sieves in an Ar-filled glove box. Fluorobenzene and C_6D_5Br were dried over CaH_2, distilled and stored over molecular sieves in an Ar-filled glove box. 1,3-bis(diisopropylphosphinomethyl)benzene (**PCP**, **515**),[199] and Ferrocenium 1-carbadodecaborate ($[Fe(Cp)_2[CHB_{11}H_{11}]$)[200] were synthesized according the previous procedures.

NMR spectra were recorded on a Varian iNova 300 spectrometer (^{1}H NMR, 299.951 MHz, ^{13}C NMR, 75.413 MHz, ^{31}P NMR, and 121.425 MHz). Chemical shifts are given in δ (ppm). ^{31}P NMR spectra were referenced externally with 85% phosphoric acid at δ 0. ^{1}H NMR and ^{13}C NMR spectra were referenced using residual protio solvent signals. Electrochemical studies were carried out using a CH Instruments Model 700D Series Electrochemical Analyzer/Workstation in conjunction with a three-electrode cell. The working electrode was a CHI 104 glassy carbon disc (3.0 mm diameter), and the auxiliary electrode a platinum wire. The reference electrode was Ag/AgCl electrode separated from the test solution by a fine porosity frit. CVs were conducted in solutions of fluorobenzene with 0.1 M $[Bu_4N][BArF^{20}]$ as supporting electrolyte at scan rates of 50 mV/s. The concentration of **516** was 0.001 M. CVs were referenced to the $Fe(\eta^5\text{-}C_5H_5)_2/Fe(\eta^5\text{-}C_5H_5)^{2+}$ redox couple. Electron paramagnetic resonance spectrum (**Figure V-3**) was recorded in a continuous wave X-band EleXsys EPR spectrometer at 288 K. Photochemical reactor used in the synthesis was manufactured by The Southern New England Ultraviolet Company equipped with 2537A° lamps (254 nm bulb). The temperature inside the reactor is approximately 60-70 ℃ without the fan.

5.4.2 Synthesis and characterization of Fe complexes

(PCP)Fe(CO)$_2$H (516) using Fe$_2$(CO)$_9$. A 75 mL PTFE-valved gas-tight quartz tube was charged with 0.186 g $Fe_2(CO)_9$ (0.50 mmol), 0.338 g **515** (1.0 mmol) and 25 ml toluene in the Glove-box [201]. The tube was degassed under vacuum, and was irradiated with UV for 2d. The light green solution was obtained and filtered through a pad of Celite. The solution was then concentrated and layered with pentane. Crystallization at -30 ℃

afforded **515** as dark green block crystals (0.331 g, 0.74 mmol, 74%). ^{1}H NMR (300 MHz, C_6D_6): δ 7.00 (m, 3H, Ar*H*), 3.13 (dvt, 2H, ArC*H*$_2$), 2.91 (dvt, 2H, ArC*H*$_2$), 2.00 (m, 2H, C*H*), 1.88 (m, 2H, C*H*), 1.20 (dd, *J* = 14.9, 7.1 Hz, 6H, C*H*$_3$), 1.06 (m, 12H, C*H*$_3$), 0.83(m, 6H, C*H*$_3$), -8.72 (t, 1H, $^{2}J_{P\text{-}H}$ = 50.4 Hz). ^{13}C NMR (75 MHz, C_6D_6): δ 217.3 (t, $^{2}J_{P\text{-}C}$ = 16.0 Hz, *C*O), 216.6 (t, $^{2}J_{P\text{-}C}$ = 16.0 Hz, *C*O), 172.8 (t, $^{2}J_{P\text{-}C}$ = 12.8 Hz, Ar*C*), 147.1 (t, $^{2}J_{P\text{-}C}$ = 10.3 Hz, Ar*C*), 123.1, 121.6 (t, $^{3}J_{P\text{-}C}$ = 7.6 Hz, Ar*C*), 39.5 (t, $^{1}J_{P\text{-}C}$ = 14.5 Hz, *C*H(CH$_3$)$_2$), 28.4 (t, 1H, $^{1}J_{P\text{-}C}$ = 9.3 Hz, Ar*C*H$_2$), 26.9 (t, $^{1}J_{P\text{-}C}$ = 14.5 Hz, *C*H(CH$_3$)$_2$), 19.0 (CH(*C*H$_3$)$_2$), 18.7 (CH(*C*H$_3$)$_2$), 18.6 (CH(*C*H$_3$)$_2$), 18.2 (CH(*C*H$_3$)$_2$) ppm. ^{31}P{^{1}H}NMR (121 MHz, C_6D_6): δ 110.3 (s) ppm. IR (KBr): 1968(s, CO), 1935(s, CO), 1881(w, Fe-H) cm^{-1}, EA (%) calcd for $FeC_{22}H_{36}O_2P_2$: C 58.68; H 8.06; found: C 58.62; H 8.13.

[(PCHP)Fe(CO)$_2$][CHB$_{11}$H$_{11}$] (519). In the Ar filled glove box, to a solution of ferrocenium 1-carbadodecaborate ($FcCHB_{11}H_{11}$, 135 mg, 0.30 mmol) in 5 ml PhF in a 25 ml Schlenk flask, a solution of **515** (135 mg, 0.30 mmol) in 2 ml PhF was added drop by drop. The light green solution of **515** turned dark green immediately upon addition. The clear solution was stirred for another 5 min, then the solvent was removed under vacuum to give a dark green oil. 15 mL (3×5 ml) pentane was added to wash away the ferrocene. The dark green solid was obtained after washing and redissolved in 3 ml PhF and filtered through a pad of Celite, and then the filtrate was layered with pentane. Slow diffusion at -35 ℃ resulted in 153 mg **519** as dark-green crystals (86%). IR (KBr): 1981(s, CO), 1917(s, CO), 1884(w, Fe-C-H) cm^{-1}. The EPR study reveals a well-defined axial spectrum of **519** (Figure V-3), where $g_{//}$ = 2.007 and $g_{\perp}$ = 2.054. The g values are close to free electron g values (g = 2.0023). Magnetic susceptibility was measured using Evans' method

(C_6D_5Br as a solvent at 22℃): μ_{eff} = 2.0 μ_B EA (%) calcd for $FeC_{23}H_{48}O_2P_2B_{11}$: C 46.56, H 8.15; found: 46.20, 8.20.

[(PCP)Fe(CO)$_2$CNCH$_3$][CH$_{12}$B$_{11}$] (518). A 50 mL culture tube was charged with 135 mg (0.30 mmol) **516** and 99 mg (0.030 mmol) Ferrocenium 1-carbadodecaborate ($FcCHB_{11}H_{11}$) and then 10 mL CH_3CN was added, the mixture bubbled for a few seconds to give a yellow solution. The resulting solution was further stirred for 1 h at room temperature before removing all the volatiles. The residual oil was washed with 15 mL pentane to afford yellow solid. The yellow compound was dissolved in PhF. Slow diffusion of pentane resulted in 120 mg **518** (63%) as yellow crystal. ^{1}H NMR (400 MHz, $CDCl_3$): δ 3.61 (m, 4H, ArC*H*$_2$), 2.54 (m, 4H, C*H*CH$_3$), 1.30 (m, 24H, CHC*H*$_3$) ppm. ^{13}C NMR (101 MHz, $CDCl_3$) δ 213.1 (t, $J_{P\text{-}C}$ = 25.9 Hz, *C*O), 208.6 (t, $J_{P\text{-}C}$ = 11.2 Hz,), 163.7 (t, $J_{P\text{-}C}$ = 8.9 Hz), 147.0 (t, $J_{P\text{-}C}$ = 7.7 Hz, Ar*C*), 130.8 (s, CH$_3$*C*N), 127.0(s, Ar*C*), 124.6 (t, $J_{P\text{-}C}$ = 7.3 Hz, Ar*C*), 51.9 (brs, 36.8 (d, $J_{P\text{-}C}$ = 13.7 Hz, Ar*C*H$_2$), 26.1 (t, $J_{P\text{-}C}$ = 9.0 Hz, *C*H(CH$_3$)$_2$), 26.0 (t, $J_{P\text{-}C}$ = 11.2 Hz, *C*H(CH$_3$)$_2$), 19.5 (s, CH(*C*H$_3$)$_2$), 19.3 (s, CH(*C*H$_3$)$_2$), 19.1 (s, CH(*C*H$_3$)$_2$), 5.0 (s, *C*H$_3$CN). ^{31}P{^{1}H} NMR (162 MHz, $CDCl_3$): δ 91.8 ppm. IR (KBr): 2017(s, CO), 1967(s, CO) cm^{-1}. EA (%) calcd for $FeC_{25}H_{50}NO_2P_2B_{11}$: C, 47.41; H, 7.96; N, 2.21; found: C, 47.53; H, 8.11; N, 2.23.

(PCP)Fe(CO)$_2$Br (517). A 25 ml Schlenk flask was charged with **516** (224 mg, 0.50 mmol), N-bromosuccinimide (90 mg, 0.55 mmol) and 10 ml toluene, the mixture was stirred for 30 min at R.T., then was filtered through a pad of silica gel. 10 ml PhF was used to wash the product through the silica gel, the solvent was removed under vacuum to give yellow powder, which can be recrystallized via cooling the saturated toluene solution in a

-35 ℃ freezer (204 mg, 77% yield). ^{1}H NMR (500 MHz, C_6D_6): δ 7.07 (m, 3H, Ar*H*), 3.56 (dvt, 2H, ArC*H*$_2$), 3.18 (dvt, 2H, ArC*H*$_2$), 3.10 (m, 2H, C*H*), 2.01 (m, 2H, C*H*), 1.23 (dvt, *J* = 7.3 Hz, 6H, C*H*$_3$), 1.03 (m, 18H, C*H*$_3$). ^{31}P{^{1}H} NMR (202 MHz, C_6D_6): δ 89.0 (s) ppm. ^{13}C{^{1}H} NMR (126 MHz, C_6D_6): δ 218.03 (t, $^{2}J_{P\text{-}C}$ = 25.4 Hz, *C*O), 213.05 (t, $^{2}J_{P\text{-}C}$ = 12.5 Hz, *C*O), 170.60 (t, $^{2}J_{P\text{-}C}$ = 12.7 Hz, Ar*C*), 148.47 (t, $^{2}J_{P\text{-}C}$ = 8.6 Hz, Ar*C*), 125.3 (s, Ar*C*), 123.00 (t, $^{3}J_{P\text{-}C}$ = 7.2 Hz, Ar*C*), 38.68 (t, $^{1}J_{P\text{-}C}$ = 14.7 Hz, Ar*C*H$_2$), 26.42 (t, $^{1}J_{P\text{-}C}$ = 9.4 Hz, *C*H(CH$_3$)$_2$), 26.39 (t, $^{1}J_{P\text{-}C}$ = 10.6 Hz, CH(*C*H$_3$)$_2$), 19.62 (s, CH(*C*H$_3$)$_2$), 19.38 (s, CH(*C*H$_3$)$_2$), 19.36 (s, CH(*C*H$_3$)$_2$). IR (KBr): 1995(s, CO), 1940(s, CO) cm^{-1}, EA (%) calcd for $FeC_{22}H_{35}O_2P_2Br$: C 49.93; H 6.67; found: C 50.28; H 6.61.

5.4.3 Electron paramagnetic resonance spectroscopy

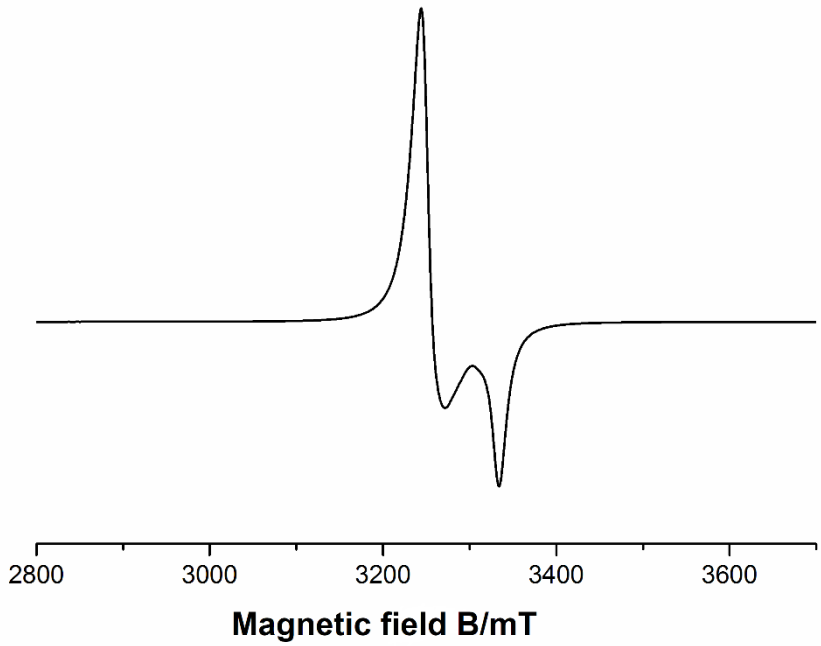

Figure V-3. The X-band EPR spectrum of **519** solid was recorded at 292 K with a microwave frequency of 9.38 GHz, microwave power 0.6 mW, and modulation width 1G. The spectrum was collected over multiple runs.

5.4.4 X-Ray structural determination details

X-Ray data collection, solution, and refinement for 516 (CCDC XXXX). A Leica MZ 75 microscope was used to identify a light green block of **516** with very well defined faces with dimensions (max, intermediate, and min) 0.20 x 0.26 x 0.34 mm^3 from a representative sample of crystals of the same habit. The crystal mounted on a nylon loop was then placed in a cold nitrogen stream (Oxford) maintained at 110 K. X-ray data were obtained on a Bruker APEXII CCD based diffractometer (Mo sealed X-ray tube, Kα = 0.71073 Å). All diffractometer manipulations, including data collection, integration and scaling were carried out using the Bruker APEX3 software. The absorption correction program SADABS was employed to correct the data for absorption effects. The space group was determined on the basis of systematic absences and intensity statistics and the structure was solved by direct methods and refined by full-matrix least squares on F^2. The structure was solved in the orthorhombic Pnma space group using XS (incorporated in SHELXLE/OLEX2).[146,147] All non-hydrogen atoms were refined with anisotropic thermal parameters. All hydrogen atoms were placed in idealized positions and refined using riding model. The structure was refined (weighted least squares refinement on F^2) and the final least-squares refinement converged.[146-148] No additional symmetry was found using ADDSYM incorporated in PLATON program.[149]

X-Ray data collection, solution, and refinement for [(PCHP)Fe(CO)$_2$]CHB$_{11}$H$_{11}$ (519) (CCDC XXXX). A Leica MZ 75 microscope was used to identify a dark green block of **519** with very well defined faces with dimensions (max, intermediate, and min) 0.25 x 0.15 x 0.05 mm^3 from a representative sample of

crystals of the same habit. The crystal mounted on a nylon loop was then placed in a cold nitrogen stream (Oxford) maintained at 110 K. X-ray data were obtained on a Bruker APEXII CCD based diffractometer (Mo sealed X-ray tube, Kα = 0.71073 Å). All diffractometer manipulations, including data collection, integration and scaling were carried out using the Bruker APEX3 software. The absorption correction program SADABS was employed to correct the data for absorption effects. The space group was determined on the basis of systematic absences and intensity statistics and the structure was solved by direct methods and refined by full-matrix least squares on F^2. The structure was solved in the orthorhombic Pnma space group using XS (incorporated in SHELXLE/OLEX2).[146,147] All non-hydrogen atoms were refined with anisotropic thermal parameters. All hydrogen atoms were placed in idealized positions and refined using riding model with the exception of the hydrogen bridged to iron and carbon which was located from the difference map. The structure was refined (weighted least squares refinement on F^2) and the final least-squares refinement converged.[146-148] No additional symmetry was found using ADDSYM incorporated in PLATON program.[149]

CHAPTER VI

DEHYDROGENATIVE DIBORATION OF ALKYNES CATALYZED BY IR/CO/^{T}BUNC SYSTEM*

6.1 Introduction

1,2-Diboration of alkynes (1,1-diboration of alkynes has also been reported)[202] is a reaction that produces 1,2-diborylalkenes,which are useful building blocks for the syntheses of polysubstituted alkenes.[96-99] It is typically conceived stoichiometrically as a formal addition of the B-B bond in a diborane across a triple bond of an alkyne.[203] The diborane usually carries heteroatom substituents on the borons, with the B_2pin_2 and B_2cat_2 being the most common reagents. This reaction has been catalyzed by a transition metal complexes such as Pt [78,103,104,204-208] or Cu,[105] by strong bases for certain substrates,[109] via organocatalysis,[110,111] and has even been shown to proceed without a catalyst for some diboranes.[109] An Ir catalyst for diboration using a B-B reagent has also been reported.[99]

* Reprinted with permission "Dehydrogenative Diboration of Alkyne Catalyzed by Ir/CO/^{t}BuNC System." Lai, Q; Ozerov, O.V. *J. Organomet. Chem.* **2021**, *931*, 121614. Copyright [2021] by the Elsevier B.V.

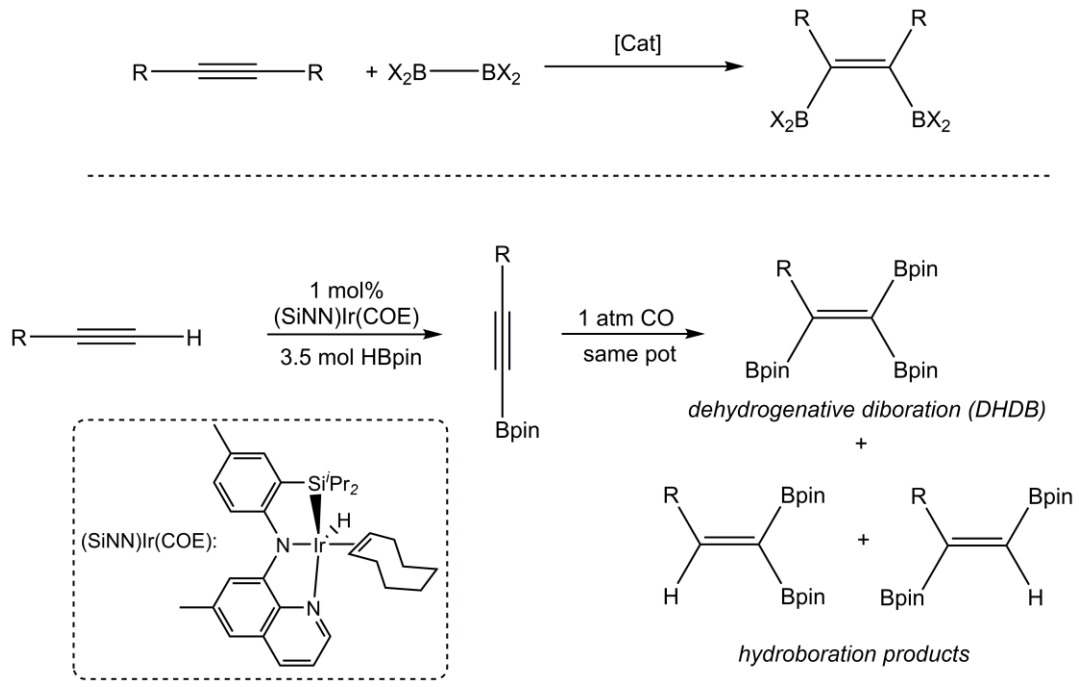

Scheme VI-1. Top: conventional diboration of alkynes with a B-B reagent. Bottom: dehydrogenative diboration of alkynylboronates with HBpin using a (SiNN)Ir catalyst.

In 2015, we reported on tandem catalysis of the conversion of terminal alkynes into triborylalkenes by the Ir complexes supported by the SiNN ligand.[113] The first step of the transformation is the dehydrogenative borylation of terminal alkynes (DHBTA), on which we and others extensively reported separately.[209-215] DHBTA results in the formation of alkynylboronates which are diborated in the second step to yield triborylalkenes by a (SiNN)Ir catalysts modified by the addition of CO. The unusual part of this reaction was that the diboration was not of a kind depicted at the top of Scheme VI-1 but instead used HBpin as the boron substrate and thus was net dehydrogenative. This is potentially an attractive alternative to the diboration with diboranes because it relies on a simpler boron starting material. We were not able to establish the mechanism by which this dehydrogenative diboration (DHDB) happens, but did isolate a

(SiNN)Ir(CO) complex which was itself a competent catalyst. The selectivity for the diboration was not perfect and competitive hydroboration also took place to some extent. Fortuitously, alkenes with three -Bpin substituents proved to be less soluble and were easily isolated by recrystallization out of mixtures containing tri- and diboryl alkenes.

We desired to explore whether an analogous DHDB can be applicable to alkynes other than alkynylboronates and also if the selectivity towards diboration could be improved. Although we intended to focus on the Ir complexes of the SiNN ligand, this report describes how it was discovered that the SiNN ligand was not necessary and that a simpler catalyst formulation was possible.

6.2 Results and discussion

6.2.1 Optimization of DHDB of 1-phenyl-1-butyne

We selected 1-phenyl-1-butyne as the test substrate to examine whether DHDB can be extended to internal, carbon-substituted alkynes. Application of 1% (SiNN)Ir(COE) as the catalyst under conditions similar to those we reported in 2015 resulted in the formation of the predominantly DHDB product along with two isomeric hydroboration products. Performing a control experiment with 1 mol% $[Ir(COD)Cl]_2$ as the catalyst (all molar percentages refer to the Ir content, not the molar amount of the dimeric precursor), we found that it furnished essentially the same product distribution. This was surprising because our control experiment with 5 mol% $[Ir(COE)_2Cl]_2$ in the 2015 paper led primarily to hydroboration and to little or no diboration products. The culprit in this instance was that 5 mol% Ir is a high catalyst loading and the introduction of CO via freeze-pump-thaw cycles takes some time (that the 2015 experiment did not

control for) after the mixing the alkyne, HBpin, and the Ir catalyst. Thus, it is possible to consume the reagents (primarily via hydroboration) before CO is properly introduced.

Having realized this, we examined a series of simple Ir precursors (**Table VI-1**) at 1 mol% Ir loading and taking care to minimize the exposure time prior to the introduction of CO. Except for $[Ir(COD)\ Br]_2$ and $[Ir(COD)\ I]_2$, all the entries in Table VI-1 resulted in approximately the same distribution of DHDB/hydroboration products. This suggests that the same active species was generated in entries 1, 2, and 5-7 and that implies that the anionic ligand attached to Ir in the precursor (Cl, OH, or OMe) was replaced with another. We hypothesize that the HBpin reagent undergoes metathesis with the Ir-O and Ir-Cl bonds to replace them with Ir-H or Ir-B, but that such metathesis is ineffective with Ir-Br or Ir-I.

Table VI-1. Alkyne diboration with different iridium precursors[a]

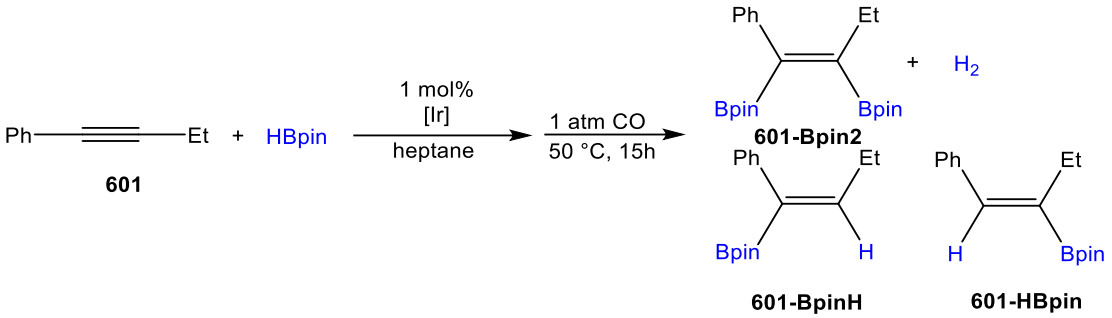

Entry	[Ir]	Yield of A1-Bpin2	Yield of A1-BpinH	Yield of A1-HBpin
1	(SiNN)IrCOE	77%	14%	7%
2	$[Ir(COD)Cl]_2$	74%	17%	7%
3	$[Ir(COD)Br]_2$	5%	85%	8%
4	$[Ir(COD)I]_2$	10%	75%	14%
5	$[Ir(COD)OH]_2$	71%	17%	10%
6	$[Ir(COD)OMe]_2$	72%	16%	10%
7	$[Ir(COE)_2Cl]_2$	76%	14%	8%

a. All reactions performed at 50 ℃ in heptane with 0.08 mmol 1-phenyl-1-butyne, 0.28 mmol HBpin, and 1 mol% catalyst loading under 1 atm CO. b. Yields were determined by ^{1}H NMR integration versus 1,4-dioxane as an internal standard.

We selected $[Ir(COD)Cl]_2$ for the next set of experiments aimed at improving the selectivity of the reaction towards DHDB. The results are summarized in Table VI-2. The selectivity for DHDB increased modestly but steadily as the polarity of the solvent decreased (entries 1-4, 9, 10). It was also noted that the selectivity increased with

increased pressure of CO (entries 4, 18, 19). We surmise that these two facts are related. CO is more soluble in less polar solvents[216] and thus the effective concentration of CO is influenced by both the nature of the solvent and by the CO pressure introduced into the reaction vessel. Increasing the reaction temperature (entries 4-6) decreased the selectivity for DHDB. Although CO solubility may increase with temperature,[217,218] it is possible that the binding of CO to Ir is less favorable at higher temperatures. Although we have not established the identity of the Ir species in the catalytic mixture, it seems reasonable to propose that DHDB requires binding of one or more CO ligands to Ir, and that the "last" CO binding to Ir is not bound very strongly, such that its concentration is affected by temperature, solvent polarity and CO pressure. Hydroboration does proceed without CO, and it may also proceed via species with CO bound to Ir, but with fewer CO ligands than may be required for DHDB.

The effect of other additives was also explored. Adding tricyclohexylphosphine or pyridine had a negligible effect on the outcome of the reaction (entries 12 and 13). The use of ^{t}BuNC *instead* of CO did not lead to any DHDB products (entry 18); however, the use of ^{t}BuNC *in addition to* CO resulted in the improvement of selectivity. Finally, it should be noted that performing the reaction in the presence of liquid mercury did not affect the outcome (entry 11), suggesting that the catalysis proceeds homogeneously.

Table VI-2. Summary of the optimization of alkyne diboration

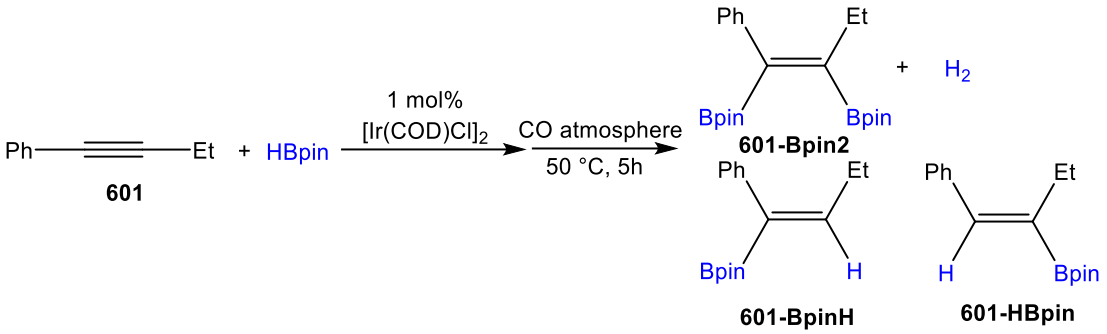

entry	Solvent	**601-Bpin2**/(**601-BpinH + 601-HBpin**)[b]	Additive	CO pressure
1	THF	42/58	none	1 atm
2	PhF	52/48	none	1 atm
3	toluene	57/43	none	1 atm
4	C_6D_6	59/41	none	1 atm
5	C_6D_6	70/16[e]	none	1 atm
6	C_6D_6	17/83[f]	none	1 atm
7	C_6D_6	N/A[g]	none	1 atm Ar
8	C_6D_6	0/0[h]	none	1atm
9	isooctane	69/31	none	1 atm
10	heptane	78/22	none	1 atm
11	C_6D_6	58/42	Hg drop	1 atm
12	C_6D_6	55/42	4 mol% P(*c*-$C_6H_{11})_3$	1 atm
13	C_6D_6	57/43	4 mol% pyridine	1 atm

Table VI-2 Continued

entry	Solvent	**601-Bpin2/(601-BpinH + 601-HBpin)**[b]	Additive	CO pressure
14	C_6D_6	65/35	1.1 mol% ^{t}BuNC	1 atm
15	C_6D_6	73/27	2.1 mol% ^{t}BuNC	1 atm
16	C_6D_6	75/25	4.1 mol% ^{t}BuNC	1 atm
17	heptane	86/14	3 mol% ^{t}BuNC	1 atm
18	C_6D_6	0/50	4.1 mol% ^{t}BuNC	1 atm Ar[c]
19	heptane	86/14	none	2 atm[d]
20	heptane	91/9	none	3 atm[d]
21	C_6D_6	59/41[i]	none	1 atm

a. All reactions performed at 50 ℃ with 0.08 mmol 1-phenyl-1-butyne, 0.28 mmol HBpin, and 1 mol% catalyst loading in a J. Y tube for 5 h. b. Yields were determined by ^{1}H NMR integration versus 1,4-dioxane as an internal standard. c. The reaction was conducted under 1 atm Ar instead of CO. d. The reaction was conducted in a top-screw capped schlenk flask. e. The reaction was performed at room temperature (25 ℃) for 3 d. f. The reaction was performed at 80 ℃. g. All of the alkyne was converted into a mixture of hydroboration, hydrogenation and other unidentified products. h. B_2Pin_2 was used as boron source. i. After all the **A1** was consumed, 1 mol % [Ir(COD)Cl] was loaded to the reaction mixture. Then the resulting mixture was degassed and back-filled with CO, then heated at 50 ℃ for 15 h.

6.2.2 Exploration of the scope of DHDB

Next, we examined the reaction of 1-phenyl-1-butyne with boranes other than HBpin (Table VI-3). The use of HBCat (entry 2) resulted in slightly less selectivity for DHDB, while the use of HBpng (entry 4) led to predominantly hydroboration, with only

9% of the DHDB product. Reactions with HBdan and HBdaz (entry 3&5) did not lead to any DHDB at all.

Table VI-3. DHDB with different boranes.

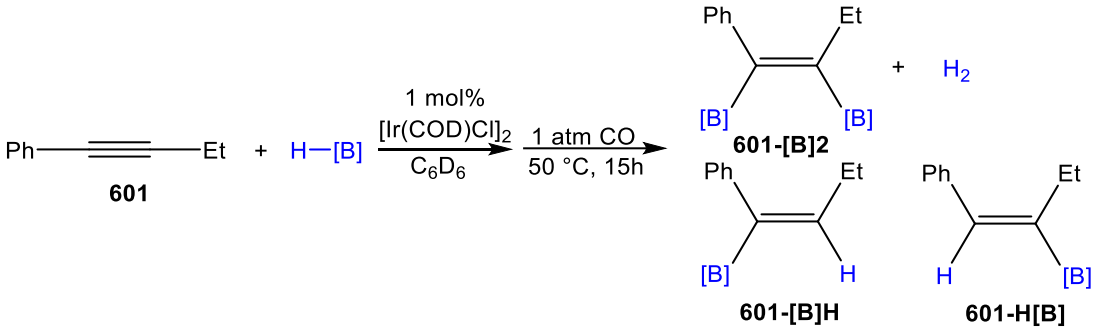

entry	H-[B] abbreviation	H-[B]	**601-[B]2**/(**601-[B]H + 601-H[B]**)	Alkyne conversion
1	HBpin	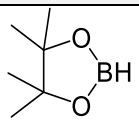	74/26	100%
2	HBcat	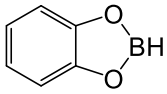	72/28	100%
3	HBdaz	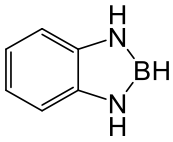	0/100	52%
4	HBpng	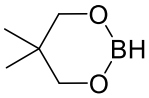	9/91	100%
5	HBdan	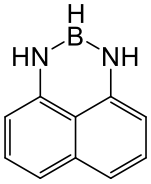	0/100	20%

The alkyne substrate scope of Ir/CO/tBuNC system was briefly examined and is outlined in table VI-4. Although lower temperature increased the DHDB selectivity, the reaction at RT was too slow, requiring days for completion. Because of this, we elected to perform the reactions at 50 ℃ and with 1 atm of CO for convenience. Heptane was used as solvent to improve CO solubility. It was found that alkyl- and aryl-substituted internal and terminal alkynes can be diborylated with HBpin to yield *cis*-diborylalkenes with modest to high selectivity. Bis(trimethylsilyl)acetylene did not engage in the reaction, possibly owing to the steric hindrance. The diboration products derived from A3 and A7 were easily isolated as pure white solids by removing the volatiles at the end of the reaction, followed by recrystallization from a toluene solution layered with pentane at -35 ℃. For terminal alkynes, the diboration products could be isolated by column chromatography.

Table VI-4. DHDB with different alkynes.[a]

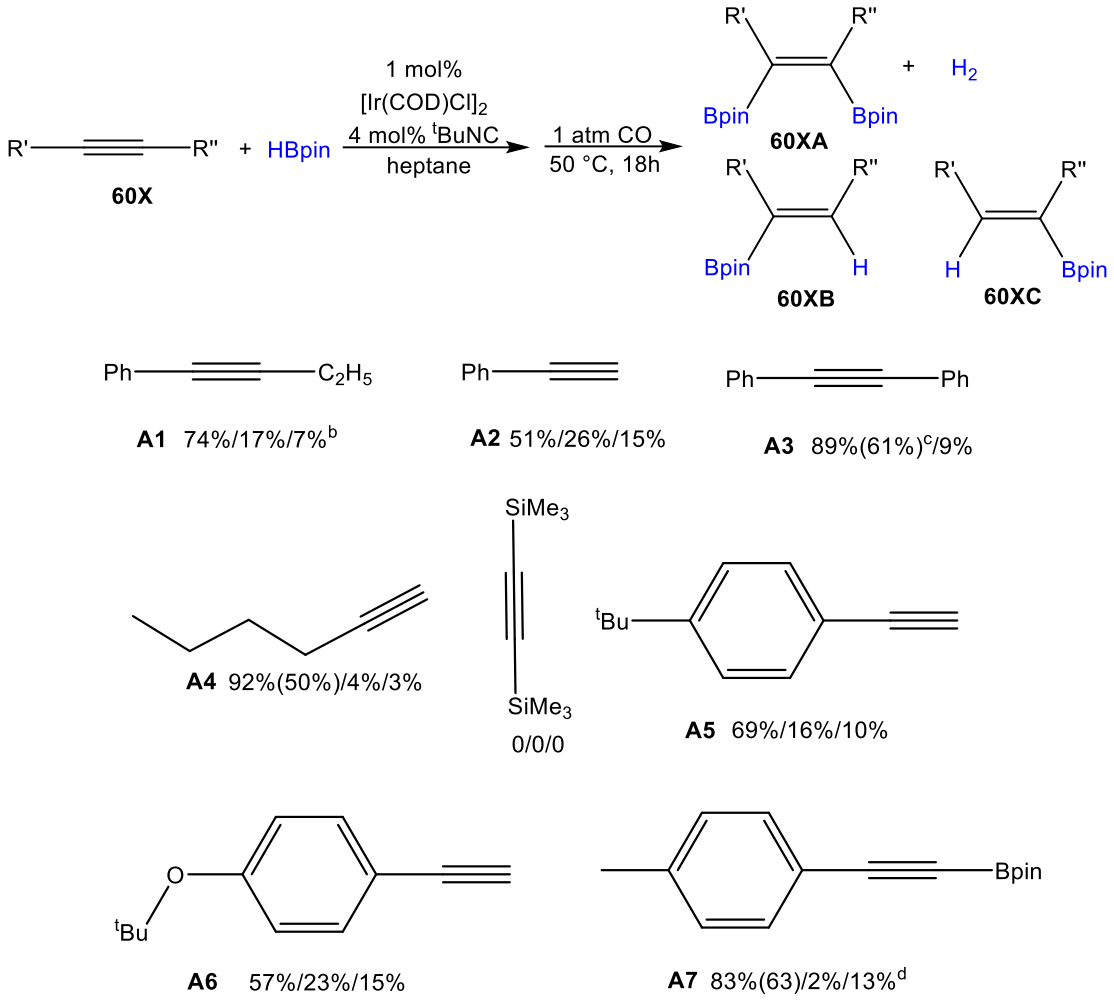

a. All the reaction performed at 50 ℃ with 0.08 mmol 1-phenyl-1-butyne, 0.28 mmol HBpin, and 1 mol% catalyst loading in a J. Y tube for 5 h b. Yields were determined by ^{1}H NMR integration versus 1,4-dioxane as an internal standard and were given in the following order: **A-Bpin2**/**A-BPinH**/**A-HBpin**. c. isolated yield in 2.0 mmol scale were given in parenthesis. d. without ^{t}BuNC.

6.3 Experimental section

6.3.1 General consideration

Unless otherwise specified, all reactions and manipulations were carried out under an argon atmosphere using glove box or Schlenk line techniques. Solvents were dried and deoxygenated via the solvent purification system and stored over molecular sieves in the

glove box filled with argon. Heptane, THF, toluene, C_6H_5F, C_6D_6 were dried over NaK /Ph_2CO/18-crown-6, distilled and stored over molecular sieves in an Ar-filled glove box. Fluorobenzene and C_6D_5Br were dried over CaH_2, distilled and stored over molecular sieves in an Ar-filled glove box. $[Ir(COD)Cl]_2$,[219] $[Ir(COD)Br]_2$,[220] $[Ir(COD)I]_2$,[221] $[Ir(COE)_2Cl]_2$,[222] $[Ir(COD)OH]_2$,[223] $[Ir(COD)OMe]_2$,[201] (SiNN)Ir(COE)[209] were prepared according to previous literature. Alkynes were deoxygenated by three freeze-pump-thaw cycles or dried under vacuum overnight prior transferring into an Ar-filled glove box. All other chemicals were used as received from commercial vendors. Benzodiazaborole (HBdaz),[55] neopentylglycolborane (HBnpg), and 1,8-naphthalenediaminatoborane (HBdan)[224] were prepared according to published procedures. NMR spectra were recorded on a Varian iNova 300 spectrometer (^{1}H NMR, 299.951 MHz, ^{13}C NMR, 75.413 MHz, ^{31}P NMR, and 121.425 MHz), Varian Inova 400 (^{1}H NMR, 399.535 MHz; ^{11}B NMR, 128.185 MHz) and NMRS 500 (^{1}H NMR, 499.703 MHz; ^{13}C NMR, 125.697 MHz) spectrometer. Chemical shifts are given in δ (ppm). ^{1}H NMR and ^{13}C NMR spectra were referenced using the solvent signals.

6.3.2 Precatalyst screening for DHDB of 1-phenyl-1-butyne with pinacolborane

A 64 μL stock solution of Ir catalyst (0.0125 M in C_6H_6, 0.00080 mol) was added to a J. Young tube. After removing C_6H_6 under vacuum, 11.3 μL 1-phenyl-1-butyne (0.080 mol), 42 μL pinacolborane (0.28 mol) and 450 μL heptane was loaded via syringe. The J. Young tube was degased via freeze-pump-thaw 3 cycles, and then refilled with 1 atm CO. the resulting mixture was heated in 50 ℃ for 15 h. The solvent was removed under vacuum and 500 μL 0.08 M 1,4-dioxane in C_6D_6 was added. The yields of the diboration and

hydroboration products were determined via ^{1}H NMR analysis (500 MHz, C_6D_6, Entry 2 is shown as an example). Diboration product **601-Bpin2**:[225] δ 7.35 – 7.33 (m, Ph*H*, 2H), 7.18 (t, $J_{H\text{-}H}$ = 7.7 Hz, Ph*H*, 2H), 7.03 (tt, $J_{H\text{-}H}$ = 7.2, 1.4 Hz, Ph*H*, 1H), 2.42 (q, $J_{H\text{-}H}$ = 7.5 Hz, C*H*$_2$CH$_3$, 2H), 1.17 (s, Bpin*H*, 12H), 1.13 (t, $J_{H\text{-}H}$ = 7.5 Hz, CH$_2$C*H*$_3$, 3H). 1.12 (s, Bpin*H*, 12H). Hydroboration product **601-BpinH**: δ 7.39 – 7.37 (m, PhH, 2H) 7.24 (t, $J_{H\text{-}H}$ = 7.7 Hz, Ph*H*, 2H), 7.12 (t, $J_{H\text{-}H}$ = 7.7 Hz, Ph*H*, 1H) 6.96 (t, $J_{H\text{-}H}$ = 7.3 Hz, PhCC*H*, 1H), 2.16 (p, $J_{H\text{-}H}$ = 7.5 Hz, C*H*$_2$CH$_3$, 2H), 1.06 (s, Bpin*H*, 12H), 0.84 (t, $J_{H\text{-}H}$ = 7.5 Hz, CH$_2$C*H*$_3$, 3H); The reason we assigned the resonances to **601-BpinH** is that for compound **601-BpinH** the ethyl CH_2 proton would couple to both the CH_3 proton and alkenyl protons, thus giving rise to a quintet instead of quartet resonances for the CH_2 protons, and triplet instead of singlet resonance for the alkenyl proton.[226] The assignment was also consistent with other reactions that afford different **601-BpinH**/**601-HBpin** ratios. Hydroboration product **601-HBpin**: δ 2 Ph*H* resonances are overlapping with product **601-Bpin2**, 7.72 (s, PhC*H*C, 1H), 7.08 (t, $J_{H\text{-}H}$ = 7.4 Hz, 1H), 1.4 Hz, Ph*H*, 1H), 2.65 (q, $J_{H\text{-}H}$ = 7.6 Hz, C*H*$_2$CH$_3$, 2H), 1.27 (t, $J_{H\text{-}H}$ = 7.5 Hz, CH$_2$C*H*$_3$, 3H), 1.12 (s, Bpin*H*, 12H);

6.3.3 Solvent screening for DHDB of 1-phenyl-1-butyne with pinacolborane

A 64 μL stock solution of [Ir(COD)Cl]$_2$ (0.0125 M in C_6H_6, 0.00080 mol) was added to a J. Young tube. After the benzene was removed under vacuum, 11.3 μL 1-phenyl-1-butyne (0.080 mol), 42 μL pinacolborane (0.28 mol) and 450 μL solvent was loaded via syringe. The J. Young tube was degased through freeze-pump-thaw 3 cycles, and then refilled with 1 atm CO. the resulting mixture was heated in 50 ℃ for 15 h. The solvent was removed under vacuum and 500 μL 0.08 M 1,4-dioxane in C_6D_6 was added.

The yields of the diboration and hydroboration products were determined via ^{1}H NMR analysis.

6.3.4 Control experiments

6.3.4.1 Reaction of 1-phenyl-1-butyne with bis(pinacolato)diboron catalyzed by [Ir(COD)Cl]$_2$ at 1 atm CO

To a J. Young tube, 32 μL stock solution of [Ir(COD)Cl]$_2$ (0.0125 M in C_6D_6, 0.00040 mol), 140 μL stock solution of B_2Pin_2 (1.0 M in C_6D_6, 0.28 mol), and 160 μL stock solution of 1-phenyl-1-butyne/1,4-dioxane ([alkyne]: 0.5 M in C_6D_6, 0.080 mol; 1,4-dioxane: 0.25 M in C_6D_6 as internal standard) were loaded via syringe. The J. Young tube was degassed by 3 cycles of freeze-pump-thaw, and then back filled with 1 atm CO. No reaction between alkyne and boron reagents after the tube was heated in 50 ℃ for 15 h.

6.3.4.2 Reaction of 1-phenyl-1-butyne with pinacolborane catalyzed by [Ir(COD)Cl]2 at 1 atm Ar

To a J. Young tube, 32 μL stock solution of [Ir(COD)Cl]$_2$ (0.0125 M in C_6D_6, 0.00040 mol), 280 μL stock solution of borane (1.0 M in C_6D_6, 0.28 mol), and 160 μL stock solution of 1-phenyl-1-butyne/1,4-dioxane ([alkyne]: 0.5 M in C_6D_6, 0.080 mol; 1,4-dioxane: 0.25 M in C_6D_6 as internal standard) were loaded via syringe. The resulting mixture was heated in 50 ℃ for 18 h. No diboration product A2-Bpin$_2$ was detected by ^{1}H NMR spectroscopy.

6.3.4.3 Reaction of 1-phenyl-1-butyne with pinacolborane catalyzed by [Ir(COD)Cl]2 at 1 atm CO, where additional 0.5% [Ir(COD)Cl]2 was added after all the alkyne was converted into diboration and hydroboration products

To a J. Young tube, 32 μL stock solution of $[Ir(COD)Cl]_2$ (0.0125 M in C_6D_6, 0.00040 mol), 32 μL stock solution of ^{t}BuNC (0.0500 M in C_6D_6, 0.0016 mol), 240 μL stock solution of borane (1.0 M in C_6D_6, 0.24 mol), and 160 μL stock solution of 1-phenyl-1-butyne/1,4-dioxane ([alkyne]: 0.5 M in C_6D_6, 0.080 mol; 1,4-dioxane: 0.25 M in C_6D_6 as internal standard) were loaded via syringe. The J. Young tube was degased via freeze-pump-thaw 3 times, and then refilled with 1 atm CO. The resulting mixture was heated in 50 ℃ for 15 h. The yields of the diboration and hydroboration products were determined via ^{1}H NMR analysis.

6.3.5 ^{t}BuNC-assisted DHDB of 1-phenyl-1-butyne

To a J. Young tube, 32 μL stock solution of $[Ir(COD)Cl]_2$ (0.0125 M in C_6D_6, 0.00040 mol), 32 μL stock solution of ^{t}BuNC (0.0500 M in C_6D_6, 0.0016 mol), 240 μL stock solution of borane (1.0 M in C_6D_6, 0.24 mol), and 160 μL stock solution of 1-phenyl-1-butyne/1,4-dioxane ([alkyne]: 0.5 M in C_6D_6, 0.080 mol; 1,4-dioxane: 0.25 M in C_6D_6 as internal standard) were loaded via syringe. The J. Young tube was degased via freeze-pump-thaw 3 times, and then refilled with 1 atm CO. The resulting mixture was heated in 50 ℃ for 15 h. The yields of the diboration and hydroboration products were determined via ^{1}H NMR analysis.

6.3.6 Borane substrate scope for DHDB of 1-phenyl-1-butyne

6.3.6.1 General procedure

To a J. Young tube, 64 μL stock solution of $[Ir(COD)Cl]_2$ (0.0125 M in C_6D_6, 0.00080 mol), 280 μL stock solution of borane (1.0 M in C_6D_6, 0.28 mol), and 160 μL stock solution of 1-phenyl-1-butyne/1,4-dioxane ([alkyne]: 0.5 M in C_6D_6, 0.080 mol; 1,4-dioxane: 0.25 M in C_6D_6 as internal standard) were loaded via syringe. The J. Young tube was degassed via freeze-pump-thaw 3 times, and then refilled with 1 atm CO. The resulting mixture was heated in 50 ℃ for 15 h. The yields of the diboration and hydroboration products were determined via ^{1}H NMR analysis.

6.3.6.2 Selected NMR data for the products and other reaction observations

HBcat as boron source: **601-Bcat2**: δ 7.31 – 7.29 (m, aromatic*H*, 2H), 7.19 (t, J_{H-H} = 7.7 Hz, aromatic*H*, 2H), 7.08 (tt, J_{H-H} = 7.2, 1.4 Hz, aromatic*H*, 1H) 6.93 (dd, J_{H-H} = 5.8, 3.3 Hz, Bcat*H*, 2H), 6.85 (dd, J_{H-H} = 5.9, 3.4 Hz, Bcat*H*, 2H), 6.76 (dd, J_{H-H} = 5.9, 3.3 Hz, Bcat*H*, 2H), 6.70 (dd, J_{H-H} = 5.9, 3.2 Hz, Bcat*H*, 2H), 2.49 (q, J_{H-H} = 7.6 Hz, C*H*$_2$CH$_3$, 2H), 1.06 (t, J_{H-H} = 7.6 Hz, CH$_2$C*H*$_3$, 3H). **601-BcatH**: δ aromatic resonances (aromatic*H*) of **601-BcatH** cannot be differentiated from that of **601-HBcat**, 2.11 (p, J_{H-H} = 7.5 Hz, C*H*$_2$CH$_3$, 2H), 0.83 (t, J_{H-H} = 7.5 Hz, CH$_2$C*H*$_3$, 3H). **601-HBcat**: δ aromatic resonances of **601-HBcat** cannot be differentiated from that of **601-BcatH**, 7.82 (s, ArC*H*C, 1H), 2.65 (q, J_{H-H} = 7.6 Hz, C*H*$_2$CH$_3$, 2H), 1.23 (t, J_{H-H} = 7.5 Hz, CH$_2$C*H*$_3$, 3H).

HBdaz as boron source: around 52% alkyne was converted into a mixture of unidentified products.

HBnpg as boron source: **601-BnpgH**: δ 7.31 – 7.25 (m, aromatic*H*, 2H), 7.29 – 7.15 (m, aromatic*H*, 2H), 7.14 – 7.08 (m, aromatic*H*, 1H), 6.87 (t, *J* = 7.3 Hz, ArCC*H*, 1H), 3.26 (s, BnpgCH_2, 4H), 2.09 (p, *J* = 7.5, CH_2CH$_3$, 2H), 0.84 (t, *J* = 7.5 Hz, CH$_2$CH_3, 3H), 0.52 (s, BnpgCH_3, 6H). **601-HBnpg**: δ 7.65 (s, ArC*H*C, 1H), 7.39 – 7.30 (m, aromatic*H*, 2H), 7.08 – 7.01 (m, aromatic*H*, 2H), 3.32 (s, BnpgCH_2, 4H), 2.62 (q, *J* = 7.4 Hz, CH_2CH$_3$, 2H), 1.24 (t, *J* = 7.5 Hz, CH$_2$CH_3, 3H), 0.51 (s, BnpgCH_3, 6H). Around 91% of hydroboration products were formed. Due to the difficulties on purification of HBnpg as well as low diboration yield, no further study was conducted using this boron source.

HBdan as boron source: **601-BdanH**: 6.75 (t, *J* = 7.3 Hz, ArCC*H*, 1H), 6.01 (dd, *J* = 6.3, 2.0 Hz, Bdan*H*, 2H), 1.99 (p, *J* = 7.4 Hz, CH_2CH$_3$, 2H), 0.86 (t, *J* = 7.5 Hz, CH$_2$CH_3, 3H). **601-HBdan**: δ 6.05 (dd, *J* = 5.9, 2.5 Hz, Bdan*H*, 2H), 2.21 (q, *J* = 8.4 Hz, CH_2CH$_3$, 2H). With only 20% of the alkyne was converted, alkenyl proton resonances of hydroboration product **601-HBdan** could be overlapped with aromatic proton resonances, which make it difficult to conclude whether **601-HBdan** or **601-Bdan2** is formed. However, based on the ratio of CH_2 resonance to Bdan resonance (1:1), it is more likely the hydroboration product **601-HBdan** (9%). According to the coupling between alkenyl proton and ethyl CH_2 proton in **601-BdanH**, it would be reasonable to claim that 11% of **601-BdanH** was formed. Therefore, for this borane no DHDB product was formed.

6.3.7 Alkyne substrate scope of DHDB

6.3.7.1 General procedure

To a J. Young tube, 20 μL stock solution of [Ir(COD)Cl]$_2$ (0.010 M in C_6D_6, 0.00020 mol), 40 μL stock solution of ^{t}BuNC (0.040 M in C_6D_6, 0.00160 mol), 44 μL

(0.30 mol) HBpin, 0.1 mmol of alkyne and 400 μL isooctane were loaded via syringe in the Glove box. The J. Young tube was degased via freeze-pump-thaw 3 cycles, and then refilled with 1 atm CO. The resulting mixture was heated in 50 ℃ for 15 h. The yield of diboration and hydroboration was revealed by ^{1}H NMR analysis.

6.3.7.2 Selected product data

602-Bpin2: ^{1}H NMR (500 MHz, C_6D_6): δ 7.65-7.63 (m, Ar*H*, 2H), 7.13 (t, $J_{H\text{-}H}$ = 7.6 Hz, Ar*H*, 2H), 7.00 (m, Ar*H*, 1H), 6.63 (s, ArCC*H*, 1H), 1.23 (s, Bpin*H*, 12H), 1.12 (s, Bpin*H*, 12H).

605-Bpin2: ^{1}H NMR (500 MHz, C_6D_6): δ 7.65-7.64 (m, Ar*H*, 2H), 7.23-7.22 (m, Ar*H*, 2H), 6.69 (s, ArCC*H*, 1H), 1.27 (s, Bpin*H*, 12H), 1.17 (s, ^{t}Bu*H*, 9H), 1.13 (s, Bpin*H*, 12H).

606-Bpin2: ^{1}H NMR (500 MHz, C_6D_6): δ 7.60-7.59 (m, Ar*H*, 2H), 6.93-6.91 (m, Ar*H*, 2H), 6.61 (s, ArCC*H*, 1H), 1.26 (s, Bpin*H*, 12H), 1.16 (s, ^{t}Bu*H*, 9H), 1.13 (s, Bpin*H*, 12H).

6.3.8 Preparative-scale of DHDB

6.3.8.1 General procedure

To a 25 mL PTFE-valved gas-tight flask, 6.7 mg (0.01 mmol) $[Ir(COD)Cl]_2$, 11 μL (0.08 mmol) ^{t}BuNC, 2.0 mmol alkyne and 871 μL (6.0 mmol) HBpin was loaded in an Argon-filled glove box. The flask was taken out of the box and degassed via freeze-pump-thaw 3 times, and then refilled with 1 atm CO. The resulting mixture was heated in 50 ℃ for 15 h. The flask was transferred to the box, and the volatile was removed under vacuum. The diboration product was then isolated by the following methods. For **603** and **607**: the

residue was dissolved with toluene and filtered through a short pad of Celite. Toluene solution was concentrated and then layered with pentane. Crystalline solid **603-Bpin2** and **607-Bpin2** were collected after slow diffusion overnight at -35 ℃ freezer. For **604**: **604-Bpin2** was purified by chromatography on silica gel with 2:1 hexane:acetone.

6.3.8.2 Product yields and NMR data

603-Bpin2: white solid, isolated yield: 528 mg (61%) ^{1}H NMR (500 MHz, $CDCl_3$) δ 7.01-7.08 (m, 6H, Ar*H*), 6.95-6.96 (m, 4H, Ar*H*), 1.32 (s, 24H, Bpin C*H*$_3$). ^{13}C NMR (125 Hz, $CDCl_3$) δ 141.38, 129.43, 127.53, 125.90, 84.17, 25.00. HR-MS [113] calcd for $C_{26}H_{35}B_2O_4$: 433.2716; found 433.2709. The NMR data were consistent with literature values.[103]

607-Bpin2: white solid, isolated yield: 622 mg (63%) ^{1}H NMR (500 MHz, $CDCl_3$) δ 7.18 (d, $^{3}J_{H\text{-}H}$ = 8.1 Hz, 2H, Ar*H*), 7.03 (d, *J* = 7.8 Hz, 2H, Ar*H*) 2.29 (s, 3H, ArC*H*$_3$), 1.30 (s, 12H, BpinC*H*$_3$), 1.27 (s, 12H, BpinC*H*$_3$), 1.10 (s, 12H, BpinC*H*$_3$). ^{13}C NMR (125 Hz, $CDCl_3$) δ 142.41, 136.36, 128.44, 127.75, 83.90, 83.47, 83.22, 25.02, 24.94, 24.64, 21.31. HR-MS calcd for $C_{27}H_{44}B_3O_6$: 496.3448; found 496.3405.The NMR data were consistent with literature values.[113]

604-Bpin2: colorless oil, yield: 340 mg (50%); ^{1}H NMR (500 Hz, $CDCl_3$) δ 0.87 (t, $^{3}J_{H\text{-}H}$ = 6.8 Hz, 3H), 1.26 (s, 12H, BpinC*H*$_3$), 1.31 (s, 12H, BpinC*H*$_3$), 1.19-1.31 (m, 6H), 1.34-1.45 (m, 2H), 2.21 (t, $^{3}J_{H\text{-}H}$ = 7.1Hz, 2H), 5.85 (s, 1H). ^{13}C NMR (125 Hz, $CDCl_3$) δ 83.72, 83.35, 39.67, 30.91, 25.03, 25.00, 22.56, 14.10. HR-MS [113] calcd for $C_{18}H_{35}B_2O_4$: 337.2716; found 337.2708. The NMR data were consistent with literature values.[103]

6.4 Conclusion

We have expanded the substrate scope of Ir-catalyzed dehydrogenative diboration (DHDB) to non-alkynylboronate alkynes from an earlier report utilizing (SiNN)Ir complexes. In the present work, we discovered that the SiNN pincer ligand is not required and that a precatalyst as simple as $[Ir(COD)_2Cl]_2$ can be used under the right conditions. The DHDB reaction is in competition with hydroboration which is also catalyzed by Ir. Although hydrogen is presumably produced as a result of DHDB, hydrogenation of the carbon-carbon double or triple bonds was not observed. For some substrates, the selectivity for DHDB was as high as 9:1. A variety of terminal or internal alkynes produced diboration products under optimized conditions and some diboration products were isolated in a pure form. Although we did not pursue the characterization of the Ir compounds present in the catalytic reaction mixture, the experimental data suggest that DHDB is favored by increasing competitive coordination of CO to Ir.

CHAPTER VII

CONCLUSIONS

Synthesis of a new tripodal alane/tris(phosphine) ligand (**207**) based on 2-(diisopropylphosphino)pyrrole, and AlP_3-supported Ni complexes are reported. The central tris(pyrrolyl)aluminum moeity acts as a stronger Lewis acid towards Ni that other related group 13 element-centered tripodal ligands, as demonstrated by the binding of H_2 to Ni and ease of reduction.

Reactions of the AlP_3 ligand with AgOTf and Ag^+ do not lead to a well-defined Ag→Al bond. Instead, Al manages to abstract either the triflate anion or one of the phosphine donors away from silver. This reinforces the notion that monovalent silver is not a good partner for Z-type ligands. Employing a stronger Lewis acid such as in AlP_3 causes the Al center to seek alternatives to Ag as a Lewis basic partner, even in spite of the significant structural preorganization favouring a direct silver-aluminum contact.

The synthesis of PAlP and PBP pincer complexes of Rh possessing a central bis(N-pyrrolyl)aluminyl or -boryl unit was developed. Complex $(PAl^{py}P)Rh(CO)_2$ (**403**) possesses an aluminyl site stabilized by coordination of pyridine, resulting in a four-coordinate Al. Attempts to the three-coordinate aluminyl by abstraction of pyridine with $BF_3{\cdot}Et_2O$ unexpectedly led to the B/Al metathesis with the preservation of the pincer structure in the product $(PBP)Rh(CO)_2$ (**405**). Abstraction of pyridine was carried out using $B(C_6F_5)_3$, but the desired $(PAlP)Rh(CO)_2$ (**404**) underwent dimerization via

isocarbonyl bridging, reflecting the elevated Lewis acidity of the N-pyrrolyl-substituted aluminyl.

We managed to synthesize **510** via cyclometalation of PCP ligand with iron nonacarbonyl. 1 e^- oxidation of **510** in non-coordinating solvent results in **513**, which show weak C_{aryl}-H-Fe interaction. While 1 e^- oxidation of **510** in coordinating solvent results in **512** accompanied by H_2 releasing.

We have expanded the substrate scope of Ir-catalyzed dehydrogenative diboration (DHDB) to non-alkynylboronate alkynes from an earlier report utilizing (SiNN)Ir complexes. In the present work, we discovered that the SiNN pincer ligand is not required and that a precatalyst as simple as $[Ir(COD)_2Cl]_2$ can be used under the right conditions. The DHDB reaction is in competition with hydroboration which is also catalyzed by Ir. Although hydrogen is presumably produced as a result of DHDB, hydrogenation of the carbon-carbon double or triple bonds was not observed. For some substrates, the selectivity for DHDB was as high as 9:1. A variety of terminal or internal alkynes produced diboration products under optimized conditions and some diboration products were isolated in a pure form. Although we did not pursue the characterization of the Ir compounds present in the catalytic reaction mixture, the experimental data suggest that DHDB is favored by increasing competitive coordination of CO to Ir.

REFERENCES

(1) Moulton, C. J.; Shaw, B. L. Transition Metal–carbon Bonds. Part XLII. Complexes of Nickel, Palladium, Platinum, Rhodium and Iridium with the Tridentate Ligand 2,6-bis[(di-t-butylphosphino)methyl]phenyl. *Journal of the Chemical Society, Dalton Transactions* **1976**, 1020-1024.

(2) Morales-Morales, D.; Jensen, C. G. *The Chemistry of Pincer Compounds*; Elsevier, 2011.

(3) Crabtree, R. H. General Properties of Organometallic Complexes. *In The Organometallic Chemistry of the Transition Metals*, 2005, 29-52.

(4) Zhang, J.; Leitus, G.; Ben-David, Y.; Milstein, D. Facile Conversion of Alcohols into Esters and Dihydrogen Catalyzed by New Ruthenium Complexes. *J Am Chem Soc* **2005**, *127*, 10840-10841.

(5) Weng, W.; Chen, C.-H.; Foxman, B. M.; Ozerov, O. V. Palladium Complexes of a P2C Ligand Containing a Central Carbene Moiety. *Organometallics* **2007**, *26*, 3315-3320.

(6) Morales-Morales, D.; Grause, C.; Kasaoka, K.; Redón, R. o.; Cramer, R. E.; Jensen, C. M. Highly Efficient and Regioselective Production of Trisubstituted Alkenes Through Heck Couplings Catalyzed by a Palladium Phosphinito PCP Pincer Complex. *Inorganica Chimica Acta* **2000**, *300-302*, 958-963.

(7) Bedford, R. B.; Draper, S. M.; Noelle Scully, P.; Welch, S. L. Palladium bis(phosphinite) 'PCP '-pincer Complexes and their Application as Catalysts in the Suzuki Reaction. *New Journal of Chemistry* **2000**, *24*, 745-747.

(8) Liang, L.-C.; Lin, J.-M.; Hung, C.-H. Nickel(II) Complexes of Bis(2-diphenylphosphinophenyl)amide. *Organometallics* **2003**, *22*, 3007-3009.

(9) Fan, L.; Foxman, B. M.; Ozerov, O. V. N−H Cleavage as a Route to Palladium Complexes of a New PNP Pincer Ligand. *Organometallics* **2004**, *23*, 326-328.

(10) Fryzuk, M. D. The 1992 Alcan Award Lecture Excursions Around the Periodic Table: Ligand Design in Inorganic Chemistry. *Canadian Journal of Chemistry* **1992**, *70*, 2839-2845.

(11) Peters, J. C.; Harkins, S. B.; Brown, S. D.; Day, M. W. Pincer-like Amido Complexes of Platinum, Palladium, and Nickel. *Inorganic Chemistry* **2001**, *40*, 5083-5091.

(12) MacInnis, M. C.; MacLean, D. F.; Lundgren, R. J.; McDonald, R.; Turculet, L. Synthesis and Reactivity of Platinum Group Metal Complexes Featuring the New Pincer-like Bis(phosphino)silyl Ligand [κ3-(2-Ph2PC6H4)2SiMe]− ([PSiP]):

Application in the Ruthenium-Mediated Transfer Hydrogenation of Ketones. *Organometallics* **2007**, *26*, 6522-6525.

(13) Okazaki, M.; Yamahira, N.; Minglana, J. J. G.; Tobita, H. Ru(xantsil)(CO)(PCy3): Facile Generation of a Coordinatively Unsaturated Ruthenium(II) Complex Bearing 14 Valence Electrons [xantsil = (9,9-dimethylxanthene-4,5-diyl)bis(dimethylsilyl)]. *Organometallics* **2004**, *23*, 4531-4533.

(14) Okazaki, M.; Yamahira, N.; Minglana, J. J. G.; Komuro, T.; Ogino, H.; Tobita, H. [Ru(xantsil)(CO)(η6-toluene)]: Synthon for a Highly Unsaturated Ruthenium(II) Complex through Facile Dissociation of the Toluene Ligand [xantsil = (9,9-dimethylxanthene-4,5-diyl)bis(dimethylsilyl)]. *Organometallics* **2008**, *27*, 918-926.

(15) Koller, J.; Sarkar, S.; Abboud, K. A.; Veige, A. S. Synthesis and Characterization of (2,6-iPrNCN)HfCl2- and (3,5-MeNCN)2Hf2- (where NCN = 2,6-bis[phenylazanidyl]methylphenyl): New Trianionic Pincer Ligands. *Organometallics* **2007**, *26*, 5438-5441.

(16) Nguyen, A. I.; Blackmore, K. J.; Carter, S. M.; Zarkesh, R. A.; Heyduk, A. F. One- and Two-Electron Reactivity of a Tantalum(V) Complex with a Redox-Active Tris(amido) Ligand. *J Am Chem Soc* **2009**, *131*, 3307-3316.

(17) Klet, R. C.; VanderVelde, D. G.; Labinger, J. A.; Bercaw, J. E. Highly Regioirregular Polypropylene from Asymmetric Group 4 Anilide(pyridine)phenoxide Complexes. *Chemical Communications* **2012**, *48*, 6657-6659.

(18) Komuro, T.; Tobita, H. Thermal Reaction of a Ruthenium Bis(silyl) Complex Having a Lutidine-based Si,N,Si Ligand: Formation of a μ-silyl(μ-silylene) Diruthenium Complex Involving a 3c–2e Ru–Si–C Interaction. *Chemical Communications* **2010**, *46*, 1136-1137.

(19) Agapie, T.; Bercaw, J. E. Cyclometalated Tantalum Diphenolate Pincer Complexes: Intramolecular C−H/M−CH3 σ-Bond Metathesis May Be Faster than O−H/M−CH3 Protonolysis. *Organometallics* **2007**, *26*, 2957-2959.

(20) Zarkesh, R. A.; Ziller, J. W.; Heyduk, A. F. Four-Electron Oxidative Formation of Aryl Diazenes Using a Tantalum Redox-Active Ligand Complex. *Angewandte Chemie International Edition* **2008**, *47*, 4715-4718.

(21) Sircoglou, M.; Bouhadir, G.; Saffon, N.; Miqueu, K.; Bourissou, D. A Zwitterionic Gold(I) Complex from an Ambiphilic Diphosphino−Alane Ligand. *Organometallics* **2008**, *27*, 1675-1678.

(22) Takaya, J.; Iwasawa, N. Synthesis, Structure, and Catalysis of Palladium Complexes Bearing a Group 13 Metalloligand: Remarkable Effect of an Aluminum-Metalloligand in Hydrosilylation of CO2. *J Am Chem Soc* **2017**, *139*, 6074-6077.

(23) Hara, N.; Saito, T.; Semba, K.; Kuriakose, N.; Zheng, H.; Sakaki, S.; Nakao, Y. Rhodium Complexes Bearing PAlP Pincer Ligands. *J Am Chem Soc* **2018**, *140*, 7070-7073.

(24) Morisako, S.; Watanabe, S.; Ikemoto, S.; Muratsugu, S.; Tada, M.; Yamashita, M. Synthesis of A Pincer-IrV Complex with A Base-Free Alumanyl Ligand and Its Application toward the Dehydrogenation of Alkanes. *Angewandte Chemie International Edition* **2019**, *58*, 15031-15035.

(25) Fujii, I.; Semba, K.; Li, Q.-Z.; Sakaki, S.; Nakao, Y. Magnesiation of Aryl Fluorides Catalyzed by a Rhodium–Aluminum Complex. *J Am Chem Soc* **2020**, *142*, 11647-11652.

(26) Schuhknecht, D.; Ritter, F.; Tauchert, M. E. Isolation and Properties of a Palladium PBP Pincer Complex Featuring an Ambiphilic Boryl Site. *Chem Commun (Camb)* **2016**, *52*, 11823-11826.

(27) Shih, W.-C.; Gu, W.; MacInnis, M. C.; Timpa, S. D.; Bhuvanesh, N.; Zhou, J.; Ozerov, O. V. Facile Insertion of Rh and Ir into a Boron–Phenyl Bond, Leading to Boryl/Bis(phosphine) PBP Pincer Complexes. *J Am Chem Soc* **2016**, *138*, 2086-2089.

(28) Spokoyny, A. M.; Reuter, M. G.; Stern, C. L.; Ratner, M. A.; Seideman, T.; Mirkin, C. A. Carborane-Based Pincers: Synthesis and Structure of SeBSe and SBS Pd(II) Complexes. *J Am Chem Soc* **2009**, *131*, 9482-9483.

(29) Eleazer, B. J.; Smith, M. D.; Peryshkov, D. V. Metal- and Ligand-Centered Reactivity of meta-Carboranyl-Backbone Pincer Complexes of Rhodium. *Organometallics* **2016**, *35*, 106-112.

(30) Segawa, Y.; Yamashita, M.; Nozaki, K. Syntheses of PBP Pincer Iridium Complexes: A Supporting Boryl Ligand. *J Am Chem Soc* **2009**, *131*, 9201-9203.

(31) Hasegawa, M.; Segawa, Y.; Yamashita, M.; Nozaki, K. Isolation of a PBP-Pincer Rhodium Complex Stabilized by an Intermolecular C H σ Coordination as the Fourth Ligand. *Angewandte Chemie International Edition* **2012**, *51*, 6956-6960.

(32) Lin, T.-P.; Peters, J. C. Boryl–Metal Bonds Facilitate Cobalt/Nickel-Catalyzed Olefin Hydrogenation. *J Am Chem Soc* **2014**, *136*, 13672-13683.

(33) Vogt, M.; Langer, R. The Pincer Platform Beyond Classical Coordination Patterns. *European Journal of Inorganic Chemistry* **2020**, 3885-3898.

(34) Braunschweig, H.; Dewhurst, R. D.; Hupp, F.; Nutz, M.; Radacki, K.; Tate, C. W.; Vargas, A.; Ye, Q. Multiple Complexation of CO and Related Ligands to a Main-group Element. *Nature* **2015**, *522*, 327-330.

(35) Kong, L.; Li, Y.; Ganguly, R.; Vidovic, D.; Kinjo, R. Isolation of a Bis(oxazol-2-ylidene)–Phenylborylene Adduct and its Reactivity as a Boron-Centered Nucleophile. *Angewandte Chemie International Edition* **2014**, *53*, 9280-9283.

(36) Kinjo, R.; Donnadieu, B.; Celik, M. A.; Frenking, G.; Bertrand, G. Synthesis and Characterization of a Neutral Tricoordinate Organoboron Isoelectronic with Amines. *Science* **2011**, *333*, 610.

(37) Shih, W.-C.; Gu, W.; MacInnis, M. C.; Herbert, D. E.; Ozerov, O. V. Boryl/Borane Interconversion and Diversity of Binding Modes of Oxygenous Ligands in PBP Pincer Complexes of Rhodium. *Organometallics* **2017**, *36*, 1718-1726.

(38) Shih, W.-C.; Ozerov, O. V. Selective ortho C–H Activation of Pyridines Directed by Lewis Acidic Boron of PBP Pincer Iridium Complexes. *J Am Chem Soc* **2017**, *139*, 17297-17300.

(39) Kwan, E. H.; Kawai, Y. J.; Kamakura, S.; Yamashita, M. A Long-tethered (P–B–P)-pincer Ligand: Synthesis, Complexation, and Application to Catalytic Dehydrogenation of Alkanes. *Dalton Transactions* **2016**, *45*, 15931-15941.

(40) Kwan, E. H.; Ogawa, H.; Yamashita, M. A Highly Active PBP–Iridium Catalyst for the Dehydrogenation of Dimethylamine–Borane: Catalytic Performance and Mechanism. *ChemCatChem* **2017**, *9*, 2457-2462.

(41) Tanoue, K.; Yamashita, M. Synthesis of Pincer Iridium Complexes Bearing a Boron Atom and iPr-Substituted Phosphorus Atoms: Application to Catalytic Transfer Dehydrogenation of Alkanes. *Organometallics* **2015**, *34*, 4011-4017.

(42) Ganguly, G.; Malakar, T.; Paul, A. Theoretical Studies on the Mechanism of Homogeneous Catalytic Olefin Hydrogenation and Amine–Borane Dehydrogenation by a Versatile Boryl-Ligand-Based Cobalt Catalyst. *ACS Catalysis* **2015**, *5*, 2754-2769.

(43) Ogawa, H.; Yamashita, M. Platinum Complexes Bearing a Boron-based PBP Pincer Ligand: Synthesis, Structure, and Application as a Catalyst for Hydrosilylation of 1-decene. *Dalton Transactions* **2013**, *42*, 625-629.

(44) Bontemps, S.; Gornitzka, H.; Bouhadir, G.; Miqueu, K.; Bourissou, D. Rhodium(I) Complexes of a PBP Ambiphilic Ligand: Evidence for a Metal→Borane Interaction. *Angewandte Chemie International Edition* **2006**, *45*, 1611-1614.

(45) Sircoglou, M.; Bontemps, S.; Mercy, M.; Saffon, N.; Takahashi, M.; Bouhadir, G.; Maron, L.; Bourissou, D. Transition-Metal Complexes Featuring Z-Type Ligands: Agreement or Discrepancy between Geometry and dn Configuration? *Angewandte Chemie* **2007**, *119*, 8737-8740.

(46) Cao, Y.; Shih, W.-C.; Ozerov, O. V. Addition of O–H, N–H, and F–H Bonds across a Boryl–Iridium Unit. *Organometallics* **2019**, *38*, 4076-4081.

(47) Shih, W.-C.; Ozerov, O. V. Synthesis and Characterization of PBP Pincer Iridium Complexes and Their Application in Alkane Transfer Dehydrogenation. *Organometallics* **2017**, *36*, 228-233.

(48) Suess, D. L. M.; Peters, J. C. H ‒ H and Si ‒ H Bond Addition to Fe≡NNR2 Intermediates Derived from N2. *J Am Chem Soc* **2013**, *135*, 4938-4941.

(49) Suess, D. L. M.; Peters, J. C. A CO-Derived Iron Dicarbyne That Releases Olefin upon Hydrogenation. *J Am Chem Soc* **2013**, *135*, 12580-12583.

(50) Harman, W. H.; Peters, J. C. Reversible H2 Addition across a Nickel–Borane Unit as a Promising Strategy for Catalysis. *J Am Chem Soc* **2012**, *134*, 5080-5082.

(51) Boone, M. P.; Stephan, D. W. A Ru−η6-Arene Complex as a C-Based Lewis Acid in the Activation of Hydrogen and Hydrogenation Catalysis. *J Am Chem Soc* **2013**, *135*, 8508-8511.

(52) Boone, M. P.; Stephan, D. W. Ru–η6-Arene Cations [{(Ph2PC6H4)2B(η6-Ph)}RuX]+ (X=Cl, H) as Lewis Acids. *Chemistry – A European Journal* **2014**, *20*, 3333-3341.

(53) Sircoglou, M.; Bontemps, S.; Mercy, M.; Miqueu, K.; Ladeira, S.; Saffon, N.; Maron, L.; Bouhadir, G.; Bourissou, D. Copper(I) Complexes derived from Mono- and Diphosphino-Boranes: Cu → B Interactions Supported by Arene Coordination. *Inorganic Chemistry* **2010**, *49*, 3983-3990.

(54) Cao, Y.; Shih, W.-C.; Bhuvanesh, N.; Ozerov, O. V. Silver Halide Complexes of a Borane/bis(phosphine) Ligand. *Dalton Transactions* **2019**, *48*, 9959-9961.

(55) Hadebe, S. W.; Robinson, R. S. Rhodium-Catalyzed Hydroboration Reactions with Sulfur and Nitrogen Analogues of Catecholborane. *European Journal of Organic Chemistry* **2006**, *2006*, 4898-4904.

(56) El-Zaria, M. E.; Arii, H.; Nakamura, H. m-Carborane-Based Chiral NBN Pincer-Metal Complexes: Synthesis, Structure, and Application in Asymmetric Catalysis. *Inorganic Chemistry* **2011**, *50*, 4149-4161.

(57) Eleazer, B. J.; Smith, M. D.; Popov, A. A.; Peryshkov, D. V. (BB)-Carboryne Complex of Ruthenium: Synthesis by Double B–H Activation at a Single Metal Center. *J Am Chem Soc* **2016**, *138*, 10531-10538.

(58) Courtemanche, M.-A.; Larouche, J.; Légaré, M.-A.; Bi, W.; Maron, L.; Fontaine, F.-G. A Tris(triphenylphosphine)aluminum Ambiphilic Precatalyst for the Reduction of Carbon Dioxide with Catecholborane. *Organometallics* **2013**, *32*, 6804-6811.

(59) Sircoglou, M.; Saffon, N.; Miqueu, K.; Bouhadir, G.; Bourissou, D. Activation of M–Cl Bonds with Phosphine–Alanes: Preparation and Characterization of Zwitterionic Gold and Copper Complexes. *Organometallics* **2013**, *32*, 6780-6784.

(60) Saito, N.; Takaya, J.; Iwasawa, N. Stabilized Gallylene in a Pincer-Type Ligand: Synthesis, Structure, and Reactivity of PGaIP-Ir Complexes. *Angewandte Chemie International Edition* **2019**, *58*, 9998-10002.

(61) Takaya, J.; Hoshino, M.; Ueki, K.; Saito, N.; Iwasawa, N. Synthesis, Structure, and Reactivity of Pincer-type Iridium Complexes Having Gallyl- and Indyl-Metalloligands Utilizing 2,5-bis(6-phosphino-2-pyridyl)pyrrolide as a New Scaffold for Metal–metal Bonds. *Dalton Transactions* **2019**, *48*, 14606-14610.

(62) Trofimenko, S. Boron-Pyrazole Chemistry. *J Am Chem Soc* **1966**, *88*, 1842-1844.

(63) Trofimenko, S. Recent Advances in Poly(pyrazolyl)borate (Scorpionate) Chemistry. *Chemical Reviews* **1993**, *93*, 943-980.

(64) Trofimenko, S. Coordination Chemistry of Pyrazole-derived Ligands. *Chemical Reviews* **1972**, *72*, 497-509.

(65) Garner, M.; Reglinski, J.; Cassidy, I.; Spicer, M. D.; Kennedy, A. R. Hydrotris(methimazolyl)borate, a Soft Analogue of Hydrotris(pyrazolyl)borate. Preparation and Crystal Structure of a Novel Zinc Complex. *Chemical Communications* **1996**, 1975-1976.

(66) Jones, J. S.; Gabba ̈ı, F. P. Coordination- and Redox-Noninnocent Behavior of Ambiphilic Ligands Containing Antimony. *Accounts of Chemical Research* **2016**, *49*, 857-867.

(67) Canary, J. W.; Wang, Y.; Roy Jr, R.; Lawrence Que, Jr.; Miyake, H. Tris[(2-Pyridyl)Methyl] Amine (TPA) and (+)-Bis[(2-Pyridyl)methyl]-1-(2-Pyridyl)-Ethylamine (α-Metpa). *Inorganic Syntheses* **1998**, 70-75.

(68) Bowen, T.; Planalp, R. P.; Brechbiel, M. W. An Improved Synthesis of Cis,cis-1,3,5-triaminocyclohexane. Synthesis of Novel Hexadentate Ligand Derivatives for the Preparation of Gallium Radiopharmaceuticals. *Bioorganic & Medicinal Chemistry Letters* **1996**, *6*, 807-810.

(69) Kl ̈ui, W.; Mocigemba, N.; Weber-Schuster, A.; Bell, R.; Frank, W.; Mootz, D.; Poll, W.; Wunderlich, H. [(C5H5)Co{P(O)(OH)2}3H]: A Novel Organometallic Tris-phosphonic Acid That Dissolves Glass to Form a Six-Coordinate Silicon Complex. *Chemistry – A European Journal* **2002**, *8*, 2335-2340.

(70) Heintz, W. Ueber Dem Ammoniaktypus Angeh ̈orige Organische S ̈auren. *Ann Chem Pharm* 1862, *122* , 257-294.

(71) Hill, A. F.; Owen, G. R.; White, A. J.; Williams, D. J. The Sting of the Scorpion: A Metallaboratrane. *Angew Chem Int Ed Engl* **1999**, *38*, 2759-2761.

(72) Braunschweig, H.; Dewhurst, R. D. Transition Metals as Lewis Bases: "Z-type" Boron Ligands and Metal-to-boron Dative Bonding. *Dalton Transactions* **2011**, *40*, 549-558.

(73) Rudd, P. A.; Liu, S.; Gagliardi, L.; Young, V. G., Jr.; Lu, C. C. Metal-alane Adducts with Zero-valent Nickel, Cobalt, and Iron. *J Am Chem Soc* **2011**, *133*, 20724-20727.

(74) Cammarota, R. C.; Vollmer, M. V.; Xie, J.; Ye, J.; Linehan, J. C.; Burgess, S. A.; Appel, A. M.; Gagliardi, L.; Lu, C. C. A Bimetallic Nickel-Gallium Complex Catalyzes CO2 Hydrogenation via the Intermediacy of an Anionic d(10) Nickel Hydride. *J Am Chem Soc* **2017**, *139*, 14244-14250.

(75) You, D.; Gabbaï, F. P. Tunable σ-Accepting, Z-Type Ligands for Organometallic Catalysis. *Trends in Chemistry* **2019**, *1*, 485-496.

(76) Sircoglou, M.; Bontemps, S.; Bouhadir, G.; Saffon, N.; Miqueu, K.; Gu, W. X.; Mercy, M.; Chen, C. H.; Foxman, B. M.; Maron, L.; Ozerov, O. V.; Bourissou, D. Group 10 and 11 Metal Boratranes (Ni, Pd, Pt, CuCl, AgCl, AuCl, and Au+) Derived from a Triphosphine-Borane. *J Am Chem Soc* **2008**, *130*, 16729-16738.

(77) Bontemps, S.; Bouhadir, G.; Gu, W.; Mercy, M.; Chen, C.-H.; Foxman, B. M.; Maron, L.; Ozerov, O. V.; Bourissou, D. Metallaboratranes Derived from a Triphosphanyl–Borane: Intrinsic C3 Symmetry Supported by a Z-Type Ligand. *Angewandte Chemie International Edition* **2008**, *47*, 1481-1484.

(78) Ishiyama, T.; Matsuda, N.; Murata, M.; Ozawa, F.; Suzuki, A.; Miyaura, N. Platinum(0)-catalyzed Diboration of Alkynes with Tetrakis(alkoxo)diborons: An Efficient and Convenient Approach to Cis-bis(boryl) Alkenes. *Organometallics* **1996**, *15*, 713-720.

(79) Cammarota, R. C.; Lu, C. C. Tuning Nickel with Lewis Acidic Group 13 Metalloligands for Catalytic Olefin Hydrogenation. *J Am Chem Soc* **2015**, *137*, 12486-12489.

(80) Vollmer, M. V.; Ye, J.; Linehan, J. C.; Graziano, B. J.; Preston, A.; Wiedner, E. S.; Lu, C. C. Cobalt-Group 13 Complexes Catalyze CO2 Hydrogenation via a Co(−I)/Co(I) Redox Cycle. *ACS Catalysis* **2020**, *10*, 2459-2470.

(81) Dunn, P. L.; Reath, A. H.; Clouston, L. J.; Young, V. G.; Tonks, I. A. Homo- and Heteroleptic Group 4 2-(diphenylphosphino)pyrrolide Complexes: Synthesis, Coordination Chemistry and Solution State Dynamics. *Polyhedron* **2014**, *84*, 111-119.

(82) Weng, W.; Parkin, S.; Ozerov, O. V. Double C−H Activation Results in Ruthenium Complexes of a Neutral PCP Ligand with a Central Carbene Moiety. *Organometallics* **2006**, *25*, 5345-5354.

(83) King, E. R.; Betley, T. A. Unusual Electronic Structure of First Row Transition Metal Complexes Featuring Redox-Active Dipyrromethane Ligands. *J Am Chem Soc* **2009**, *131*, 14374-14380.

(84) Yang, W.; Gao, X.; Wang, B. Boronic acid compounds as potential pharmaceutical agents. *Medicinal Research Reviews* **2003**, *23*, 346-368.

(85) Hall, D. G.: *Boronic Acids: Preparation, Applications in Organic Synthesis and Medicine*; John Wiley & Sons, 2006.

(86) Miyaura, N.; Suzuki, A. Palladium-Catalyzed Cross-Coupling Reactions of Organoboron Compounds. *Chemical Reviews* **1995**, *95*, 2457-2483.

(87) Brewster, J. H.; Negishi, E.-I. Brown: Passes Through the Mountains (1). *Science* **1980**, *207*, 44.

(88) Suzuki, A. Cross‐coupling Reactions of Organoboranes: an Easy Way to Construct C-C Bonds (Nobel Lecture). *Angewandte Chemie International Edition* **2011**, *50*, 6722-6737.

(89) Touchet, S.; Carreaux, F.; Carboni, B.; Bouillon, A.; Boucher, J.-L. Aminoboronic Acids and Esters: From Synthetic Challenges to the Discovery of Unique Classes of Enzyme Inhibitors. *Chemical Society Reviews* **2011**, *40*, 3895-3914.

(90) Magano, J.; Dunetz, J. R. Large-Scale Applications of Transition Metal-Catalyzed Couplings for the Synthesis of Pharmaceuticals. *Chemical Reviews* **2011**, *111*, 2177-2250.

(91) Soriano-Ursúa, M. A.; Das, B. C.; Trujillo-Ferrara, J. G. Boron-containing Compounds: Chemico-biological Properties and Expanding Medicinal Potential in Prevention, Diagnosis and Therapy. *Expert Opinion on Therapeutic Patents* **2014**, *24*, 485-500.

(92) Smoum, R.; Rubinstein, A.; Dembitsky, V. M.; Srebnik, M. Boron Containing Compounds as Protease Inhibitors. *Chemical Reviews* **2012**, *112*, 4156-4220.

(93) Diaz, D. B.; Yudin, A. K. The Versatility of Boron in Biological Target Engagement. *Nature Chemistry* **2017**, *9*, 731-742.

(94) Adams, J.; Palombella, V. J.; Sausville, E. A.; Johnson, J.; Destree, A.; Lazarus, D. D.; Maas, J.; Pien, C. S.; Prakash, S.; Elliott, P. J. Proteasome Inhibitors: A Novel Class of Potent and Effective Antitumor Agents. *Cancer Research* **1999**, *59*, 2615.

(95) Babu, K. N.; Massarwe, F.; Reddy, R. R.; Eghbarieh, N.; Jakob, M.; Masarwa, A. Unsymmetrical 1,1-Bisboryl Species: Valuable Building Blocks in Synthesis. *Molecules* **2020**, *25*.

(96) Ishiyama, T.; Yamamoto, M.; Miyaura, N. A Synthesis of (E)-(1-Organo-1-alkenyl)boronates by the Palladium-Catalyzed Cross-Coupling Reaction of (E)-1,2-Bis(boryl)-1-alkenes with Organic Halides: A Formal Carboboration of Alkynes via the Diboration-Coupling Sequence. *Chemistry Letters* **1996**, *25*, 1117-1118.

(97) Shimizu, M.; Nakamaki, C.; Shimono, K.; Schelper, M.; Kurahashi, T.; Hiyama, T. Stereoselective Cross-Coupling Reaction of 1,1-Diboryl-1-alkenes with Electrophiles: A Highly Stereocontrolled Approach to 1,1,2-Triaryl-1-alkenes. *J Am Chem Soc* **2005**, *127*, 12506-12507.

(98) Nishihara, Y.; Miyasaka, M.; Okamoto, M.; Takahashi, H.; Inoue, E.; Tanemura, K.; Takagi, K. Zirconocene-Mediated Highly Regio- and Stereoselective Synthesis of Multisubstituted Olefins Starting from 1-Alkynylboronates. *J Am Chem Soc* **2007**, *129*, 12634-12635.

(99) Iwadate, N.; Suginome, M. Differentially Protected Diboron for Regioselective Diboration of Alkynes: Internal-Selective Cross-Coupling of 1-Alkene-1,2-diboronic Acid Derivatives. *J Am Chem Soc* **2010**, *132*, 2548-2549.

(100) Urry, G.; Kerrigan, J.; Parsons, T. D.; Schlesinger, H. I. Diboron Tetrachloride, B2Cl4, as a Reagent for the Synthesis of Organo-boron Compounds. I. The Reaction of Diboron Tetrachloride with Ethylene1. *J Am Chem Soc* **1954**, *76*, 5299-5301.

(101) Ceron, P.; Finch, A.; Frey, J.; Kerrigan, J.; Parsons, T.; Urry, G.; Schlesinger, H. I. Diboron Tetrachloride and Tetrafluoride as Reagents for the Synthesis of Organoboron Compounds. II. The Behavior of the Diboron Tetrahalides toward Unsaturated Organic Compounds1. *J Am Chem Soc* **1959**, *81*, 6368-6371.

(102) Brotherton, R. J.; McCloskey, A. L.; Boone, J. L.; Manasevit, H. M. The Preparation and Properties of Some Tetraalkoxydiborons1. *J Am Chem Soc* **1960**, *82*, 6245-6248.

(103) Ishiyama, T.; Matsuda, N.; Miyaura, N.; Suzuki, A. Platinum(0)-catalyzed Diboration of Alkynes. *J Am Chem Soc* **1993**, *115*, 11018-11019.

(104) Thomas, R. L.; Souza, F. E. S.; Marder, T. B. Highly Efficient Monophosphine Platinum Catalysts for Alkyne Diboration. *Journal of the Chemical Society, Dalton Transactions* **2001**, 1650-1656.

(105) Yoshida, H.; Kawashima, S.; Takemoto, Y.; Okada, K.; Ohshita, J.; Takaki, K. Copper-catalyzed Borylation Reactions of Alkynes and Arynes. *Angew Chem Int Ed Engl* **2012**, *51*, 235-238.

(106) Ansell, M. B.; Menezes da Silva, V. H.; Heerdt, G.; Braga, A. A. C.; Spencer, J.; Navarro, O. An Experimental and Theoretical Study into the Facile, Homogenous (N-heterocyclic carbene)2-Pd(0) Catalyzed Diboration of Internal and Terminal Alkynes. *Catalysis Science & Technology* **2016**, *6*, 7461-7467.

(107) Nakagawa, N.; Hatakeyama, T.; Nakamura, M. Iron-catalyzed Diboration and Carboboration of Alkynes. *Chemistry* **2015**, *21*, 4257-4261.

(108) Nagashima, Y.; Hirano, K.; Takita, R.; Uchiyama, M. Trans-diborylation of Alkynes: Pseudo-intramolecular Strategy Utilizing a Propargylic Alcohol Unit. *J Am Chem Soc* **2014**, *136*, 8532-8535.

(109) Kojima, C.; Lee, K. H.; Lin, Z.; Yamashita, M. Direct and Base-Catalyzed Diboration of Alkynes Using the Unsymmetrical Diborane(4), pinB-BMes2. *J Am Chem Soc* **2016**, *138*, 6662-6669.

(110) Nagao, K.; Ohmiya, H.; Sawamura, M. Anti-selective Vicinal Silaboration and Diboration of Alkynoates through Phosphine Organocatalysis. *Org Lett* **2015**, *17*, 1304-1307.

(111) Yoshimura, A.; Takamachi, Y.; Han, L. B.; Ogawa, A. Organosulfide-Catalyzed Diboration of Terminal Alkynes under Light. *Chemistry* **2015**, *21*, 13930-13933.

(112) Dhillon, R. S.: *Hydroboration and organic synthesis: 9-Borabicyclo [3.3. 1] Nonane (9-BBN)*; Springer Science & Business Media, 2007.

(113) Lee, C. I.; Shih, W. C.; Zhou, J.; Reibenspies, J. H.; Ozerov, O. V. Synthesis of Triborylalkenes from Terminal Alkynes by Iridium-Catalyzed Tandem C-H Borylation and Diboration. *Angew Chem Int Ed Engl* **2015**, *54*, 14003-14007.

(114) Amgoune, A.; Bourissou, D. σ-Acceptor, Z-type ligands for transition metals. *Chemical Communications* **2011**, *47*, 859-871.

(115) Harman, W. H.; Lin, T.-P.; Peters, J. C. A d10 Ni–(H2) Adduct as an Intermediate in H H Oxidative Addition across a Ni B Bond. *Angewandte Chemie International Edition* **2014**, *53*, 1081-1086.

(116) Anderson, J. S.; Rittle, J.; Peters, J. C. Catalytic Conversion of Nitrogen to Ammonia by an Iron Model Complex. *Nature* **2013**, *501*, 84-87.

(117) Moore, J. T.; Lu, C. C. Catalytic Hydrogenolysis of Aryl C–F Bonds Using a Bimetallic Rhodium–Indium Complex. *J Am Chem Soc* **2020**, *142*, 11641-11646.

(118) Foreman, M. R. S. J.; Hill, A. F.; White, P.; Williams, D. J. Polyazolyl Chelate Chemistry. 13. An Osmaboratrane1. *Organometallics* **2004**, *23*, 913-916.

(119) Mihalcik, D. J.; White, J. L.; Tanski, J. M.; Zakharov, L. N.; Yap, G. P. A.; Incarvito, C. D.; Rheingold, A. L.; Rabinovich, D. Cobalt Tris(mercaptoimidazolyl)borate Complexes: Synthetic Studies and the Structure of the First Cobaltaboratrane. *Dalton Transactions* **2004**, 1626-1634.

(120) Pang, K.; Tanski, J. M.; Parkin, G. Reactivity of the Ni→B Dative σ -bond in the Nickel Boratrane Compounds [κ 4-B(mimBut)3]NiX (X = Cl, OAc, NCS, N3): Synthesis of a Series of B-functionalized Tris(2-mercapto-1-tert-butylimidazolyl)borato Complexes, [YTmBut]NiZ. *Chemical Communications* **2008**, 1008-1010.

(121) Moret, M.-E.; Zhang, L.; Peters, J. C. A Polar Copper–Boron One-Electron σ-Bond. *J Am Chem Soc* **2013**, *135*, 3792-3795.

(122) Moloy, K. G.; Petersen, J. L. N-Pyrrolyl Phosphines: An Unexploited Class of Phosphine Ligands with Exceptional .pi.-Acceptor Character. *J Am Chem Soc* **1995**, *117*, 7696-7710.

(123) Cohen, S. M.; Halper, S. R. Dipyrromethene Complexes of Iron. *Inorganica Chimica Acta* **2002**, *341*, 12-16.

(124) Li, S.; Wang, Y.; Yang, W.; Li, K.; Sun, H.; Li, X.; Fuhr, O.; Fenske, D. N2 Silylation Catalyzed by a Bis(silylene)-Based [SiCSi] Pincer Hydrido Iron(II) Dinitrogen Complex. *Organometallics* **2020**, *39*, 757-766.

(125) Clegg, W.; J. Edwards, A.; Clegg, W.; S. Mair, F.; M. Nolan, P. A 3:1 Mixed Aggregate of Diphenylamidolithium with Lithium Chloride: Crystal Structure of [(Ph2NLi)3LiCl • 3tmen] (tmen = N,N,N′ ,N′ -tetramethylethylenediamine). *Chemical Communications* **1998**, 23-24.

(126) Semmelhack, M. F.; Chlenov, A.; Ho, D. M. Accelerated Arene Ligand Exchange in the (Arene)Cr(CO)2L Series. *J Am Chem Soc* **2005**, *127*, 7759-7773.

(127) Deeming, A. J.; Shinhmar, M. K. 2-Diphenylphosphinoazacyclopentadienylmanganese Tricarbonyl as a New Bridging Ligand. *Journal of Organometallic Chemistry* **1999**, *592*, 235-239.

(128) Dunn, P. L.; Beaumier, E. P.; Tonks, I. A. Synthesis and Characterization of Tantalum-based Early-late Heterobimetallic Complexes Supported by 2-(diphenylphosphino)pyrrolide Ligands. *Polyhedron* **2020**, *181*, 114471.

(129) Dunn, P. L.; Chatterjee, S.; MacMillan, S. N.; Pearce, A. J.; Lancaster, K. M.; Tonks, I. A. The 4-Electron Cleavage of a N═N Double Bond by a Trimetallic TiNi2 Complex. *Inorganic Chemistry* **2019**, *58*, 11762-11772.

(130) Murphy, L. J.; Hollenhorst, H.; McDonald, R.; Ferguson, M.; Lumsden, M. D.; Turculet, L. Selective Ni-Catalyzed Hydroboration of CO2 to the Formaldehyde Level Enabled by New PSiP Ligation. *Organometallics* **2017**, *36*, 3709-3720.

(131) Wassenaar, J.; Reek, J. N. H. INDOLPhos: Novel Hybrid Phosphine-phosphoramidite Ligands for Asymmetric Hydrogenation and Hydroformylation. *Dalton Transactions* **2007**, 3750-3753.

(132) Mishra, S. J.; Ghosh, S.; Stothert, A. R.; Dickey, C. A.; Blagg, B. S. J. Transformation of the Non-Selective Aminocyclohexanol-Based Hsp90 Inhibitor into a Grp94-Seletive Scaffold. *ACS Chemical Biology* **2017**, *12*, 244-253.

(133) Salman, H.; Abraham, Y.; Tal, S.; Meltzman, S.; Kapon, M.; Tessler, N.; Speiser, S.; Eichen, Y. 1,3-Di(2-pyrrolyl)azulene: An Efficient Luminescent Probe for Fluoride. *European Journal of Organic Chemistry* **2005**, *2005*, 2207-2212.

(134) Cordero, B.; Gómez, V.; Platero-Prats, A. E.; Revés, M.; Echeverría, J.; Cremades, E.; Barragán, F.; Alvarez, S. Covalent Radii Revisited. *Dalton Transactions* **2008**, 2832-2838.

(135) Parkin, G. Valence, Oxidation Number, and Formal Charge: Three Related but Fundamentally Different Concepts. *Journal of Chemical Education* **2006**, *83*, 791.

(136) Hill, A. F. An Unambiguous Electron-Counting Notation for Metallaboratranes. *Organometallics* **2006**, *25*, 4741-4743.

(137) Parkin, G. A Simple Description of the Bonding in Transition-Metal Borane Complexes. *Organometallics* **2006**, *25*, 4744-4747.

(138) Bonanno, J. B.; Henry, T. P.; Wolczanski, P. T.; Pierpont, A. W.; Cundari, T. R. Evidence for Strong Tantalum-to-Boron Dative Interactions in (silox)3Ta(BH3) and (silox)3Ta(η2-B,Cl-BCl2Ph) (silox = tBu3SiO)1. *Inorganic Chemistry* **2007**, *46*, 1222-1232.

(139) Desrosiers, P. J.; Cai, L.; Lin, Z.; Richards, R.; Halpern, J. Assessment of the" T1 criterion" for Distinguishing Between Classical and Nonclassical Transition-metal Hydrides: Hydride Relaxation Rates in Tris (triarylphosphine) osmium Tetrahydrides and Related Polyhydrides. *J Am Chem Soc* **1991**, *113*, 4173-4184.

(140) Crabtree, R. H. Dihydrogen Complexation. *Chemical Reviews* **2016**, *116*, 8750-8769.

(141) Cammarota, R. C.; Xie, J.; Burgess, S. A.; Vollmer, M. V.; Vogiatzis, K. D.; Ye, J.; Linehan, J. C.; Appel, A. M.; Hoffmann, C.; Wang, X.; Young, V. G.; Lu, C. C. Thermodynamic and Kinetic Studies of H2 and N2 Binding to Bimetallic Nickel-group 13 Complexes and Neutron Structure of a Ni(η2-H2) Adduct. *Chemical Science* **2019**, *10*, 7029-7042.

(142) Tsay, C.; Peters, J. C. Thermally Stable N2 and H2 Adducts of Cationic Nickel(ii). *Chemical Science* **2012**, *3*, 1313-1318.

(143) Vollmer, M. V.; Cammarota, R. C.; Lu, C. C. Reductive Disproportionation of CO2 Mediated by Bimetallic Nickelate(-I)/Group 13 Complexes. *European Journal of Inorganic Chemistry* **2019**, *2019*, 2140-2145.

(144) González-Sebastián, L.; Flores-Alamo, M.; García, J. J. Reduction of CO2 and SO2 with Low Valent Nickel Compounds under Mild Conditions. *Dalton Transactions* **2011**, *40*, 9116-9122.

(145) Lee, G. M.; Korobkov, I.; Baker, R. T. d8 Nickel and Palladium Difluorocarbenes Derived from Trifluoromethyl POCOP-type Pincer Complexes. *Journal of Organometallic Chemistry* **2017**, *847*, 270-277.

(146) Sheldrick, G. A Short History of SHELX. *Acta Crystallographica Section A* **2008**, *64*, 112-122.

(147) Sheldrick, G. Crystal Structure Refinement with SHELXL. *Acta Crystallographica Section C* **2015**, *71*, 3-8.

(148) Dolomanov, O. V.; Bourhis, L. J.; Gildea, R. J.; Howard, J. A. K.; Puschmann, H. OLEX2: a Complete Structure Solution, Refinement and Analysis Program. *Journal of Applied Crystallography* **2009**, *42*, 339-341.

(149) Spek, A. Single-crystal Structure Validation with the Program PLATON. *Journal of Applied Crystallography* **2003**, *36*, 7-13.

(150) Strauss, S. H. The Search for Larger and More Weakly Coordinating Anions. *Chemical Reviews* **1993**, *93*, 927-942.

(151) Reed, C. A. Carboranes: A New Class of Weakly Coordinating Anions for Strong Electrophiles, Oxidants, and Superacids. *Accounts of Chemical Research* **1998**, *31*, 133-139.

(152) Reed, C. A. H+, CH3+, and R3Si+ Carborane Reagents: When Triflates Fail. *Accounts of Chemical Research* **2010**, *43*, 121-128.

(153) Engesser, T. A.; Lichtenthaler, M. R.; Schleep, M.; Krossing, I. Reactive p-block Cations Stabilized by Weakly Coordinating Anions. *Chemical Society Reviews* **2016**, *45*, 789-899.

(154) Mömming, C. M.; Frömel, S.; Kehr, G.; Fröhlich, R.; Grimme, S.; Erker, G. Reactions of an Intramolecular Frustrated Lewis Pair with Unsaturated Substrates: Evidence for a Concerted Olefin Addition Reaction. *J Am Chem Soc* **2009**, *131*, 12280-12289.

(155) Axenov, K. V.; Mömming, C. M.; Kehr, G.; Fröhlich, R.; Erker, G. Structure and Dynamic Features of an Intramolecular Frustrated Lewis Pair. *Chemistry – A European Journal* **2010**, *16*, 14069-14073.

(156) McMahon, C. N.; Barron, A. R. Molecular structure of (tBu)3AlP(nPr)3. *Journal of Chemical Crystallography* **1997**, *27*, 195-197.

(157) Fryzuk, M. D.; Giesbrecht, G. R.; Olovsson, G.; Rettig, S. J. Synthesis and Characterization of Four- and Five-Coordinate Organoaluminum Complexes Incorporating the Amido Diphosphine Ligand System N(SiMe2CH2PPri2)2. *Organometallics* **1996**, *15*, 4832-4841.

(158) Farrugia, L. WinGX and ORTEP for Windows: an Update. *Journal of Applied Crystallography* **2012**, *45*, 849-854.

(159) Xie, Z.; Jelinek, T.; Bau, R.; Reed, C. A. New Weakly Coordinating Anions. III. Useful Silver and Trityl Salt Reagents of Carborane Anions. *J Am Chem Soc* **1994**, *116*, 1907-1913.

(160) Morales-Morales, D.; Jensen, C. M.: The Chemistry of Pincer Compounds. Elsevier: Amsterdam ;, 2007.

(161) van Koten, G.; Milstein, D.: The Monoanionic ECE-Pincer Ligand: A Versatile Privileged Ligand Platform-General Considerations. Springer, 2013.

(162) van der Boom, M. E.; Milstein, D. Cyclometalated Phosphine-Based Pincer Complexes: Mechanistic Insight in Catalysis, Coordination, and Bond Activation. *Chemical Reviews* **2003**, *103*, 1759-1792.

(163) Selander, N.; Szabó, K. J. Catalysis by Palladium Pincer Complexes. *Chemical Reviews* **2011**, *111*, 2048-2076.

(164) Choi, J.; MacArthur, A. H. R.; Brookhart, M.; Goldman, A. S. Dehydrogenation and Related Reactions Catalyzed by Iridium Pincer Complexes. *Chemical Reviews* **2011**, *111*, 1761-1779.

(165) Peris, E.; Crabtree, R. H. Key Factors in Pincer Ligand Design. *Chemical Society Reviews* **2018**, *47*, 1959-1968.

(166) Green, M. L. H.; Parkin, G. Application of the Covalent Bond Classification Method for the Teaching of Inorganic Chemistry. *Journal of Chemical Education* **2014**, *91*, 807-816.

(167) Kuriakose, N.; Zheng, J.-J.; Saito, T.; Hara, N.; Nakao, Y.; Sakaki, S. Characterization of Rh–Al Bond in Rh(PAlP) (PAlP = Pincer-type Diphosphino-Aluminyl

Ligand) in Comparison with Rh(L)(PMe3)2 (L = AlMe2, Al(NMe2)2, BR2, SiR3, CH3, Cl, or OCH3): Theoretical Insight. *Inorganic Chemistry* **2019**, *58*, 4894-4906.

(168) Hill, A. F.; McQueen, C. M. A. Dihydroperimidine-Derived PNP Pincer Complexes as Intermediates en Route to N-Heterocyclic Carbene Pincer Complexes. *Organometallics* **2014**, *33*, 1909-1912.

(169) Semba, K.; Fujii, I.; Nakao, Y. A PAlP Pincer Ligand Bearing a 2-Diphenylphosphinophenoxy Backbone. *Inorganics* **2019**, *7*, 140-149.

(170) Stephen Hartman, J.; Shoemaker, J. A. W.; Janzen, A. F.; Ragogna, P. J.; Szerminski, W. R. The Coordination Chemistry of (py)2BF2+ and Related Difluoroboron Cations. *Journal of Fluorine Chemistry* **2003**, *119*, 125-139.

(171) Westcott, S.; Marder, T.; Baker, R.; Calabrese, J. Reactions of Catecholborane with Iridium Complexes: Molecular Structure of Trans-IrHCl(CO)(Bcat)(PPh3)2. *Canadian Journal of Chemistry* **2011**, *71*, 930-936.

(172) Knorr, J. R.; Merola, J. S. Synthesis and Structure of a [(1,2-phenylenedioxy)boryl]iridium Hydride Complex: a Model System for Studying Catalytic Hydroboration. *Organometallics* **1990**, *9*, 3008-3010.

(173) Vela, J.; Lief, G. R.; Shen, Z.; Jordan, R. F. Ethylene Polymerization by Palladium Alkyl Complexes Containing Bis(aryl)phosphino-toluenesulfonate Ligands. *Organometallics* **2007**, *26*, 6624-6635.

(174) Alich, A.; Nelson, N. J.; Strope, D.; Shriver, D. F. Solution Infrared Study of Carbon- and Oxygen-bonded Carbon Monoxide. Interaction of Bridging Carbonyl Ligands with Aluminum Alkyls. *Inorganic Chemistry* **1972**, *11*, 2976-2983.

(175) Plečnik, C. E.; Liu, S.; Chen, X.; Meyers, E. A.; Shore, S. G. Lanthanide−Transition-Metal Carbonyl Complexes: New [Co4(CO)11]2- Clusters and Lanthanide(II) Isocarbonyl Polymeric Arrays. *J Am Chem Soc* **2004**, *126*, 204-213.

(176) Dickie, C. M.; Nippe, M. Magnetization Dynamics of a Heterometallic Dy-isocarbonyl Complex. *Inorganic Chemistry Frontiers* **2016**, *3*, 97-103.

(177) Goettel, J. T.; Braunschweig, H. Recent Advances in Boron-centered Ligands and their Transition Metal Complexes. *Coordination Chemistry Reviews* **2019**, *380*, 184-200.

(178) Taniguchi, T.; Wang, J.; Irle, S.; Yamaguchi, S. TICT Fluorescence of N-borylated 2,5-Diarylpyrroles: a Gear Like Dual Motion in the Excited State. *Dalton Transactions* **2013**, *42*, 620-624.

(179) Sivula, K.; Le Formal, F.; Grätzel, M. Solar Water Splitting: Progress Using Hematite (α-Fe2O3) Photoelectrodes. *ChemSusChem* **2011**, *4*, 432-449.

(180) Sun, C.-L.; Li, B.-J.; Shi, Z.-J. Direct C−H Transformation via Iron Catalysis. *Chemical Reviews* **2011**, *111*, 1293-1314.

(181) Bauer, I.; Knölker, H.-J. Iron Catalysis in Organic Synthesis. *Chemical Reviews* **2015**, *115*, 3170-3387.

(182) Morris, R. H. Exploiting Metal–Ligand Bifunctional Reactions in the Design of Iron Asymmetric Hydrogenation Catalysts. *Accounts of Chemical Research* **2015**, *48*, 1494-1502.

(183) Jia, F.; Li, Z. Iron-catalyzed/mediated Oxidative Transformation of C–H Bonds. *Organic Chemistry Frontiers* **2014**, *1*, 194-214.

(184) Himmelbauer, D.; Mastalir, M.; Stöger, B.; Veiros, L. F.; Pignitter, M.; Somoza, V.; Kirchner, K. Iron PCP Pincer Complexes in Three Oxidation States: Reversible Ligand Protonation To Afford an Fe(0) Complex with an Agostic C–H Arene Bond. *Inorganic Chemistry* **2018**, *57*, 7925-7931.

(185) Rachlewicz, K.; Wang, S.-L.; Peng, C.-H.; Hung, C.-H.; Latos-Grażyński, L. Remarkable Paramagnetically Shifted 1H and 2H NMR Spectra of Iron(II) Complexes of 2-Aza-21-carbaporphyrin: An Evidence for Agostic Interaction. *Inorganic Chemistry* **2003**, *42*, 7348-7350.

(186) Chen, W.-C.; Hung, C.-H. Synthesis and Characterization of Iron N-Confused Porphyrins: Structural Evidences of Agostic Interaction. *Inorganic Chemistry* **2001**, *40*, 5070-5071.

(187) Hamon, P.; Hamon, J.-R.; Lapinte, C. Isolation and Characterization of a Cationic 19-electron Iron(III) Hydride Complex; Electron Transfer Induced Hydride Migration by Carbon Monoxide at an Iron(III) Centre. *Journal of the Chemical Society, Chemical Communications* **1992**, 1602-1603.

(188) Drover, M. W.; Schild, D. J.; Oyala, P. H.; Peters, J. C. Snapshots of a Migrating H-Atom: Characterization of a Reactive Iron(III) Indenide Hydride and its Nearly Isoenergetic Ring-Protonated Iron(I) Isomer. *Angew Chem Int Ed Engl* **2019**, *58*, 15504-15511.

(189) Malischewski, M.; Seppelt, K.; Sutter, J.; Heinemann, F. W.; Dittrich, B.; Meyer, K. Protonation of Ferrocene: A Low-Temperature X-ray Diffraction Study of [Cp2FeH](PF6) Reveals an Iron-Bound Hydrido Ligand. *Angewandte Chemie International Edition* **2017**, *56*, 13372-13376.

(190) Creaser, C. S.; Kaska, W. C. Complexes of 1,3-Bis(dimethylphosphinomethyl)benzene with Nickel(II), Palladium(II) and Iron(II) Halides. *Inorg. Chim. Acta* **1978**, *30*, L325-L326.

(191) Bhattacharya, P.; Krause, J. A.; Guan, H. Iron Hydride Complexes Bearing Phosphinite-Based Pincer Ligands: Synthesis, Reactivity, and Catalytic Application in Hydrosilylation Reactions. *Organometallics* **2011**, *30*, 4720-4729.

(192) Jiang, S.; Quintero-Duque, S.; Roisnel, T.; Dorcet, V.; Grellier, M.; Sabo-Etienne, S.; Darcel, C.; Sortais, J. B. Direct Synthesis of Dicarbonyl PCP-iron Hydride

Complexes and Catalytic Dehydrogenative Borylation of Styrene. *Dalton Trans* **2016**, *45*, 11101-11108.

(193) Wu, C.-Y.; Chen, Y.; Jing, S.-Y.; Lee, C.-S.; Dinda, J.; Hwang, W.-S. Reactions of Diiron Nonacarbonyl with Pyrrolyl-, pyridyl- and thienyl-substituted Azines: N-N Bond Cleavage, Cyclometallation and C-N σ and π-Bonding. *Polyhedron* **2006**, *25*, 3053-3065.

(194) Hirotsu, M.; Santo, K.; Hashimoto, H.; Kinoshita, I. Carbon- and Sulfur-Bridged Diiron Carbonyl Complexes Containing N,C,S-Tridentate Ligands Derived from Functionalized Dibenzothiophenes: Mimics of the [FeFe]-Hydrogenase Active Site. *Organometallics* **2012**, *31*, 7548-7557.

(195) Bhattacharya, P.; Krause, J. A.; Guan, H. Activation of Dihydrogen and Silanes by Cationic Iron Bis(phosphinite) Pincer Complexes. *Organometallics* **2014**, *33*, 6113-6121.

(196) Ryan, O. B.; Tilset, M.; Parker, V. D. Chemical and Electrochemical Oxidation of Group 6 Cyclopentadienylmetal Hydrides. First Estimates of 17-electron Metal-hydride Cation-radical Thermodynamic Acidities and their Decomposition of 17-Electron Neutral Radicals. *J Am Chem Soc* **1990**, *112*, 2618-2626.

(197) Guan, H.; Saddoughi, S. A.; Shaw, A. P.; Norton, J. R. Ruthenium-Catalyzed Ionic Hydrogenation of Aziridinium Cations. *Organometallics* **2005**, *24*, 6358-6364.

(198) Brookhart, M.; Green, M. L. H.; Parkin, G. Agostic Interactions in Transition Metal Compounds. *Proc Natl Acad Sci U S A* **2007**, *104*, 6908-6914.

(199) Shih, W.-C.; Ozerov, O. V. One-Pot Synthesis of 1,3-Bis(phosphinomethyl)arene PCP/PNP Pincer Ligands and Their Nickel Complexes. *Organometallics* **2015**, *34*, 4591-4597.

(200) Yu, C.-H.; Yang, X.; Ji, X.; Wang, C.-H.; Lai, Q.; Bhuvanesh, N.; Ozerov, O. V. Redox Communication between Two Diarylamido/Bis(phosphine) (PNP)M Moieties Bridged by Ynediyl Linkers (M = Ni, Pd, Pt). *Inorganic Chemistry* **2020**, *59*, 10153-10162.

(201) Uson, R.; Oro, L. A.; Cabeza, J. A. Dinuclear Methoxy Cyclooctadiene and Barrelene Complexes of Rhodium(I) and Iridium(I). *Inorganic Syntheses* **1985**, *23*, 126-130.

(202) Krautwald, S.; Bezdek, M. J.; Chirik, P. J. Cobalt-Catalyzed 1,1-Diboration of Terminal Alkynes: Scope, Mechanism, and Synthetic Applications. *J Am Chem Soc* **2017**, *139*, 3868-3875.

(203) Zhao, F.; Jia, X.; Li, P.; Zhao, J.; Zhou, Y.; Wang, J.; Liu, H. Catalytic and Catalyst-free Diboration of Alkynes. *Organic Chemistry Frontiers* **2017**, *4*, 2235-2255.

(204) Takaya, J.; Iwasawa, N. Catalytic, Direct Synthesis of Bis(boronate) Compounds. *ACS Catalysis* **2012**, *2*, 1993-2006.

(205) Lesley, G.; Nguyen, P.; Taylor, N. J.; Marder, T. B.; Scott, A. J.; Clegg, W.; Norman, N. C. Synthesis and Characterization of Platinum(II)−Bis(boryl) Catalyst Precursors for Diboration of Alkynes and Diynes: Molecular Structures of cis-[(PPh3)2Pt(B-4-Butcat)2], cis-[(PPh3)2Pt(Bcat)2], cis-[(dppe)Pt(Bcat)2], cis-[(dppb)Pt(Bcat)2], (E)-(4-MeOC6H4)C(Bcat)CH(Bcat), (Z)-(C6H5)C(Bcat)C(C6H5)(Bcat), and (Z,Z)-(4-MeOC6H4)C(Bcat)C(Bcat)C(Bcat)C(4-MeOC6H4)(Bcat) (cat = 1,2-O2C6H4; dppe = Ph2PCH2CH2PPh2; dppb = Ph2P(CH2)4PPh2). *Organometallics* **1996**, *15*, 5137-5154.

(206) Lillo, V.; Mata, J.; Ram ́ırez, J.; Peris, E.; Fernandez, E. Catalytic Diboration of Unsaturated Molecules with Platinum(0)−NHC: Selective Synthesis of 1,2-Dihydroxysulfones. *Organometallics* **2006**, *25*, 5829-5831.

(207) Abu Ali, H.; Goldberg, I.; Kaufmann, D.; Burmeister, C.; Srebnik, M. Novel C1-Bridged Bisboronate Derivatives by Insertion of Diazoalkanes into Bis(pinacolato)diborane(4). *Organometallics* **2002**, *21*, 1870-1876.

(208) Grirrane, A.; Corma, A.; Garcia, H. Stereoselective Single (Copper) or Double (Platinum) Boronation of Alkynes Catalyzed by Magnesia-Supported Copper Oxide or Platinum Nanoparticles. *Chemistry – A European Journal* **2011**, *17*, 2467-2478.

(209) Lee, C.-I.; Zhou, J.; Ozerov, O. V. Catalytic Dehydrogenative Borylation of Terminal Alkynes by a SiNN Pincer Complex of Iridium. *J Am Chem Soc* **2013**, *135*, 3560-3566.

(210) Pell, C. J.; Ozerov, O. V. Catalytic Dehydrogenative Borylation of Terminal Alkynes by POCOP-supported Palladium Complexes. *Inorganic Chemistry Frontiers* **2015**, *2*, 720-724.

(211) Lee, C.-I.; DeMott, J. C.; Pell, C. J.; Christopher, A.; Zhou, J.; Bhuvanesh, N.; Ozerov, O. V. Ligand Survey Results in Identification of PNP Pincer Complexes of Iridium as Long-lived and Chemoselective Catalysts for Dehydrogenative Borylation of Terminal Alkynes. *Chemical Science* **2015**, *6*, 6572-6582.

(212) Tsuchimoto, T.; Utsugi, H.; Sugiura, T.; Horio, S. Alkynylboranes: A Practical Approach by Zinc-Catalyzed Dehydrogenative Coupling of Terminal Alkynes with 1,8-Naphthalenediaminatoborane. *Advanced Synthesis & Catalysis* **2015**, *357*, 77-82.

(213) Romero, E. A.; Jazzar, R.; Bertrand, G. Copper-catalyzed Dehydrogenative Borylation of Terminal Alkynes with Pinacolborane. *Chemical Science* **2017**, *8*, 165-168.

(214) Wei, D.; Carboni, B.; Sortais, J.-B.; Darcel, C. Iron-Catalyzed Dehydrogenative Borylation of Terminal Alkynes. *Advanced Synthesis & Catalysis* **2018**, *360*, 3649-3654.

(215) Procter, R. J.; Uzelac, M.; Cid, J.; Rushworth, P. J.; Ingleson, M. J. Low-Coordinate NHC–Zinc Hydride Complexes Catalyze Alkyne C–H Borylation and Hydroboration Using Pinacolborane. *ACS Catalysis* **2019**, *9*, 5760-5771.

(216) Muccitelli, J.; Wen, W.-Y. Solubilities of Hydrogen and Deuterium Gases in Water and Their Isotope Fractionation Factor. *Journal of Solution Chemistry* **1978**, *7*, 257-267.

(217) Gjaldbæk, J. C. The solubility of Hydrogen, Oxygen, and Carbon Monoxide in Some Non-polar Solvents. *Acta Chemica Scandinavica* **1952**, *6*, 11.

(218) Liu; Takemura, F.; Yabe, A. Solubility and Diffusivity of Carbon Monoxide in Liquid Methanol. *Journal of Chemical & Engineering Data* **1996**, *41*, 589-592.

(219) Herde, J. L.; Lambert, J. C.; Senoff, C. V.; Cushing, M. A. Cyclooctene and 1,5-Cyclooctadiene Complexes of Iridium(I). *Inorganic Syntheses* **1974**, 18-20.

(220) Bartels, B.; Garcá-Yebra, C.; Rominger, F.; Helmchen, G. Iridium-Catalysed Allylic Substitution: Stereochemical Aspects and Isolation of IrIII Complexes Related to the Catalytic Cycle. *European Journal of Inorganic Chemistry* **2002**, *2002*, 2569-2586.

(221) Socol, S. M.; Yang, C.; Meek, D. W.; Glaser, R. Spectroscopic and Reactivity Studies of Diastereomeric Iridium(III) Hydride Complexes of the Chelating Tritertiary Phosphine Ligand Cyttp. *Canadian Journal of Chemistry* **1992**, *70*, 2424-2433.

(222) van der Ent, A.; Onderdelinden, A. L.; Schunn, R. A. Chlorobis(cyclooctene)rhodium(I) and -Iridium(I) Complexes. *Inorganic Syntheses* **1973**, 92-95.

(223) Green, L. M.; Meek, D. W. Synthesis, Characterization and Reactivity of Alkoxide and Hydroxide Complexes of Rhodium(I) and Iridium(I). *Organometallics* **1989**, *8*, 659-666.

(224) Iwadate, N.; Suginome, M. Synthesis of Masked Haloareneboronic Acids via Iridium-catalyzed Aromatic C–H Borylation with 1,8-Naphthalenediaminatoborane (danBH). *Journal of Organometallic Chemistry* **2009**, *694*, 1713-1717.

(225) Zhou, Y.; You, W.; Smith, K. B.; Brown, M. K. Copper-Catalyzed Cross-Coupling of Boronic Esters with Aryl Iodides and Application to the Carboboration of Alkynes and Allenes. *Angewandte Chemie International Edition* **2014**, *53*, 3475-3479.

(226) Ho, G.-M.; Segura, L.; Marek, I. Ru-catalyzed Isomerization of ω-alkenylboronates Towards Stereoselective Synthesis of Vinylboronates with Subsequent in situ Functionalization. *Chemical Science* **2020**, *11*, 5944-5949.

(227) Incerti–Pradillos, C. A.; Kabeshov, M. A.; Malkov, A. V. Highly Stereoselective Synthesis of Z-Homoallylic Alcohols by Kinetic Resolution of Racemic Secondary Allyl Boronates. *Angewandte Chemie International Edition* **2013**, *52*, 5338-5341.

(228) Gu, W.; McCulloch, B. J.; Reibenspies, J. H.; Ozerov, O. V. Improved Methods for the Halogenation of the [HCB11H11]− Anion. *Chemical Communications* **2010**, *46*, 2820-2822.

APPENDIX A

SYNTHESIS OF BIS-(2-DIISOPROPYLPHOSPHINOPYRROLYL) ALANE (ALMEP2) LIGANDS AND THEIR RHODIUM AND IRIDIUM COMPLEXES

A.1 Results and discussion

The protolysis of $AlMe_3$ with 2 equiv **204** at room temperature leads to **701** with 95% purity. **701** exhibits an expected C_{2v} symmetric ^1H NMR spectrum. The Al-Me resonance of **701** appears as a triplet at 0.05 ppm with a J_{P-H} coupling equals to 3.2 Hz.

The **701** was directly used in cyclometalation reactions without further purification. Treatment of **701** in toluene with 0.5 equiv $[Rh(COD)Cl]_2$ in the presence of pyridine gives rise to **702** at room temperature, which is poorly dissolved in toluene. 72% isolation yield was achieved via filtration. Single crystals of **702** for X-ray analysis was obtained via cooling a THF solution in -35 ℃ freezer. The ^1H NMR spectrum of **702** is C_s symmetric, and one set of the ^{i}Pr methyl protons resonate at far more up-field than the rest(0.33 ppm) due to the aromatic ring current effect from pyridine.

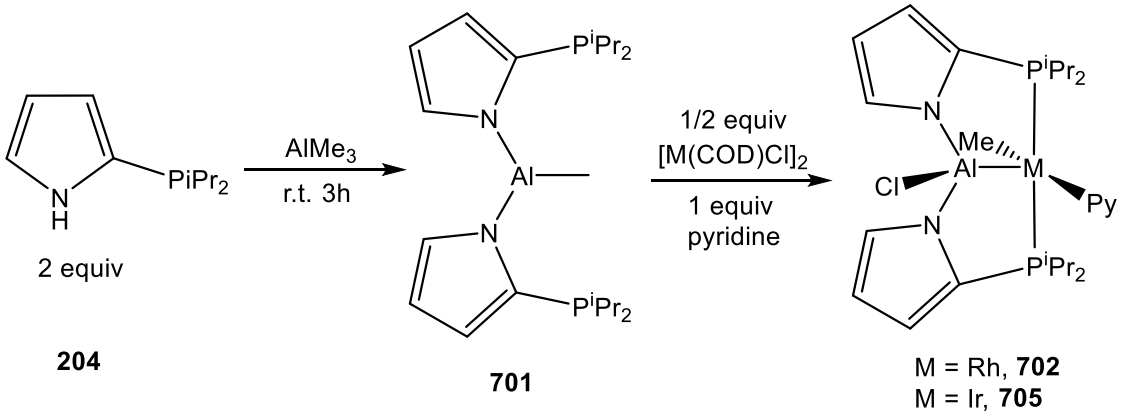

Scheme VII-1. Synthesis of **701** and its metal complexes

With the similar synthetic procedure **705** was isolated in 70% yield. The single crystals suitable for X-ray analysis was obtained with the similar condition. The 5 different protons resonances of pyridine ligand was observed in ^{1}H NMR spectrum, suggesting a restricted rotation of pyridine around Ir-N bond and is consistent with upfield resonances of one set of ^{i}Pr methyl.

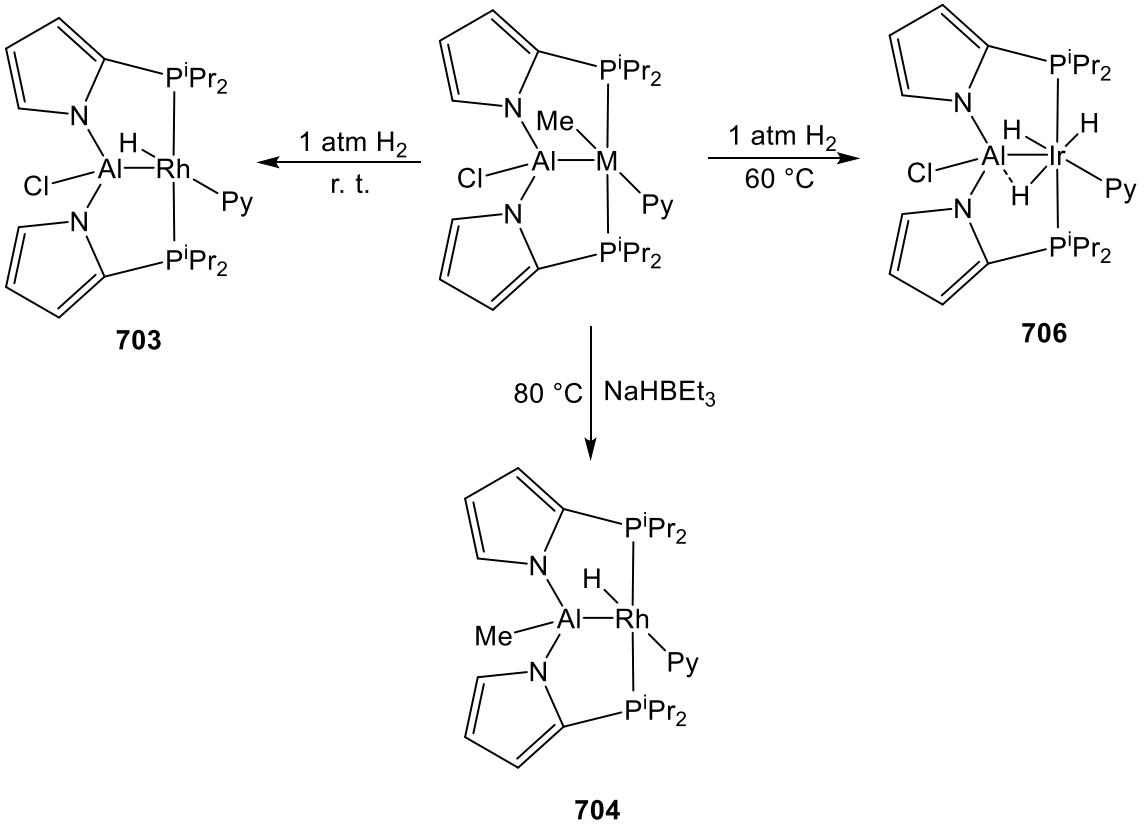

Scheme VII-2. Reactions of (PAlClP)MPyMe with H_2 and $NaHBEt_3$

The reaction of **702** with 1 atm H_2 at room temperature leads to **703** within 3 h. While reaction of **705** with 1 atm H_2 is slower and requires heating at 60 ℃ for 2 h. Both **706** and **703** have poor solubility in toluene and can be recrystallized from a hot toluene solution.

The treatment of 702 with $NaHBEt_3$ in the presence of pyridine leads to 704, where Al-Cl bond is replaced with methyl and Rh-Me bond is replace with Rh-H bond.

A.2 Experimental section

A.2.1 General consideration

Unless otherwise specified, all reactions and manipulations were carried out inside an argon-filled glove box or using Schlenk line techniques. THF, toluene, and pentane were dried and deoxygenated via the solvent purification system and stored over molecular sieves in the glove box filled with argon. C_6D_6 were dried over NaK /Ph_2CO/18-crown-6, distilled and stored over molecular sieves in an Ar-filled glove box. Fluorobenzene was dried over CaH_2, distilled and stored over molecular sieves in an Ar-filled glove box. NMR spectra were recorded on a Varian Inova 500 spectrometer (^{1}H NMR, 499.703 MHz, ^{13}C NMR 125.580 MHz), Varian Inova 400 (^{11}B NMR, 128.191 MHz, ^{27}Al NMR, 104.223 MHz) spectrometer. Chemical shifts are reported in δ (ppm). For ^{1}H and ^{13}C NMR spectra, the residual solvent peak was used as an internal reference (^{1}H NMR: δ 7.16 for C_6D_6, 5.32 for CD_2Cl_2, 2.08 for d_8-toluene; ^{13}C NMR: δ 128.06 for C_6D_6, 53.84 for CD_2Cl_2). Elemental analyses were performed by CALI Labs, Inc. (Highland Park, NJ). 1H-pyrrole was purchased from Oakwood chemicals, then was dried with CaH_2 and distilled before use. Other chemicals were purchased from commercial vendors and used without further

purification. 1H-2-diisopropylphosphinopyrrole (**204**) was synthesized according to the procedure in chapter II.

A.2.2 Synthesis of PAlMeP ligand and the rhodium and iridium complexes

Reaction of 1 with $AlMe_3$. To a J. Young tube, 18.3 mg (0.010 mmol) of **204** was loaded with 0.5 mL C_6D_6. 25 μL 2.0 M (0.050 mmol) $AlMe_3$ solution in toluene was added to the above solution via micro syringe at room temperature. The resulting clear solution was stirred at room temperature for 3 h, which turned light yellow. The reaction process to form **701** was monitored by NMR spectroscopy. ^{1}H NMR (500 MHz, C_6D_6): δ 7.33 (s, 2H), 6.77 (t, *J* = 2.7 Hz, 2H), 6.65 – 6.57 (m, 2H), 1.95 (octet, *J* = 7.0 Hz, 4H), 0.96 (dd, *J* = 12.9, 7.0 Hz, 12H), 0.93 (dd, *J* = 16.5, 7.0 Hz, 12H), 0.05 (t, *J* = 3.2 Hz, 3H). ^{13}C{^{1}H} NMR (125 MHz, C_6D_6): δ . ^{31}P{^{1}H} NMR (202 MHz, C_6D_6): δ -3.1 (s) ppm.

Synthesis of (PAlClP)RhPyMe (702). To a 50 mL Schlenk flask, 670 mg (3.66 mmol) of **201** was loaded with 10 mL toluene. 915 μL 2.0 M (1.83 mmol) $AlMe_3$ solution in toluene was added to the above solution via micro syringe at room temperature. The resulting clear solution was stirred at room temperature for 3 h before 158 mg (2.01 mmol) Py was added. 656 mg (0.92 mmol) $[Rh(COE)_2Cl]_2$ in 10 mL toluene was then added to the resulting mixture. The yellow precipitate form immediately upon mixing. The suspension was stirred at room temperature for 2 h before filtration. The filtrate was washed with cold 4.5 mL (1.5 mL×3) toluene to afford 822 mg **702** (72%) as yellow powder. The single crystal for X-ray analysis was obtained via recrystallization from concentrated THF solution. ^{1}H NMR (500 MHz, C_6D_6): δ 9.58 (brs, Py*H*, 1H), 8.52 (brs, Py*H*, 1H), 7.61 (dd, *J* = 2.3, 1.3 Hz, Pyrrole*H*, 2H), 6.78 (t, *J* = 1.9 Hz, Pyrrole*H*, 4H),

6.70 – 6.59 (m, Py*H*, 1H), 6.36 (brs, Py*H*, 2H), 2.41 (dtd, *J* = 12.0, 7.3, 2.7 Hz, C*H*(CH_3)$_2$, 2H), 2.18 – 2.00 (m, C*H*(CH_3)$_2$, 2H), 1.31 (dvt, *J* = 8.8, 7.6 Hz, CH(C*H*$_3$)$_2$, 6H), 1.23 (dvt, *J* = 7.2, 6.1 Hz, CH(C*H*$_3$)$_2$, 6H), 0.89 (dvt, *J* = 7.3 Hz, CH(C*H*$_3$)$_2$, 6H), 0.33 (dvt, *J* = 7.2 Hz, CH(C*H*$_3$)$_2$, 6H), 0.29 (td, *J* = 6.8, 1.7 Hz, Rh-C*H*$_3$, 3H). $^{31}P\{^1H\}$ NMR (202 MHz, C_6D_6): δ 33.71 (d, J_{Rh-P} = 119.6 Hz) .

Synthesis of (PAlClP)RhPyH (703). To a 10 mL top-screw-cap Schlenk flask, 62 mg (0.10 mmol) **702** was loaded with 5 mL toluene. The flask was degassed via freeze-pump-thaw 3 cycles and then back-filled with 1 atm H_2. After the solution was stirred at room temperature for 3 h, yellow precipitate was formed. The suspension was heated in a 90 ℃ oil bath to give a clear solution. 32 mg of **703** (54%) as yellow crystals was obtained upon cooling the solution from 90 ℃ to back to room temperature. The crystals collected are suitable for X-ray analysis. ^1H NMR (500 MHz, C_6D_6): δ 8.81 (d, *J* = 5.4 Hz, Py*H*, 2H), 7.57 (dd, *J* = 2.4, 1.2 Hz, Pyrrole*H*, 2H), 6.81 (t, *J* = 2.7 Hz, Pyrrole*H*, 2H), 6.74 – 6.67 (m, Py*H*, 1H), 6.65 (dd, *J* = 3.2, 1.0 Hz, Pyrrole*H*, 2H), 6.49 – 6.41 (m, Py*H*, 2H), 2.24 – 2.13 (m, C*H*(CH_3)$_2$, 2H), 1.60 (h, *J* = 7.1 Hz, C*H*(CH_3)$_2$, 2H), 1.16 – 1.08 (m, CH(C*H*$_3$)$_2$, 6H), 1.11 – 1.03 (m, CH(C*H*$_3$)$_2$, 6H), 0.94 (dvt, *J* = 6.8 Hz, CH(C*H*$_3$)$_2$, 6H), 0.78 (dvt, *J* = 8.5, 7.1 Hz, CH(C*H*$_3$)$_2$, 6H), -17.96 (q, *J* = 20.0 Hz, Rh-*H*, 1H). $^{31}P\{^1H\}$ NMR (202 MHz, C_6D_6): δ 35.0 (dd, *J* = 120.3, 17.7 Hz) ppm.

Synthesis of (PAlMeP)RhPyH (704). To a 50 mL culture tube, 312 mg (0.50 mmol) **702** and 60 μL (0.50 mmol) Py was loaded with 15 mL toluene. 500 μL 1.0 M (0.50 mmol) $NaHBEt_3$ was added to the mixture via micro syringe. The resulting mixture was then heated in 80 ℃ oil bath or 4 h before cooled down to the room temperature and

filtered through a short pad of Celite. All the volatile was removed under vacuum, and the residue was dissolve with 5 mL THF. The THF solution was layered with pentane. Slow diffusion in a -35 ℃ freezer afforded 150 mg **704** (50%) as yellow crystals which are suitable for X-ray analysis. ^{1}H NMR (500 MHz, C_6D_6): δ 8.61 (d, *J* = 5.4 Hz, Py*H*, 2H), 7.55 (t, *J* = 1.7 Hz, Pyrrole*H*, 2H), 6.89 (t, *J* = 2.7 Hz, Pyrrole*H*, 2H), 6.69 (d, *J* = 3.2 Hz, Pyrrole*H*, 2H), 6.65 (tt, *J* = 7.7, 1.9 Hz, Py*H*, 1H), 6.41 – 6.34 (m, Py*H*, 2H), 2.24 - 2.16 (m, *J* = 7.0, 3.4 Hz, C*H*$(CH_3)_2$, 2H), 1.63 (hept, *J* = 6.9 Hz, C*H*$(CH_3)_2$, 2H), 1.18 (dvt, *J* = 7.2 Hz, CH(C*H*$_3)_2$, 6H), 1.12 (dvt, *J* = 8.5, 7.0 Hz, CH(C*H*$_3)_2$, 6H), 0.94 (dvt, *J* = 6.7 Hz, CH(C*H*$_3)_2$, 6H), 0.80 – 0.63 (m, CH(C*H*$_3)_2$, 6H), 0.19 (s, Al-C*H*$_3$, 3H), -17.84 (dt, *J* = 23.9, 18.8 Hz, Rh-*H*, 1H). ^{31}P{^{1}H} NMR (202 MHz, C_6D_6): δ 35.6 (d, *J* = 125.3 Hz) ppm.

Synthesis of (PAlClP)IrPyMe (705). To a 50 mL Schlenk flask, 670 mg (3.66 mmol) of **204** was loaded with 10 mL toluene. 915 μL 2.0 M (1.83 mmol) $AlMe_3$ solution in toluene was added to the above solution via micro syringe at room temperature. The resulting clear solution was stirred at room temperature for 3 h before 158 mg (2.01 mmol) Py was added. 819 mg (0.92 mmol) $[Ir(COE)_2Cl]_2$ in 10 mL toluene was then added to the resulting mixture. The yellow precipitate form immediately upon mixing. The suspension was stirred at room temperature for 2 h before filtration. The residue was washed with cold 4.5 mL (1.5 mL×3) toluene to afford 910 mg **705** (70%) as yellow powder. The single crystal for X-ray analysis was obtained via recrystallization from concentrated THF solution. ^{1}H NMR (500 MHz, C_6D_6): δ 9.81 (d, *J* = 5.6 Hz, Py*H*, 1H), 8.48 (d, *J* = 5.6 Hz, Py*H*, 1H), 7.63 (dd, *J* = 2.3, 1.2 Hz, Pyrrole*H*, 2H), 6.83 – 6.74 (m, Pyrrole*H*, 4H), 6.59 (tt, *J* = 7.7, 1.7 Hz, Py*H*, 1H), 6.31 (dt, *J* = 22.2, 6.7 Hz, Py*H*, 2H), 2.65 – 2.57 (m,

C*H*(CH_3)$_2$, 2H), 2.41 – 2.29 (m, C*H*(CH_3)$_2$, 2H), 1.33 – 1.26 (m, CH(C*H*$_3$)$_2$, 6H), 1.23 (dvt, *J* = 6.7 Hz, CH(C*H*$_3$)$_2$, 6H), 0.90 – 0.82 (m, CH(C*H*$_3$)$_2$ and Ir-C*H*$_3$, 9H), 0.37 (dvt, *J* = 7.2 Hz, CH(C*H*$_3$)$_2$, 6H). ^{31}P{^{1}H} NMR (202 MHz, C_6D_6): δ 31.2 (s) ppm.

Synthesis of (PAlClP)IrPyH$_3$ (706). To a 25 mL top-screw-cap Schlenk flask, 142 mg (0.20 mmol) **705** was loaded with 10 mL toluene. The flask was degassed via freeze-pump-thaw 3 cycles and then back-filled with 1 atm H_2. The resulting solution was heated in a 90 ℃ oil bath for 4 h. 101 mg of **7** (72%) as yellow crystals was obtained upon cooling the solution from 90 ℃ to room temperature. The crystals collected are suitable for X-ray analysis. 14 mg crystals of **706** was loaded to a J. Young tube to prepare a sample of NMR spectroscopy, however the solubility of **706** is quite poor in benzene, in addition, around 15% new species (**707**) of dissolved **706** was observed in the solution according to the NMR spectroscopy. ^{1}H NMR (500 MHz, C_6D_6): δ 8.76 (d, *J* = 5.5 Hz, Py*H*, 2H), 7.81 – 7.59 (m, Pyrrole*H*, 2H), 6.91 (t, *J* = 2.8 Hz, Pyrrole*H*, 2H), 6.62 (d, *J* = 3.2 Hz, Pyrrole*H*, 2H), 6.57 (t, *J* = 7.7 Hz, Py*H*, 1H), 6.26 – 5.71 (m, Py*H*, 2H), 2.27 - 2.20 (m, C*H*(CH_3)$_2$, 2H), 1.29 (hept, *J* = 6.9 Hz, C*H*(CH_3)$_2$, 2H), 1.15 – 1.05 (m, CH(C*H*$_3$)$_2$, 6H), 0.99 – 0.89 (m, CH(C*H*$_3$)$_2$, 18H), -5.95 (s, Ir-*H*, 1H), -10.03 (qd, $J_{P\text{-}H}$ = 14.1, $J_{H\text{-}H}$ = 4.1 Hz, Ir-*H*, 1H), -21.94 (td, $J_{P\text{-}H}$ = 14.8, $J_{H\text{-}H}$ = 4.1 Hz, Ir-*H*, 1H). ^{31}P{^{1}H} NMR (202 MHz, C_6D_6): δ 19.7 (s) ppm. NMR spectroscopy of the isomer **707** in equilibrium with **706**: ^{1}H NMR (500 MHz, C_6D_6): δ 12.03 (s, PyN*H*, 1H), 9.31 (d, *J* = 5.5 Hz, Py*H*, 2H), 6.84 (dd, *J* = 3.3, 1.8 Hz, Pyrrole*H*, 2H), 6.72 (tt, *J* = 7.5, 1.7 Hz, Py*H*, 1H), 6.39 (m, Pyrrole*H*, 4H), 6.36 – 6.30 (m, Py*H*, 2H), 2.35 – 2.27 (m, C*H*(CH_3)$_2$, 2H), 1.45 (h, *J* = 7.2 Hz, C*H*(CH_3)$_2$, 2H), 1.16 – 1.08 (m, CH(C*H*$_3$)$_2$, 6H), 0.82 (dvt, *J* = 6.4 Hz, CH(C*H*$_3$)$_2$, 6H), 2 sets of CH(C*H*$_3$)$_2$ was

overlapped with Me resonances of **706**, -23.32 (td, J_{P-H} = 17.1, J_{H-H} = 7.9 Hz, Ir-*H*, 1H), -24.82 (td, J_{P-H} = 18.0, J_{H-H} = 7.8 Hz, Ir-*H*, 1H). $^{31}P\{^{1}H\}$ NMR (202 MHz, C_6D_6): δ 6.6 (s) ppm.

A.2.3 X-ray structural determination details

X-Ray data collection, solution, and refinement for (PAlClP)RhPyH (703) (CCDC xxxxxxx). (Figure VII-1) A Leica MZ 75 microscope was used to identify a light yellow block of suitable size with very well defined faces with dimensions (max, intermediate, and min) 0.26 x 0.28 x 0.32 mm^3 from a representative sample of crystals of the same habit. The crystal mounted on a nylon loop was then placed in a cold nitrogen stream (Oxford) maintained at 110 K. X-ray data were obtained on a Bruker APEXII CCD based diffractometer (Mo sealed X-ray tube, Kα = 0.71073 Å). All diffractometer manipulations, including data collection, integration and scaling were carried out using the Bruker APEX3 software. The absorption correction program SADABS was employed to correct the data for absorption effects. The space group was determined on the basis of systematic absences and intensity statistics and the structure was solved by direct methods and refined by full-matrix least squares on F^2. The structure was solved in the orthorhombic $P2_1/n$ space group using XS (incorporated in SHELXLE/OLEX2).[146,147] All non-hydrogen atoms were refined with anisotropic thermal parameters. All hydrogen atoms were placed in idealized positions and refined using riding model. The structure was refined (weighted least squares refinement on F^2) and the final least-squares refinement converged.[146-148] No additional symmetry was found using ADDSYM incorporated in PLATON program.[149]

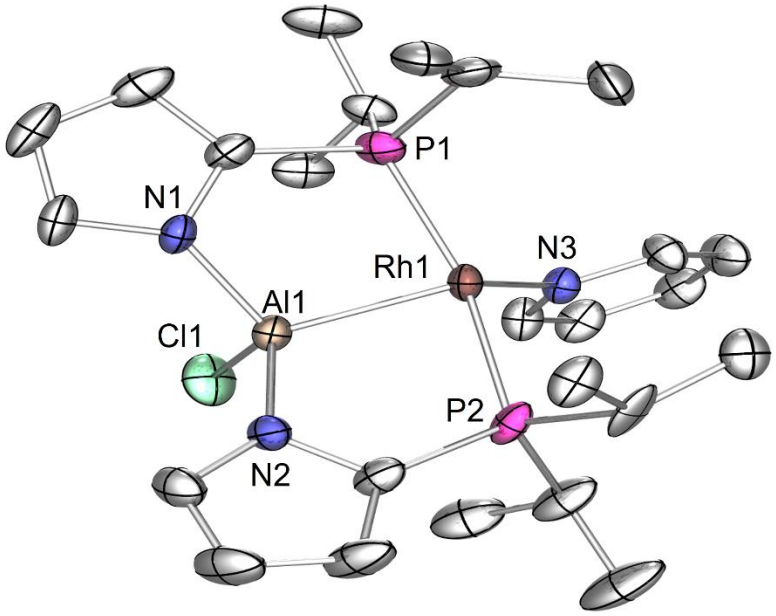

Figure VII-1. The ORTEP drawing (50% thermal ellipsoids) of **703** showing selected atom labeling. Hydrogen atoms and THF solvent were omitted for clarity. Selected bond distances (Å) and angles ( ):Rh1-P2, 2.2987(6); Rh1-P1, 2.2936(6); Rh1-Al1, 2.3407(6); Rh1-N3, 2.1470(15); Al1-Cl1, 2.1569(8); Al1-N1, 1.8752(18); Al1-N2, 1.8752(18); P2-Rh1-Al1, 83.74(2); P1-Rh1-P2, 161.212(19); P1-Rh1-Al1, 84.28(2); N3-Rh1-P2, 98.05(5); N3-Rh1-P1, 100.60(5); N3-Rh1-Al1, 122.79(5); N1-Al1-Rh1, 105.62(6); N1-Al1-Cl1, 104.99(6); N1-Al1-N2, 119.22(8).

X-Ray data collection, solution, and refinement for (PAlMeP)RhPyH (704) (CCDC xxxxxxx) (Figure VII-2). A yellow, multi-faceted block of suitable size (0.20 x 0.21 x 0.18 mm) was selected from a representative sample of crystals of the same habit using an optical microscope and mounted onto a nylon loop. Low temperature (110 K) X-ray data were obtained on a Bruker APEXII CCD based diffractometer (Mo sealed X-ray tube, K_α = 0.71073 Å). All diffractometer manipulations, including data collection, integration and scaling were carried out using the Bruker APEXII software. An absorption correction was applied using SADABS. The space group was determined on the basis of systematic absences and intensity statistics and the structure was solved by direct methods and refined by full-matrix least squares on F^2. The structure was solved in the

orthorhombic $P2_1/n$ space group using XS (incorporated in SHELXLE).[146,147] All non-hydrogen atoms were refined with anisotropic thermal parameters. All hydrogen atoms were placed in idealized positions and refined using riding model. The structure was refined (weighted least squares refinement on F^2) and the final least-squares refinement converged.[146-148] No additional symmetry was found using ADDSYM incorporated in PLATON program.[149]

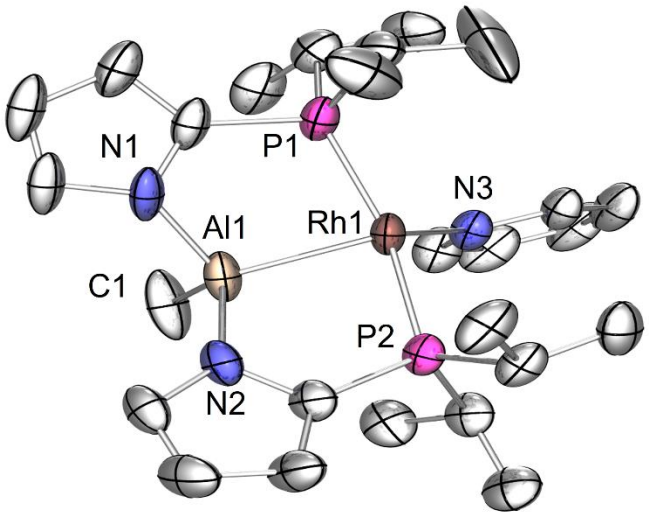

Figure VII-2. The ORTEP drawing (50% thermal ellipsoids) of **704** showing selected atom labeling. Hydrogen atoms and C_6D_6 solvent were omitted for clarity. Selected bond distances (Å) and angles (°):Rh1-P1, 2.2900(11); Rh1-P2, 2.2850(12); Rh1-Al1, 2.3754(12); Rh1-N3, 2.153(3); Al1-N1, 1.895(4); Al1-N2, 1.900(4); Al1-C1, 1.971(5); P1-Rh1-Al1, 83.95(4); P2-Rh1-P1, 160.09(3); P2-Rh1-Al1, 85.06(5); N1-Al1-Rh1, 103.53(13); N1-Al1-N2, 115.51(15); N1-Al1-C1, 106.5(2).

X-Ray data collection, solution, and refinement for (PAlClP)IrPyMe (705) (CCDC xxxxxxx) (Figure VII-3). A Leica MZ 75 microscope was used to identify a light yellow block of suitable size with very well defined faces with dimensions (max, intermediate, and min) 0.025 x 0.025 x 0.015 mm^3 from a representative sample of crystals of the same habit. The crystal mounted on a nylon loop was then placed in a cold nitrogen

stream (Oxford) maintained at 110 K. X-ray data were obtained on a Bruker APEXII CCD based diffractometer (Mo sealed X-ray tube, Kα = 0.71073 Å). All diffractometer manipulations, including data collection, integration and scaling were carried out using the Bruker APEXII software. An absorption correction was applied using SADABS. The space group was determined on the basis of systematic absences and intensity statistics and the structure was solved by direct methods and refined by full-matrix least squares on F^2. The structure was solved in the monoclinic $P2_1/c$ space group using XS (incorporated in SHELXLE).[146,147] All non-hydrogen atoms were refined with anisotropic thermal parameters. All hydrogen atoms were placed in idealized positions and refined using riding model with the exception of the hydrogen bridged to iron and carbon which was located from the difference map. The structure was refined (weighted least squares refinement on F^2) and the final least-squares refinement converged.[146-148] No additional symmetry was found using ADDSYM incorporated in PLATON program.[149]

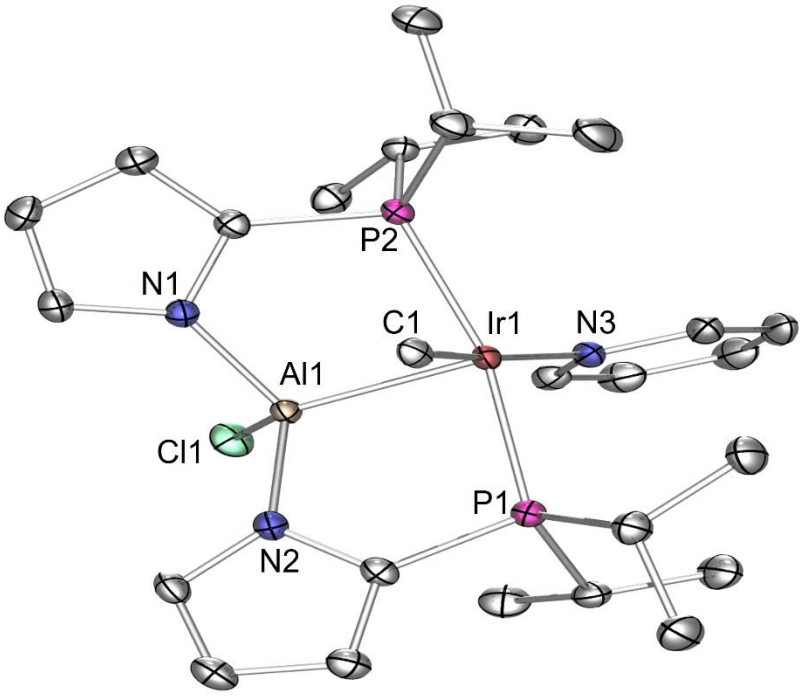

Figure VII-3. The ORTEP drawing (50% thermal ellipsoids) of **705** showing selected atom labeling. Hydrogen atoms and C_6H_5F solvent were omitted for clarity. Selected bond distances (Å) and angles ( ):Ir1-P1, 2.3137(6); Ir1-P2, 2.3150(6); Ir1-Al1, 2.3509(6); Ir1-N3, 2.1408(19); Ir1-C1, 2.127(2); Al1-N1, 1.870(2); Al1-N2, 1.871(2); Cl1-Al1, 2.1757(9); P1-Ir1-P2, 163.86(2); P1-Ir1-Al1, 84.44(2); P2 Ir1-Al1, 84.76(2); N3-Ir1-P1, 98.70(5); N3-Ir1-P2, 96.26(5); N3-Ir1-Al1, 110.14(5); C1-Ir1-P1, 83.40(6); C1-Ir1-P2, 83.31(6); C1-Ir1-Al1, 82.39(6); C1-Ir1-N3, 167.40(8); Cl1-Al1-Ir1, 123.38(3); N1-Al1-Ir1, 103.52(6); N1-Al1-Cl1, 104.54(7);

X-Ray data collection, solution, and refinement for (PAlClP)IrPyH (706) (CCDC xxxxxxx) (Figure VII-4). A Leica MZ 75 microscope was used to identify a light yellow block of suitable size with very well defined faces with dimensions (max, intermediate, and min) 0.26 x 0.28 x 0.32 mm^3 from a representative sample of crystals of the same habit. The crystal mounted on a nylon loop was then placed in a cold nitrogen stream (Oxford) maintained at 110 K. X-ray data were obtained on a Bruker APEXII CCD based diffractometer (Mo sealed X-ray tube, Kα = 0.71073 Å). All diffractometer manipulations, including data collection, integration and scaling were carried out using

the Bruker APEX3 software. The absorption correction program SADABSwas employed to correct the data for absorption effects. The space group was determined on the basis of systematic absences and intensity statistics and the structure was solved by direct methods and refined by full-matrix least squares on F^2. The structure was solved in the orthorhombic $P2_1/n$ space group using XS (incorporated in SHELXLE/OLEX2).[146,147] All non-hydrogen atoms were refined with anisotropic thermal parameters. All hydrogen atoms were placed in idealized positions and refined using riding model. The structure was refined (weighted least squares refinement on F^2) and the final least-squares refinement converged.[146-148] No additional symmetry was found using ADDSYM incorporated in PLATON program.[149]

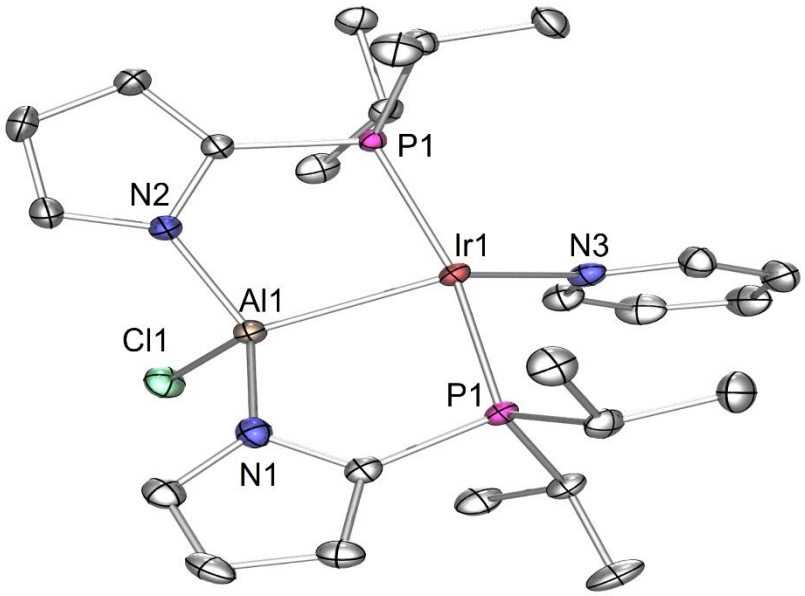

Figure VII-4. The ORTEP drawing (50% thermal ellipsoids) of **706** showing selected atom labeling. Hydrogen atoms and C_6D_6 solvent were omitted for clarity. Selected bond distances (Å) and angles ( ): Ir1-P1, 2.3112(7); Ir1-P2, 2.3073(8); Ir1-Al1, 2.5104(9); Ir1-N3, 2.176(3); Cl1-Al1, 2.1669(12); Al1-N1, 1.881(3); Al1-N2, 1.890(3); P1-Ir1-Al1, 85.23(3); P2-Ir1-P1, 164.84(3); P2-Ir1-Al1, 85.66(3); N3-Ir1-P1, 99.63(7); N3-Ir1-P2, 95.53(7); N3-Ir1-Al1, 128.29(7); N1-Al1-Ir1, 98.81(9); N1-Al1-Cl1, 102.49(9); N1-Al1-N2, 124.39(13).

APPENDIX B

CARBORANE C-H FUNCTIONALIZATION

B.1 General considerations.

Unless specified otherwise, all manipulations were performed under an Ar atmosphere using standard Schlenk line of glovebox techniques. Toluene, pentane, C_6D_6 and THF were dried over NaK/Ph_2CO/18-crown-6, distilled or vacuum transferred and stored over molecular sieves in an Ar-filled glovebox. NMR spectra were recorded on a Varian Inova 500 spectrometer (^{1}H NMR, 499.703 MHz, ^{13}C NMR 125.580 MHz), Varian Inova 400 (^{11}B NMR, 128.191 MHz) spectrometer, Bruker 400 (^{13}C 100, ^{11}B 102 MHz). Chemical shifts are reported in δ (ppm). For ^{1}H and ^{13}C NMR spectra, the residual solvent peak was used as an internal reference (^{1}H NMR: δ 7.16 for C_6D_6, 1.94 for CD_3CN, 7.26 for $CDCl_3$; ^{13}C NMR: δ 77.16 for $CDCl_3$, 1.32 for CD_3CN). MALDI mass spectrometric analyses of the carborane anions were carried out by the Texas A&M University Laboratory for Biological Mass Spectrometry, and simulated MALDI[227] spectra were generated using a publicly available isotope distribution calculator and mass spectrometry plotter.[1] For ^{11}B NMR, spectra were referenced externally to δ = 0 ppm by using $BF_3 \cdot Et_2O$. NaH was purchased from Sigma-Aldrich and washed with hexane before using; 6-bromo-1-hexene, 4-bromo-1-butene, allybromide and 1-iododecane was purchased from Matrix Scientific and used without further purification. 4-vinylbenzylchloride was purchased from Sigma Aldrich. $[Me_3NH][CHB_{11}Cl_{11}]$[228] was synthesized according to the published procedure.

B.2 Synthesis of [HNMe($C_{18}H_{37}$)$_2$][Cl]

[HNMe($C_{18}H_{37}$)$_2$][Cl]. A 50 mL Schlenk flask was charged with $(C_{18}H_{37})_2NMe$ (3.56 g, 6.6 mmol, 1 equiv.) and dry MeOH (536 μL, 13.2 mmol, 2 equiv.) and Et_2O (20 mL). Me_3SiCl (1.66 mL, 13.2 mmol, 2 equiv.) was then added to the above mixture dropwise. Upon mixing, the title product precipitated out as white solid. The solid was filtered, washed with pentane, and dried *in vacuo* to afford the product as a white solid, 3.42 g (90%). ^{1}H NMR (400 MHz, $CDCl_3$): δ 12.2 (br s, 1H, N*H*), 3.95 (s, 1H, C*H*$B_{11}Cl_{11}$), 2.81-2.99 (m, 4H, NC*H*$_2$), 2.69 (d, *J* = 4.8 Hz, 3H, NC*H*$_3$), 1.81-1.72 (m, 4H, C*H*$_2$), 1.29-1.20 (m, 60H, C*H*$_2$), 0.83 (t, *J* = 6.9 Hz, 6H, CH_3). $^{13}C\{^1H\}$ NMR (100 MHz, CD_3CN): δ 55.7 (s, alpha-CH_2, 2C), 39.9 (s, N–Me), 32.0 (s, CH_2, 2C), 29.8-29.1 (m, CH_2, 24C), 26.8 (s, CH_2, 2C), 23.6 (s, CH_2, 2C), 22.8 (s, CH_2, 2C), 14.2 (s, terminal CH_3, 2C).

B.3 Carborane C-H alkylation towards alkyl and alkenyl monoanion

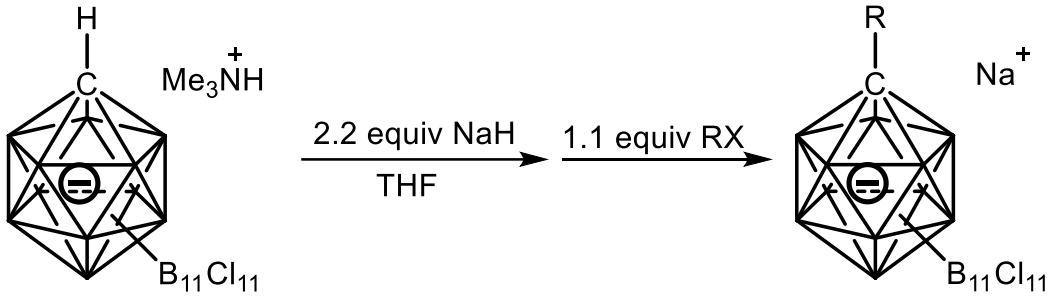

Scheme VII-3. C-H alkylation of carborane anion

General procedure for the synthesis of Na[$RCB_{11}Cl_{11}$]: To a 50 mL Schlenk flask, 500 mg $[Me_3NH][CHB_{11}Cl_{11}]$ and 2.5 equiv NaH were loaded with 20 mL THF. The resulting suspension was stirred at room temperature for 2 h until it stopped bubbling. All volatiles were removed under vacuum, and then 20 mL THF was added with 1.1 equiv R-Hal (allyl bromide, 4-bromo-1-butene, 6-bromo-1-hexene, 4-chloromethylstyrene, or

decyl iodide). The suspension was further stirred at room temperature overnight. NaCl was removed by filtering the solution through a short pad of Celite. All volatiles were removed under vacuum. The residue was washed with cold pentane and further dried under vacuum to yield Na[$RCB_{11}Cl_{11}$] as a white solid.

R = Allyl 708:

Na[Allyl-$CB_{11}Cl_{11}$]: 427 mg (85% yield). ^{1}H NMR (500 MHz, CD_3CN): δ 6.10 (ddt, *J* = 17.2, 9.9, 7.4 Hz, 1H), 5.13 (dq, *J* = 16.7, 1.4 Hz, 1H), 5.08 – 5.01 (dq, *J* = 16.7, 1.4 Hz, 1H), 3.01 (d, *J* = 7.3 Hz, 3H). ^{11}B{^{1}H NMR (128 MHz, CD_3CN): δ -3.03, -10.10, -11.73. ^{13}C{^{1}H} NMR (100 MHz, CD_3CN): δ 130.5 (s, *C*H*C*H_2), 120.4 (s, *C*H*C*H_2), 49.5 (brs, carborane-C), 35.6 (s, *C*H_2CHCH_2).

R = Butenyl 709

Na[Butenyl-$CB_{11}Cl_{11}$]: 427 mg Na[Butenyl-$CB_{11}Cl_{11}$] (85% yield) ^{1}H NMR (500 MHz, $CDCl_3$): δ 5.72 (ddt, *J* = 17.0, 10.3, 6.6 Hz, 1H), 5.08 (ddd, *J* = 17.4, 3.1, 1.6 Hz, 1H), 5.03 (ddd, *J* = 10.2, 3.1 Hz, 1.6 Hz, 1H), 2.69 – 2.61 (m, 2H), 2.37 (t, *J* = 8.9 Hz, 2H). ^{11}B(^{1}H decoupled) NMR (128 MHz, $CDCl_3$): δ -3.87, -10.52, -11.63. ^{13}C{^{1}H} NMR (100 MHz, CD_3CN): δ 137.6 (s, CH_2CH_2*C*H*C*H_2), 116.6 (s, *C*H*C*H_2), 50.6 (brs, carborane-C), 31.4 (s, *C*$H_2CH_2CHCH_2$), 29.6 (s, CH_2*C*H_2CHCH_2).

R = Hexenyl 710

Na[hexenyl-$CB_{11}Cl_{11}$]: 300 mg Na[hexenyl-$CB_{11}Cl_{11}$] (87% yield) ^{1}H NMR (400 MHz, CD_3CN): δ 5.77 (ddt, *J* = 17.0, 10.2, 6.7 Hz, 1H), 4.99 (dq, *J* = 17.2, 1.7 Hz, 1H), 4.93 (ddt, *J* = 10.2, 2.3, 1.2 Hz, 1H). 2.30 – 2.20 (m, 2H), 2.07 – 1.97 (m, 2H), 1.90 – 1.75 (m, 2H) 1.32 (p, *J* = 7.4 Hz, 2H). ^{11}B(^{1}H decoupled) NMR (128 MHz, CD_3CN): δ -2.94,

-9.96, -11.58. $^{13}C\{^{1}H\}$ NMR (100 MHz, CD_3CN): δ 139.2 (s, *C*H*C*H_2), 115.3 (s, *C*H*C*H_2), 51.4 (brs, carborane-C), 33.6 (s, *alpha-C*H_2), 31.8 (s, *C*H_2),29.9 (s, *C*H_2), 24.6 (s, *C*H_2).

R = Vinylbenzyl 711

Na[vinylbenzylCB$_{11}$Cl$_{11}$]: 449 mg (89%).^{1}H NMR (500 MHz, CD_2Cl_2) δ 7.46 (d, *J* = 8.2 Hz, 2H), 7.27 (d, *J* = 8.2 Hz, 2H), 6.69 (dd, *J* = 17.6, 10.9 Hz, 1H), 5.75 (d, *J* = 17.6 Hz, 1H), 5.24 (d, *J* = 11.2 Hz, 1H), 3.67 (s, 2H). $^{11}B(^{1}H$ decoupled) NMR (128 MHz, CD_2Cl_2): δ -3.32, -10.18, -11.16. $^{13}C\{^{1}H\}$ NMR (100 MHz, CD_3CN): δ 137.5 (s, *C*H*C*H_2), 137.0 (s, *Ph*) 134.8 (s, *Ph*), 131.0 (s, *Ph*), 125.4 (s, *Ph*), 114.6 (s, *Ph*), 49.5 (brs, carborane-C), 36.1 (s, Ph*C*H_2).

R = decyl 712

Na[DecylCB$_{11}$Cl$_{11}$]: 1.46 g (95%). ^{1}H NMR (500 MHz, $CDCl_3$) δ 2.27 (t, *J* = 9.2 Hz, 2H), 2.10 (s, 4H), 1.41 – 1.07 (m, 12H), 0.87 (t, *J* = 6.9 Hz, 3H). $^{11}B(^{1}H$ decoupled) NMR (128 MHz, $CDCl_3$): δ -4.14, -10.59, -11.52. $^{13}C\{^{1}H\}$ NMR (100 MHz, CD_3CN): δ 49.5 (brs, carborane-*C*), 32.4 (s, decyl*C*H_2), 31.8 (s, decyl*C*H_2), 30.5 (s, decyl*C*H_2), 30.0 (s, decyl*C*H_2), 29.9 (s, decyl*C*H_2), 29.8 (s, decyl*C*H_2), 29.4 (s, decyl*C*H_2), 24.9 (s, decyl*C*H_2), 23.2 (s, decyl*C*H_2), 14.4 (s, decyl*C*H_3).

B.4 Synthesis of activators (I)

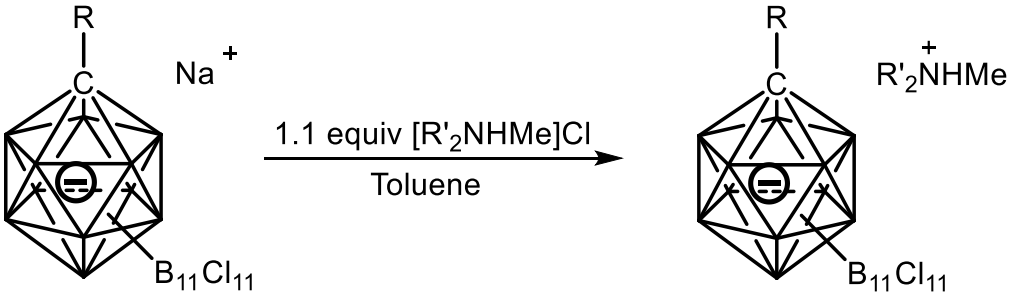

Scheme VII-4. Synthesis of ammonium carboranes

General synthesis of [R'$_2$MeNH][RCB$_{11}$Cl$_{11}$]: In a 50 mL Schlenk flask, a solution of 300 mg Na[RCB$_{11}$Cl$_{11}$] in 10 mL THF was added to a solution of 1.1 equiv [R'$_2$MeNH]Cl in 10 mL THF. Upon mixing, precipitate formed immediately. The mixture was further stirred for 2 h, then filtered through a short pad of Celite. The filtrate was concentrated *in vacuum*, and the resulting oil was dissolved in toluene. The toluene solution was passed through a short pad of silica gel (to remove excess [R'$_2$MeNH]Cl) and concentrated under vacuum to afford the product.

R = Allyl, R' = ^{n}Octyl 713

[^{n}Octyl$_2$MeNH][Allyl-CB$_{11}$Cl$_{11}$]: 360 mg (78%).^{1}H NMR (500 MHz, $CDCl_3$): δ 6.16 (ddt, *J* = 17.2, 9.9, 7.4 Hz, 1H), 5.20 (dq, *J* = 16.7, 1.4 Hz, 1H), 5.12 (dq, *J* = 16.7, 1.4 Hz, 1H), 3.01 (d, *J* = 7.3 Hz, 3H), 3.15 (vt, *J* = 7.5 Hz, 4H), 3.08 (d, *J* = 7.4 Hz, 2H), 2.97 (s, 3H), 1.80 (p, *J* = 8.0 Hz, 4H), 1.44 – 1.21 (m, 22H), 0.89 (t, *J* = 7.0 Hz, 3H). ^{11}B(^{1}H decoupled) NMR (128 MHz, $CDCl_3$): δ -3.53, -10.47, -11.75. ^{13}C NMR (126 MHz, CD_3CN): δ 137.6 (s, *C*H*C*H$_2$, 1C), 116.5 (s, *C*H*C*H$_2$, 1C), 57.1 (s, alpha-CH$_2$, 2C), 54.0 (brs, carborane-C, 1C), 40.8 (s, N-Me, 1C), 32.3 (s, CH$_2$, 2C), 29.6 (s, CH$_2$, 2C), 29.5 (s, *C*H$_2$CHCH$_2$, 1C), 26.9 (s, CH$_2$, 2C), 24.5 (s, CH$_2$, 2C), 23.3 (s, CH$_2$, 2C), 14.4 (s, terminal-Me, 2C).

R = Butenyl, R' = ^{n}Octyl 714

[^{n}Octyl$_2$MeNH][Butenyl-CB$_{11}$Cl$_{11}$]: 360 mg (80%).^{1}H NMR (500 MHz, $CDCl_3$): δ 6.16 (ddt, *J* = 17.2, 9.9, 7.4 Hz, 1H), 5.20 (dq, *J* = 16.7, 1.4 Hz, 1H), 5.12 (dq, *J* = 16.7, 1.4 Hz, 1H), 3.01 (d, *J* = 7.3 Hz, 3H), 3.15 (vt, *J* = 7.5 Hz, 4H), 3.08 (d, *J* = 7.4 Hz, 2H), 2.97 (s, 3H), 1.80 (p, *J* = 8.0 Hz, 4H), 1.44 – 1.21 (m, 22H), 0.89 (t, *J* = 7.0 Hz, 3H).

$^{11}B(^{1}H$ decoupled) NMR (128 MHz, $CDCl_3$): δ -3.81, -10.58, -11.80. $^{13}C\{^{1}H\}$ NMR (126 MHz, $CDCl_3$): δ 136.5 (s, *C*H*C*H_2, 1C), 116.1 (s, *C*H*C*H_2, 1C), 57.7 (s, alpha-CH_2, 2C), 50.4 (brs, carborane-C, 1C), 41.5 (s, N–Me), 31.5 (s, CH_2, 2C), 30.4 (s, *C*H_2*C*H_2CHCH_2, 1C), 28.9 (s, CH_2, 2C), 28.7 (s, *C*H_2*C*H_2CHCH_2, 1C), 26.2 (s, CH_2, 2C), 24.5 (s, CH_2, 2C), 22.5 (s, CH_2, 2C), 14.0 (s, terminal CH_3, 2C).

R = Hexenyl, R' = ^{n}Octyl 715

[^{n}Octyl$_2$MeNH][Hexenyl-$CB_{11}Cl_{11}$]: 410 mg (85%).^{1}H NMR (500 MHz, $CDCl_3$): δ 7.04 (s, 1H), 5.77 (ddt, *J* = 17.0, 10.2, 6.7 Hz, 1H), 5.00 (dq, *J* = 17.5, 3.3 Hz, 1H), 4.94 (dq, *J* = 17.5, 3.3 Hz, 1H), 3.12 (t, *J* = 8.3 Hz, 4H), 2.93 (s, 3H),2.28 (t, *J* = 9.0 Hz, 2H), 2.05 (dd, *J* = 14.7, 6.9 Hz, 2H), 1.96 – 1.85 (m, 2H), 1.84 – 1.73 (m, 2H), 1.45 – 1.20 (m, 24H), 0.88 (t, *J* = 6.9 Hz, 6H). $^{11}B(^{1}H$ decoupled) NMR (128 MHz, $CDCl_3$): δ -3.61, -10.39, -11.70. $^{13}C\{^{1}H\}$ NMR (126 MHz, $CDCl_3$): δ 138.1 (s, *C*H*C*H_2, 1C), 114.8 (s, *C*H*C*H_2, 1C), 57.8 (s, alpha-CH_2, 2C), 51.1 (brs, carborane-C, 1C), 41.6 (s, N–Me), 33.0 (s, hexyl-CH_2, 1C), 31.6 (s, CH_2, 2C), 31.0 (s, hexyl-CH_2, 1C), 29.4 (s, hexyl-CH_2, 1C), 28.9 (s, CH_2, 2C), 26.3 (s, CH_2, 2C), 24.6 (s, CH_2, 2C), 23.9(s, hexyl-CH_2, 1C), 22.6 (s, CH_2, 2C), 14.1 (s, terminal CH_3, 2C).

R = vinylbenzyl, R' = ^{n}Octyl 716

[^{n}Octyl$_2$MeNH][CH_2=CH$C_6H_4CH_2CB_{11}Cl_{11}$]: 500 mg (82%). ^{1}H NMR (500 MHz, $CDCl_3$) δ 7.46 (d, *J* = 8.3 Hz, 2H), 7.25 (d, *J* = 8.3 Hz, 2H), 6.67 (dd, *J* = 17.7, 10.8 Hz, 1H), 5.73 (d, *J* = 17.6 Hz, 1H), 5.23 (d, *J* = 10.9 Hz, 1H), 3.67 (s, 2H), 3.15 (t, *J* = 8.4 Hz, 4H), 2.97 (s, 3H), 1.84 – 1.71 (m, 4H), 1.43 – 1.18 (m, 22H), 0.88 (t, *J* = 7.0 Hz, 6H). $^{11}B(^{1}H$ decoupled) NMR (128 MHz, $CDCl_3$): δ -3.18, -10.42, -11.78. . $^{13}C\{^{1}H\}$ NMR (126

MHz, $CDCl_3/CD_3CN$) δ 137.6 (s, sp^2-C, 1C), 137.2 (s, sp^2-C, 1C), 134.9 (s, Ar, 1C), 131.2 (s, Ar, 1C), 125.5 (s, Ar, 1C), 114.5 (s, Ar, 1C), 57.0 (s, N-CH_2, 2C), 49.5 (brs, carborane-C, 1C), 40.7 (s, N-Me, 1C), 36.2 (s, benzylic-C, 1C), 32.2 (s, CH_2, 2C), 29.5 (s, CH_2, 4C), 26.9 (s, CH_2, 2C), 24.4 (s, CH_2, 2C), 23.2 (s, CH_2, 2C), 14.3 (s, CH_2, 2C).

R = decyl, R' = ^{n}Octyl 717

[^{n}Octyl$_2$MeNH][Decyl-CB$_{11}$Cl$_{11}$]: 400 mg (88%). ^{1}H NMR (500 MHz, C_6D_6) δ 4.67 (s, 1H), 2.76 (t, *J* = 8.4 Hz, 2H), 2.33 – 2.17 (m, 4H), 2.10 – 2.00 (m, 2H), 1.90 (d, *J* = 5.5 Hz, 3H), 1.42 – 1.33 (m, 4H), 1.33 – 1.06 (m, 30H), 0.99 (t, *J* = 7.2 Hz, 6H), 0.90 (t, *J* = 7.0 Hz, 3H). ^{11}B NMR (128 MHz, $CDCl_3$): δ -3.09, -10.04, -11.72. ^{13}C{^{1}H} NMR (100 MHz, CD_3CN) δ 57.3 (s, alpha-CH_2, 2C), 51.5 (brs, carborane-C, 1C), 41.0 (s, N–Me), 32.6 (s, decyl-alpha-CH_2, 1C), 32.4 (s, CH_2, 2C), 32.0 (s, decyl-CH_2, 1C), 30.6 (s, decyl-CH_2, 1C), 30.1 (s, decyl-CH_2, 1C), 30.0 (s, decyl-CH_2, 1C), 29.9 (s, decyl-CH_2, 1C), 29.7 (s, CH_2, 2C), 29.6 (s, CH_2, 2C), 29.4 (s, decyl-CH_2, 1C), 27.0 (s, CH_2, 2C), 25.1 (s, decyl-CH_2, 1C), 24.8(s, CH_2, 2C), 23.4 (s, decyl-CH_2, 1C), 23.3 (s, CH_2, 2C), 14.4 (s, terminal CH_3, 3C).

R = Allyl, R' = C$_{18}$H$_{37}$ 718

[(^{n}C$_{18}$H$_{37}$)$_2$MeNH][Allyl-CB$_{11}$Cl$_{11}$]: 425 mg (85%). ^{1}H NMR (500 MHz, C_6D_6): δ 6.40 (brs, NH), 6.05 (ddt, *J* = 17.2, 9.9, 7.4 Hz, 1H), 5.09 (dq, *J* = 16.7, 1.4 Hz, 1H), 5.02 (dq, *J* = 16.7, 1.4 Hz, 1H), 3.14 – 2.96 (m, 6H, N-CH_2,alpha-CH_2), 2.88 (d, *J* = 5.4 Hz, 3H, N-CH_3), 1.75- 1.66 (m, 4H, CH_2), 1.32-1.16 (m, 60H, CH_2), 0.78 (t, *J* = 6.9 Hz, 3H, terminal-Me). ^{11}B{^{1}H} NMR (128 MHz, CD_3CN): δ ^{13}C{^{1}H} NMR (126 MHz, acetone-d_6): δ 137.6 (s, *C*H*C*H_2, 1C), 116.5 (s, *C*H*C*H_2, 1C), 57.1 (s, alpha-CH_2, 2C), 54.0

(brs, carborane-C, 1C), 40.9 (s, N–Me), 32.6 (s, CH_2, 2C), 30.4-29.6(m, CH_2, 24C), 29.5 (s, *C*H_2CHCH_2, 1C), 26.8 (s, CH_2, 2C), 24.4 (s, CH_2, 2C), 23.3 (s, CH_2, 2C), 14.4 (s, terminal CH_3, 2C).

R = Butenyl, R' = $C_{18}H_{37}$ 719

[(^{n}$C_{18}H_{37}$)$_2$MeNH][Butenyl-$CB_{11}Cl_{11}$]: 300 mg (85%). ^{1}H NMR (500 MHz, $CDCl_3$): δ 5.70 (ddt, *J* = 16.9, 10.2, 6.6 Hz, 1H), 5.06 (dq, *J* = 17.1, 1.5 Hz, 1H), 5.00 (dq, *J* = 10.2, 1.4 Hz, 1H), 3.14 – 2.96 (m, 6H, N-CH_2,alpha-CH_2), 2.98 (s, 3H, N-CH_3), 2.65-2.60 (m, 2H, hexyl-CH_2), 2.35 (t, *J* = 8.9 Hz, 2H, hexyl-CH_2), 1.82- 1.76 (m, 4H, CH_2), 1.41-1.25 (m, 60H, CH_2), 0.88 (t, *J* = 7.0 Hz, 3H, terminal-Me). ^{11}B{^{1}H} NMR (128 MHz, CD_3CN): δ -2.87, -9.93, -11.60. ^{13}C{^{1}H} NMR (126 MHz, $CDCl_3$): δ 138.9 (s, *C*H*C*H_2, 1C), 116.2 (s, *C*H*C*H_2, 1C), 57.8 (s, alpha-CH_2, 2C), 51.2 (brs, carborane-C, 1C), 41.8 (s, N–Me), 32.0 (s, CH_2, 2C), 30.6 (s, *C*H_2*C*H_2CHCH_2, 1C), 30.4-29.6(m, CH_2, 24C), 28.9 (s, *C*H_2CHCH_2, 1C), 26.5 (s, CH_2, 2C), 24.5 (s, CH_2, 2C), 22.8 (s, CH_2, 2C), 14.3 (s, terminal CH_3, 2C).

R = Hexenyl, R' = $C_{18}H_{37}$ 720

[(^{n}$C_{18}H_{37}$)$_2$MeNH][Hexenyl-$CB_{11}Cl_{11}$]: 300 mg (83%). ^{1}H NMR (500 MHz, $CDCl_3$): δ 6.19 (brs, NH), 5.77 (ddt, *J* = 16.9, 10.2, 6.7 Hz, 1H), 5.00 (dq, *J* = 17.1, 1.6 Hz, 1H), 4.94 (dq, *J* = 10.2, 1.2 Hz, 1H), 3.25 – 3.08 (m, 6H, N-CH_2,alpha-CH_2), 2.99 (d, *J* = 4.9 Hz, 3H, N-CH_3), 2.29 (vt, *J* = 9.6 Hz, 2H, alpha C of hexyl), 2.05 (qt, *J* = 6.8, 1.3 Hz, 2H, hexyl-CH_2), 1.93- 1.77 (m, 6H, CH_2), 1.32-1.16 (m, 62H, CH_2), 0.88 (t, *J* = 7.0 Hz, 3H, terminal-Me). ^{11}B{^{1}H} NMR (128 MHz, CD_3CN): δ -2.97, -9.99, -11.62. ^{13}C{^{1}H} NMR (126 MHz, $CDCl_3$): δ ^{13}C{^{1}H} NMR (126 MHz, $CDCl_3$): δ 138.4 (s, *C*H*C*H_2, 1C),

114.9(s, *C*H*C*H_2, 1C), 57.9 (s, alpha-CH_2, 2C), 51.7 (brs, carborane-C, 1C), 41.9 (s, N–Me), 33.2 (s, hexyl-CH_2, 1C), 32.1 (s, CH_2, 2C), 31.2 (s, hexyl-CH_2, 1C), 30.4-29.6(m, CH_2, 24C), 29.6 (s, hexyl-CH_2, 1C), 26.4 (s, CH_2, 2C), 24.5 (s, CH_2, 2C), 24.0 (s, hexyl-CH_2, 1C), 22.8 (s, CH_2, 2C), 14.3 (s, terminal CH_3, 2C).

R = styrenyl, R' = $C_{18}H_{37}$ 721

[(^{n}$C_{18}H_{37}$)$_2$MeNH][Styrenyl-$CB_{11}Cl_{11}$]: 330 mg (82%). ^{1}H NMR (400 MHz, Chloroform-*d*) δ 7.47 (d, *J* = 8.1 Hz, 2H), 7.24 (d, *J* = 8.1 Hz, 2H), 6.66 (dd, *J* = 17.6, 10.9 Hz, 2H), 5.73 (d, *J* = 17.6 Hz, 1H), 5.23 (d, *J* = 10.9 Hz, 0H), 3.67 (s, 2H), 3.24 – 2.93 (m, 4H), 2.86 (d, *J* = 5.1 Hz, 3H, N-Me), 1.35 - 1.26 (m, $CH_2$60H), 0.88 (t, *J* = 6.8 Hz, 6H). ^{11}B{^{1}H} NMR (128 MHz, CD_3CN): δ -2.70, -9.95, -11.35. ^{13}C{^{1}H} NMR (126 MHz, $CDCl_3$): δ 136.8 (s, *C*H*C*H_2, 1C), 136.5 (s, Ar, 1C), 134.1 (s, Ar, 2C), 130.2 (s, Ar, 1C), 124.9 (s, Ar, 2C), 114.0(s, *C*H*C*H_2, 1C), 57.5 (s, alpha-CH_2, 2C), 49.2 (brs, carborane-C, 1C), 41.3 (s, N–Me, 1C), 35.6 (s, benzyl-CH_2, 1C), 32.0 (s, CH_2, 4C), 29.8-29.6(m, CH_2, 22C), 29.5 (s, CH_2, 2C), 29.4 (s, CH_2, 2C), 29.3 (s, CH_2, 2C), 29.0 (s, CH_2, 2C), 26.3 (s, CH_2, 2C), 24.4 (s, CH_2, 2C), 22.7 (s, CH_2, 2C), 14.2 (s, terminal CH_3, 2C).

R = Decyl, R' = $C_{18}H_{37}$ 722

(^{n}$C_{18}H_{37}$)$_2$MeNH][Decyl-$CB_{11}Cl_{11}$]: 340 mg (80%). ^{1}H NMR (400 MHz, Chloroform-*d*) δ 6.16 (brs, N-H, 1H), 3.27 – 3.08 (m, N-CH_2, 4H), 2.99 (d, *J* = 5.2 Hz, N-Me, 3H), 2.28 – 2.24 (m, alpha-decyl-CH_2, 2H), 1.87 - 1.74 (m, CH_2, 6H), 1.41 - 1.26 (m, CH_2, 76H), 0.87 (t, *J* = 6.7 Hz, terminal-CH_3, 9H). ^{11}B{^{1}H} NMR (128 MHz, CD_3CN): δ -3.22, -10.05, -11.38. ^{13}C{^{1}H} NMR (126 MHz, $CDCl_3$): δ 58.1 (s, alpha-CH_2, 2C), 51.5 (brs, carborane-C, 1C), 41.9 (s, N–Me, 1C), 32.01 (s, N-alkyl-CH_2, 2C) 31.96(s, decyl-

CH_2, 1C), 31.3 (s, decyl-CH_2, 1C), 30.3 (s, decyl-CH_2, 1C), 29.8-29.3(m, CH_2, 34C), 29.0 (s, CH_2, 2C), 26.4 (s, CH_2, 2C), 24.7 (s, CH_2, 2C), 24.5 (s, decyl-CH_2, 2C), 22.77 (s, N-alkyl-CH_2, 2C), 22.74 (s, decyl-CH_2, 1C), 14.21 (s, N-alkylterminal CH_3, 2C), 14.19 (s, decyl-terminal-CH_3).

B.5 Carborane C-H alkylation towards dianion

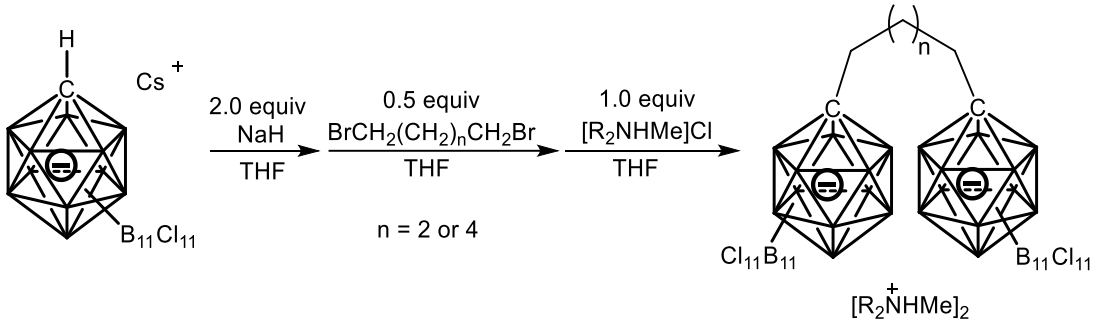

Scheme VII-5. Synthesis of ammonium dicarboranes.

General Procedures For The Synthesis of $[R_2NMeH][Cl_{11}B_{11}CCH_2(CH_2)_nCH_2CB_{11}Cl_{11}](n=2, 4)$. To a 50 mL Schlenk flask, ~500 mg $Cs[CHB_{11}Cl_{11}]$ and 2 equiv NaH were loaded with 20 mL THF. The resulting suspension was stirred at room temperature for 2 h until it stopped bubbling. Then 0.47 equiv $BrCH_2(CH_2)_nCH_2Br$ (n= 2, 4). The suspension was further stirred at room temperature overnight. Inorganic chloride salts was removed by filtering the solution through a short pad of Celite. The filtrate was concentrated and treated with a solution of 1.0 equiv $[R_2MeNH]Cl$ in 10 mL THF. Upon mixing, precipitate formed immediately, and the mixture was further stirred for 2 h, THF was removed under vacuum. The residue was dissolved in C_6H_5F and filtered through a short pad of Celite. After removing the solvent of the filtrate. The oil was triturated with toluene 4 times to remove remaining THF.

n = 2, R' = ^{n}Octyl 723

For [^{n}Octyl$_2$MeNH][B$_{11}$Cl$_{11}$CCH$_2$CH$_2$CH$_2$CH$_2$CB$_{11}$Cl$_{11}$]. 538 mg (88%). ^{1}H NMR (500 MHz, $CDCl_3/CD_3CN$): δ 7.13 (brs, NH, 2H), 2.90 (vt, *J* = 8.5 Hz, N-CH_2, 8H), 2.67 (s, N-CH_3, 6H), 2.13 (vt, *J* = 8.1 Hz, alphaC*H*$_2$, 4H), 1.72 – 1.67 (m, betaC*H*$_2$, 4H), 1.56 (p, *J* = 7.7 Hz, NCH_2CH_2, 8H), 1.33 – 1.14 (m, 44H), 0.82 – 0.74 (m, octylC*H*$_3$, 12H). ^{11}B{^{1}H} NMR (128 MHz, $CDCl_3/CD_3CN$): δ -2.49, -9.57, -11.21.

n = 4, R' = ^{n}Octyl 724

For [^{n}Octyl$_2$MeNH][B$_{11}$Cl$_{11}$CCH$_2$CH$_2$CH$_2$CH$_2$CH$_2$CH$_2$CB$_{11}$Cl$_{11}$]. 560 mg (90%). ^{1}H NMR (500 MHz, $CDCl_3/CD_3CN$): δ 7.13 (brs, NH, 2H), 2.90 (brs, N-CH_2, 8H), 2.67 (s, N-CH_3, 6H), 2.11 (vt, *J* = 8.1 Hz, alphaC*H*$_2$, 4H), 1.75 – 1.67 (m, betaC*H*$_2$, 4H), 1.57 (p, *J* = 7.7 Hz, NCH_2CH_2, 8H), 1.33 – 1.14 (m, 44H), 1.13 (p, *J* = 3.3 Hz, gamaC*H*$_2$, 4H), 0.82 – 0.74 (m, octylC*H*$_3$, 12H). ^{11}B{^{1}H} NMR (128 MHz, $CDCl_3/CD_3CN$): δ -2.68, -9.57, -11.27.

n = 2, R' = C$_{18}$H$_{37}$ 725

For [(^{n}C$_{18}$H$_{37}$)$_2$MeNH][B$_{11}$Cl$_{11}$CCH$_2$CH$_2$CH$_2$CH$_2$CB$_{11}$Cl$_{11}$]. 781 mg (94%). ^{1}H NMR (500 MHz, $CDCl_3$): δ 7.13 (brs, NH, 2H), 3.02 - 2.85 (m, N-CH_2, 8H), 2.72 (d, *J* = 5.0 Hz, N-CH_3, 6H), 2.16 (vt, *J* = 8.1 Hz, alphaC*H*$_2$, 4H), 1.75 – 1.67 (m, betaC*H*$_2$, 4H), 1.64 – 1.54 (m, NCH_2CH_2, 8H), 1.26 – 1.17 (m, 120H), 0.79 (t, *J* = 6.8 Hz, octylC*H*$_3$, 12H). ^{11}B{^{1}H} NMR (128 MHz, $CDCl_3/CD_3CN$): δ -3.01, -10.12, -11.75.

n = 4, R' = C$_{18}$H$_{37}$ 726

For [(^{n}C$_{18}$H$_{37}$)$_2$MeNH][B$_{11}$Cl$_{11}$CCH$_2$CH$_2$CH$_2$CH$_2$CH$_2$CH$_2$CB$_{11}$Cl$_{11}$]. 801 mg (95%). ^{1}H NMR (500 MHz, $CDCl_3/CD_3CN$): δ 6.90 (brs, NH, 2H), 3.11 - 2.90 (m, N-

CH_2, 8H), 2.73 (s, N-CH_3, 6H), 2.11 (vt, J = 8.1 Hz, alphaCH_2, 4H), 1.84 – 1.78 (m, betaCH_2, 4H), 1.70 – 1.60 (m, NCH_2CH_2, 8H), 1.33 – 1.26 (m, 120H), 1.23 – 1.20 (m, gamaCH_2, 4H), 0.91 – 0.81 (m, octylCH_3, 12H). $^{11}B\{^1H\}$ NMR (128 MHz, $CDCl_3$): δ -2.65, -9.70, -11.31.

B.6 Carborane C-H amination

Synthesis of Na[$NH_2CB_{11}Cl_{11}$] 727. To a 250 mL Schlenk flask, 1.37 g (2.35 mmol) [Me_3NH][$CHB_{11}Cl_{11}$] and 0.25 g (2.35 mmol) Na2CO3 was loaded. 75 mL MeOH and 25 mL H_2O was added to the mixture. The resulting solution was refluxed at 70 ℃ oil bath for 3 h. All the volatiles were removed under vacumm to yield Na[$CHB_{11}Cl_{11}$] and inorganic sodium salts as white solid, which was dissolved in 50 mL H2O. To the water solution, 0.40 g NaOH and 0.40 g NH_2OSO_3H was added. The resulting mixture was stirred for 4 h at r. t. After removing the water under vacumm, 60 mL was used to abstract the Na[$NH_2CB_{11}Cl_{11}$]. The THF was removed under vacuum to afford Na[$NH_2CB_{11}Cl_{11}$] as white solid, which was further dried at 100 ℃ to yield 1.20 g white solid. ^1H NMR (400 MHz, CD_3CN,): δ 2.60 (brs, NH_2). $^{11}B\{^1H\}$ NMR (128 MHz, CD_3CN): δ -5.20 (brs, 1B), -11.33 (brs, 10B).

APPENDIX C

(PBP)IRPHCL CATALYZED DEHYDROGENATIVE SILYLATION OF TERMINAL ALKENES

C.1 General considerations

Unless otherwise specified, all reactions and manipulations were carried out under an argon atmosphere using glove box or Schlenk line techniques. Solvents were dried and deoxygenated via the solvent purification system and stored over molecular sieves in the glove box filled with argon. C_6D_6 were dried over NaK /Ph_2CO/18-crown-6, distilled and stored over molecular sieves in an Ar-filled glove box. (PBP)IrPhCl, (PBP)IrH4, and (PBP)IrHCl were prepared by published procedure.[27] Other reagents were purchased from commercial suppliers and used without further purification. NMR spectra were recorded on a Varian iNova 300 spectrometer (^{1}H NMR, 299.951 MHz, ^{13}C NMR, 75.413 MHz, ^{31}P NMR, and 121.425 MHz), Varian Inova 400 (^{1}H NMR, 399.535 MHz; ^{11}B NMR, 128.185 MHz) and NMRS 500 (^{1}H NMR, 499.703 MHz; ^{13}C NMR, 125.697 MHz) spectrometer. Chemical shifts are given in δ (ppm). ^{31}P NMR spectra were referenced externally with 85% phosphoric acid at δ 0. ^{1}H NMR and ^{13}C NMR spectra were referenced using the solvent signals.

C.2 (PBP)Ir catalyzed dehydrogenative silylation of terminal alkene

Reaction of tert-butylethylene (728) with bis-(trimethylsiloxyl)methylsilane catalyzed by (PBP)IrPhCl. To a J. Young tube, 54 μL bis-(trimethylsiloxyl)methylsilane (0.20 mol), 100 μL stock solution of (PBP)IrPhCl (0.10 M in C_6D_6, 0.010 mol), 26 μL tert-butylethylene (0.20 mmol) and 500 μL 0.08 M 1,4-dioxane (internal standard) in C_6D_6

was added was loaded. The resulting mixture was heated in 130 ℃ for 8 h. 42% of silylated product **729** was formed: ^{1}H NMR (500 MHz, C_6D_6) δ 6.35 (d, *J* = 19.0 Hz, vinyl*H*, 1H), 5.63 (d, *J* = 19.0 Hz, vinyl*H*, 1H), 0.98 (s, ^{t}Bu*H*, 9H), 0.19 (s, SiMe*H*, 18H).

Reaction of 1-hexene (730) with bis-(trimethylsiloxyl)methylsilane catalyzed by (PBP)IrPhCl. To a J. Young tube, 54 μL bis-(trimethylsiloxyl)methylsilane (0.20 mol), 100 μL stock solution of (PBP)IrPhCl (0.10 M in C_6D_6, 0.010 mol), 25 μL 1-hexene (0.20 mmol) and 500 μL 0.08 M 1,4-dioxane (internal standard) in C_6D_6 was added was loaded. The resulting mixture was heated in 130 ℃ for 8 h. 47% of silylated product **731** was formed: ^{1}H NMR (500 MHz, C_6D_6) δ 6.29 (dt, *J* = 18.7, 6.3 Hz, vinyl*H*, 1H), 5.69 (d, *J* = 18.7 Hz, vinyl*H*, 1H), resonances of ^{n}Bu were overlapped with olefins and hexane, 0.19 (s, SiMe*H*, 18H).

APPENDIX D

LIST OF PUBLICATIONS RESULTING FROM PHD WORK

1. Lai, Q; Cosio, M.; Ozerov, O.V. Ni Complexes of an Alane/Tris(phosphine) Ligand Built Around a Strongly Lewis Acidic Tris(N-pyrrolyl)aluminium. *Chem. Comm.* **2020**, *56*, 14845-14848.

2. Lai, Q; Bhuvanesh, N.; Ozerov, O.V. Unexpected B/Al Transelementation within a Rh Pincer Complex. *J. Am. Chem. Soc.* **2020**, *142*, 20920-20923.

3. Lai, Q; Ozerov, O.V. Dehydrogenative Diboration of Alkyne Catalyzed by Ir/CO/^{t}BuNC System. *J. Organomet. Chem.* **2021,** *931*, 121614.

4. Gunther, S.; Lai, Q.; Huacuja, R.; Bremer, S.; Pearson, D. M.; Demott, J. C.; Bhuvanesh, N.; Ozerov, O. V.; Klosin, J. Highly Efficient Carborane-Based Activators for Molecular Olefin Polymerization Catalysts. *ACS Catal.* **2021**, Accepted

5. Yu, C.-H.; Yang, X.; Ji, X.; Wang, C-H.; Lai, Q.; Bhuvanesh, N.; Ozerov, O. V. Redox Communication between Two Diarylamido/Bis(phosphine) (PNP)M Moieties Bridged by Ynediyl Linkers (M = NI, Pd, Pt), *Inorg. Chem.* **2020**, *59*, 10153-10162